



TECHNISCHE UNIVERSITÄT MÜNCHEN

FAKULTÄT FÜR CHEMIE

**DISCOVERY AND MECHANISTIC ANALYSIS OF A
SORAFENIB-DERIVED ANTIBIOTIC ACTIVE AGAINST
DRUG-RESISTANT *S. AUREUS*, PERSISTERS AND BIOFILMS**

DISSERTATION

ZUR ERLANGUNG DES AKADEMISCHEN GRADES EINES
DOKTORS DER NATURWISSENSCHAFTEN VON

ELENA KUNOLD

MÜNCHEN 2018



Technische Universität München

Fakultät für Chemie

Lehrstuhl für Organische Chemie II

**Discovery and Mechanistic Analysis of a
Sorafenib-derived Antibiotic Active Against
Drug-resistant *S. aureus*, Persisters and Biofilms**

Elena Kunold

Vollständiger Abdruck der von der Fakultät für Chemie der Technischen
Universität München zur Erlangung des akademischen Grades eines

Doktors der Naturwissenschaften (Dr. rer. nat.)

genehmigten Dissertation.

Vorsitzender: Prof. Dr. Michael Groll

Prüfer der Dissertation: 1. Prof. Dr. Stephan A. Sieber

2. Prof. Dr. Matthias Feige

Die Dissertation wurde am 04.12.2017 bei der Technischen Universität München eingereicht
und durch die Fakultät für Chemie am 16.01.2018 angenommen.

Summary

The rise of multidrug resistant bacteria has started to outpace the discovery of novel antibiotics and now poses a severe public health threat. *Staphylococcus aureus* is a good example of a dangerous human pathogen, which has a remarkable ability to develop resistance mechanisms within a short time. Resistances against all established antibiotics are known, including reserve drugs such as linezolid and daptomycin. Due to this, the prevalence of severe staphylococcal hard-to-treat infections and life-threatening conditions has dramatically increased during the last decades. Thus, discovery and development of new antibacterial agents addressing novel resistance-free targets are urgently needed.

In this thesis, the human kinase inhibitor sorafenib, a drug approved for oncological indications, was found to exhibit antibiotic potency in *S. aureus*. Subsequent work comprised optimization of its scaffold for further development as a drug candidate as well as mechanistic studies of the antibiotic mode of action.

The scaffold of sorafenib was used as basis for the design of a library of 72 small molecule-derivatives. Structure-activity relationship studies led to compound PK150, which showed a ten-fold increase in antibiotic potency compared to sorafenib in *S. aureus*. Furthermore, PK150 was able to inhibit growth of drug-resistant *S. aureus* strains as well as other gram-positive pathogens, such as *Mycobacterium tuberculosis* and vancomycin-resistant enterococci. In addition, PK150 was able to kill persisters and to eradicate established biofilms. Most strikingly, the compound did not induce *in vitro* resistance, showed comparable toxicity to sorafenib, and exhibited good oral bioavailability as well as plasma stability *in vivo*. In a mouse bloodstream infection model, it significantly reduced bacterial loads in heart and lungs, thus rendering PK150 a promising therapeutic drug development candidate.

Affinity-based protein profiling target identification strategy with a sorafenib-derived photoprobe revealed signal peptidase IB (SpsB) as the strongest hit in the performed analysis. Binding was confirmed via competitive labeling and activity-based assays with recombinantly expressed protein. Interestingly, binding of PK150 to SpsB resulted in a stimulation of SpsB. Furthermore, docking and dynamics simulations suggested a binding location adjacent to the active site, which is in accordance with the stimulating effect, as the indicated position does not block the substrate binding pocket. SpsB is an essential protein that cleaves signal peptides from extracellular proteins resulting in their release and maturation and therefore plays an important role in the last step of protein translocation. In line with the SpsB stimulation, a secretome analysis revealed elevated levels of SpsB-substrates in the extracellular space, supporting the target hypothesis. Autolysins, which are cell-wall degrading

enzymes, were among the secreted proteins suggesting their contribution to the antibiotic mechanism by dysregulation of bacterial autolysis. Mode of action analysis showed bactericidal activity of PK150 with accompanied cell lysis, as observed by electron microscopy. The strong antibiotic effect likely stems from an involvement of further targets to the overall mechanism of action. This is supported by the observed lack in resistance development for PK150.

In light of the antibacterial and pharmacological properties, PK150 represents a founding member of a novel class of highly active antibiotics.

Zusammenfassung

Die Verbreitung von Antibiotika-Resistenzen und der gleichzeitige Rückgang an neu entwickelten und zugelassenen Antibiotika stellen heutzutage eine ernsthafte Gefahr für die öffentliche Gesundheit dar. *Staphylococcus aureus* ist ein gutes Beispiel für einen gefährlichen humanen Krankheitserreger, der äußerst effizient Resistenzen entwickelt. Resistente Stämme gegen alle etablierten Antibiotika sind bekannt, einschließlich Reservemedikamente wie Linezolid und Daptomycin. Die Häufigkeit schwerwiegender schlecht behandelbarer Infektionen und lebensbedrohlicher Zustände hat deshalb in den letzten Jahrzehnten stark zugenommen. Die Entdeckung und Entwicklung neuer antibakterieller Wirkstoffe sind daher dringend erforderlich. Diese sollten idealerweise neuartige Zielmoleküle adressieren, die nicht mit bereits bestehenden Resistenzmechanismen assoziiert sind.

Der Ausgangspunkt dieser Arbeit war die Entdeckung der antibiotischen Wirkung des humanen Kinaseinhibitors Sorafenib, eines zugelassenen onkologischen Medikaments, gegen *S. aureus*. Der weitere Verlauf der Arbeit umfasste auf der einen Seite die Verbesserung der Struktur für die weitere Entwicklung als Wirkstoff-Kandidat und auf der anderen Seite die mechanistische Analyse der antibiotischen Wirkungsweise.

Sorafenib wurde als Ausgangspunkt für die Synthese einer Bibliothek von 72 Derivaten genutzt. Auf dieser Basis wurden Struktur-Aktivitätsbeziehungs-Studien durchgeführt, die zur Entdeckung der Verbindung PK150 geführt haben. Diese Verbindung zeigte eine zehnfach stärkere antibiotische Wirkung im Vergleich zu Sorafenib. PK150 hemmte das Wachstum von Antibiotika-resistenten *S. aureus*-Stämmen sowie von weiteren grampositiven Erregern wie *Mycobacterium tuberculosis* und Vancomycin-resistenten Enterokokken. Außerdem tötete es Persister-Zellen und löste etablierte Biofilme auf, die in der Klinik mit schwer behandelbaren Infektionsmanifestationen assoziiert sind. Bemerkenswerterweise induzierte PK150 keine In-vitro-Resistenz, zeigte zudem eine zu Sorafenib vergleichbare Toxizität sowie gute orale Bioverfügbarkeit und Plasmastabilität. Die In-vivo-Wirksamkeit konnte im Maus-Infektionsmodell gezeigt werden, was PK150 zu einem vielversprechenden Kandidaten für die Weiterentwicklung zum therapeutischen Mittel macht.

Durch Affinitäts-basiertes Protein-Profilung mit einer Sorafenib-verwandten Photosonde wurde die Signalpeptidase IB (SpsB) als das wahrscheinlichste Zielprotein der Verbindung identifiziert. SpsB ist ein essentielles Protein, das für die Abspaltung des Signalpeptids von extrazellulären Proteinen nach ihrem Transport durch die Zytoplasmamembran zuständig und damit für die Reifung und Freisetzung von extrazellulären Proteinen von zentraler Bedeutung ist. Die Bindung wurde über kompetitive Markierung und aktivitätsbasierte Assays mit rekombinant exprimiertem Protein bestätigt.

Interessanterweise wurde ein stimulierender Effekt von PK150 auf die Aktivität von SpsB gefunden. Zudem deuteten Docking- und Dynamiksimulationen auf eine Bindung von PK150 in der Nähe des aktiven Zentrums des Enzyms hin, was mit einer Aktivitätssteigerung vereinbar ist, da die Substratbindetasche in dieser Position nicht blockiert ist. Im Einklang mit der Aktivierung von SpsB zeigte die Analyse des bakteriellen Sekretoms eine Anreicherung von SpsB-Substraten im extrazellulären Raum an, was die Hypothese von SpsB als das Zielmolekül von PK150 stützt. Autolysine, Zellwand-abbauende Enzyme, wurden unter den im Sekretom angereicherten Proteinen gefunden, was darauf hindeutet, dass diese eine Rolle in der antibiotischen Wirkung spielen. Passend hierzu ergab die weitere Analyse des Wirkungsmechanismus, dass PK150 eine bakterizide Aktivität besitzt und zudem Zell-Lyse auslöst, was aus elektronenmikroskopischen Aufnahmen ersichtlich wurde. Der starke antibiotische Effekt kann wahrscheinlich auf einen Beitrag weiterer beteiligter Zielmoleküle zum Wirkmechanismus von PK150 zurückgeführt werden. Darauf deutet auch die fehlende Resistenzentwicklung hin.

Aufgrund der gezeigten antibakteriellen und pharmakologischen Eigenschaften repräsentiert PK150 den ersten Vertreter einer neuen Klasse von potenten Antibiotika.

Contents

Summary	III
Zusammenfassung.....	V
Contents	VII
Introductory Remarks	IX
1 Introduction	1
1.1 Antimicrobial Resistance Crisis	1
1.2 <i>Staphylococcus aureus</i>	4
1.3 Approaches for the Discovery of Antibacterials	9
1.4 Target Deconvolution	10
1.5 Scope of this work	15
2 Results and Discussion	17
2.1 Discovery of a Novel Sorafenib-derived and Highly Potent Antibiotic.....	17
2.1.1 Antibacterial Screen of Kinase Inhibitors	17
2.1.2 Screening of Sorafenib Derivatives and SAR studies.....	18
2.1.3 Antibacterial Spectrum of Sorafenib and PK150.....	20
2.1.4 Resistance Development.....	22
2.1.5 Killing of Persisters	23
2.1.6 Eradication of Biofilms	27
2.1.7 Cytotoxicity, Hemolysis and Plasma Stability.....	29
2.1.8 Kinobead Pull-Downs with Human Cells	30
2.1.9 <i>In vivo</i> Activity	31
2.2 Mechanistic Insights into the Antibiotic Action of Sorafenib and PK150.....	35
2.2.1 Identification of Protein Targets via AfBPP	35
2.2.2 Biochemical Validation of SpsB as a Target.....	40
2.2.3 Docking and Molecular Dynamics	49
2.2.4 Genomic Approaches	51
2.2.5 Secretome and Surfaceome Analyses	53
2.2.6 Mode of Antibiotic Action	56
2.2.7 SpsB and the Mode of Action.....	60
3 Conclusions and Outlook	65
4 Materials and Methods.....	71
4.1 Microbiology.....	71
4.1.1 Bacterial Strains and Media	71
4.1.2 Cultivation Methods.....	73
4.1.3 Determination of Minimum Inhibitory Concentration (MIC).....	74

4.1.4	Resistance Development Assay.....	75
4.1.5	Persister Cell Assays	75
4.1.6	Biofilm Assays.....	76
4.1.7	Time-Kill Assays	77
4.1.8	Cell Membrane Permeability Assay	78
4.1.9	Zymography.....	78
4.2	Drug Candidate Development Assays.....	79
4.2.1	<i>In vitro</i> assays	79
4.2.2	<i>In vivo</i> animal studies	83
4.3	Proteomics.....	85
4.3.1	AfBPP with Sorafenib Photoprobe SFN-P in <i>E. coli</i> BL21(DE3)pLysS harboring pET-DEST-55-fl-SpsB.....	85
4.3.2	AfBPP with Sorafenib Photoprobe SNF-P in <i>S. aureus</i> NCTC 8325.....	86
4.3.3	Secretome and Surfaceome analyses	89
4.3.4	Kinobead Pull-downs.....	91
4.4	Molecular Biology and Protein Biochemistry	93
4.4.1	Cloning of Full-length SpsB (fl-SpsB)	93
4.4.2	Expression and Purification of Full-length SpsB.....	94
4.4.3	Western Blot Analysis	95
4.4.4	Intact Protein Mass Spectrometry	95
4.4.5	Preparation of Membrane Fractions from <i>E. coli</i> and <i>S. aureus</i> NCTC 8325.....	96
4.4.6	FRET Assays	96
4.5	Other Methods	97
4.5.1	Computational methods - Molecular Docking and Dynamic Simulations ...	97
4.5.2	Electron Microscopy.....	98
4.5.3	Next-Generation Sequencing	99
5	Contributions	101
6	References.....	103
7	Abbreviations, Units and Symbols	117
8	Supporting Information	121
8.1	Supporting Figures.....	121
8.2	Supporting Tables	127

Introductory Remarks

The present doctoral dissertation was accomplished between February 2013 and November 2017 under the supervision of Prof. Dr. Stephan A. Sieber at the Chair of Organic Chemistry II of the Technische Universität München.

Parts of this thesis have been/will be published as listed below:

Kunold, E.,* Kleiner, P.,* Rox, K., Jennings, M. C., Ugur, I. M., Reinecke, M., Kuster, B., Antes, I., Rohde, M., Wuest, W. M., Medina, E., Sieber, S. A. Repurposing human kinase inhibitors to create an antibiotic active against drug-resistant *Staphylococcus aureus* (submitted).

*contributed equally

Kunold, E., Kleiner, P., Sieber S. A. Identification of the molecular target of a growth inhibiting compound in *Staphylococcus aureus* using a chemical proteomics strategy, oral presentation, 21st International Mass Spectrometry Conference, Toronto, Canada, 08/2016.

Sieber, S. A., Kleiner, P., **Kunold, E.** Urea motif containing compounds and derivatives thereof as antibacterial drugs. 16171906.7 - 1462, filed May 30, 2017, issued July 11, 2017.

1 Introduction

1.1 Antimicrobial Resistance Crisis

Antibiotics have shown the most outstanding beneficial effect on human life expectancy in the entire history of medicine.¹ However, the rise of antibiotic-resistant pathogens over the past decades and the simultaneous decline in introduction of new compound classes into clinical practice has now led to a global health crisis, in which even simple infections could become life-threatening again.² In February 2017, the World Health Organization (WHO) published a list of twelve antibiotic-resistant bacterial pathogens that in addition to *M. tuberculosis* represent a major threat to public health (Table 1).^{3,4} This document strongly emphasizes the urgency of actions that need to be undertaken to fight resistant bacterial infections. Indeed, scientists and healthcare experts have been ringing the alarm bell for years warning of a “post-antibiotic era” to come.^{5,6}

Table 1: Global priority list of antibiotic-resistant pathogens to guide research, discovery and development of new antibiotics. The catalogue was released in February 2017 by the World Health Organization to point out which 12 antibiotic-resistant strains additionally to *M. tuberculosis* represent the major health threat worldwide. Modified from Tacconelli *et al.*⁴

Priority 1: CRITICAL
<i>Mycobacterium tuberculosis</i> <i>Acinetobacter baumannii</i> , carbapenem-resistant <i>Pseudomonas aeruginosa</i> , carbapenem-resistant <i>Enterobacteriaceae</i> *, carbapenem-resistant, 3 rd generation cephalosporin-resistant
Priority 2: HIGH
<i>Enterococcus faecium</i> , vancomycin-resistant <i>Staphylococcus aureus</i> , methicillin-resistant, vancomycin-intermediate and resistant <i>Helicobacter pylori</i> , clarithromycin-resistant <i>Campylobacter</i> , fluoroquinolone-resistant <i>Salmonella spp.</i> , fluoroquinolone-resistant <i>Neisseria gonorrhoeae</i> , 3 rd cephalosporin-resistant, fluoroquinolone-resistant
Priority 3: MEDIUM
<i>Streptococcus pneumoniae</i> , penicillin-non-susceptible <i>Haemophilus influenzae</i> , ampicillin-resistant <i>Shigella spp.</i> , fluoroquinolone-resistant

The phenomenon of antibiotic resistance is as old as antibiotics themselves. The presence of resistance genes on plasmids, for example coding for serine β -lactamases thus conferring resistance to penicillins, cephalosporins and carbapenems, could be traced back to millions of years ago by phylogenetic analyses.⁷⁻⁹ A common belief is that bacteria naturally developed antibiotics to compete with each other, which has been shown to be only true to some extent.¹⁰ Several hypotheses for the natural

functions of these second metabolites exist.¹¹ The observation that antibiotic concentration levels produced by environmental bacteria are commonly far below the minimum inhibitory concentrations (MICs)¹² and that even very low concentrations (1/100 of MIC) are sufficient to substantially modulate transcriptional profiles^{13,14} lead to the assumption that these metabolites are used as signal molecules.^{10,15} At higher concentrations they are able to inhibit the growth or even kill bacteria, a trait which was accidentally discovered by Alexander Fleming in 1929.¹⁶ Since then, these metabolites have been in the focus of research and were meticulously looked for to exploit them for therapeutic purposes under the name “antibiotics”, introduced by Selman Waksman in 1941.¹⁷ For every acting molecule, however, a modulating silencing counterpart exists.¹² The majority of the fast occurring resistances today is therefore just the immediate recall of mechanisms that coevolved together with the molecules that we have borrowed from nature as antibiotics.¹⁸ The first raised finger to sensitize the community about the topic of responsible handling of antibiotics came as early as 1945 from Alexander Fleming himself, who recognized how easily resistances emerge.¹⁹

Antibiotic resistances occur when bacteria are placed under selective pressure upon treatment with the respective drug. The bacterial resistance repertoire comprises a multitude of different mechanisms (Figure 1). Some of them are intrinsic, whereas others can be acquired through horizontal gene transfer by conjugation, transformation or transduction²⁰ or evolved through spontaneous mutations.²¹ Examples of intrinsic insensitivity are absent targets for the respective drug in some species and natural barriers, such as the outer membrane of gram-negative bacteria. Acquired resistance mechanisms comprise inactivation of the drug by enzymatic metabolism and reduced effective concentration of a drug due to prevention of target access or increased efflux. Additionally, targets can be modified by mutations or post-translational modifications (PTMs), either rendering them inaccessible for the drug or resulting in structural changes of secondary, non-protein targets such as peptidoglycan. It has also been found that the induction of alternative pathways can enable bypassing of the target pathway.^{18,21,22}

Resistance mechanisms known today likely represent just a sample of the full range of existing resistance pathways. The majority of currently available antibiotics target only a very limited number of pathways or structures within the bacteria (Figure 1). There are five main target categories of antibiotics – 1) cell-wall biosynthesis (targeted by e.g. β -lactam antibiotics and glycopeptides), 2) protein biosynthesis (e.g. rifamycin prevents transcription and tetracyclines, macrolides, aminoglycosides and oxazolidinones prevent translation of proteins), 3) deoxyribonucleic acid (DNA) replication (quinolones), 4) folate synthesis (sulfonamides, trimethoprim), and 5) membrane structures (polymyxins, lipopeptides).²³ This narrow scope of exploited antibacterial targets aggravates the resistance problem as resistance mechanisms often render several antibiotics with similar points

of attack inactive at once. To overcome this problem, novel chemical entities targeting alternative pathways are desperately needed. The estimated number of approximately 200 conserved essential proteins displays the enormous spectrum of potential targets that still await exploitation.²⁴

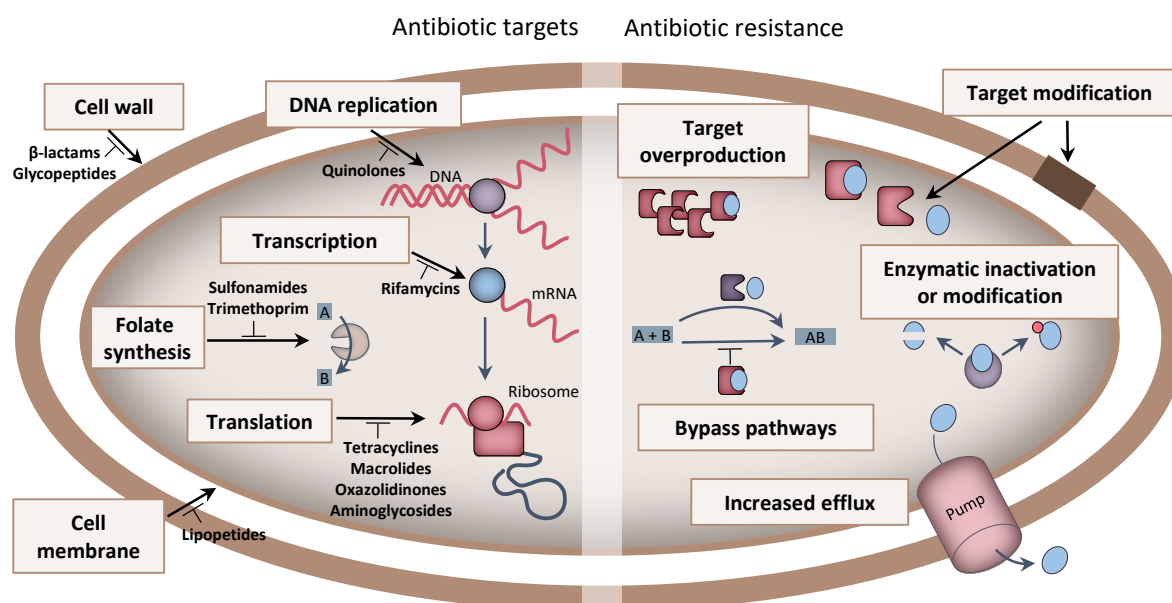


Figure 1: Antibiotic targets and resistance mechanisms. Modified from Lewis²⁴ and Wright.²⁵

The discovery of novel chemical entities, however, is currently challenged by the lack of interest of the pharmaceutical industry in the development of antibiotics. After the “golden era” of antibiotics between 1940 and 1960, during which novel classes of natural products with antibacterial properties were easily identified mainly from soil bacteria, the pharmaceutical industry went through a long-lasting drought period (Figure 2). Enormous efforts based on high-throughput screening platforms failed, not paying off the high costs of investment that initially had to be paid.^{24,26} Novel classes of antibiotics were introduced in the last two decades. However, they are narrow-spectrum, resulting in a fairly limited clinical use.²⁴ Although the “post-antibiotic era” is imminent, the current market for hard-to-treat resistant infections is small and standard antibiotics are prescribed with priority. In addition, antibiotic treatment regimens are often short-termed, curative and cheap compared to the treatment of chronic diseases and therefore less profitable.²⁷ Furthermore, regulatory hurdles aggravate the situation.^{1,28} Due to the feared low return on investments, the majority of the largest pharmaceutical companies abandoned their antibiotic R&D divisions, leading to a strong decline in research activities.²⁹ By 2013, only four multinational companies still invested in this research area.²⁷ Due to the decline in antibacterial research activities of the pharmaceutical industry, the antibiotic development pipelines are almost empty today.

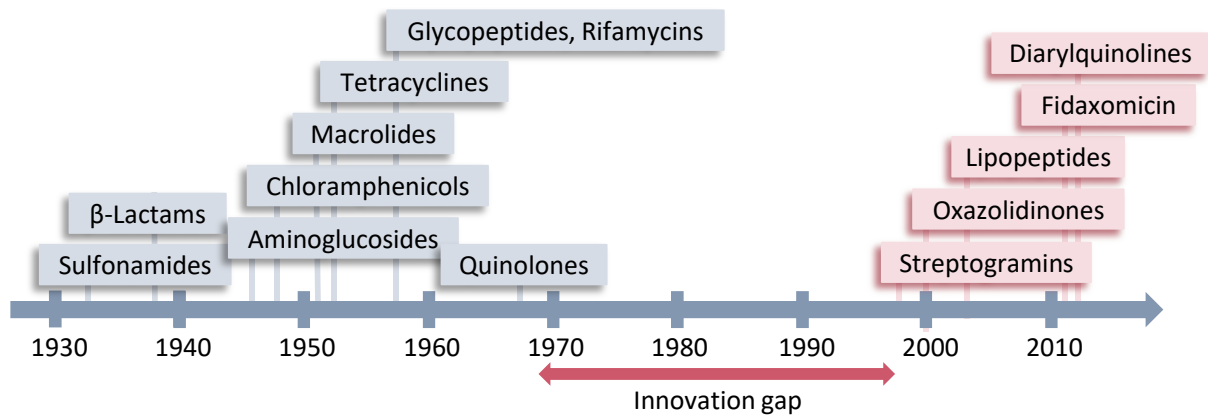


Figure 2: “Innovation gap” of new antibiotic leads. There were no major classes of antibiotics introduced in the years between 1968 and 1998.²⁴

The current resistance crisis is further aggravated by the careless use of antibiotics. Inappropriate prescription and overuse of antibacterial drugs, general lack of public knowledge on proper and responsible use of antibiotics, and the misuse of antibiotics in food-producing animals, have led to faster emergence and spread of resistant strains.^{27,30}

Summarized, the fast spread of resistant strains and the simultaneous lack in discovery of new antibiotics that address novel resistance-free targets are the main causes of the current crisis of more frequently occurring untreatable bacterial infections. *Staphylococcus aureus* is a prominent example of such a pathogen. These days, multidrug resistant *S. aureus* strains are the norm rather than the exception, causing infections that are difficult to treat.³¹ Therefore, the WHO recently set a high priority on finding novel antibiotics against methicillin-resistant (MRSA) as well as vancomycin-intermediate (VISA) and -resistant (VRSA) strains (Table 1).⁴

1.2 *Staphylococcus aureus*

Staphylococcus aureus is a gram-positive commensal eubacterium and an opportunistic pathogen. Most often it asymptomatically colonizes skin, anterior nares and gastrointestinal tract in about 20 – 30% of the population permanently and in 30% transiently.^{32–34} The harmless colonization, however, serves as a reservoir for the development of potentially severe infections, once the immune system is compromised by disease, surgery or therapeutic interventions.³⁵ Under these circumstances, *S. aureus* can cause severe infections of skin and soft tissues and enter the blood stream resulting in bacteremia. Once in the bloodstream it can disseminate to almost every organ and cause endocarditis, pneumonia and meningitis as well as osteomyelitis, and even urinary tract infections. It can cause acute life-threatening conditions such as sepsis and toxic shock syndrome.^{36,37} Surgical interventions and

introduction of catheters and other invasive devices represent a higher potential risk of bacteremia and deep-seated organ infections. Presence of foreign material, furthermore, provides a perfect surface for attachment of bacteria and formation of biofilms, which are especially challenging to treat.³⁸ The difficulties in *S. aureus* treatment arise from multiple causes. The pathogenicity of *S. aureus* is characterized by an ingenious combination of various immune-evasion mechanisms and a broad spectrum of virulence factors which are responsible for the broad range of different infection manifestations and symptoms as well as several mechanisms for the very rapid adaptation to changing conditions.^{39,40} The pathogen employs different ways to circumvent or inactivate the action of antibiotics by efficient and fast development of resistances or switching its phenotype to antibiotics-unsusceptible, dormant variants such as metabolically inactive persisters residing in biofilms.⁴¹

Microbiology, Pathogenicity and Virulence

At the microscopic level, staphylococci are round (“kókkos”, Greek for “grain, corn, berry”), approximately 0.8 – 1.2 µm in diameter and form clusters similar to bunches of grapes (staphylé, Greek for “grape”). This irregular appearance stems from sequential division of cells in three orthogonal planes (Figure 3).^{42,43} On agar plates, *Staphylococcus aureus* forms round colonies that are characterized by a typical golden color (*aureus*, Latin for “golden”) originating from the yellowish-orange carotenoid pigment staphyloxanthin.^{44,45} It protects the bacterium against neutrophils and reactive oxygen species from the immune system⁴⁶ and promotes virulence in animal models.⁴⁷ The pigment represents one of many virulence factors, which are the determinants of pathogenesis of *S. aureus*. They allow the bacterium to attach to tissues and cells as well as to hide from, inactivate or hijack the immune system. Many of these processes directly result in harmful toxic effects for the host.⁴⁰

The *S. aureus* genome comprises about 2.8 Mbp⁴⁸ and approximately 2900 genes.⁴⁹ A total of up to 170 different existing virulence genes in *S. aureus* species were reported.⁵⁰ The arsenal of virulence factors expressed by *S. aureus* can be functionally divided into two major groups. The first group comprises surface proteins that are involved in the initial stages of infection and promote attachment and colonization of host cells. Proteins called microbial surface components recognizing adhesive matrix molecules (MSCRAMMs), for example, mediate the binding to the surface molecules of target tissues. After successful colonization, the second group of virulence factors, mainly secretory proteins, mediates detachment and spread of bacteria within the host and helps to evade the immune system. An example are cytolytic toxins, i.e. hemolysins or leucocidins, which induce lysis of erythrocytes, leukocytes and other blood cells via membrane permeabilization or by formation of pores.^{51–53}

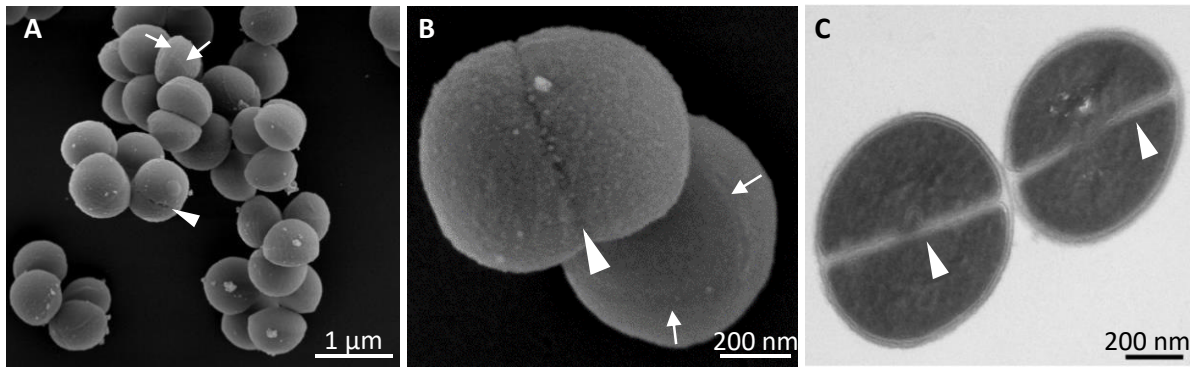


Figure 3: Field emission scanning electron micrographs (FESEM) (A, B) and transmission electron micrographs (C) of exponentially dividing *S. aureus* NCTC 8325. Arrow heads point to division septa and arrows to scars from septa of previous divisions. Images by Manfred Rohde, Central Facility for Microscopy (ZEIM), Helmholtz Centre for Infection Research (HZI), Braunschweig, Germany.

Expression coordination of various groups of virulence factors at different stages of staphylococcal infection – with mainly surface proteins during early and secreted proteins at later stages – is tightly controlled by regulative mechanisms. Adapting to changing conditions requires sensing of environmental changes (supply of nutrients and oxygen, pH, temperature, osmolarity), communication between cells, and coordination of their growth and density. The regulative processes associated with sensing of external conditions and the response to them are called quorum-sensing. Regulation of virulence factor expression is an interactive regulatory network mainly including two two-component regulatory systems (accessory gene regulator (*agr*) and staphylococcal accessory element (*sae*)) and the global regulatory system with staphylococcal accessory regulator A (*sarA*) as the central molecule.^{40,52}

As virulence factors act outside the cells, these surface-bound or secreted proteins need to be translocated across the cytoplasmic membrane. The majority of virulence factors is transported via the Sec pathway, which comprises the main translocase SecYEG, several auxiliary components for translocation (e.g. SecDF-YajC, YidC), the ATPase motor SecA, and the signal peptidase IB (SpsB). The latter recognizes and removes signal peptides of substrate pre-proteins that are designated for translocation, thereby releasing them into the extracellular space, which is the reason why most of the virulence factors contain a signal peptide sequence.^{53,54} In this regard, targeting virulence factors, quorum-sensing regulators, and bacterial secretion systems, is an attractive strategy for fighting this pathogen.⁵⁵ Especially, the essential endopeptidase SpsB has been repeatedly described as an attractive drug target and many efforts have been undertaken to develop molecules that address this enzyme.⁵⁵⁻⁵⁷

Antibiotic Resistance, Persisters and Biofilms

Staphylococcus aureus is an excellent example for a pathogen that is remarkably efficient in resistance development. Virtually susceptible to any antibiotic, it rapidly acquired resistances after the clinical introduction of drugs throughout the history. First spread of resistance against penicillin has been reported only one year after the first broader trial phase on patients in 1941 had taken place.⁵⁸ Resistance to methicillin, the first penicillinase-resistant penicillin, was reported in 1961, only two years after its first use.⁵⁹ Since then, epidemic waves of methicillin-resistant *S. aureus* (MRSA) have been reported repeatedly, first as nosocomial infections associated with hospital environments and since the late 1990s as community-acquired (CA-MRSA) infections.⁶⁰ Spread of MRSA led to a broader use of vancomycin from the 1980s on, resulting in the emergence of VISA in 1997 and VRSA in 2002.⁶¹ Further examples are resistances against the last resort drugs daptomycin and linezolid, which were reported one year after the discovery of daptomycin and introduction of linezolid in 1986 and 2000, respectively.²⁴ Resistances to the majority of existing antibiotics are known (Table 2), emphasizing the high demand for development of novel drugs against *S. aureus* which address alternative unexploited targets.

Table 2: Examples of mechanisms of *S. aureus* resistance to antibiotics.^{31,61,62} Modified from Lowy 2003.³¹

Antibiotic	Resistance gene(s)	Resistance determinant	Mechanism(s) of resistance	Location(s)
β-Lactams	<i>blaZ</i>	β-Lactamase	Enzymatic hydrolysis	PI:Tn
	<i>mecA</i>	PBP2a	Reduced affinity	C: SCC <i>mec</i>
Glycopeptides (VISA)	Different, mostly <i>rpoB</i>	Altered peptidoglycan	Trapping of vancomycin in the cell wall	C
Glycopeptides (VRSA)	<i>vanA</i>	D-Ala-D-Lac	Synthesis of dipeptide with reduced affinity for vancomycin	PI:Tn
Quinolones	<i>parC</i>	ParC component of topo IV	Mutations in the QRDR region, reducing affinity of enzyme-DNA complex for quinolones	C
	<i>gyrA, gyrB</i>	Gyrase components		C
Aminoglycosides	Different (e.g. <i>aac, aph</i>)	Acetyltransferase, phosphotransferase	Modification of aminoglycosides	PI, PI:Tn
Trimethoprim	<i>dfrB</i>	Dihydrofolate reductase	Reduced affinity for DHFR	C
Sulfamethoxazole (Sulfonamide)	<i>sulA</i>	Dihydropteroate synthase	Overproduction of <i>p</i> -aminobenzoic acid by enzyme	C
Oxazolidinone	<i>rrn</i>	23S rRNA	Mutation in 23S rRNA component of 50S ribosome interferes with ribosomal binding	C
Quinupristin	<i>ermA, ermB, ermC</i>	Ribosomal methylases	Reduce binding to the 23S ribosomal subunit	PI, C
Dalfopristin	<i>Vat, vatB</i>	Acetyltransferases	Enzymatic modification	PI
Daptomycin	<i>mrpF, cls2, pgsA</i>	Enzymes of phospholipid biosynthesis	Reduce binding by changing the charge of the membrane	C

PI, Plasmid; C, Chromosome; Tn, Transposon; QRDR, Quinolone resistance-determining region

Major clinical treatment challenges apart from antibiotic resistance are represented by altered *S. aureus* phenotypes. These genetically identical cells are characterized by a very slow or nonexistent growth (dormant state).⁶³ They are responsible for the majority of resistance-independent, recurrent, hard-to-treat infections strongly contributing to the number of treatment failures.⁴¹ Persister cells represent the most prominent dormant phenotype variant of *S. aureus*. They are present as a subpopulation of every bacterial culture and are especially highly abundant in stationary phase-cultures characterized by limited nutrient and oxygen supply and high cell densities. Due to the fact that most antibiotics act on actively growing cells, persisters - being metabolically inactive - are inherently less susceptible to drug treatment.⁶⁴ These bacteria can survive until the environmental stress disappears and revert back to the actively growing phenotype. Upon antibiotic treatment, the characteristic biphasic killing curve shows an initial phase of fast killing kinetics, in which cells of normal phenotype are rapidly killed, followed by a second phase, during which the killing stagnates as only tolerant persister cells remain.⁶⁵ The formation and regulation of this state is highly complex and has been studied in detail for gram-negative bacteria such as *E. coli* and *S. typhimurium*. However, persister formation in gram-positives is poorly understood yet. Several mechanisms known from *E. coli*, for example an involvement of toxin-antitoxin modules, could not be experimentally confirmed in *S. aureus*.⁶³ Although expression of stationary markers and depletion of ATP levels was shown to be correlated with an increase in antibiotic tolerance, the exact mechanisms leading to persister formation in gram-positives remain elusive.^{66,67}

The connection between persister cells and biofilms, however, is evident.⁴¹ Biofilms are layers of bacteria adhering to a surface that are embedded in an extracellular matrix of polysaccharides, DNA, and proteins. Antibiotic tolerance of such communities was first attributed to a decreased accessibility and penetration of drugs into these matrices but experiments have demonstrated that this is not the prime cause for tolerance. The matrix rather functions as a protective shield against the immune system during infection. Conditions in biofilms appear to be similar to that of stationary phases of planktonic bacteria with high densities and limited nutrients. The decreased metabolic behavior and the antibiotic tolerance, which are the hallmarks of persisters in planktonic cultures, are also hallmarks of bacteria residing in biofilms.⁶⁸

Evolutionarily, these phenotypes might have arisen as an immediate protection mechanism for unpredictable environmental stresses. Their presence in every culture represents a back-up survival strategy, if other mechanisms fail. Additionally, phenotypic switching is beneficial compared to irreversible mutations that represent a fitness cost once the stressor is gone.⁵²

1.3 Approaches for the Discovery of Antibacterials

Major current research goals lie in the identification of novel chemical scaffolds with antibacterial activity, ideally targeting unexploited pathways, resulting in novel modes of action.

Targeted vs. Untargeted Approaches

Identification of novel antibacterial drugs requires a platform for the assessment of the antibacterial activity. Two major strategies herein are targeted and untargeted approaches. Untargeted strategies employ the evaluation of antibacterial activity of a compound based on phenotypic assays using whole cells. Most often this is conducted via determination of the lowest concentration of a compound that inhibits visible growth of bacteria.⁶⁹ Untargeted strategies are used for initial discovery of novel antibacterial agents without a preliminary idea of the underlying mechanism. In contrast to this, targeted strategies are based on proteins that have been previously suggested as attractive points of attack. During the 1990s whole-genome sequencing became a fast and easy methodology. Associated genomics approaches led to the identification of druggable targets, which are essential and ideally have no human homologues to avoid adverse side effects and have favorable accessibility for drugs.^{26,70} Apart from focusing on essential targets, targeting virulence factors of pathogens has emerged as a novel attractive strategy during the past years.⁷¹ Antivirulence approaches aim to overcome the problem of resistance by disarming the pathogens rather than killing them. These approaches are believed to largely circumvent the selective pressure, which causes resistance development when antibiotics against essential targets are used.⁷² Main targets in antivirulence approaches are quorum-sensing molecules, regulating the expression of virulence determinants and virulence factors such as adhesins and toxins.^{73,74} Furthermore, secretion systems, responsible for the translocation and release of virulence factors into the extracellular space, are regarded as attractive targets as well.^{55,72}

Sources of Antibacterial Molecules

Finding novel antibacterial scaffolds requires the exploration of new chemical spaces. The broad majority of antibiotics used these days are natural products and derivatives thereof. Nature itself is the richest source of structurally diverse and unique bioactive compounds. Thus, most of the recently discovered bioactive scaffolds are natural products from organisms found in previously unexplored habitats, such as the desert and the ocean.^{75,76} Interestingly, the human body can be regarded as a niche for the identification of novel natural products, as well. The observation that there are individuals who have never been carriers of *S. aureus* has led to the discovery of *Staphylococcus lugdunensis* and its antibacterial metabolite lugdunin.⁷⁷ An interesting example is furthermore the

recently discovered antibiotic teixobactin from uncultivable soil bacteria. Researchers used a special trick – namely semipermeable membranes as part of the iChip technology – in order to be able to cultivate these bacteria directly in their natural habitat.⁷⁸ This strategy is very promising for future discoveries, as 99% of the soil bacteria have never been explored, and could initiate the revival of bacteria mining.^{79,80} Another strategy for the discovery of natural metabolites is the so called genome-mining.^{69,81} Genomics has led to the identification of the underlying biosynthetic machineries for the production of secondary metabolites, including antibiotically active agents. The majority of these specialized metabolite biosynthetic gene clusters (BGCs) remains silent under laboratory conditions and the encoded metabolites remain elusive. Approaches to activate or to heterologously express those genes represent an elegant strategy to discover novel chemical compounds from otherwise exhaustively studied organisms.

Targeted high-throughput screening (HTS) approaches have been unsuccessful in the identification of antibacterial compounds in the past. The major reason for this overall failure is attributed to the inappropriate matter of the used compound libraries as well as the starting material for subsequent syntheses. The properties of the available libraries had been optimized to address human drug targets (e.g. Lipinski rules) and thus often do not meet the requirements for bacterial targets.^{26,82} Penetration into bacterial cells represented one of the main obstacles.²⁴ However, systematic deepening of the knowledge about physicochemical properties of antibiotics is believed to enable the design of appropriate chemical libraries and revive HTS platforms as a powerful strategy for the identification of new lead compounds.^{24,82} Furthermore, HTS screenings can be useful to identify combinations of antibacterial agents that would slow down the development of resistances.²⁴

Another attractive strategy is the repurposing of already existing drugs for novel indication areas.⁸³ The wealth of readily available scaffolds represents a good source for systematic screens against pathogenic bacteria.⁸⁴ Additionally, drug repurposing can reduce the time and costs associated with the drug development process, which is a major advantage compared to a *de novo* development process.⁸⁵ Repositioning has already been successful in several other disease areas.⁸⁵ Recently, this strategy led to the discovery of antibiotic activity of small molecules that originated from approaches to discover drugs for human targets, such as ebselen,⁸⁶ 5-fluoro-2'-deoxyuridine⁸⁷, terfenadine⁸⁸ and pyridopyrimidines.⁸⁴

1.4 Target Deconvolution

For further rational development and optimization of antibacterial compounds, knowledge of the involved targets and underlying mechanisms of action is required. In this regard, target-based

approaches have the advantage that hits can be directly optimized through medicinal chemistry efforts. However, many hits from target-based approaches lack activity when using whole cells. This is mostly caused by inefficient penetration, efflux or interference with other structures within and outside the cells.²⁴

In contrast to that, the major advantage of phenotype-based approaches is that they are more intuitive and straight-forward, directly revealing the antibiotic potency.⁸⁹ Whole cell-based approaches provide an unbiased view and allow the detection of compounds that address multiple targets.⁸⁹ A disadvantage is that target deconvolution for these hits can be a challenging task due to the countless number of structures that can be addressed by small molecules, especially regarding proteins.⁸⁹ However, recent advances in mass spectrometry-based proteomic approaches enabled the study of proteins at the level of whole cellular proteomes. Combined with chemical strategies, target deconvolution of small molecules has become feasible. One powerful technology for this task is the activity-based protein profiling (ABPP), developed by Cravatt^{90,91} and Bogyo.^{92,93}

Target Identification: Activity-Based Protein Profiling

Activity-based protein profiling is a powerful tool for all kinds of experiments, in which the binding of a small molecule to a protein enables investigation of its targets. The main advantage of this technique is that the binding provides information about the proteins' activity states (i.e. their correct folding and respective post-translational modifications) and not just their abundance.^{91,94} This versatile method can be used for different kinds of investigations. It enables identification and functional annotation of unknown proteins or protein classes (e.g. ATP-binding proteins with an ATP-probe).^{95,96} Furthermore, activity-based profiling can be used for comparisons of known proteins or protein classes between various conditions (e.g. serine hydrolase family enzymes with fluorophosphonate-based probes).⁹⁶⁻⁹⁸ In drug discovery the most interesting application of this method is its use for identification of previously unknown targets of bioactive molecules.⁹⁹

The central piece of an ABPP-approach is a probe, consisting of 1) the selectivity group that directs specific binding to a protein, 2) a reactive moiety that facilitates binding to the target and 3) a reporter tag that enables the visualization or identification of the bound target (Figure 4).

The selectivity group is mostly a small molecule that determines the scope of protein targets. Most often, it is either a natural product or a synthetic molecule with known bioactivity, used for identification of its targets and off-targets. Alternatively it can be a previously described binder of a protein class, which is used as a tool for comparative monitoring of these proteins or for functional annotation of unknown proteins.⁹⁹

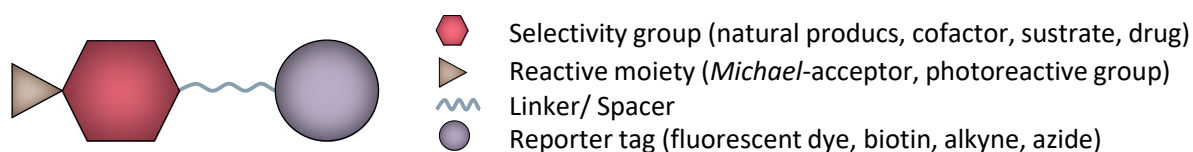


Figure 4: Schematic representation of an activity-based probe (ABP).

The reactive part of the probe is either an intrinsic electrophilic moiety for direct covalent attachment to a protein or a photocrosslinker for covalent linking of reversibly binding molecules. The most common photocrosslinker groups are benzophenones, diazirines, and aryl azides. They are chemically inert, but form extremely reactive intermediates (biradicals, carbenes, and nitrenes, respectively) upon irradiation with ultraviolet (UV) light. These species form covalent bonds with residues in their vicinity.^{100,101} In cases, in which a photocrosslinker is applied, the respective workflow is called affinity-based protein profiling (AfBPP). This strategy has been successfully used in a variety of protein studies, for example of metalloproteases^{102,103} and histone deacetylases.^{104,105}

Reporter tags are used for the visualization or isolation and subsequent identification of the bound proteins. Recent advances in chemical biology have led to the development of several bioorthogonal ligation methods, enabling the introduction of reporter tags after binding of the probe to a protein and subsequent cell lysis. This strategy substantially minimizes interfering effects and permeability issues.^{105–108} In this respect, terminal azides and alkynes have gained broad application in recent years. They can be bioorthogonally clicked to each other in a Copper(I)-catalyzed azide-alkyne cycloaddition reaction (CuAAC) (Figure 5).^{109–111} The small size has the advantage to be able to modify small molecules without significant alteration of their structure and physicochemical properties. The possibility to introduce reporter tags after the binding event enabled the use of more complex reporter tags, such as rhodamine biotin-azide tri-functional linkers (TFL). With such linkers in place, a combination of workflows for visualization and subsequent pull-down analyses is possible.¹¹²

The design of the probe is critical for the outcome of the experiment. Ideally, the specificity of binding should be preserved and the activity retained. Reactive groups as well as reporter tags therefore need to be added at sites that do not interfere with the original interactions of the compound and its target. This can be a challenging task, especially for scaffolds with completely unknown binding modes. A possibility to estimate the applicability is the comparison of the bioactivity of the probe to the original molecule.

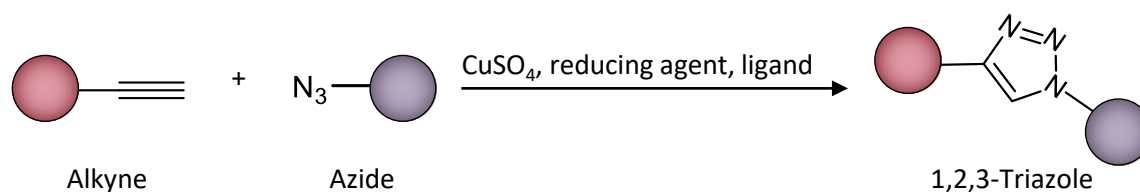


Figure 5: Schematic representation of the Copper(I)-catalyzed azide-alkyne cycloaddition reaction (CuAAC). Preferred functionalization is indicated by the red circle for probe and by the violet circle for the reporter tag.

Affinity-Based Protein Profiling Workflow

Depending on membrane permeability of the probes, ABPP- and AfBPP experiments can be performed *in situ* using whole cells or *in vitro* using lysates. Using whole cells is preferred due to the preservation of the *status quo* of the proteome *versus* unpredictable changes of the proteome upon lysis. The basic steps of a typical A(f)BPP-workflow *in situ* comprise labeling, tagging and reporting (Figure 6).

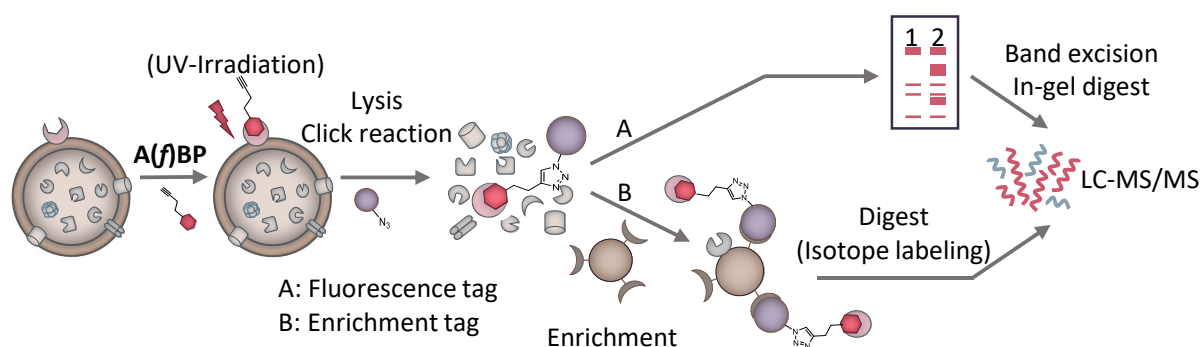


Figure 6: Schematic representation of an activity/affinity-based protein profiling with alternative reporting strategies – click chemistry-mediated attachment of (A) a fluorescent dye and subsequent analysis on an SDS-PAGE or (B) attachment of an enrichment tag, pull-down and subsequent analysis via LC-MS/MS.

Intact cells are incubated with the probe over a suitable period of time that allows the small molecule to bind to its interaction partners. In case of binding to cytosolic targets, a preceding passage through the cellular envelope is required. If the reactive group is intrinsically electrophilic, it is attacked by a nucleophilic residue, which is most often an activated cysteine or lysine in the active pocket of the protein. In case of non-covalent binders with attached photocrosslinkers, cells need to be irradiated with UV light to promote covalent linking. Afterwards, proteins are released upon mechanic disruption or enzymatic lysis of cells and clicked to a reporter tag. When using a fluorescence tag (e.g. rhodamine), the protein extracts can be separated using sodium dodecyl sulfate - polyacrylamide gel electrophoresis (SDS-PAGE) and visualized via fluorescence detection. Optionally, bands of interest can be excised, proteins digested using the in-gel digestion method,¹¹³ and identified using liquid

chromatography tandem mass spectrometry (LC-MS/MS). In case of an affinity tag, such as biotin or desthiobiotin, proteins are enriched via a pull-down using beads coated with avidin, streptavidin or neutrAvidin.¹¹⁴ Subsequently, the proteins can be eluted from the beads for their further analysis.

Target Identification via LC-MS/MS

Many approaches require the identification and a precise quantification of probe-labeled proteins beyond the mere visualization of molecular weight and abundance as seen in SDS-PAGE. Advances in high-resolution mass spectrometry and liquid chromatography, especially with respect to sensitivity, accuracy, resolution, and throughput, have made quantitative analyses of complex protein samples feasible.^{115–117} Chemical proteomics, combining the powers of A(f)BPP and mass spectrometry, enables quantitative profiling of targets and off-targets of small molecules at the level of entire proteomes.¹¹⁸

For mass spectrometry-based identification and quantification of ABPP-labeled proteins, digestion of proteins into peptides (bottom-up proteomics) is a central step for the subsequent workflow.^{117,119} The so generated peptides are then fractionated by liquid chromatography and analyzed on an on-line coupled tandem mass spectrometer.

Several possibilities exist to enable quantitative comparisons between samples treated under different conditions (such as control conditions or varying concentrations of the probe) or between samples from different strains (e.g. comparison of pathogenic vs. non-pathogenic strains). The quantification methods can be divided into two major categories – label free- and stable-isotope labeling-mediated quantification approaches.¹²⁰

Label-free quantification (LFQ) allows the comparison of an unlimited number of conditions, whereas labeling by isotopes is mostly limited by the number of available labels as well as by resolution power of the mass spectrometer. The advantage of isotopic labeling is that it provides more accurate quantification and is less prone to quantification errors by variations in sample handling. However, it requires modification of proteins or peptides prior to mass spectrometric analysis. This is achieved by the introduction of stable isotopes with different masses. After the modification, differently labeled samples are combined and analyzed together. Different isotopes are present in the same precursor scans enabling their relative quantification. Stable isotopes can be introduced at several stages of the proteomic workflow. Metabolic labeling (e.g. stable isotope labeling by amino acids in cell culture, SILAC) allows direct modification of proteins, whereas chemical labeling (e.g. dimethyl labeling, tandem mass tag, TMT) is conducted at the peptide level.^{120,121} Metabolic labeling is only possible for organisms that are auxotrophic for the isotopic amino acids (e.g. human cell cultures) and requires genetic manipulations for prototrophic organisms. Therefore, chemical labeling is preferred for bacterial analysis.

One popular stable isotope labeling approach is dimethyl labeling, in which three isobaric dimethyl tags are introduced into lysines and N-termini of peptides via reductive amination (Figure 7).¹²²

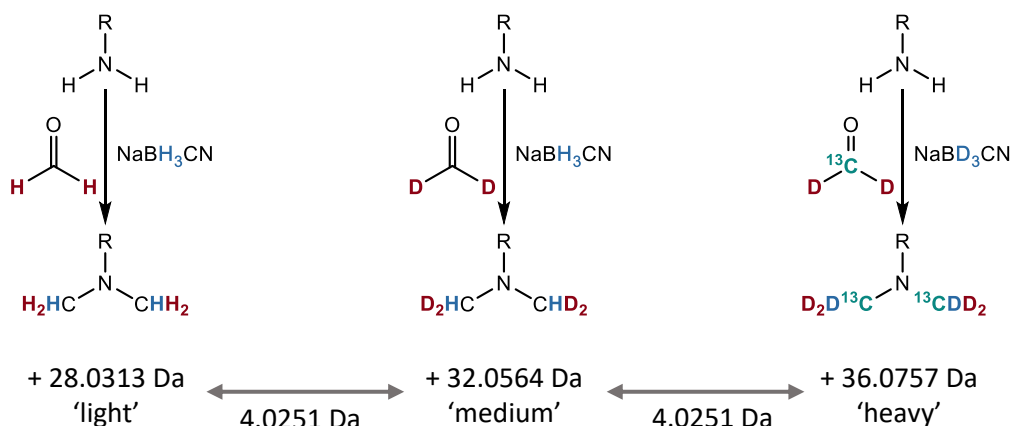


Figure 7: Dimethyl labeling reactions for comparison of three samples. Only with this combination of dimethyl labeling reagents mass shifts of 4 Da between the labeling states for triplex experiments are obtained. Modified from Boersema *et al.*¹²²

The mass spectrometric analysis is followed by database-assisted identification and quantification of peptides and proteins using analysis software (e.g. MaxQuant).^{123–125} Eventually, the obtained quantitative data are statistically analyzed in order to reveal significant changes in protein abundances.

1.5 Scope of this work

The spread of antibiotic-resistant *S. aureus* strains demands the development of drugs against unexploited targets very urgently. To identify molecules that address novel target(s) with essential functions in *S. aureus*, a phenotype-based screening of a panel of human kinase inhibitors was conducted in the present work. This class of molecules was chosen as bacterial signaling largely relies on phosphorylation pathways, similar to eukaryotic systems. For example, regulation of the expression of virulence factors by the two-component Agr regulatory system is mediated by kinases and transcriptional activators.^{126,127} While research in the field of bacterial kinases and their possible use as drug targets is comparably new,^{128–130} efforts to elaborate human kinase inhibitors date back to the 1950s.¹³¹ The created wealth of compounds represents a rich source available for repurposing to antibacterial research. This approach has previously led to the identification of antibiotic activity of a series of pyridopyrimidines, which were part of a library originally designed for the development of a human tyrosine kinase inhibitor.⁸⁴

The human kinase inhibitor screen resulted in the identification of antibiotic activity of sorafenib against *S. aureus*. This finding built the basis for further work, which comprised optimization of antibacterial activity of sorafenib on the one hand, and elucidation of target structures and the underlying antibiotic mechanism on the other.

Chapter 2.1 describes the identification of the antibiotic potency of sorafenib, the discovery of the sorafenib-derived compound PK150 and work performed for the assessment of its potential as a drug candidate. The identification of PK150 with a ten-fold higher antibiotic potency than sorafenib was the result of structure-activity-relationship studies based on a library of 72 derivatives of the parent compound. Furthermore, the scope of the antibacterial activity was determined in terms of susceptible pathogens, including clinically challenging variants of *S. aureus* – drug-resistant strains, persistent phenotypes as well as biofilms. The prevalence of the occurrence of spontaneous *in vitro* resistances against sorafenib and PK150 was assessed. For further development, drug-like parameters, such as cellular toxicity as well as *in vitro* pharmacokinetic parameters were determined. Finally, pharmacokinetic and -dynamic properties of PK150 were studied in *in vivo*-mouse infection models.

Chapter 2.2 covers the studies performed in order to elucidate the underlying mechanism that leads to antibacterial activity of sorafenib and PK150. For the identification of the target proteins, an AfBPP approach was used. Subsequent target validation comprised recombinant overexpression of the most promising target candidate, a signal peptidase, *in vitro* labeling experiments, biochemical activity assays as well as docking- and molecular dynamics-studies. Based on the gained insights, follow-up experiments were conducted utilizing proteomics to assess SpsB-dependent changes in the abundances of secreted as well as cell surface-attached proteins upon treatment with the respective compounds. Furthermore, microbiological assays and electron microscopic studies were performed to elucidate the antibiotic mode of action. Obtained results were eventually used to develop a hypothesis how the antibiotic activity of sorafenib and PK150 can be related to the observed changes at the molecular level.

2 Results and Discussion

2.1 Discovery of a Novel Sorafenib-derived and Highly Potent Antibiotic

2.1.1 Antibacterial Screen of Kinase Inhibitors

To find novel essential targets in *Staphylococcus aureus*, a phenotypic screen was conducted using a panel of 233 commercially available kinase inhibitors. Compounds were selected to cover a broad variety of scaffolds. The selection comprised compounds already approved in cancer treatment such as imatinib (approved in 2001)¹³² and lenvatinib (approved in 2015)¹³³, development candidates from all three clinical phases (e.g. danusertib (phase II)¹³⁴, tofacitinib (phase III)¹³⁵ as well as compounds in early discovery or preclinical development phases (Table S1). In order to assess the antibiotic activity of the compounds, the methicillin-sensitive strain NCTC 8325 was used. An initial cut-off concentration of 30 μM was chosen to identify all potentially interesting molecules for further examination. Nine kinase inhibitors displayed a growth inhibiting effect at this concentration (Table 3).

Table 3: MIC values of the nine most potent compounds from the screen in *S. aureus* NCTC 8325.

Kinase Inhibitor	MIC (μM)
Sorafenib Tosylate (Bay 43-9006)	3
Regorafenib (Bay 73-4506)	3
Degrasyn (WP1130)	10
TAK-285	30
RAF265 (CHIR-265)	30
MK-2461	30
Gandotinib (LY2784544)	30
Brivanib alaninate (BMS-582664)	30
AZ 960	30

For the each of the respective hits the minimum inhibitory concentration (MICs) was determined. MIC is the lowest concentration, at which the visible growth of bacteria is inhibited. Sorafenib (**SFN**) and regorafenib (Figure 8), two structurally related compounds, exhibited the lowest MIC values of 3 μM (1.4 $\mu\text{g}/\text{mL}$) among the nine hits. Both drugs, developed and marketed by Bayer AG as Nexavar[®] and Stivarga[®] have been first approved in 2005¹³⁶ and 2012¹³⁷ by the U.S Food and Drug Administration (FDA) for cancer treatment. Sorafenib and regorafenib are promiscuous multi-target kinase inhibitors, addressing both tyrosine as well as serine/threonine kinases.^{138,139} Both are classified as type II kinase

inhibitors occupying a part of the ATP binding pocket and an adjacent allosteric pocket, which is only available when the kinase is in a catalytically inactive conformation.¹⁴⁰

Determination of MIC values in further pathogens revealed that **SFN** inhibits growth of different MRSA strains (Table 5 and Table S3), *Mycobacterium tuberculosis* and *Listeria monocytogenes*, rendering the compound an interesting candidate to be tested in further studies.

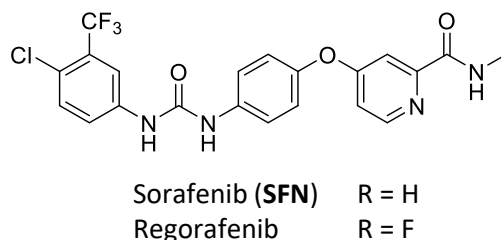


Figure 8: Structures of the approved kinase inhibitors **SFN** and regorafenib, which showed the lowest MICs in the screen.

2.1.2 Screening of Sorafenib Derivatives and SAR studies

For the further investigation of **SFN**'s antibacterial activity and assessment of its potential to be optimized as a drug, a library of 72 **SFN** analogs (Table S4) was synthesized (Chapter 5: Contributions). The library was designed to cover a range of group variations that is as broad as possible to assess which parts of the molecule are indispensable for activity and which modifications are tolerable. Initially, 40 compounds were synthesized with systematic modifications of the three moieties of the **SFN** scaffold – the 4-chloro-3-(trifluoromethyl) phenyl, the urea and the heteroaryl ether. Variations in these groups resulted in changes of MIC values in *S. aureus* NCTC 8325 allowing for conclusions to be made regarding the connection between scaffold features and antibiotic activity (Figure 9 and Table S4). Interestingly, modifications of the left phenyl moiety, regardless of whether the phenyl residue was replaced by other aromatic (e.g. compounds **1-105**, **1-109**, Table S4) or aliphatic groups (e.g. compounds **1-108**, **1-110**), were totally intolerable and led to the complete loss of antibiotic activity. Surprisingly, even minor modifications of the aromatic ring substituents such as the replacement of the trifluoromethyl-group by a methyl group (**1-134**, Figure 9) or the removal of the 4-chloro substituent (**1-163**) fully abolished antibiotic activity. During the course of this work, Chang et al.¹⁴¹ independently developed active derivatives based on the **SFN** structure, as well. Although derivatives within that study were different to the ones presented here, the most potent molecules contained 4-chloro-3-(trifluoromethyl) phenyl groups. This is in line with results obtained in the present work emphasizing the importance of this motif for the antibiotic potency.

Removal or replacement of hydrogens at the central urea motif were not tolerated (e.g. compounds **1-182**, Figure 9 and **5-009**, Table S4). Substitution of the urea by a thiourea (**3-001**, Figure 9), led to a substantially decreased MIC value of 10 μM .

In contrast to this, variations of the heteroaryl ether moiety were mostly tolerable (e.g. **2-013**) or even resulted in an increase of the antibiotic activity (e.g. **3-006**).

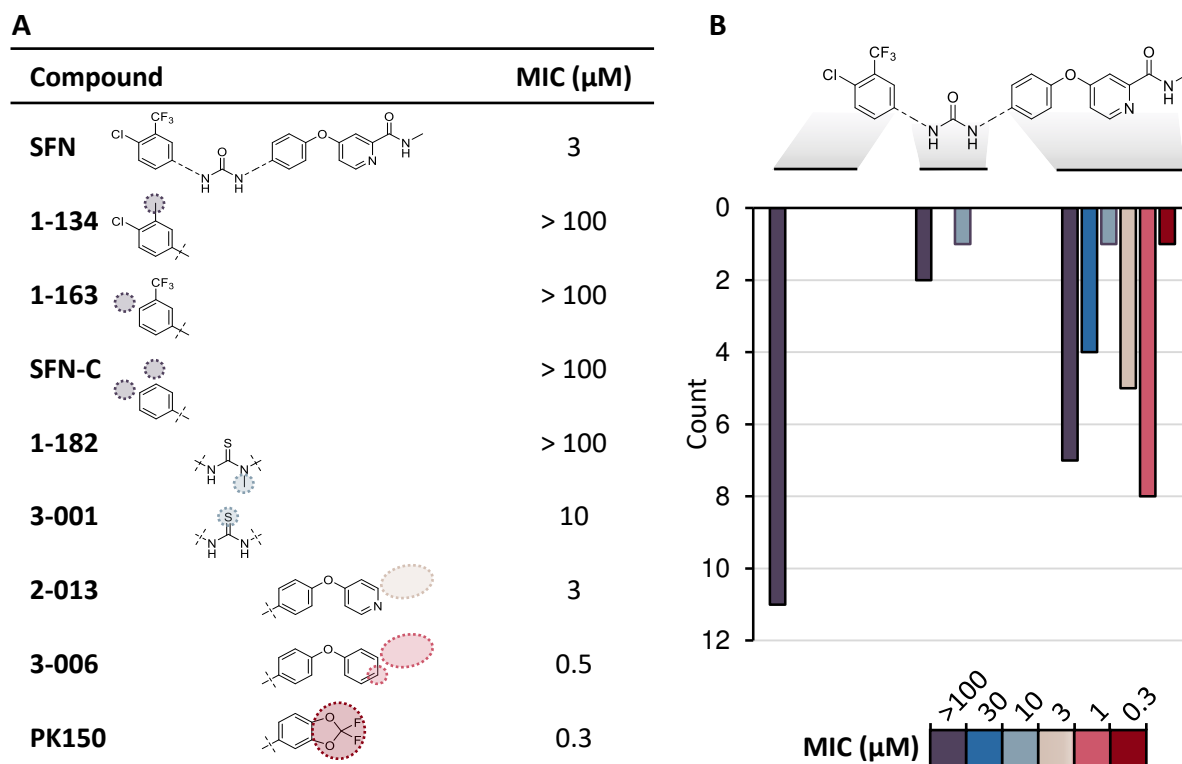


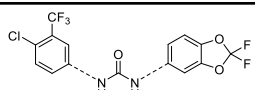
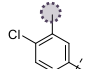
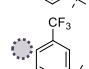
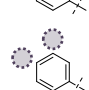
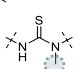
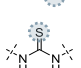
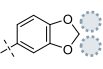
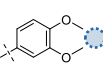
Figure 9: Structure-activity relationship study with analogs of **SFN**. (A) Examples of variations of **SFN**'s moieties are shown with respective MIC values in *S. aureus* NCTC 8325. (B) Correlation between modifications of the **SFN** scaffold and MIC values in *S. aureus* NCTC 8325 (color code). Bars represent counts of the analogs, classified by their MIC values. In total, the diagram comprises 40 close analogs of **SFN**. See Table S4 for the full overview of analogs.

The most intriguing part of the scaffold dissection studies was the replacement of the heteroaryl ether by a 2,2-difluoro-1,3-benzodioxole moiety, resulting in compound **PK150** with an even 10 times lower MIC of 0.3 μM (118 ng/mL) compared to the original compound **SFN**. Further alterations in this structural motif, such as the removal of the fluorine substituents (**1-159**, Table 4) or opening of the acetal (**1-160**) resulted in a significant decrease of the MIC values rendering it crucial for the antibiotic potency. In contrast to **SFN**, minor changes of substituents of the 4-chloro-3-(trifluoromethyl) phenyl moiety were tolerable (e.g. **4-017**, **4-018**). However, removal of both substituents (**PK150-C**) was again associated with a complete loss of activity emphasizing its important role for activity. While the

substitution of urea by thiourea only slightly changed activity (**1-166**), further modifications of this moiety resulted in substantially decreased or fully abolished activities (e.g. **5-016**).

A valuable byproduct of the SAR studies was the identification of **PK150-C** and **SFN-C**, compounds that are structurally very similar to their counterparts **PK150** and **SFN**, but inactive in MIC assay. These derivatives lacking the chlorine and trifluoromethyl groups on the phenyl ring represent appropriate controls in further experiments, especially for target validation (Chapter 2.2.2).

Table 4: Structure-activity relationship study with analogs of **PK150**. Examples of modified structures are shown with respective MIC values in *S. aureus* NCTC 8325. See Table S4 for the full overview of analogs.

Compound	MIC (μM)
PK150 	0.3
4-017 	0.5
4-018 	0.7
PK150-C 	> 100
5-016 	> 100
1-166 	0.5
1-159 	10
1-160 	30

2.1.3 Antibacterial Spectrum of Sorafenib and PK150

The antibacterial spectra of **SFN** and **PK150** were further determined against a panel of gram-positive and gram-negative bacteria (Table 5).

Whereas both compounds showed good activities in gram-positive bacteria, no growth inhibition could be observed in gram-negative bacteria. The missing activity in gram-negatives is a common phenomenon for small molecules. This is often caused by a lower permeability of their cell envelopes, comprising an additional protective barrier, the outer membrane. Furthermore, gram-negative bacteria possess an efficient system of efflux pumps which are constantly removing toxic agents from the cells.^{142,143}

Table 5: Antibiotic activities of **SFN** and **PK150** in non-pathogenic and pathogenic bacteria, determined as MIC values; 100 μM was the highest concentration tested. See Table S2 for the full list of tested strains and Table S3 for the resistance spectrum of the clinical MRSA isolates.

Organism		MIC (μM)	
		SFN	PK150
Gram-positive			
<i>Staphylococcus aureus</i>	MSSA	3	0.3
	MRSA	3-10	0.3 – 1
	MRSA, clinical isolates	3-10	0.3
	VISA	3	0.3
<i>Mycobacterium tuberculosis</i>	H37Rv	25	2
<i>Listeria monocytogenes</i>		3	0.3
<i>Bacillus subtilis</i>		5	1
<i>Enterococcus faecalis</i>	VRE	> 100	3
<i>Enterococcus faecium</i>	VRE	> 100	1
Gram-negative*		> 100	> 100

MSSA, methicillin-sensitive *S. aureus*; MRSA, methicillin-resistant *S. aureus*, VISA, vancomycin-intermediate *S. aureus*; VRE, vancomycin-resistant enterococci;
 **A. baumannii*, *E. aerogenes*, *E. cloacae*, *E. coli*, *K. pneumoniae*, *P. aeruginosa*, *S. typhimurium*, *S. enteritides*.

With MIC values of 3 – 10 μM **SFN** exhibited good antibiotic activity in different established MRSA strains as well as several clinical MRSA isolates. As these MRSA strains bore resistances to several established antibiotics^{144,145} (see Table S3 for resistance spectra), but were similarly sensitive to **SFN**, an involvement of a novel antibacterial target in the mechanism of action is reasonable.

PK150 had a ten-fold higher activity (0.3 – 1 μM) against MSSA and MRSA strains than **SFN** and was more potent than several approved antibiotics, including vancomycin (MIC: 1.4 $\mu\text{g}/\text{mL}$; 1 μM) and the reserve antibiotic linezolid (MIC: 1 $\mu\text{g}/\text{mL}$; 3 μM) (Table 6). Solely rifampicin and penicillin exhibited lower MIC values among the tested antibiotics. The high prevalence of resistance development to these drugs, however, limits their clinical application.^{31,60,146–148}

Moreover, with an MIC of 2 μM , **PK150** exhibited a 10-fold higher activity against *Mycobacterium tuberculosis*, as well. This is another, clinically highly relevant feature of this compound as there is a high demand for research and development of new antibiotics against the causative agent of tuberculosis.^{4,149}

Strikingly and, in contrast to **SFN**, **PK150** exhibited antimicrobial activity against enterococci, including vancomycin-resistant strains (VRE). The respective MICs were 1 μM in *Enterococcus faecium* and 3 μM in *Enterococcus faecalis*. Differences in antibiotic susceptibilities of staphylococci and enterococci have been observed before and were mostly associated with differences regarding intrinsic and acquired resistance mechanisms between the species.^{150,151} It might therefore be possible that a resistance

mechanism contributes to tolerance against **SFN**, but not **PK150** due to differences in structure and chemical properties. Regardless of resistance mechanisms, differences in the spectrum of or in affinities to target(s) in general might explain different responsiveness to **SFN** and **PK150**.

Table 6: MIC values of established antibiotics compared to **SFN** and **PK150** in *S. aureus* NCTC 8325.

Compound	MIC	
	(μ M)	(μ g/mL)
Rifampicin	0.009	0.01
Penicillin G	0.05	0.02
Tetracycline	0.5	0.2
Ofloxacin	0.5 - 2	0.2 - 0.7
Ciprofloxacin	0.754	0.25
Gentamicin	-	0.5
Vancomycin	1	1.4
Linezolid	3	1.0
Oxacillin	2.5	1.0
PK150	0.3	0.1
SFN	3	1.4

2.1.4 Resistance Development

Emerging resistances are the major clinical challenge in modern anti-infective medicine. Whereas acquisition of resistance determining factors via gene transfer is dependent on the presence of resistant organisms in the environment,¹⁸ and is therefore difficult to imitate in a laboratory experiment, the prevalence of evolving resistance due to mutations is measurable. The probability of obtaining resistant mutants increases with the number of bacterial cell divisions. Thus, sequential culturing of bacteria at sub-MIC levels allows to reliably test a large number of generations for the occurrence of spontaneous resistance-conferring *de novo* mutations upon antibiotic treatment.¹⁵² Hence, for the assessment of resistance development, sequential passaging in the presence of sub-inhibitory concentrations of **PK150**, **SFN** and the control antibiotic ofloxacin (OFLOX) was performed.⁷⁹ Bacterial cells were treated with 0.25 \times , 0.5 \times , 1 \times , 2 \times and 4 \times MIC concentrations of the respective compounds. Passaging intervals were 24 h. If a shift in MIC occurred, concentrations were adjusted accordingly. Cultures containing the second highest concentration that allowed growth (optical density at 600 nm (OD_{600}) ≥ 2) were used for passaging as they contained more cells, thus increasing the number of spontaneous mutations and with that the probability to obtain a resistant clone. The passaging was repeated daily for the period of 27 days.

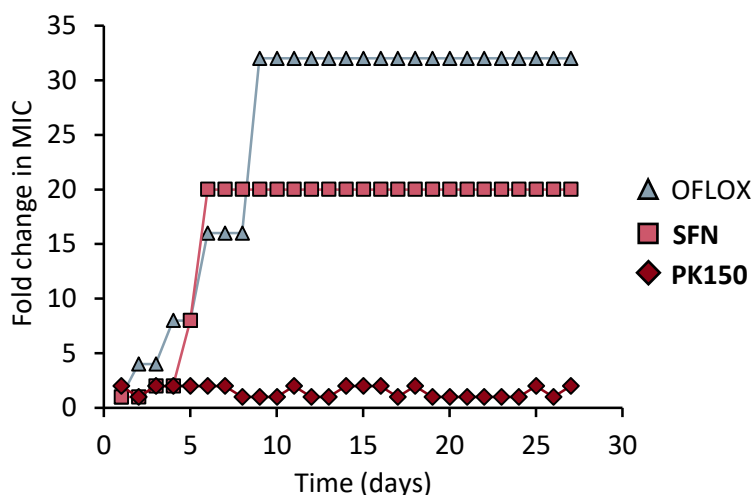


Figure 10: Resistance development during serial passaging in presence of sub-MIC concentrations of antimicrobials. For **SFN**, 20-fold MIC was the highest concentration tested (solubility limit). The figure is representative of 3 independent experiments.

Interestingly, no resistances were observed for **PK150**, whereas cells rapidly became unsusceptible to **SFN** and ofloxacin. The lack of mutation-based resistances might hint to either a non-specific mode of action⁷⁹ such as membrane disintegration, or targeting multiple proteins and by that rendering evolution of several resistance mechanisms at once unlikely.^{153,154} Sorafenib-resistant strains were still sensitive to **PK150**, additionally indicating a change in the spectrum of targets addressed by **PK150**.

The ultimate prevalence of resistance development can be only assessed after an introduction of a drug into clinical practice. However, an absence of spontaneous resistance development as well as an absence of cross-resistance to **PK150**, as several clinical MRSA were susceptible to the compound, are promising results.

2.1.5 Killing of Persisters

As introduced before, persisters and their presence in biofilms represent a major clinical challenge. Persister research in gram-positive bacteria is a young discipline and there are many inconsistencies between results from different groups.⁶³ They are most often caused by differences in protocols of persister isolation, treatment and accompanying methodical details,^{67,155–157} which can significantly influence the outcome. Major differences are the conditions used for persister isolation, such as the growth phase, the class and concentration of the antibiotic used for persister selection, as well as the duration of the selection step. Simultaneous vs. subsequent treatment with the isolating antibiotic and the tested compound as well as the cultivation conditions during treatment with the compounds (e.g. medium or buffer) also play an important role.^{158,159} Regarding these differences, the activity of **PK150** was evaluated in two independent persister cell assays.

In the first experiment, based on the protocols from Conlon *et al.*¹⁶⁰ and Kim *et al.*,¹⁵⁶ persister cells were isolated from stationary phase with gentamicin, washed to get rid of the antibiotic, diluted to an $OD_{600} = 0.4$, and subsequently treated with the compounds in phosphate-buffered saline (PBS). For the determination of the numbers of viable cells, i.e. surviving persisters, cells were plated and incubated on agar, followed by the counting of individual colonies (Figure 11).

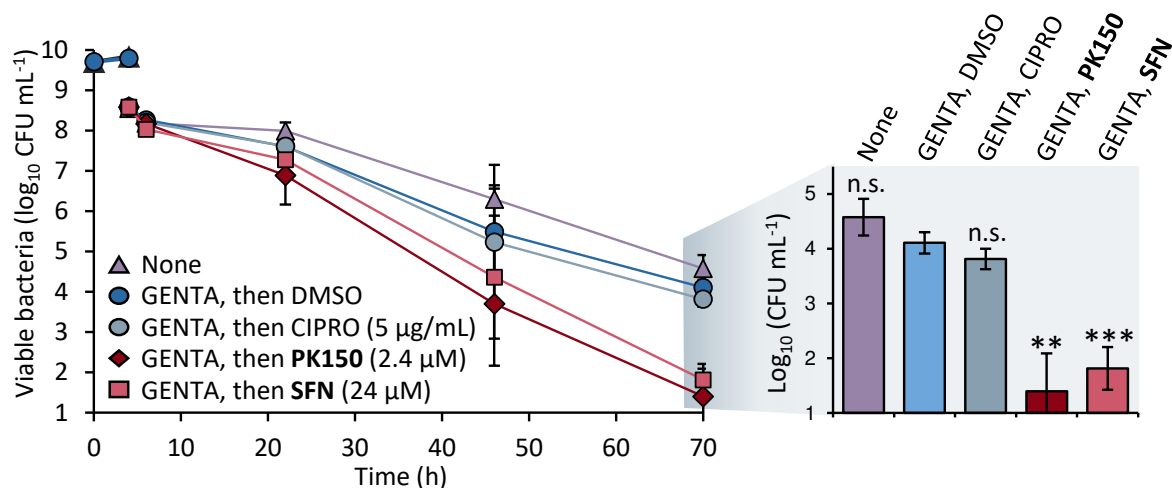


Figure 11: Persister cell assay No.1. *S. aureus* NCTC 8325 cells were incubated either with gentamicin (20 µg/mL, blue circles) or without antibiotic (violet triangles) or for 4 h to isolate persister cells. Persisters were then washed, diluted to $OD_{600}=4$ (approximately 3.8×10^8 CFU/mL) and either left untreated or treated with ciprofloxacin (CIPRO, 5 µg/mL, 20 × MIC), **PK150** (2.4 µM, 8 × MIC), **SFN** (24 µM, 8 × MIC) or DMSO for 66 h. Bars represent surviving persisters (Log_{10} CFU/mL) after 66 h of compound treatment. Data represent mean values \pm SD ($n = 3$ per group); n.s., not significant, ** $p < 0.01$, *** $p < 0.001$ (Student's *t*-test) for compound- vs. DMSO-treated groups.

No cells were killed by gentamicin during the initial selection period of 4 h indicating that the cells in the initial stationary culture were in persister state. This was furthermore confirmed by the observation that cells showed similar time-dependent responses, regardless if they were subsequently treated with ciprofloxacin, with dimethyl sulfoxide (DMSO) or left untreated. These observations are in accordance with previous studies stating that all stationary culture *S. aureus* cells are persisters.^{156,160–162}

The number of persister cells was significantly reduced after 70 h of treatment with 8 × MIC concentrations of **PK150** (2.4 µM) as well as with **SFN** (24 µM) compared to DMSO-treatment.

The ability of both related compounds to kill persisters indicates a similar mode of action. It is worth to highlight that the absolute concentration of **PK150** was based on its MIC and thus ten times lower than the concentration of **SFN**.

In the second persister cell assay (modified from Springer *et al.*),¹⁵⁵ cells were grown either to an OD₆₀₀ of 4 (starting condition A) or of 11 (starting condition B), representing cell cultures that were either growing or in stationary phase, respectively. Treatment of both cultures for 20 h with oxacillin alone (Figure 12) did not lead to a reduction in viable cell numbers compared to the starting culture (indicated as “inoculum”), suggesting that the majority of the present cells were persisters. After 70 h, cells from starting condition A showed a slightly decreased cell number compared to the inoculum indicating that these cells were not completely tolerant to oxacillin. In contrast to this, culture B seemed to contain exclusively persisters, as no killing could be observed with oxacillin alone even after 70 h. This observation is consistent with the fact that the percentage of persister cells increases with the density of cells and limitation of both nutrients as well as oxygen.

To assess the effects of **SFN** and **PK150**, cells were simultaneously incubated with the compounds and persister selecting antibiotic oxacillin (OXA) in rich medium (Figure 12). Significant reductions of persisters from both growth phases (OD₆₀₀ = 4 or 11) were achieved after 20 h of treatment. After 70 h, the effects were even more pronounced. At this time point the absolute reduction of persister cells was about 6 – 7 logs of CFU/mL for the combinations of oxacillin with **PK150** or **SFN** compared to DMSO. In contrast to that, oxacillin as well as the control compounds **PK150-C** and **SFN-C** did not show any or only slight reductions in viable cell numbers. As described above, cells in the used starting cultures were predominantly (starting OD₆₀₀ of 4) or completely (starting OD₆₀₀ of 11) in persister state. Therefore, the same starting cultures were treated with compounds alone (*i. e.* without addition of oxacillin). By doing so, possible influences of mutual synergistic or antagonistic effects of the agents were eliminated. The killing activities were still significant for both **SFN** and **PK150** compared to the inoculum. As the absolute reductions, however, were less prominent than for the combination with oxacillin, synergistic effects between the action of oxacillin and **PK150** or **SFN** are likely. Control compounds (**SFN-C** and **PK150**) again did not show reduction in viable cell numbers.

In summary, it can be concluded that **SFN** and **PK150** both lead to significant reductions of persister cell numbers independent of the assay method. The ability to kill persisters is a highly valuable feature of the compounds regarding the lack of clinical treatment options for this phenotype.

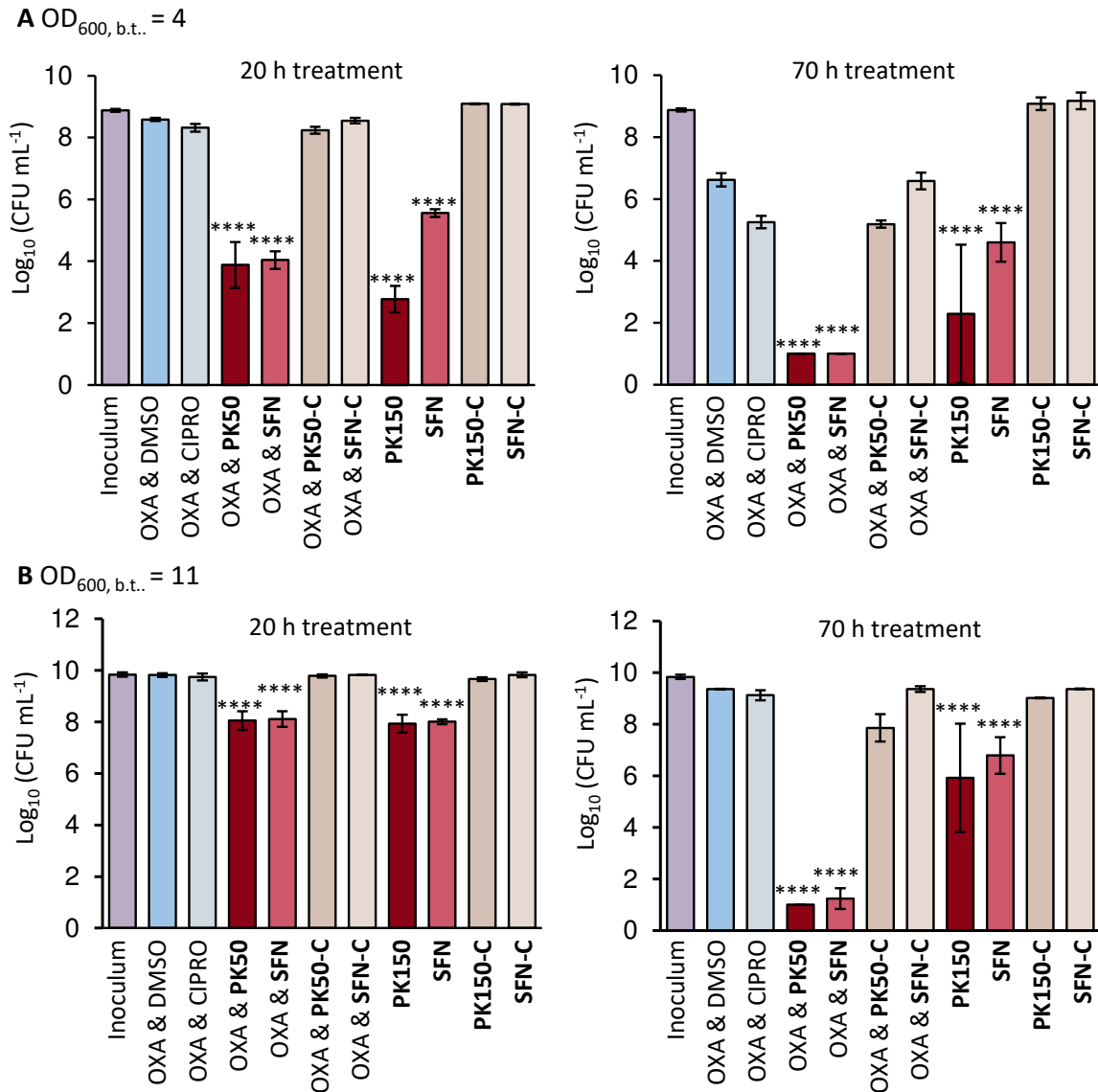


Figure 12: Persister cell assay № 2. *S. aureus* NCTC 8325 bacteria were grown to either (A) $OD_{600} = 4$ (early stationary phase) or (B) $OD_{600} = 11$ (stationary phase) and treated with either combinations of the persister-selecting antibiotic oxacillin (OXA, 30 $\mu\text{g}/\text{mL}$, 30 \times MIC) and tested compounds ciprofloxacin (CIPRO, 5 $\mu\text{g}/\text{mL}$, 20 \times MIC), **PK150** or **PK150-C** (2.4 μM , 8 \times MIC) and **SFN** or **SFN-C** (24 μM , 8 \times MIC) or the tested compounds alone for 20 h or 70 h. Data represent mean values \pm SD ($n = 3$ per group); n.s., not significant; ** $p < 0.01$, *** $p < 0.001$, **** $p < 0.0001$ (Student's *t*-test) for compound- vs. DMSO/OXA-treated groups. $OD_{600, b.t.}$, OD_{600} before treatment.

2.1.6 Eradication of Biofilms

As established biofilms are largely composed of persister cells and represent a major challenge in antibiotic therapies, the assessment of activity of compounds against these multicellular surface-bound bacterial communities is highly interesting.

Biofilm formation undergoes different stages of development. First, planktonic cells change their phenotype and adhere to a surface. These cells produce extracellular polymeric substance (EPS) and mature. In the late stage, some cells revert to a planktonic phenotype, detach from the biofilm, disseminate, and can again establish a biofilm at a new site.¹⁶³ Current efforts in the control of biofilms comprise two major strategies: 1) compounds that interfere with biofilm formation and 2) substances that eradicate pre-established biofilms.¹⁶⁴ Whereas there are several biofilm formation inhibitors known, often derived from quorum-sensing molecules,¹⁶⁵ biofilm-destructing molecules have been sparsely reported.^{164,166}

To assess the potential of **PK150** as a biofilm eradicator, a regrowth assay for the determination of minimum biofilm eradication concentration (MBEC) was performed. MBEC is the lowest concentration of a compound that results in an optical density of less than 0.1 (i.e. clear well) after the pre-treated biofilm has been incubated in fresh medium. The absence of bacterial regrowth represents a > 95% clearance of biofilm bacteria.^{164,167}

Biofilms could be successfully eradicated by **PK150** in a concentration dependent manner for both MSSA (NCTC 8325) and MRSA (USA300-0114) strains (Figure 13). Strikingly, the MBEC values were as low as 25 μ M for 20 h of treatment with the compound (Table 7). The values are in the same range as for quaternary ammonium cations (QACs), which are the strongest biofilm eradicators reported to date.¹⁶⁴

Table 7: Minimum biofilm eradication concentration (MBEC) values for treatment of MSSA and MRSA-strains for 20 and 70 hours. MBEC values were defined by regrowth assays that result in OD₅₉₅ values below 0.1.¹⁶⁴

		NCTC 8325* (MSSA)		USA300-0114 (MRSA)	
MIC (μ M)	PK150	0.78		1.56	
	OXA	25		> 25	
MBEC (μ M)	Treatment duration	20 h	70 h	20 h	70 h
	PK150	25	12.5	25	50
	PK150 & OXA	25	12.5	25	25

*Strain (DSM-4910) was obtained from Deutsche Sammlung von Mikroorganismen und Zellkulturen (DSMZ).

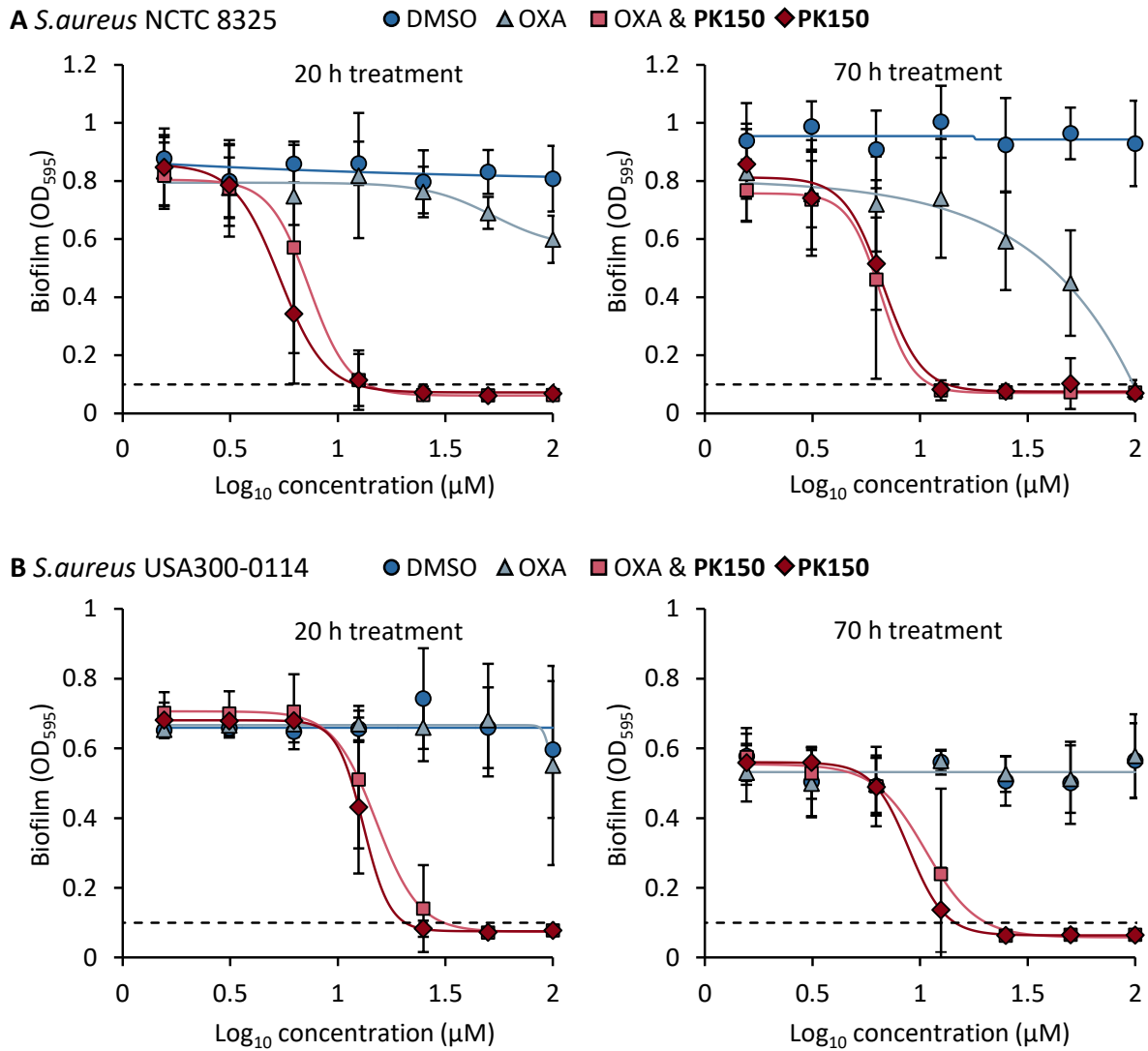


Figure 13: Residual biofilms of *S. aureus* NCTC 8325 (A) and USA300-0114 (B) after 20 h of treatment with DMSO, various concentrations of **PK150** and a combination of equal concentrations of oxacillin (OXA) and **PK150**. The dashed line represents the minimum biofilm eradication concentration (MBEC) value (OD₅₉₅ = 0.1). Data represent mean values \pm SD ($n = 9$ per group).

The MBEC values (25 μ M) were significantly higher than the MIC values (0.3 μ M), allowing two hypotheses about the mechanism of action. It is possible that the EPS matrix effectively protects the bacteria from the compound lowering the effective concentration. Once the compounds are within the matrix, cells are killed and biofilms degrade. A further possibility is that the compounds directly interact with matrix molecules leading to a dispersion of the biofilm, so that the planktonic cells are washed away before the regrowth step. To test the hypotheses, minimum biofilm inhibitory concentration (MBIC) were determined with sub-MIC concentrations of **PK150** to examine the ability to prevent biofilm establishment. **PK150** did not show any inhibition of biofilm development at sub-MIC concentrations suggesting direct killing of cells as the mechanism of biofilm eradication.

2.1.7 Cytotoxicity, Hemolysis and Plasma Stability

Given the excellent antibiotic potency, **PK150** is a highly interesting therapeutic candidate for further pre-clinical development. However, before testing a compound's toxicity and efficacy *in vivo*, a demonstration of favorable drug properties in *in vitro* human-based experimental systems is required.¹⁶⁸ Several drug-like properties can be examined assisting the selection process towards the most promising candidates for animal studies. The major aim here is to estimate the expected toxicity and risk of adverse side effects.

In vitro toxicity was assessed with an MTT assay in four different cell lines (three human cell lines A549, HeLa and HepG2 and one murine cell line NIH/3T3) (Table 8). IC₅₀ values for **PK150** were between 7 and 16 μM and in the same range as for the approved parent molecule **SFN** (1.7 to 20 μM) indicating tolerable cytotoxicity for further animal studies. However, the accepted toxicity for oncologic indications is often higher than for infectious diseases. Nevertheless, the selectivity ratios, i.e. the ratios of IC₅₀ to MIC values, were much higher in case of **PK150** (23 – 52) compared to **SFN** (1 – 7) providing a broader therapeutic window for **PK150** for treatment of bacterial infections.

Table 8: Cytotoxicity of **SFN** and **PK150** against a panel of human and murine cell lines. The selectivity ratio represents the ratio of IC₅₀ (cytotoxicity) to MIC values (antibacterial activity against *S. aureus* NCTC 8325); *n* = min. 3 independent experiments in triplicates.

		A549	HeLa	HepG2	NIH/3T3
SFN	IC ₅₀ (μM)	19.93	9.52	1.69	7.56
	95% CI	17.13 - 23.19	8.20 - 11.05	1.07 - 2.67	6.45 - 8.86
	Selectivity ratio	6.64	3.17	0.56	2.52
PK150	IC ₅₀ (μM)	15.50	7.04	10.45	7.93
	95% CI	12.74 - 18.86	5.68 - 8.73	6.77 - 16.13	6.80 - 9.24
	Selectivity ratio	51.67	23.46	34.83	26.42

CI, confidence interval; selectivity ratio = IC₅₀ / MIC (*S. aureus* NCTC 8325)

In vitro hemolysis assays evaluate hemoglobin release in the plasma indicating lysis of red blood cells. They serve as further toxicity measure as drug-induced hemolysis is a serious safety issue when an intravenous administration route is intended.^{169,170} Similarly to **SFN**, **PK150** did not cause hemolysis of erythrocytes at concentrations around the MIC values. (Figure 14 A). A slight increase of up to 15% compared to full lysis by Triton X-100 was observed at 50 μM, a concentration that is almost 170-fold higher than the MIC.

Furthermore, *in vitro* stability of the compound in plasma is an important pharmacokinetic parameter for the assessment of potential early metabolic and degradation processes after administration. Only drugs that show a stable profile in plasma over a reasonable period of time are able to achieve concentrations high enough for desirable pharmacological effects.¹⁷¹ Both compounds, **PK150** and **SFN** showed stable concentration levels in mouse plasma over the course of 6 h as determined by mass spectrometry (Figure 14 B). In contrast, the positive control U1, a β -lactone,¹⁷² was rapidly hydrolyzed with a half-life of few minutes.

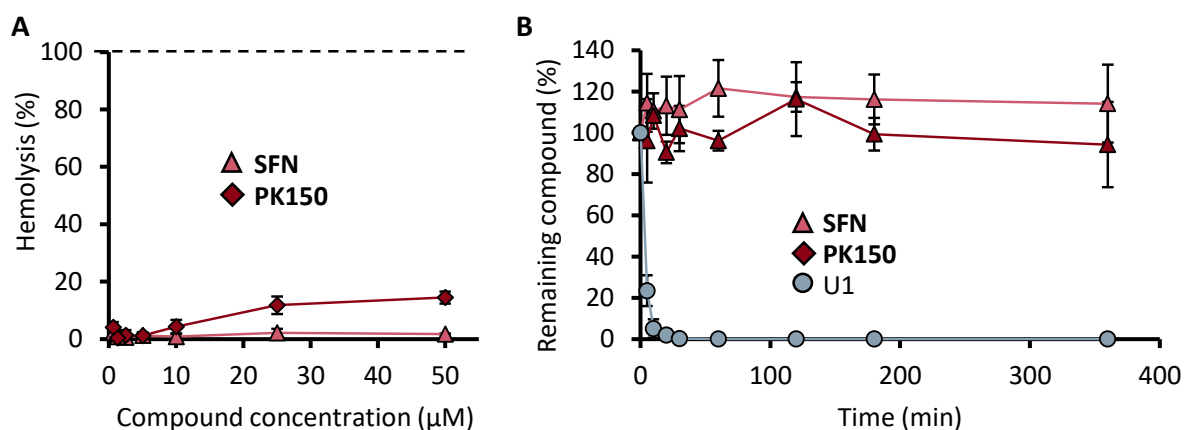


Figure 14: Hemolysis and plasma stability assays. (A) Hemolysis of sheep erythrocytes at increasing concentrations of **SFN** and **PK150** as a measure of the effect on red blood cell integrity. Hemolysis, determined by the absorbance of free hemoglobin at 414 nm, was normalized to a negative control (DMSO; hemolysis 0%) and Triton X-100 (0.2% v/v) as a positive control (hemolysis 100%, dashed line). Data represent mean values \pm SD; $n = 4$ independent experiments in triplicates. (B) Plasma stability of **SFN** and **PK150** in murine blood plasma (10 μ M compound concentration). U1 (50 μ M compound concentration), a β -lactone with known low plasma stability, was used as control.¹⁷² Compound levels were determined using a LC-MS based method. The time-dependent peak decline was expressed relative to 100% at $t = 0$ min. Data represent mean values \pm SD; $n = \text{min. } 3$ independent experiments in triplicates.

2.1.8 Kinobead Pull-Downs with Human Cells

Similar levels of toxicity of **PK150** and **SFN** indicate that **PK150** likely addresses targets in human cells. As **PK150** is a derivative of a multikinase inhibitor, a kinobead pull-down experiment was performed¹⁷³ to elucidate whether and to which extent it is still targeting human kinases. Kinobeads, comprising a panel of irreversibly attached kinase inhibitors, capture a vast variety of more than 250 human kinases. By performing competition experiments with varying concentrations of a compound, the residual binding of kinases can be estimated and IC_{50} values determined. Lysates of four human cancer cell lines (K562, Colo205, SKNBE2 and MV4 11) were incubated with kinobeads in presence of varying

concentrations of **SFN** and **PK150**. Mass spectrometry-assisted quantification of these competitive affinity pull-downs revealed targeting of eight human kinases by **SFN**, namely RET ($K_d^{app} = 32$ nM), DDR1 ($K_d^{app} = 86$ nM), ZAK ($K_d^{app} = 221$ nM), FLT3 ($K_d^{app} = 453$ nM), DDR2 ($K_d^{app} = 610$ nM), MAPK11 ($K_d^{app} = 1.2$ μ M), MAPK14 ($K_d^{app} = 8.8$ μ M) and MAP3K1 ($K_d^{app} = 14.3$ μ M) (Figure 15 and Table S5). In contrast to this, **PK150** exhibited no affinity to any kinase. Although further kinase targets not captured by kinobead technology might exist, the original targets of **SFN** were not targeted by its derivative. The removal of the crucial ATP-mimicking pyridine moiety most likely had a major impact on the decrease of affinity to kinases.^{174,175} Thus, the toxicity of **PK150** likely stems from other off-targets. Further experiments, for example target deconvolution using the AfBPP technology, are required to elucidate their identity.

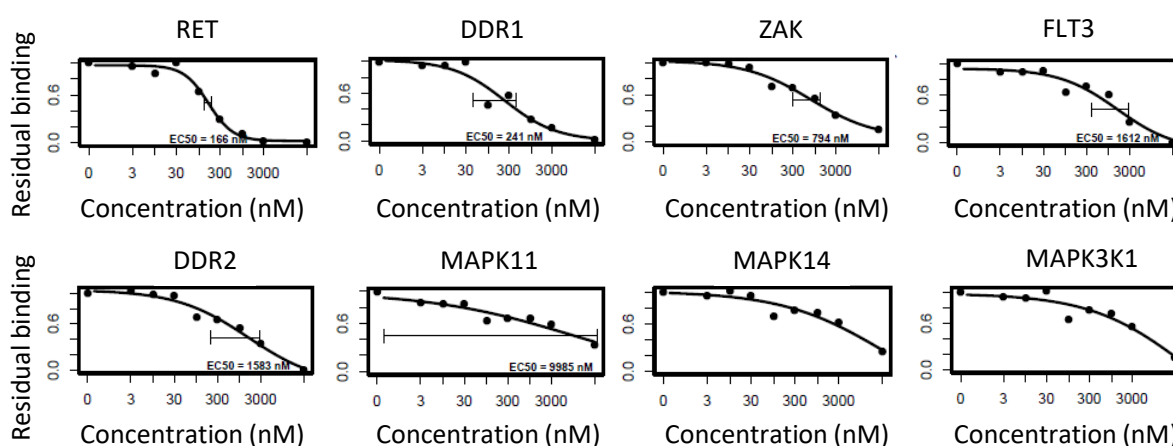


Figure 15: Competition binding curves derived from kinobead pull-downs with **SFN** in a human cell lysate mixture.

2.1.9 *In vivo* Activity

With the promising results of **PK150** regarding antibiotic activity and *in vitro* pre-evaluation indicating both low toxicity effects and favorable stability, further pharmacokinetic and -dynamic parameters were evaluated *in vivo*.

For the assessment of pharmacokinetic parameters, **PK150** was administered to outbred CD-1 mice with concentrations of 10 and 20 mg/kg of compound orally (p.o.) and 10 mg/kg of compound intravenously (i.v.) (Figure 16 and Table 9). The maximum plasma concentration (C_{max}) reached values of approximately 6 μ g/mL for the 10 mg/kg i.v. dosing and 1 – 1.6 μ g/mL for 10 and 20 mg/kg p.o. dosing, respectively. It took 5 – 6 h until the highest plasma concentration for oral administration was reached. Although there were no obvious signs of toxicity neither for oral administration nor for 10 mg/kg of intravenous injection, 20 mg/kg i.v. dosing showed severe side effects. The intravenous route of administration was therefore omitted in subsequent experiments.

Apart from the toxic effect at higher i.v. dosing the pharmacokinetic parameters were favorable. The compound was orally bioavailable (63%) as indicated by the areas under curve (AUC) for 10 mg/kg p.o. vs. i.v. administration routes. AUC increased by 30% when doubling the p.o. dose from 10 to 20 mg/kg. Furthermore, **PK150** maintained plasma levels higher than the MIC (0.1 µg/mL) for a period longer than 24 h for the 10 mg/kg p.o. administration and almost twice as long for the double dose. In line with this, plasma clearance was slow (Figure 16).

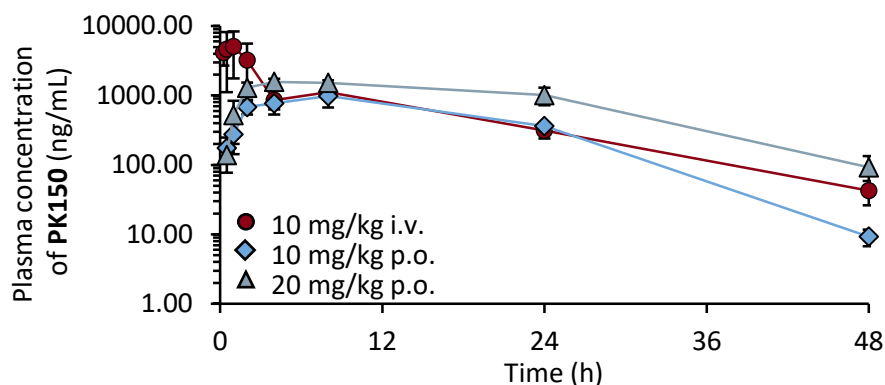


Figure 16: *In vivo* pharmacokinetics in mice. Pharmacokinetic analysis of **PK150** in murine plasma following oral (p.o.) or intravenous (i.v.) administration. Time dependent plasma concentrations after the administration of 10 mg/kg p.o. (circle), 20 mg/kg (squares) p.o. or 10 mg/kg i.v. (triangles), respectively, are shown. Compound levels in plasma were determined by LC-MS/MS analysis. Data represent means \pm SD ($n = 3$ per group).

Table 9: *In vivo* pharmacokinetics in mice. Pharmacokinetic parameters for **PK150** in murine plasma following oral (p.o.) or intravenous (i.v.) administration. Data represent means \pm SD ($n = 3$ per group).

PK parameter	Description	10 mg/kg i.v.	10 mg/kg p.o.	20 mg/kg p.o.
$t_{1/2}$ (h)	Half-life	11.69 \pm 1.5	9.67 \pm 0.2	9.37 \pm 0.5
C_{max} (µg/mL)	Maximum plasma concentration	6.19 \pm 3.0	1.02 \pm 0.3	1.58 \pm 0.2
T_{max} (h)	Time point of C_{max}	-	6.67 \pm 2.3	5.33 \pm 2.3
AUC (µg/mL*h)	Area under curve	33.61 \pm 3.3	21.09 \pm 4.0	45.09 \pm 5.1
MRT (h)	Mean residence time	10.10 \pm 1.7	13.78 \pm 0.5	16.71 \pm 1.9
V_z (L/kg)	Volume of distribution	5.00 \pm 0.2	6.78 \pm 1.3	6.07 \pm 1.1
CL (mL/kg/h)	Clearance	299.64 \pm 31.0	484.77 \pm 83.7	447.62 \pm 53.2

For the assessment of direct pharmacological benefits of **PK150**, a pharmacodynamic efficacy model with neutropenic mice was used in a first step (Figure 17). CD-1 mice were immunocompromised by administration of cyclophosphamide and infected with *S. aureus* ATCC 33591 (MRSA) by injection of approximately 2.2×10^3 CFUs into each thigh muscle. 20 mg/kg of **PK150** were orally administered, 4 and 8 h post-infection. Colony-forming units in thighs were determined 24 h after infection. **PK150**-treated mice showed a significant 10-fold reduction in CFU/g compared to vehicle-treated mice. The intraperitoneal control with levofloxacin (5 mg/kg) showed a higher average reduction (100x), but

with higher variance. The difference between bacterial loads after **PK150**- and levofloxacin-treatments was not significant, indicating comparable efficacy for the novel compound and the approved antibiotic.

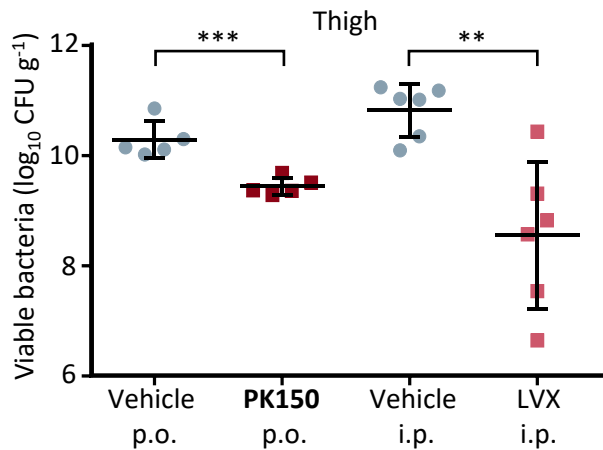


Figure 17: Efficacy of **PK150** and levofloxacin (LVX) against *S. aureus* ATCC 33591 (MRSA) in the neutropenic murine thigh model. **PK150** (20 mg/kg p.o.) or the corresponding vehicle were administered p.o. 30 min, 4 and 8 h after bacterial infection, whereas LVX (5 mg/kg) and the corresponding vehicle were administered intraperitoneally after 2, 6 and 10 h after bacterial infection. Data are expressed as mean values \pm SD; $n = 6$ for vehicle i.p., LVX i.p. and for **PK150**; $n = 5$ for vehicle p.o); **, $p < 0.01$; ***, $p < 0.001$ (Student's *t*-test).

Furthermore, the antimicrobial efficacy was validated in a bloodstream infection model with immunocompetent C57BL/6J mice. The animals were intravenously infected with 4×10^7 CFUs of *S. aureus* SH1000 (MSSA). On day three post-infection, all mice were fully symptomatic and the oral treatment started with two doses of 20 mg/kg of **PK150** separated by a 6 h interval. Single doses of 20 mg/kg were administered on days 4, 6 and 8 post-infection. On the ninth day, the count of viable bacteria was determined in liver, heart and kidneys (Figure 18). Significant reduction in CFU/g by approximately factor 100 was observed in liver and heart, while there was no such effect in kidneys.

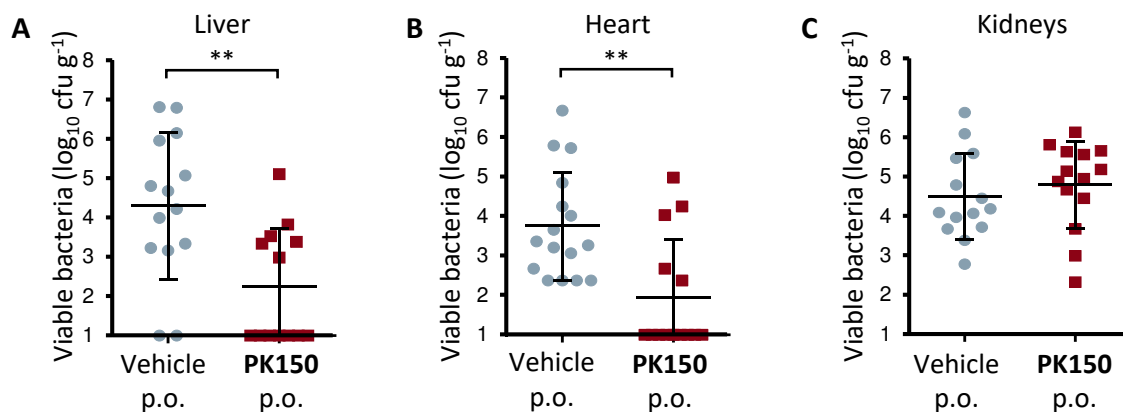


Figure 18: Efficacy of **PK150** against *S. aureus* SH1000 in a murine bloodstream infection model. Bacterial loads in the liver (A), heart (B) and kidneys (C) of *S. aureus*-infected mice treated with **PK150** (20 mg/kg p.o., squares) or vehicle alone (circles). Each symbol represents an individual mouse. Data compiled from three independent experiments are presented. Horizontal lines represent the mean values \pm SD; $n = 14$ for vehicle and **PK150**. **, $p < 0.01$ (Student's *t*-test).

2.2 Mechanistic Insights into the Antibiotic Action of Sorafenib and PK150

2.2.1 Identification of Protein Targets via AfBPP

As presented in the previous chapter, **SFN** and **PK150** exhibit excellent antibacterial activities against gram-positive pathogens. **PK150** furthermore showed a promising pharmacological profile for the further development as a potential drug against *S. aureus*. Therefore, the antibiotic mechanism of **SFN** and **PK150** remained another question to be answered. Gaining insights about targets of the compounds would be highly beneficial for further rational optimization of the drug candidate. Sorafenib is a multikinase inhibitor in human cells targeting serine/threonine kinases of the Raf family (C-Raf, B-Raf, oncogenic B-Raf V600E) as well as tyrosine kinases (e.g. VEGFR1 and 2, PDGFR, Flt-3, c-Kit, RET) and dual-action kinases such as the mitogen-activated protein kinases (MAPK) p38 and MEK1.¹³⁶ In bacterial cells DnaK was suggested as target of **SFN**.^{176,177} This assumption, however, was solely based on homology to the human target GRP78 and the observation that DnaK expression levels were reduced upon treatment with **SFN**, but direct evidence for binding was not shown.

In order to find targets of **SFN** and **PK150**, a target identification analysis using AfBPP was performed. For this, a photoprobe based on the scaffold of **SFN** was designed (Figure 19). As the compound lacks any reactive moiety, a noncovalent, reversible binding mode was assumed. In order to ensure covalent crosslinking to the target proteins during AfBPP, a photocrosslinker had to be introduced as well as an alkyne tag for subsequent click reaction with reporter tags. Based on structure-activity relationship studies a modification at the 2-pyridinecarboxamide moiety seemed to be most favorable site for modification to maintain the activity of the molecule. The diazirine group was chosen as photocrosslinking moiety due to its small size and superior crosslinking efficiency.^{178,179}

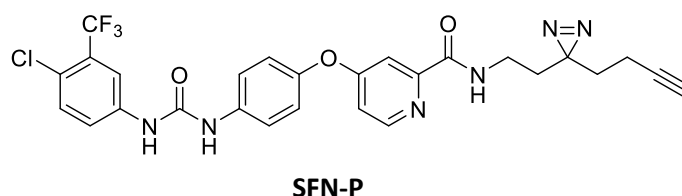


Figure 19: Structure of the photoprobe **SFN-P**. The photoprobe is based on the core structure of **SFN** that is synthetically equipped with a diazirine photocrosslinker and an alkyne tag required for AfBPP experiments.

Satisfyingly, **SFN-P** revealed an MIC value of 10 μM in NCTC 8325 as well as in USA300. As the antibiotic activity was only slightly decreased compared to **SFN**, the photoprobe was assumed as an appropriate tool for proteomic target deconvolution studies.

First, gel-based AfBPP was performed in order to optimize the labeling conditions for subsequent quantitative mass spectrometry-based analysis. The general steps of the final protocol were as follows: *S. aureus* NCTC 8325 cells were treated *in situ* with 50 μM of photoprobe **SFN-P** and irradiated with UV-light to covalently attach the probe. Lysis was performed by mechanical disruption and by an additional enzymatic lysis step using the peptidoglycan hydrolyzing enzyme lysostaphin. This was introduced to enhance the release, especially of cell wall-attached proteins.¹⁸⁰ Proteins were separated into soluble and insoluble fractions and attached to a trifunctional rhodamine-biotin azide linker (TFL)¹¹² via Copper(I)-catalyzed azide-alkyne click-reaction. Proteins were then precipitated with acetone, washed and enriched on avidin beads. Subsequently, SDS-PAGE was performed. Labeled proteins were then visualized by fluorescence detection of the rhodamine moiety (Figure 20). Visualization revealed binding to several proteins. Interestingly, the patterns were similar for soluble and insoluble fractions indicating an incomplete separation. As expected, no labeling was observed for the DMSO control. Furthermore, a competition experiment with a ten-fold excess of the parent compound **SFN** was performed, resulting in an efficient displacement of the photoprobe. Residual labeling likely remained possible because the actual chemical equilibrium is skewed during the UV-irradiation step as covalently binding photoprobe time-dependently displaces reversibly bound **SFN** molecules.

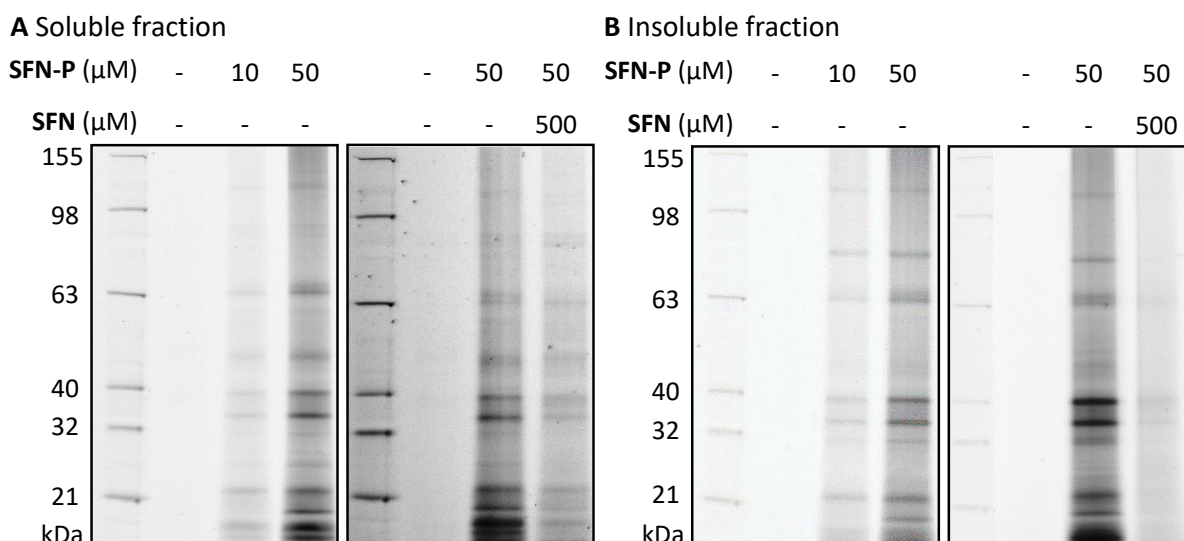


Figure 20: Fluorescence detection of SDS-PAGEs shows protein labeling pattern of *S. aureus* NCTC 8325 cells treated with **SFN-P** (10 and 50 μM) only and in competition of 50 μM **SFN-P** with a ten-fold excess of **SFN** (500 μM). After the treatment, cells were irradiated with UV-light and lysed. Soluble (A) and insoluble (B) fractions were separated before clicking to TFL and enrichment on avidin beads.

For identification and quantification of enriched proteins, the optimized workflow was combined with isotopic labeling and mass spectrometry-based analysis. For this, protein samples were prepared as described above. After enrichment, proteins were solubilized for subsequent reduction of disulfides and carbamidomethylation of resulting thiols to prevent re-oxidation. Further, proteins were on-bead digested using the proteolytic enzymes LysC and trypsin. Isotopic dimethyl groups were introduced to facilitate quantitative analysis. Labeled and desalted peptides were then separated on a C18-reversed phase column via nano high performance liquid chromatography (HPLC) and analyzed on an on-line coupled orbitrap mass spectrometer. Identification and quantification as well as statistical analysis of the proteins was subsequently performed using MaxQuant^{124,125} and Perseus,¹⁸¹ respectively.

Three control experiments were included. First, comparison to DMSO was conducted to exclude unspecific binding to avidin beads. Second, a competition experiment with an excess of the parent **SFN** was performed to confirm that both compounds address the same binding sites. Third, a comparison to minimal photocrosslinker probes was conducted to determine the extent of background binding.¹⁰¹

The comparison of **SFN-P**-labeled proteins to DMSO-treatment revealed signal peptidase IB (SpsB) (Uniprot: Q2FZT7) as the strongest hit in both fractions with enrichment ratios > 16 and p -values < 0.01 ($-\log_{10} p$ -value of 2) (Figure 21 and **Figure S1**).

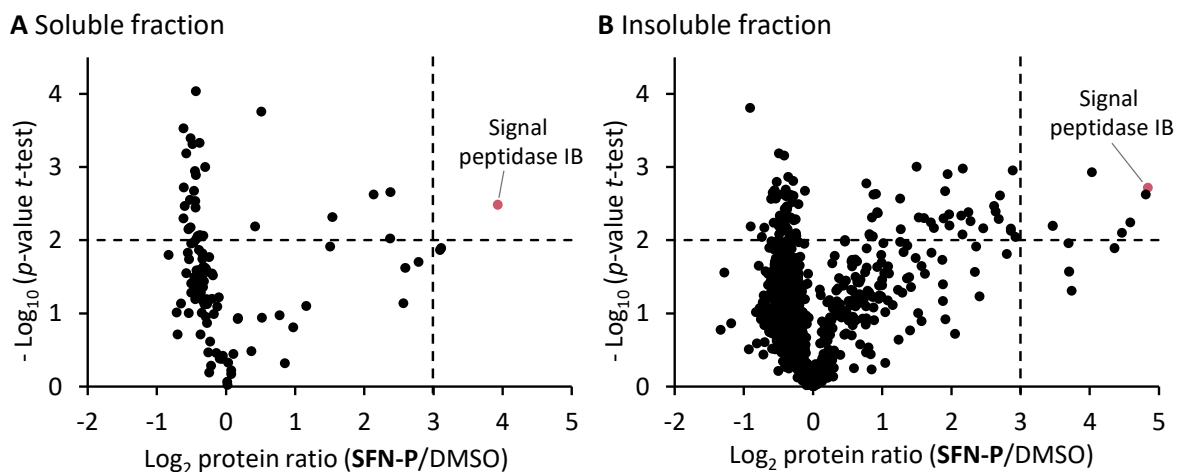


Figure 21: Volcano plots showing \log_2 fold enrichment of proteins in the soluble (A) and insoluble (B) fractions after treatment of *S. aureus* NCTC 8325 cells with **SFN-P** (50 μ M) compared to DMSO-treated cells. Dashed lines represent significant p -values < 0.01 ($-\log_{10} p$ -value of 2, horizontal) and an enrichment ratio cut-off criterion of 8-fold for selection of candidate targets for further analysis (vertical). The red dot represents the essential protein SpsB. Data represent mean values; $n = 3$ independent experiments performed in triplicates. For full list of detected proteins see Table S6 and Table S7).

Next, probe binding to the same targets as **SFN** was validated by competition experiments. For this, *S. aureus* cells were preincubated with a ten-fold excess of **SFN** prior to the labeling with **SFN-P** (Figure 22). Again, in both fractions SpsB showed up as the strongest hit with enrichment ratios > 16 and p -values < 0.01, indicating that this protein is targeted by both **SFN** and the respective photoprobe.

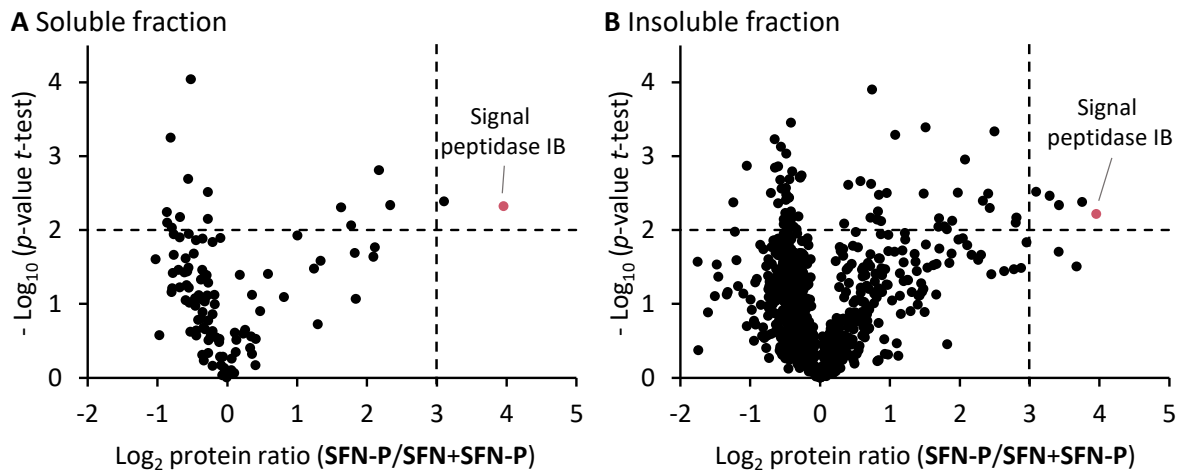


Figure 22: Volcano plots showing log₂ fold enrichment of proteins in the soluble (A) and insoluble (B) fractions after treatment of *S. aureus* NCTC 8325 cells with **SFN-P** (50 μM) compared to competition with a 10-fold excess of **SFN** (500 μM). Dashed lines represent significant p -values < 0.01 ($-\log_{10} p$ -value of 2, horizontal) and an enrichment ratio cut-off criterion of 8-fold for selection of candidate targets for further analysis (vertical). The red dot represents the essential protein SpsB. Data represent mean values; $n = 3$ independent experiments performed in triplicates. For full list of detected proteins see Table S8 and Table S9).

To control for photocrosslinker-associated off-target binding, the AfBPP workflow was applied to minimal photoprobes lacking the ligand-specific structure. Slight enrichment of SpsB became evident, especially for the photoprobe **DA-1** (Figure 23 A), but the enrichment with **SFN-P** was still almost 16-fold stronger compared to the minimal photoprobe (Figure 23 B). Background enrichment of SpsB by **DA-2** and **DA-3** were less pronounced (Figure S2 and Figure S3). Background binding of photoprobes can be explained by their high reactivity upon UV-excitation. The resulting reactive intermediates unspecifically react with any protein in proximity leading to a labeling bias towards highly abundant proteins or proteins with a preference for small-molecule binding.¹⁰¹ SpsB's location at the outer leaflet of the membrane makes it easily accessible for photoprobes as no passaging through the bacterial envelope is required, which might explain the background binding.

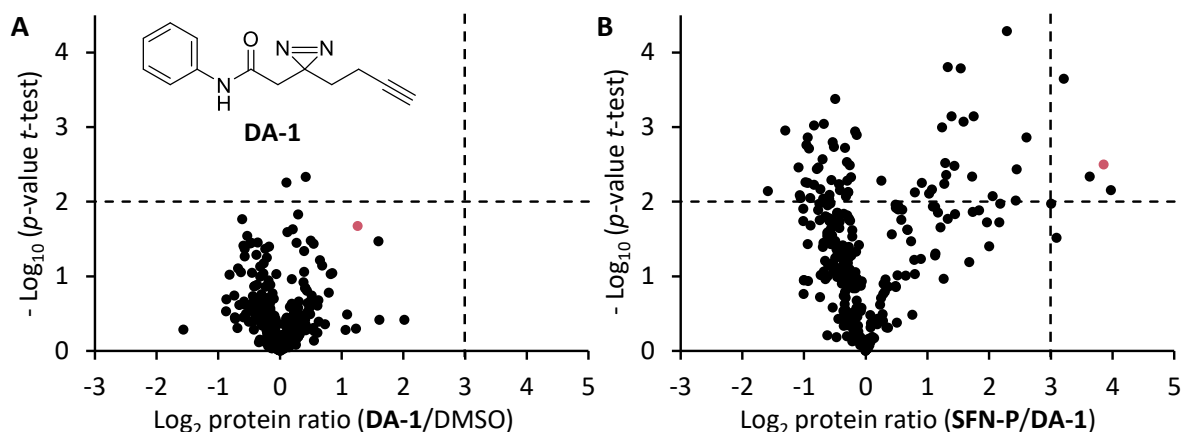


Figure 23: Photocrosslinker background binding. Volcano plots show \log_2 fold enrichment of proteins after treatment of *S. aureus* NCTC 8325 cells with the minimal photocrosslinker probe **DA-1** ($50 \mu\text{M}$)¹⁰¹ compared to treatment with (A) DMSO or (B) **SFN-P** ($50 \mu\text{M}$). Dashed lines represent \log_2 enrichment ratio of 3 and a $-\log_{10}$ p -value of 2. The red dot represents SpsB. Data represent mean values; $n = 3$ independent experiments performed in triplicates. Note: No separation of soluble and insoluble fractions was conducted here.

Proteins with at least 8-fold enrichment (\log_2 ratio > 3) in labeling or competition experiments were considered as target candidates (Table 10).

Table 10: Overview of the target candidates with 8-fold enrichment ratios (\log_2 ratio > 3) in labeling and competition experiments. For an overview of transposon mutants see Table S10.

Protein IDs	Protein names	Log ₂ ratio				TM
		Soluble fraction		Insoluble fraction		
		SFN-P/ DMSO	SFN-P/ Comp.	SFN-P/ DMSO	SFN-P/ Comp.	
Q2FZT7	Signal peptidase IB, putative	3.9	4.0	4.8	4.0	n. a.
Q2FWA8	Lytic regulatory protein, putative	3.1	3.1	n. d.	n. d.	NE721
Q2FVS2	Putative uncharacterized protein	3.1	2.3	3.7	n. d.	NE1076
Q2FVZ5	Putative uncharacterized protein	2.8	2.1	4.6	3.0	NE866
Q2G193	Putative uncharacterized protein	2.6	n. d.	4.4	3.1	NE733
Q2G2W2	Putative uncharacterized protein	n. d.	n. d.	4.8	3.4	NE419
Q2G117	Putative uncharacterized protein	n. d.	n. d.	4.5	3.8	NE323
Q2G1C5	Membrane protein, putative	n. d.	n. d.	4.0	3.3	NE166
Q2G2N2	Putative uncharacterized protein	n. d.	n. d.	3.7	3.7	NE779
Q2FZQ2	Putative uncharacterized protein	n. d.	n. d.	3.7	2.9	NE1270
Q2FV70	Putative uncharacterized protein	n. d.	n. d.	3.5	2.3	NE1204
Q2FWD0	Probable DNA-directed RNA polymerase subunit delta	n. d.	n. d.	n. d.	3.4	NE646

TM, Transposon mutant (Nebraska transposon mutant library), USA300; n. a., not available; n. d., not detected

Interestingly, no known bacterial protein kinases were among the enriched proteins. Sorafenib is considered as quite promiscuous inhibitor in human cells, targeting more than ten kinases.¹⁷⁴ However, the majority of human and bacterial kinases are structurally very different.¹⁸² Presumably, **SFN-P** did not bind staphylococcal kinases due to structural differences.

Out of the twelve proteins with highest enrichment ratios, SpsB was the only protein essential for cell viability.⁵⁵ For the remaining eleven proteins, the respective transposon mutants (from Nebraska transposon mutant library) were screened for MIC shifts upon treatment with **SFN** or **PK150** (Table S10).

Strikingly, only one transposon mutant, bearing the transposon in the gene coding for lytic regulatory protein (Lrp, Uniprot Q2FWA8), revealed a slight increase in the MIC of approximately 3-fold upon incubation with **SFN**. Although this protein of unknown function seems to have a slight contribution to the overall antibiotic mechanism, further studies were focused on SpsB because this protein was the strongest enrichment hit and is furthermore essential.

2.2.2 Biochemical Validation of SpsB as a Target

Type I signal peptidases (SPases) are membrane-bound serine-endopeptidases. They cleave signal peptides from secretory pre-proteins crossing the cytoplasmic membrane and are therefore responsible for their release and maturation.¹⁸³ About one third of all bacterial proteins are translocated through the cytoplasmic membrane and function outside the cytosol in soluble as well as membrane- or cell wall-attached forms.⁵⁴ These proteins execute diverse tasks including nutrient uptake, communication, excretion, maintaining of cellular structure, cell division as well as infection of foreign organisms. Thus, many of the extracellular proteins are virulence factors and play a major role in pathogenicity. The majority of the secreted proteins are processed by a signal peptidase in the last step of translocation.

In *S. aureus*, genes for two types of signal peptidases have been identified upon homology with other SPases - *spsB* and *spsA*. Only SpsB has been found to contain catalytic amino acids required for the functionality of the enzyme.^{184,185}

SpsB is proposed as an attractive drug target for several reasons. Most importantly, the enzyme is essential for viability. A great advantage of targeting SpsB is furthermore that its enzymatic pocket is located extracellularly. The direct accessibility to drugs in gram-positive bacteria circumvents the requirement for small molecules to penetrate the bacterial envelope as well as potential problems regarding efflux. Moreover, structural differences to essential proteases in eukaryotes enable selective targeting, thereby reducing the risk of host toxicity.^{55,186} Finding an inhibitor for SpsB, however, is a

challenging task as the enzyme is insensitive to classical serine protease inhibitors due to a unique catalytic mechanism employing a Ser/Lys catalytic dyad. The mechanism is characterized by a *si-face* attack of substrates, in contrast to the classical *re-face* attack conducted by canonical catalytic triads of the most Ser-dependent proteases. In light of the intriguing druggable properties, many efforts have been undertaken to find an inhibitor of SpsB,⁵⁵ revealing the natural product class of arylomycins as the most promising one.¹⁸⁷ Inhibition of SpsB by arylomycins has been shown to result in cell death, presumably caused by an accumulation of unprocessed proteins.¹⁸⁸ With this being said, targeting SpsB by **SFN** is a highly promising result. Hence, the validity and mode of binding were examined experimentally as described in the following chapters.

Labeling of recombinant SpsB *in vitro* and *in situ* in *E. coli*

In the present work the native full-length SpsB (fl-SpsB) sequence from *S. aureus* NCTC 8325 was cloned into the expression vector pET-55-DEST. The resulting SpsB-overexpression vector (pET-55-DEST-SpsB) was transformed into *E. coli* BL21(DE3)pLysS cells and used for an inducible expression of the enzyme, containing an N-terminal *Strep*-tag II. The full sequence of the overexpressed protein comprised 220 amino acids, resulting in a molecular weight of 24951.4 Da (average mass) (Figure S4).

For the validation of SpsB as a target protein of **SFN-P**, first *in situ* labeling experiments were conducted in *E. coli* BL21(DE3)pLysS harboring the SpsB-overexpression vector (Figure 24).

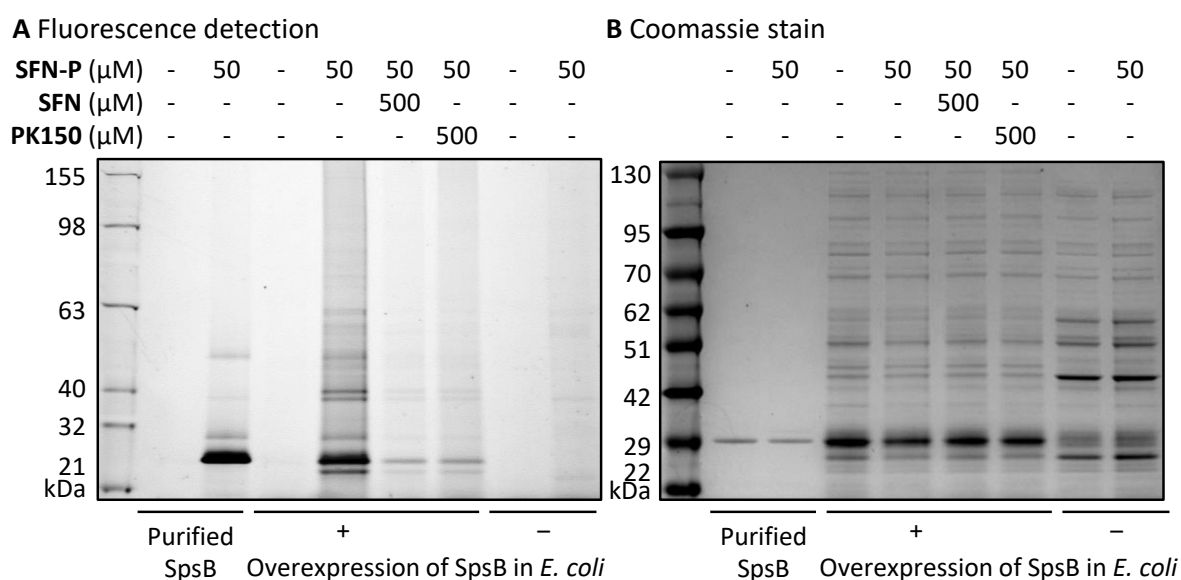


Figure 24: SDS-PAGEs of SpsB labeled by **SFN-P**. (A) Fluorescence gel shows labeling patterns of purified SpsB (5 μ M) or after *in situ* labeling of *E. coli* cells harboring SpsB overexpression vector (with either induced (+) or not induced (-) overexpression of SpsB) by **SFN-P** (50 μ M) with and without pre-treatment by **SFN** or **PK150** (500 μ M; competition). (B) Coomassie-staining of gel in (A). Note: No separation of soluble and insoluble fractions and no enrichment on avidin beads were conducted here.

Treatment of purified SpsB with a 10-fold excess of the photoprobe revealed strong labeling of the protein and served as molecular weight control for comparison of labeling in intact *E. coli*. *In situ* labeling in *E. coli* was conducted 3 h after induction of the protein expression by treatment of the bacteria with 50 μM of **SFN-P**. Binding to the protein was successful in induced *E. coli*, whereas no protein labeling was detected in non-induced cells. Furthermore, competition with either **SFN** or **PK150** significantly reduced labeling by **SFN-P**, indicating that the three molecules are targeting SpsB and moreover, act at the same binding site.

FRET-based Activity Assays with Purified SpsB

In order to assess the catalytic activity of SpsB, a fluorimetric assay was used as designed by Rao *et al.*¹⁸⁵ In this assay, the cleavage substrate is a peptide derived from the *Staphylococcus epidermis* SceD pre-protein, which is a natural substrate of SpsB. The peptide is modified by a fluorescence donor-acceptor pair facilitating monitoring of SpsB activity via Förster resonance energy transfer (FRET). Upon cleavage of the peptide by SpsB the distance dependent quenching of the donor by the acceptor is abolished and an increase in fluorescence signal from the donor can be monitored (Figure 25).

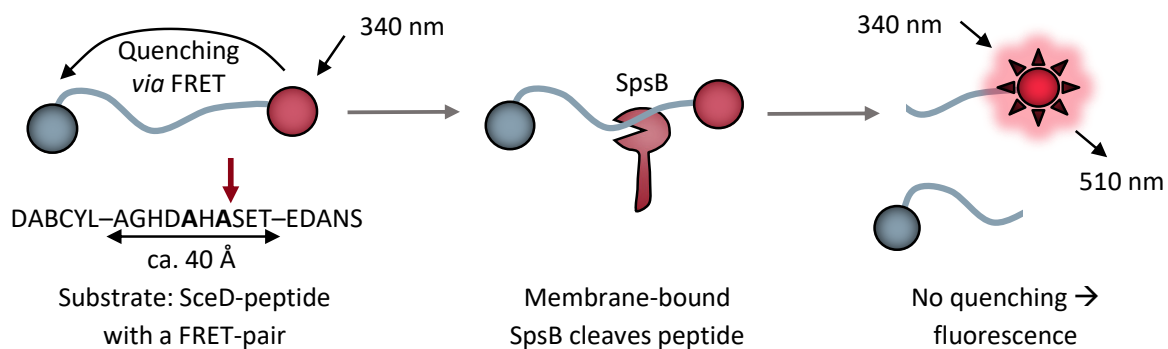


Figure 25: Basic principle of the fluorescence resonance energy transfer (FRET)-assay for measuring the activity of SpsB via the cleavage of a FRET-peptide substrate. The FRET-peptide substrate is based on the signal peptide sequence of *Staphylococcus epidermis* SceD pre-protein modified with the fluorescent donor 5-((2-aminoethyl)amino)-1-naphthalenesulfonic (EDANS) acid and the quenching acceptor 4-((4-(dimethylamino)phenyl)azo)benzoic (DABCYL) acid.

Arylomycin A4, a close analog of the known *in vitro* inhibitor of SpsB arylomycin A2,^{185,189,190} was used as a control. A concentration-dependent decrease of SpsB activity was observed demonstrating desired specificity of this assay (Figure 26 A).¹⁹¹ Purified SpsB furthermore exhibited substrate cleavage activity in contrast to controls containing either no substrate or no protein (Figure 26 B). Similarly to other members of the SPase family, SpsB is known to undergo self-cleavage *in vitro*.¹⁸⁵ Thus, the stability of the protein under assay conditions was determined. (Figure 26 B). SpsB was stable during an incubation period of 50 min at 37 °C. However, the activity strongly decreased after addition of 0.5% Triton X-100 to the buffer, probably due to its self-cleavage.⁵⁵ The activity-stimulating effect of

detergents on recombinant SPases is a known phenomenon.⁵⁵ Crystallization of the homologous *E. coli* SPase LepB had revealed a large hydrophobic surface which is probably responsible for a close contact to the membrane.¹⁹² Due to their membrane-mimicking properties, detergents are assumed to interact with hydrophobic surfaces of the protein resulting in enhanced activity. *In vivo*, however, the protein is believed to be protected from self-degradation due to the localization of both the catalytic and the autolysis sites at opposite sides of the membrane.^{185,193} This protective barrier is absent in purified proteins. Therefore, the enhancement of activity likely results in an increased self-degradation.

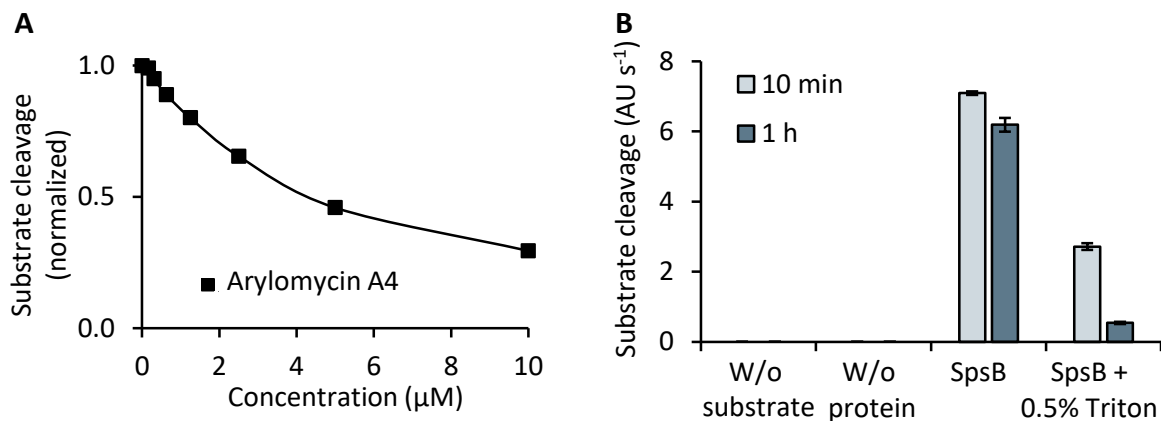


Figure 26: FRET assays with purified fl-SpsB (0.2 μM). (A) Concentration-dependent inhibition of SpsB by arylomycin A4. (B) Stability of the protein after preincubation with and without addition of 0.5% Triton X-100 in the assay buffer. Assays were started after 10 min or 1 h of preincubation at 37 °C by adding 1 μM SceD-FRET substrate and measuring fluorescence at 510 nm (340 nm for excitation). Initial slopes of the fluorescence increase are represented. Data represent mean values ± SD; $n = 3$.

Nevertheless, in order to determine the influence of **SFN** on SpsB activity, assays were first performed with Triton X-100 added in the assay buffer. Surprisingly, no change in activity was observed for even a very high concentration of 1 mM **SFN** (Figure 27 A). To evaluate the relation of this observation to the antibiotic activity, MICs were determined for different triton X-100 concentrations. An MIC shift was already observed at a very low detergent concentration of 0.005%, which is even below the critical micelle concentration of 0.016% (Figure 27 B).¹⁹⁴ At a concentration of 0.5% Triton X-100, the antibiotic activity of **SFN** was completely abolished (MIC > 100 μM). This result indicates strong interference between the detergent and binding of **SFN** to the target protein.

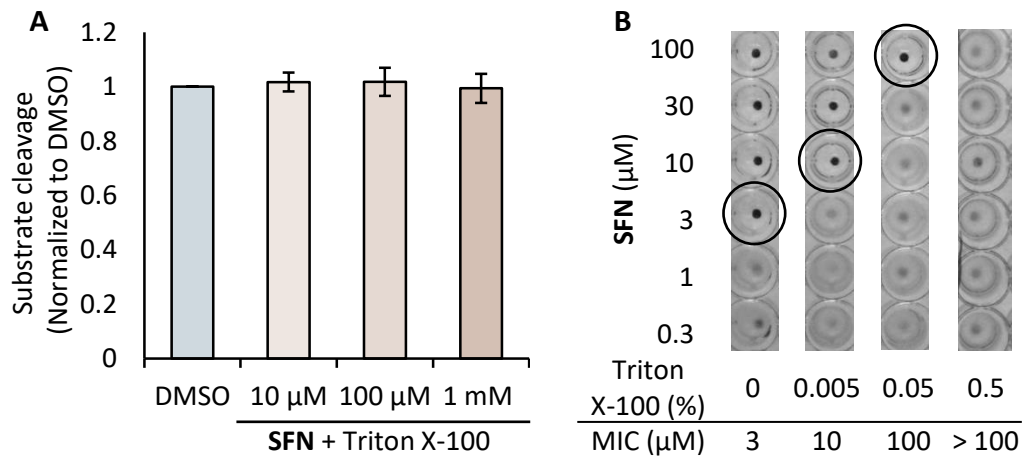


Figure 27: Influence of Triton X-100 on the activity of **SFN**. (A) FRET-based activity assay with fl-SpsB in presence of different concentrations of **SFN** and 0.5% Triton X-100. Substrate cleavage rates are normalized to DMSO-treated samples. Data represent mean values \pm SD; $n = 3$. (B) MIC-determination of **SFN** in presence of varying concentrations of detergent Triton X-100 (critical micelle concentration, CMC = 0.016%).¹⁹⁴

To circumvent the influence of the detergent, FRET-assays were subsequently performed without addition of Triton X-100 (Figure 28). Surprisingly, the enzyme showed a concentration-dependent increase in activity upon **SFN**-treatment. Incubation with **PK150** revealed even stronger stimulation. In contrast to this, the control compound **SFN-C** and **PK150-C** revealed no stimulation.

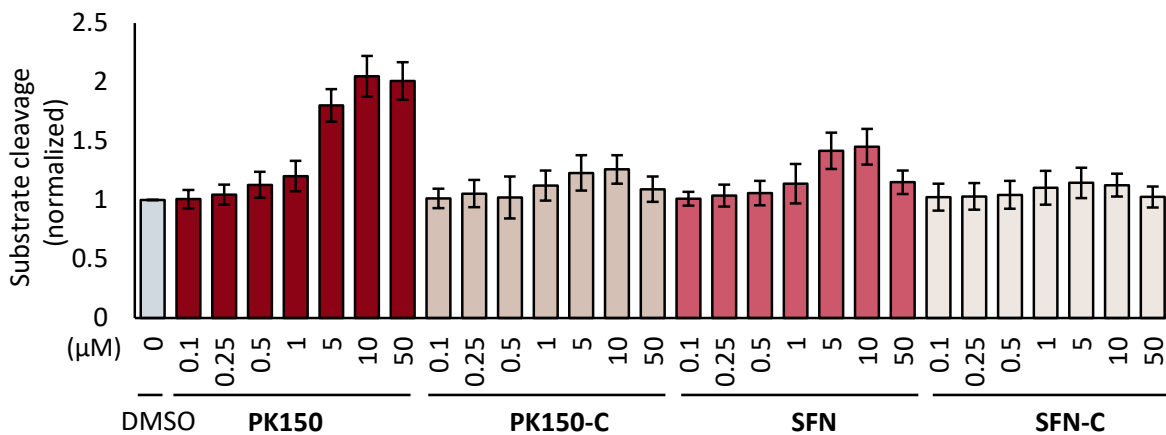


Figure 28: FRET-based activity assay with overexpressed and purified fl-SpsB (0.2 μM). Substrate cleavage rates are normalized to DMSO-treated samples. Data represent mean values \pm SD; $n = 3$ replicate experiments in triplicates.

FRET-based Activity Assays with Membranes Harboring SpsB

To validate the results obtained with purified protein, FRET-assays were performed with endogenous membranes of *S. aureus* containing native SpsB. These conditions more closely simulate the protein's natural conditions.¹⁸⁷ Furthermore, as mentioned before, being located in the membrane, the enzyme is assumed to be protected from self-degradation.¹⁸⁵ Membranes of *S. aureus* or *E. coli* were collected via extensive centrifugation after disruption of cells and removal of cell debris. Treatment with arylomycin A4 revealed concentration-dependent inhibition indicating desired specificity of the membrane-based assay-variant as well (Figure 29 A). Membrane-bound SpsB showed stable activity over a period of 50 min at the assay temperature (37 °C), corroborating a protective function of the membrane regarding self-cleavage.

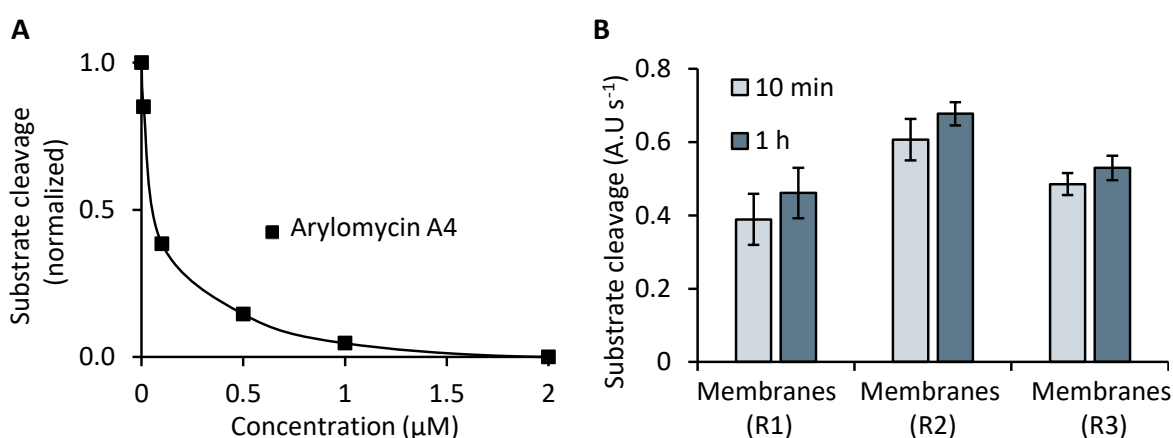


Figure 29: FRET assays with *S. aureus* membranes harboring endogenous SpsB (200 μg/mL total membrane protein concentration) (A) Concentration-dependent inhibition of SpsB with arylomycin A4. Substrate cleavage rates are normalized to DMSO-treated samples. (B) Activity of membrane-bound SpsB after 10 min and 1 h of preincubation at 37 °C. Data represent mean values ± SD from three independent membrane preparations (R1 – R3) measured in triplicates.

Treatment of *S. aureus* membranes with **PK150** and **SFN** resulted in a significant concentration-dependent stimulation of the substrate-cleaving activity (Figure 30). This observation supports the results obtained with the purified protein. The activities rose to 1.2-fold for both compounds at a concentration of 10 μM, and 1.7- and 2.8-fold at 50 μM for **SFN** and **PK150**, respectively. No significant increase in activity could be observed for the structurally similar but antibioticly inactive control compounds **PK150-C** and **SFN-C** (Figure 30). Control compounds based on the minimal photocrosslinkers did not influence the activity of SpsB (Figure S5). This supports the assumption that background binding of photocrosslinkers to SpsB in AfBPP experiments was indeed unspecific (Figure 23 and Figure S2).

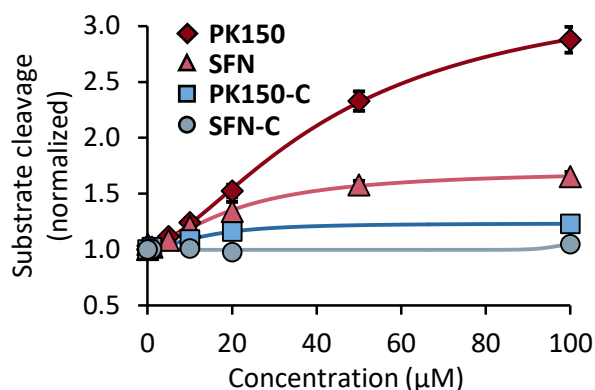


Figure 30: FRET assay with *S. aureus* NCTC 8325 membranes (200 μg/mL total membrane protein concentration) and different concentrations of **SFN**, **PK150** and their antibioticly inactive counterparts **SFN-C** and **PK150-C**. Substrate cleavage rates are normalized to DMSO-treated samples. Data represent mean values ± SD; $n = 3$ independent experiments in triplicates.

Finally, for a further confirmation of the obtained results, *E. coli* membranes overexpressing SpsB were used to perform the same assay (Figure 31). Again, antibioticly active compounds led to a concentration-dependent activity stimulation upon treatment with the compounds, whereas there was no stimulation with the control compounds. At 10 μM the activity was already significantly increased to 1.3-fold and 1.7-fold for **SFN** and **PK150**, respectively (Figure 31 B). The maximum stimulation was achieved at 50 μM yielding in a 1.3- and 2.3-fold activity for **SFN** and **PK150**, respectively. Interestingly, no stimulating effect was observed for uninduced *E. coli* membranes, indicating that its endogenous SPase LepB is not capable of binding the compounds. This in turn might be a reason for the lack of antibiotic activity in gram-negative bacteria. In fact, previous reports have shown that the sequence homology between SpsB and LepB is considerably low (approximately 26%) and although the two proteins share structural similarity in the active domain, their response to small molecules is distinctly different.^{186,195}

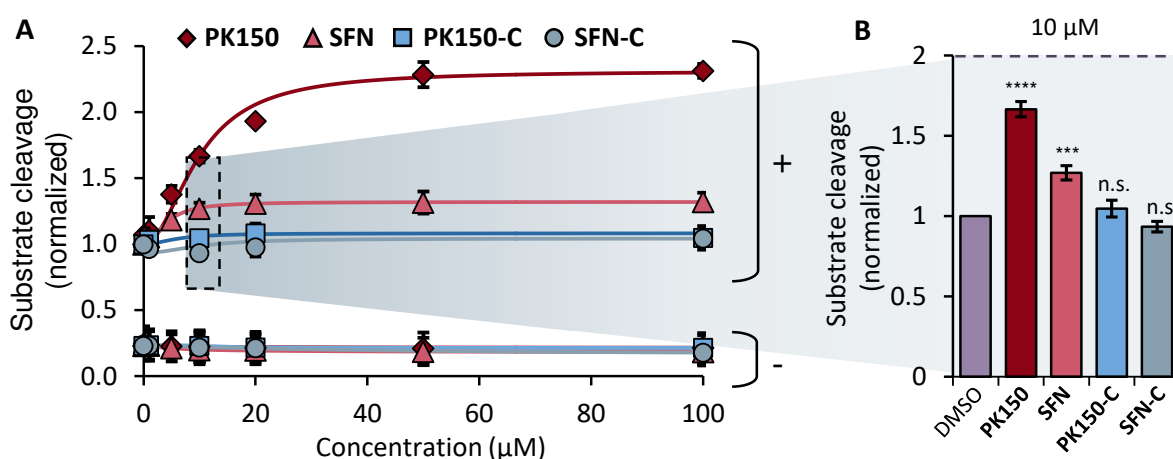


Figure 31: FRET assays with membranes from *E. coli* (50 μg/mL total membrane protein concentration). Membranes were extracted from cells harboring the SpsB overexpression vector, in which the overexpression of SpsB was either induced (+) or not induced (-). Assays were performed with different concentrations of **SFN** and **PK150** as well as of the control compounds **SFN-C** and **PK150-C**. Substrate cleavage rates are normalized to DMSO-treated samples from the induced membranes. Data represent mean values ± SD; $n = 3$ independent triplicates per group.

Based on the library of **SFN** derivatives, it was previously shown that the modifications of different moieties of the **SFN** scaffold have different influences on the MIC values (Chapter 2.1.2). The library can also be exploited to assess whether there is a correlation between MIC values and SpsB activities as determined in FRET-based assays (Figure 32). Interestingly, most compounds that are inactive in the phenotypic screen (Figure 32, dark violet dots, MIC > 100 μ M) do not stimulate SpsB. Although the values regarding of SpsB stimulation are spreading for compounds with higher antibiotic activity (1 – 30 μ M), a trend towards increasing activities of SpsB with higher MIC values can be observed. **PK150** remains the most prominent compound regarding both, antibiotic as well as SpsB-stimulating activities. This result indicates a functional relation between stimulation of SpsB and the antibiotic activity. However, there are also compounds with high antibiotic activity, which do not show stimulation of SpsB, suggesting that in these cases other targets likely contribute to the antibiotic activity. For close analogs of **SFN**, the stimulating effect can be furthermore related to the systematic structural variations within the scaffold moieties (Figure 32 B). Whereas variation of the 4-chloro-3-(trifluoromethyl) phenyl moiety did not influence intrinsic SpsB activities, changes in the heteroaryl ether moiety resulted in different levels of SpsB activity changes. This result resembles observations made for comparison of structural variation and resulting antibiotic activities (Chapter 2.1.2).

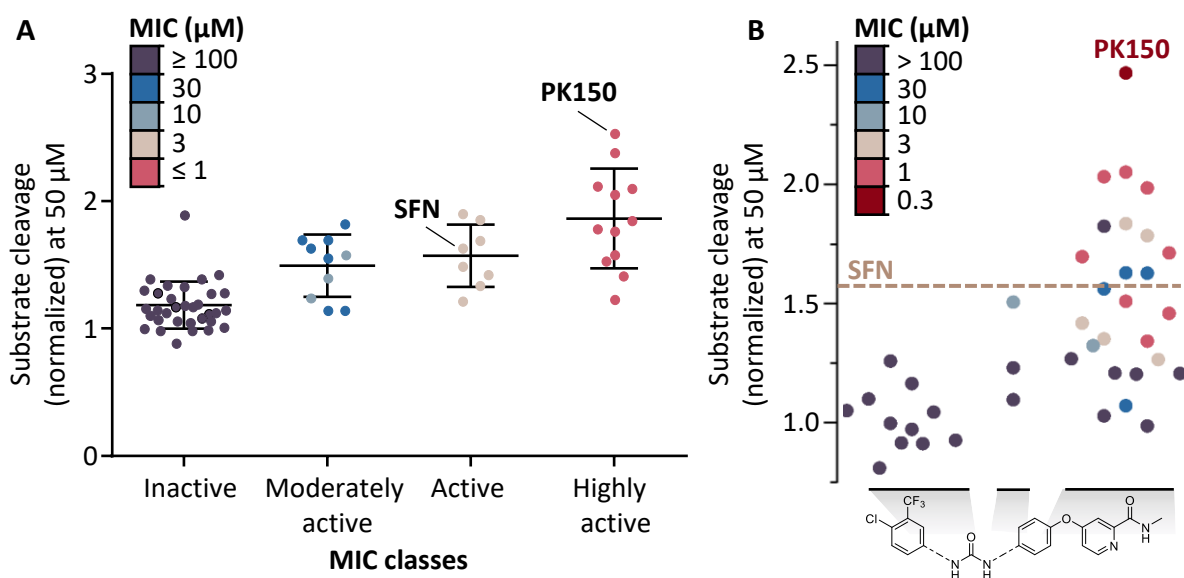


Figure 32: (A) Correlation between MIC values and SpsB activities for the whole library of derivatives. See Table S4 for structures and values. (B) Correlation analysis of close analogs of **SFN** (40 scaffolds). Substrate cleavage activities of *S. aureus* NCTC 8325 membranes at 50 μ M compound concentrations are plotted, classified according to the moieties that were varied. Corresponding MIC values are indicated via color coding. See Figure S6 for 10 and 100 μ M compound concentrations.

Colloid Formation and Specificity of the Stimulating Effect

It is known that many small molecule compounds, including approved drugs, self-associate into colloidal aggregates in aqueous solutions.^{196–198} Presence of these aggregates often leads to the discovery of false-positive inhibitors in high-throughput enzyme-centered screenings. Cause for this effect is the fact is that these aggregates can adsorb to the protein leading to its partial denaturation and unspecific inhibition.^{199,200} For inhibition artefacts this problem has been recognized decades ago and assay adjustments such as the use of colloidal breaking detergents as well as prediction methods for colloid formation were introduced.^{201,202} Similar effects were later recognized for small molecule activators as well.^{203,204} Thus, an identification of colloids and careful evaluation of their influence on protein activities is required. **SFN** is known to form colloidal aggregates.²⁰⁵ Similarly to **SFN**, **PK150** tends to form aggregates as well, but at higher concentrations, as shown by dynamic light scattering (DLS) experiments (Figure 33 A). The detergent Tween-80 was able to disrupt the colloids, which is in accordance with previously published results.²⁰⁵ However, it also reduced antibiotic activity in the cell-based MIC assay (Figure 33 B), similarly to the effects observed with Triton X-100 (Figure 27). Nonetheless, **PK150** and **SFN** formed colloids at concentrations (critical aggregation concentration, CAC) that were well above the MIC and thus not responsible for the antibiotic effect (Figure 33 B). Furthermore, the activities of SpsB residing in membranes (Figure 31) as well as of the purified SpsB (Figure 28) were stimulated at concentrations of **PK150** and **SFN** that were under the CAC, excluding unspecific stimulation by colloids. In contrast to that, the observed decrease in the stimulating effect on purified SpsB at higher concentrations of the compounds (50 μM) (Figure 28) is likely due to the formation of colloids at these concentrations.

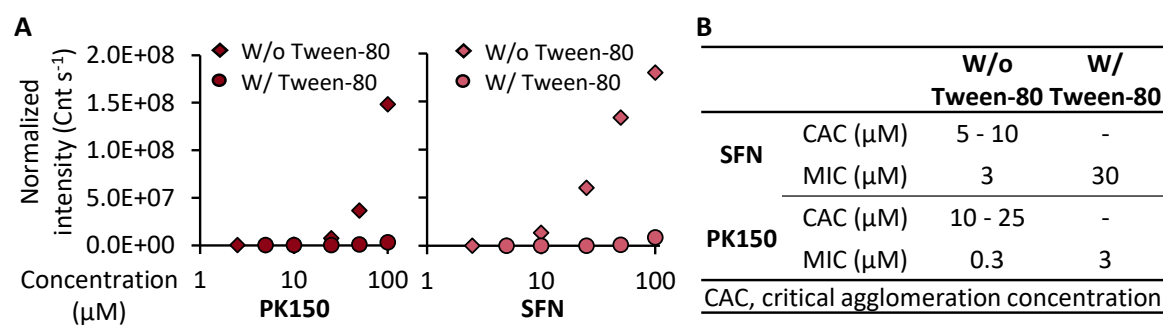


Figure 33: (A) Colloid formation by **PK150** (left panel) and **SFN** (right panel) in 50 mM sodium phosphate buffer, pH 7.0. Colloidal aggregation was measured by dynamic light scattering (DLS) in presence and absence of Tween-80 (0.023% v/v). DLS signal intensities were reduced by the addition of Tween 80, indicating the disappearance of colloidal aggregates at the respective concentration. The Figure is representative for 2 independent experiments. (B) Detergent-based MIC shift assay. MIC values were determined against *S. aureus* NCTC 8325 in B-medium and B-medium supplemented with Tween 80 (0.023% v/v). CAC, Critical aggregation concentration (determined by DLS).

2.2.3 Docking and Molecular Dynamics

In situ competitive AfBPP experiments as well as *in vitro* FRET-based assays showed compound-protein interaction between **PK150** and SpsB. The mechanism of activation was therefore studied by subsequent *in silico* experiments in form of docking and molecular dynamics (MD) simulations (Figure 34).²⁰⁶ A crystal structure of *S. aureus* SpsB fused to maltose-binding protein was used as the basis for the docking experiments (PDB: 4wvj).¹⁹⁵ The original, crystallized enzyme contained a bound inhibitory peptide, which was removed for calculations. Docking was performed in two steps comprising a broad sampling, followed by a molecular dynamic based energy refinement of the selected poses. **PK150** was found to have the lowest free binding energy when located adjacent to the substrate binding pocket with a distance of 12 Å to the C α -atoms of the active site residues Ser36 and Lys77 in the refined docking pose (Figure 34 A, B). In this position, the urea group of **PK150** forms hydrogen bonds with Asp147 (Figure 34 C). Moreover, the trifluoromethyl group of **PK150** interacts with the hydrophobic surface, formed by non-polar amino acid residues Leu41 in a flexible loop and Val47, Val64, and Val170 residing on stable β -sheets (Figure 34 A). The central role of these residues in binding is supported by the observed SpsB activities (Table 11). Removal of the trifluoromethyl group (**4-017**, **PK150-C**) or changes in the urea motif, such as the replacement of a hydrogen bond donor (**5-016**), led to a substantial drop in the activity stimulation. The binding site being located adjacent to the active site is furthermore consistent with the stimulating effect observed in FRET assays, as the substrate can still bind at the unoccupied active site.

To investigate the structural changes, which lead to the stimulating effect, MD simulations were carried out. **PK150** binding resulted in changes of the secondary structure of the protein, including destabilizing as well as stabilizing effects (Figure 34 D, E). Residues in regions that are involved in the signal peptide substrate binding (beige areas), residues within 5 Å sphere of the catalytic dyad (pink areas) and the loop, on which the catalytic dyad Ser36 / Lys77 lies (gray area), are critical for the activity of the protein. Some of these residues folded into higher order secondary structures, resulting in a limitation of the conformational space. Regulation of various enzymes has been shown to be dependent on intrinsic protein dynamics.^{207,208} Thus, it is likely that **PK150** causes the increase of catalytic activity of SpsB by constraining the protein in an active state with a rigidified active site. A similar mode of action had been shown for acyldepsipeptide-induced stimulation of the caseinolytic peptidase ClpP recently.²⁰⁹

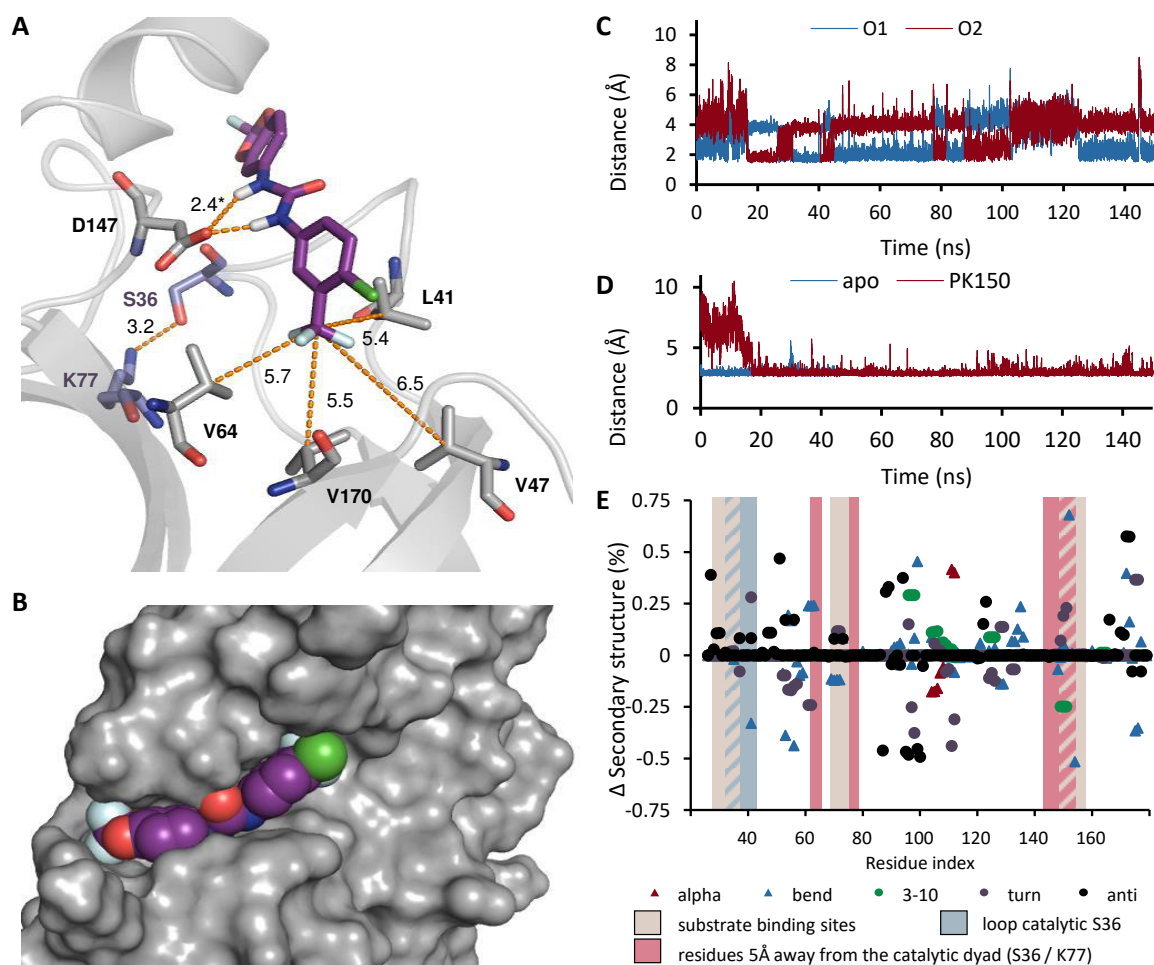
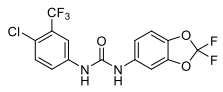
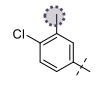
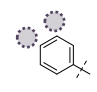
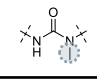


Figure 34: Molecular docking and dynamic simulations. (A) Detailed representation of the binding site showing **PK150** (purple), important active site residues (blue), and residues coordinating to **PK150** (gray) in stick representation within SpsB (cartoon). The distances shown correspond to the mean values (Å) over the last 150 ns of the simulation; *2.4 Å represents the average of the minimum distance between the urea group hydrogens and either one of the side chain oxygens of D147 (see panel C for details). (B) Surface representation of the binding cleft within SpsB. **PK150** is shown as spheres, carbon, oxygen, nitrogen, chloride, and fluorine atoms are colored purple, red, blue, green, and cyan, respectively. (C) Distance between the centers of the two hydrogen atoms of the urea motif of **PK150** and the side chain oxygens (O1, blue lines and O2, red lines) of residue D147. A hydrogen bond (2 Å) is formed between the hydrogens of the urea motif and either O1 or O2 during the simulation. (D) Distance between side chain oxygen of catalytic S36 and side chain nitrogen of K77 in the apo (red lines) and **PK150** bound simulation (blue lines). (E) The differences in the secondary structure formation percentage between the apo and **PK150** bound simulations (over 150 ns) are given with respect to the residue index. Only secondary structure elements that display a major difference between the simulations (apo vs. **PK150** bound) are plotted (i.e. alpha helix, bend, 3-10 helix, β -turn, anti-parallel). Three critical regions of the protein are highlighted, namely the signal peptide substrate binding sites (beige area), the loop involving the catalytic S36 (gray area) and the residues within 5 Å sphere of the catalytic dyad (S36 / K77) (pink area). Positive and negative values represent stabilizing and destabilizing changes, respectively.

Table 11: Examples of SpsB activity in *S. aureus* NCTC 8325 membranes at 50 μ M compound concentrations for analogs of **PK150**. See Table S4 for the full overview of analogs.

Compound		SpsB activity (normalized)
PK150		2.54 \pm 0.39
4-017		1.23 \pm 0.05
PK150-C		1.15 \pm 0.01
5-016		1.39 \pm 0.11

Experiments, involving mutations of residues responsible for binding, should be performed in the future to biologically confirm the predicted binding location. Ideally, the binding location should be confirmed by a co-crystal structure of SpsB and **PK150**. However, crystallization of SpsB is very challenging due to its self-cleavage. In previously published work, crystallization could be achieved only for the inactive mutant and for a fusion construct with maltose binding protein with tethered substrate or inhibitory peptides.^{195,210} Therefore, these strategies will be applied in future work to obtain a crystal structure with bound **PK150**.

2.2.4 Genomic Approaches

Knockout of SpsB

Since SpsB is an essential protein, a direct knockout is not available. However, a strain resistant to arylomycin, identified by Craney *et al.*,²² is able to bypass the essentiality of SpsB. It overexpresses an ABC-transporter, which is able to compensate for essential functions of the signal peptidase.^{211,212}

The SpsB knockout-mutant of such a strain (ARC0001 Δ SpsB),²¹³ was used to determine the MICs upon treatment with **SFN** and **PK150**. Unfortunately, no difference in MIC values was observed compared to the wild-type strain N315 (Table 5). However, the mutant displayed a largely different phenotype, characterized by clumping of cells and slow growth compared to the wild type. Therefore, a general loss in fitness cannot be excluded. Furthermore, in a previous study it was shown that in the double mutant the secretion of virulence factors is severely impaired. Furthermore, it is unable to establish an *in vivo* infection, which additionally pinpoints to substantial physiological changes.²¹² Thus, it is difficult to evaluate, if an absence of the MIC-shift in this mutant strain means that SpsB is not the bioactivity-defining target of **SFN** or **PK150** in wild-type strains. With respect to this finding, however,

the existence of alternative , including non-protein, targets is a possible explanation. Therefore, further investigation regarding the involvement of SpsB in the antibiotic mechanism is required. For example, genetic or chemical (with i.e. arylomycin 103)²¹² knockdown experiments could provide valuable insights.

Genome-Sequencing of SFN-resistant mutants

As resistances often arise from a mutation in the target or associated genes,^{21,214} sequencing of resistant strains can reveal target(s) of the respective drug or provide hints towards the underlying antibiotic mechanism. Therefore, next-generation sequencing of genomes of three independently obtained **SFN**-resistant *S. aureus* NCTC 8325 strains (Chapter 2.1.4) was performed. Analysis revealed mutations in several genes (Table S11).

SpsB was not among the genes that were mutated upon **SFN**-treatment, indicating SpsB-independent resistance mechanisms. Craney *et al.* had previously shown, that strains resistant to arylomycin, a known inhibitor of SpsB, did not bear mutations in the SpsB gene either.²² Instead, they were overexpressing a native gene cassette encoding the operon *ayrRABC*.²¹¹ A resistance-associated loss-of-function mutation in the *cro/cl* locus (coding for AyrR) leads to a derepression of the *ayrRABC* operon. Its product, an ABC transporter, is able to take over the essential function of SpsB.^{22,213} However, strains resistant to **SFN** did not reveal an involvement of the *ayrRABC* operon (for homologous genes in *S. aureus* NCTC 8325 see Table S12), indicating a presence of other resistance mechanism(s) here.

Mutations in genes for the kinase PknB (SAOUHSC_01187) and Protein A (SAOUHSC_02265) as well as in an intergenic region upstream of an ABC transporter were found in only one of the three replicates. Two genes evolved mutations in two of the three **SFN**-resistant strains, namely *fmtC* (SAOUHSC_01359) and *rluD* (SAOUHSC_00944), and were thus inspected more closely.

FmtC (MprF) is a membrane enzyme that decorates the membrane lipid phosphatidylglycerol (PG) with lysine residues at the outer leaflet. This modification influences the charge of the membrane²¹⁵ and is furthermore associated with other changes in membrane properties such as fluidity.²¹⁶ MprF (Multiple peptide resistance factor) has been shown to be involved in resistance to cationic antimicrobial peptides (AMPs)²¹⁵ and daptomycin.^{216,217} A closer inspection of the target identification study via AfBPP revealed that the protein FmtC/MprF was moderately enriched in the insoluble fraction upon **SFN-P** labeling compared to DMSO (\log_2 protein ratio of 1.15 and $-\log_{10}$ *p*-value of 1.12) as well as to competition experiments with **SFN** (\log_2 protein ratio of 1.14 and $-\log_{10}$ *p*-value of 1.11). It is therefore possible that MprF is a target of **SFN**, contributing to the antibacterial mechanism. For

example, an indirect influence of MprF-dependent changes in membrane properties on membrane-residing proteins, including SpsB, is conceivable.

Pseudouridine synthases (rluD) post-transcriptionally modify RNAs and are supposed to act as RNA chaperones, but their exact function is unknown.^{218,219} Their involvement in antibiotic resistance has not been described yet. RluD was not identified in AfBPP experiments here.

For both genes, corresponding transposon mutants were tested for MIC-shifts upon treatment with **SFN** and **PK150** revealing no influence on the antibiotic activities. Thus, these proteins were not further investigated as putative targets in this work.

However, deeper examination of the resistant strains and mutated genes should be carried out in the future, in order to obtain insights into the resistance mechanism against **SFN**.

2.2.5 Secretome and Surfaceome Analyses

Because of the fact that the cleavage of peptide sequences and release of secreted proteins is the main function of SpsB, changes in the secretome upon treatment with **SFN** and **PK150** were analyzed. For that, NCTC 8325 cells were grown up to the stationary phase and subsequently washed to remove proteins from prior cell lysis as well as to facilitate sensitive detection of secreted proteins upon incubation with the compounds. Concentrations of 0.5-fold MIC of **SFN** and **PK150** were used for treatment in order to avoid secondary effects and to prevent cell lysis. Cells were incubated for 1.5 h with the compounds and afterwards removed to collect the supernatants. Secreted proteins from the supernatants were obtained by precipitation, tryptically digested and eventually analyzed via label-free LC-MS/MS-based quantification.¹²⁵

The number of viable cells was determined for all conditions via plating and counting of grown colonies. No cell death or lysis could be detected across all experiments, confirming that the majority of detected proteins were due to active secretion and not passive lysis.

The overall change in protein abundances in the secretome was small due to the low concentrations of compounds (Figure 35 A). SpsB-substrates are characterized by a signal peptide, which is recognized and cleaved by the enzyme.⁵⁴ The canonical N-terminal recognition signal sequences typically share common features comprising the first 25 – 32 amino acids of the protein. The sequence consists of a positively charged N-terminus, followed by a hydrophobic region with a Gly or Pro residue at its end, and the SPase recognition site at the C-terminus. The site is characterized by small, aliphatic residues (mostly Ala) at positions -1 and -3 with respect to the cleaved bond.²²⁰ The prediction of this sequence can be used to annotate proteins as putative SpsB substrates.²²¹

Interestingly, proteins, predicted to have a signal peptide and thus regarded as SpsB substrates,²²¹ were found to be enriched in the secretome upon incubation with the active compounds compared to treatment with DMSO. Furthermore, a comparison to treatments with inactive control compounds **SFN-C** and **PK150-C**, revealed enrichment of these proteins as well, confirming that solely **PK150** and **SFN** evoke this effect. (Figure 35 B). Additionally, the same result was obtained for proteins that had been classified as SpsB substrates in a previous work by Schallenberger *et al.*²²⁰ In that study, 46 proteins had been identified, the secretion of which was decreased by the SpsB inhibitor arylomycin A-C₁₆, representing experimentally supported SpsB substrates.

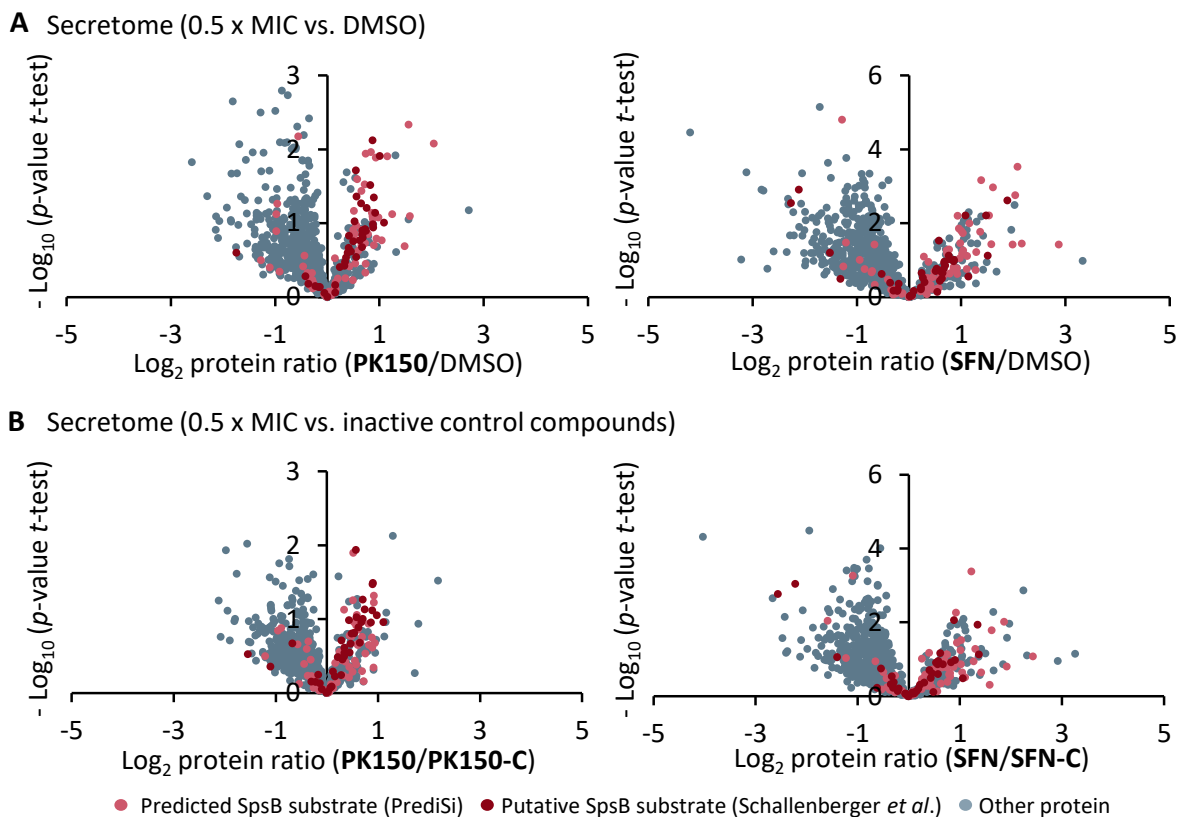
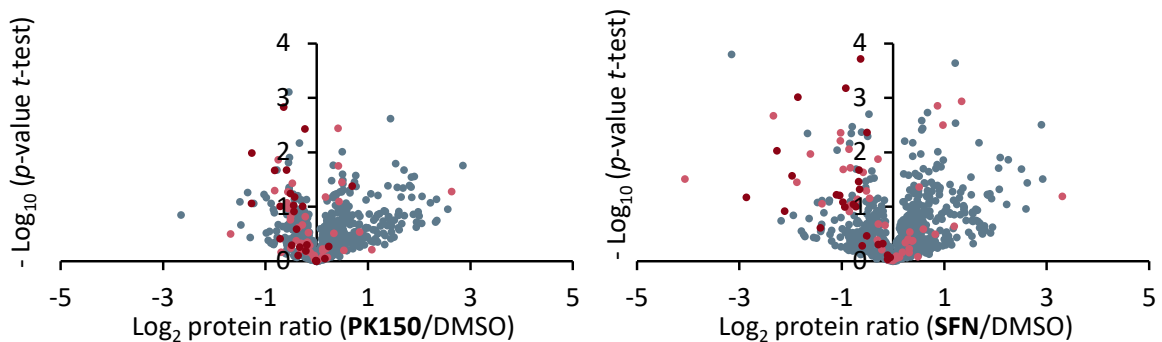


Figure 35: Secretome analysis. (A) Volcano plots showing log_2 fold changes of protein levels in the secretome after treatment of *S. aureus* NCTC 8325 cells with **PK150** (0.15 μM , 0.5 \times MIC, left panel) or **SFN** (1.5 μM , 0.5 \times MIC, right panel) compared to DMSO-treatment. (B) Log_2 fold changes of secreted proteins from cells treated with **PK150** or **SFN** compared to respective control compounds **PK150-C** (0.15 μM , left panel) and **SFN-C** (1.5 μM , right panel). Light red dots represent proteins that are predicted to have a SpsB signal peptide motif by PrediSi.²²¹ Dark red dots represent proteins, secretion of which has been found to be inhibited by arylomycin A-C₁₆ (experimentally proposed SpsB substrates).²²⁰ Data represent mean values; $n = 4$ independent experiments per group.

Taken together, these observations support the role of SpsB as a target of **SFN** and **PK150**. Furthermore, it can be concluded that the stimulation of SpsB cleavage activity is not limited to a single peptide substrate used in *in vitro* FRET-assays, but can be generally observed for the enzyme's endogenous substrates *in vivo* as well.

In previous studies, several SpsB- and Sec- dependent proteins have been identified in the surfaceome, which exert their actual functions unattached to the membrane.²²²⁻²²⁴ Therefore, the surfaceome might serve as a depot for secretory proteins, facilitating rapid adaption of cells to changing conditions by release of these proteins. To analyze the changes of surface proteins, **PK150**- and **SFN**-treated (0.5 × MIC) and washed bacteria were shaved with trypsin and analyzed via LC-MS/MS (Figure 36). Reduced abundance of SpsB substrate proteins was observed compared to DMSO- as well as to **PK150-C**- and **SFN-C**-treated cells indicating that SpsB might indeed directly deplete these proteins from the surface for their release into the secretome.

A Surfaceome (0.5 x MIC vs. DMSO)



B Surfaceome (0.5 x MIC vs. inactive control compounds)

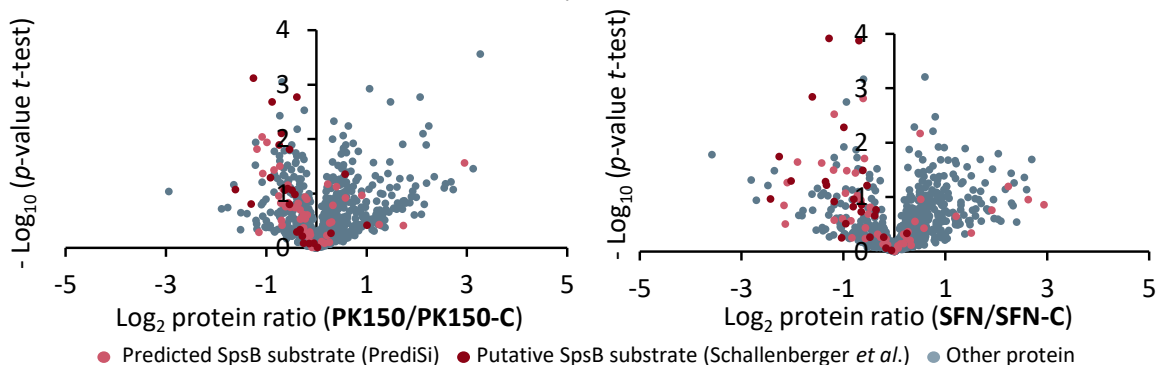


Figure 36: Surfaceome analysis. (A) Volcano plots showing log₂ fold changes of protein levels in the surfaceome after treatment of *S. aureus* NCTC 8325 cells with **PK150** (0.15 μM, 0.5 × MIC, left panel) or **SFN** (1.5 μM, 0.5 × MIC, right panel) compared to DMSO- treatment. (B) Log₂ fold changes of surface proteins from cells treated with **PK150** or **SFN** compared to respective control compounds **PK150-C** (0.15 μM, left panel) and **SFN-C** (1.5 μM, right panel). Light red dots represent proteins that are predicted to have a SpsB signal peptide motif by PrediSi.²²¹ Dark red dots represent proteins, secretion of which has been found to be inhibited by arylomycin A-C₁₆ (experimentally proposed SpsB substrates).²²⁰ Data represent mean values; *n* = 4 independent experiments per group.

2.2.6 Mode of Antibiotic Action

So far, MIC experiments had shown that **SFN** and **PK150** inhibit growth of gram-positive bacteria. Persister and biofilm assays furthermore indicated bactericidal activities of the compounds. A deeper investigation of their direct effect on cells was therefore conducted to elucidate the mode of the antibiotic action.

Antibiotic drugs are subdivided into two major groups, namely bacteriostatic drugs that inhibit bacterial growth until the drug is removed, and bactericidal drugs that kill > 99.9% of bacteria.²²⁵ Killing of bacteria can thereby be mediated via irreversible changes in the DNA, protein or membrane structures (e.g. quinolones, aminoglycosides, lipopeptides) or via lysis.^{226,227} The latter is mostly attributed to agents interfering with cell wall-modifying enzymes (e.g. β -lactams).^{226,228}

To elucidate the mode of action of **SFN** and **PK150**, time-kill assays were first performed using exponentially growing bacteria (Figure 37 A). Both compounds revealed rapid concentration-dependent killing kinetics using 1-, 2- and 8-fold MIC concentrations, with **PK150** achieving 99.9% killing efficiency slightly faster than **SFN**. To study bacteria that were arrested in growth, protein biosynthesis was inhibited by a 2-fold MIC concentration (i.e. 1 μ M) of the bacteriostatic antibiotic tetracycline, blocking the access of aminoacyl-tRNAs to the 30S ribosome (Figure 37 B).²²⁹ Again, killing was rapid and a 99.9% reduction was achieved slightly faster than for exponentially growing bacteria, indicating a synergistic effect between the compounds and tetracycline.

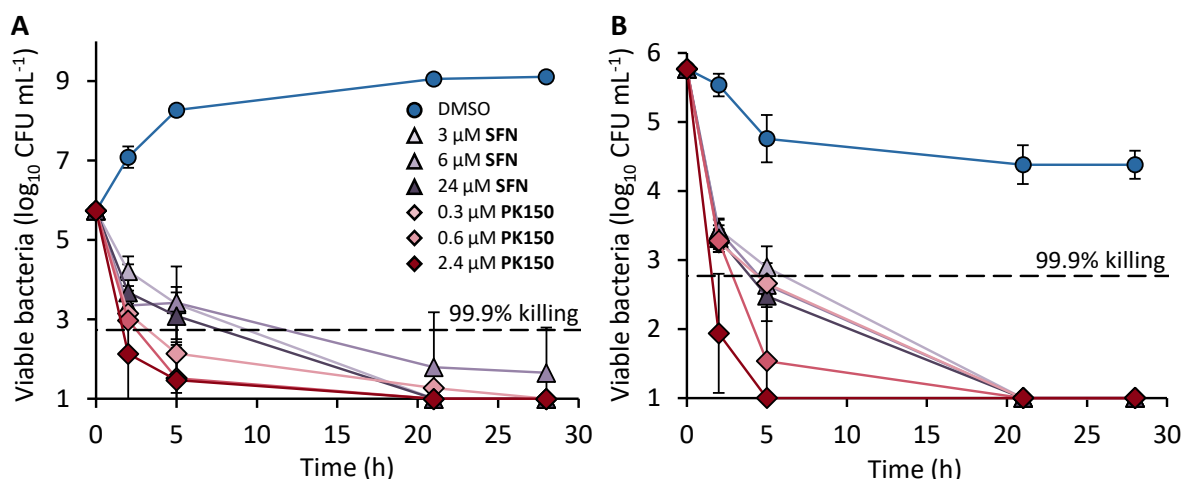


Figure 37: (A) Time-dependent killing of exponentially growing *S. aureus* NCTC 8325 by different concentrations of **SFN** and **PK150**. (B) Time-dependent killing of bacteria, arrested in growth by the addition of tetracycline at 2 \times MIC (i.e. 1 μ M) by different concentrations of **SFN** and **PK150**. Data represent mean values \pm SD ($n = 3$ per group). The dashed line represents 99.9% of killed bacteria.

In comparison to the persister cell assay (Chapter 2.1.5), killing was much faster here. This is due to the composition of cells in the starting cultures. Persisters were recovered from stationary cultures, containing 100% cells displaying the persister phenotype. In contrast to this, growth inhibition by tetracycline was conducted on a culture that was exponentially growing at the time of arrest, and therefore contained a smaller subpopulation of persister cells.

To reveal further hints on the antibiotic mechanism of **PK150**, cell morphology was studied by field emission scanning (FESEM) and transmission electron microscopy (TEM). For that, staphylococcal cells were treated with 8-fold MIC concentrations of **PK150** and **PK150-C** for 3 h (Figure 38 and Figure S7). Whereas cells treated with DMSO (Figure S7 A and B) as well as with the control compound **PK150-C** (Figure 38 A) showed round and smooth shape indicating a healthy state, **PK150**-treated cells showed strong deviations in cell appearance. Two main effects could be observed – 1) formation of extracellular vesicles (EVs) (Figure 38 B and Figure S7 D, E, F and I, arrows point to EVs) by protrusion of cytoplasmic membrane (CM) through gaps in the cell wall (CW) (Figure 38 E, F and Figure S7 I) and 2) lysis of cells (Figure 38 C, D and Figure S7 C, E, L and M, arrow heads point to damaged *S. aureus*). Furthermore, direct release of cytoplasmic material was observed (Figure 38 E and Figure S7 J).

For a long time, extracellular vesicles have been connected to gram-negative bacteria only as they have an outer membrane, from which EVs can be easily pinched off without having to cross a cell wall barrier. Additionally, such vesicles were either not observed under conditions investigated by EM or just overlooked in gram-positives. Only very recently, release of EVs has been shown to occur in gram-positive bacteria as well. The exact mechanism of their protrusion through the cell wall, however, is not known. One hypothesis is that the release is facilitated through loosening of the cell wall by enzymes that are capable of peptidoglycan hydrolysis.²³⁰ The perforation in the cell wall at sites of EV formation, as observed in electron microscopic images of cells treated with **PK150** (Figure 38 E, F), might be a result of peptidoglycan hydrolase activity. The mechanism seems to be out of control as peptidoglycan is disrupted at some sites of vesicle formation (Figure 38 F), likely resulting in release of the entire cytoplasmic content leaving cell wall relicts (Figure 38 D and Figure S7 E, L, M). In addition, the direct release of DNA was observed (Figure 38 E and Figure S7 K) which has been previously attributed to the activity of peptidoglycan hydrolases.^{231,232}

Lytic cell death mechanisms mainly comprise induction of lytic prophages, unspecific membrane permeabilization by surfactants such as saponins and antimicrobial lipopeptides,²³³ and interference with peptidoglycan synthesis by β -lactam and glycopeptide antibiotics.

Induction of prophages could be ruled out as a possible mechanism, as *S. aureus* NCTC 8325-4, a prophage-cured strain, exhibited the same MIC values for **SFN** and **PK150** (Table 5).

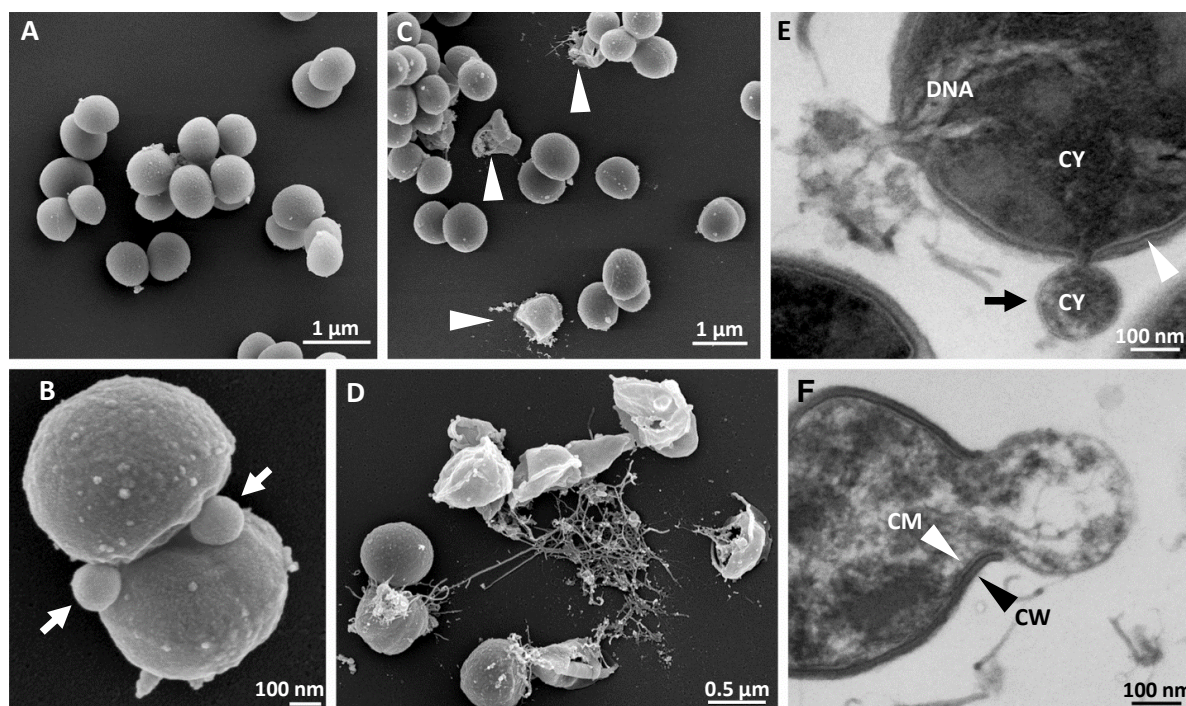


Figure 38: Electron microscopy. (A, B, C and D) Field emission scanning electron micrographs (FESEM) of *S. aureus* NCTC 8325 treated with the inactive control compound **PK150-C** (2.4 μM, A) or **PK150** (1.2 μM, B; 2.4 μM, C and D). Normally growing *S. aureus* cells can be observed for **PK150-C**- (A) as well as DMSO-treatments, whereas **PK150**-treated cells show deviations in cell appearance (B, C, D). Arrow heads point to damaged *S. aureus* (C). (B) Extracellular vesicles are formed, predominantly in the division zone of bacteria (arrows). (D) Lysis of cells and extrusion of DNA containing material. (E and F) Transmission electron micrographs (TEM) of *S. aureus* NCTC 8325 treated with 2.4 μM **PK150**. Formation of extracellular vesicles (black arrow heads cytoplasmic membrane of vesicle). DNA, Deoxyribonucleic acid; CY, cytoplasm; CM, cytoplasmic membrane; CW, cell wall.

Further, membrane permeabilizing properties of **SFN** and **PK150** were studied. In the performed assay, the DNA intercalator propidium iodide (PI) is trapped by intact membranes and released upon membrane permeabilization. It can then bind to DNA, and the resulting complex formation can be monitored via fluorescence intensity measurement (Figure 39). In contrast to the cationic surfactant benzalkonium chloride, which instantly led to PI-DNA complex formation through lysis, daptomycin treatment led to only a slight increase in fluorescence intensity. This is in agreement with published results, stating that lysis is a negligible effect in daptomycin-promoted cell death.²²⁷ Besides a similarly slight effect caused by the 8-fold MIC concentration of **SFN**, none of the other concentrations of the compounds showed an increase in fluorescence intensity, excluding a rapid, unspecific membrane disintegration and permeabilization as the cell killing mechanism.

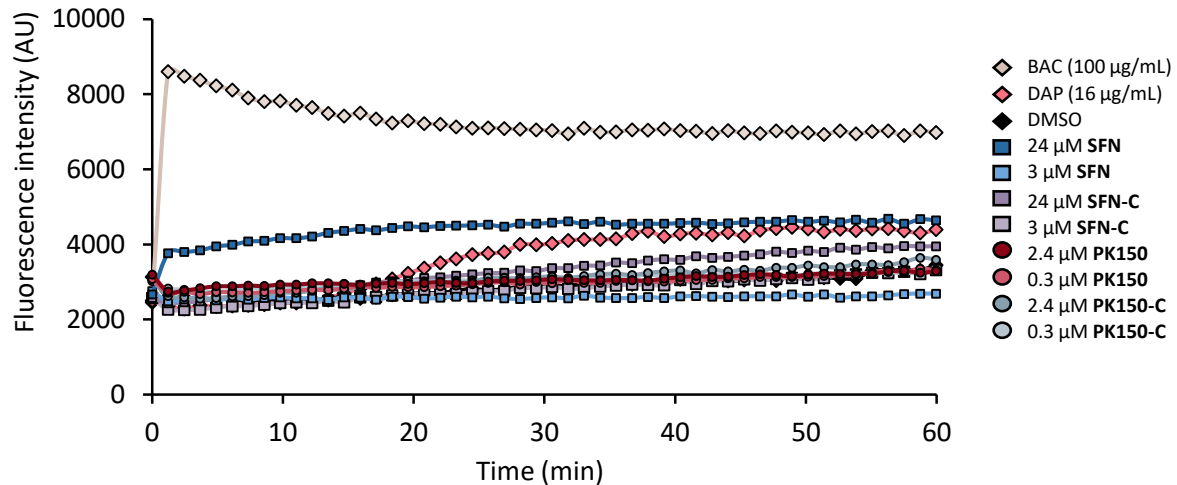


Figure 39: Examination of cell permeability via treatment of cells with propidium iodide (PI), which fluoresces at 617 nm (excitation at 535 nm) upon interaction with DNA. As positive controls, 100 µg/mL benzalkonium chloride (BAC) and 16 µg/mL daptomycin (DAP) + 50 µg/mL Ca^{2+} were used. Data represent mean measured values \pm SD ($n = 3$ per group, Note: error bars are smaller than symbols) and is representative for three biological replicates.

Beta-lactam antibiotics induce cell death via inhibition of penicillin-binding proteins (PBPs), enzymes that catalyze peptidic cross-linking of peptidoglycan units.²²⁶ A closer look into AfBPP-based target identification analysis revealed that three of the four staphylococcal penicillin-binding proteins are slightly enriched upon photoprobe treatment in comparison to DMSO as well as in the competition experiment (Figure 40). As enrichment ratios lie in the background area, it is unlikely that PBP-binding plays a major role in the antibiotic mechanism, but a contribution is possible.

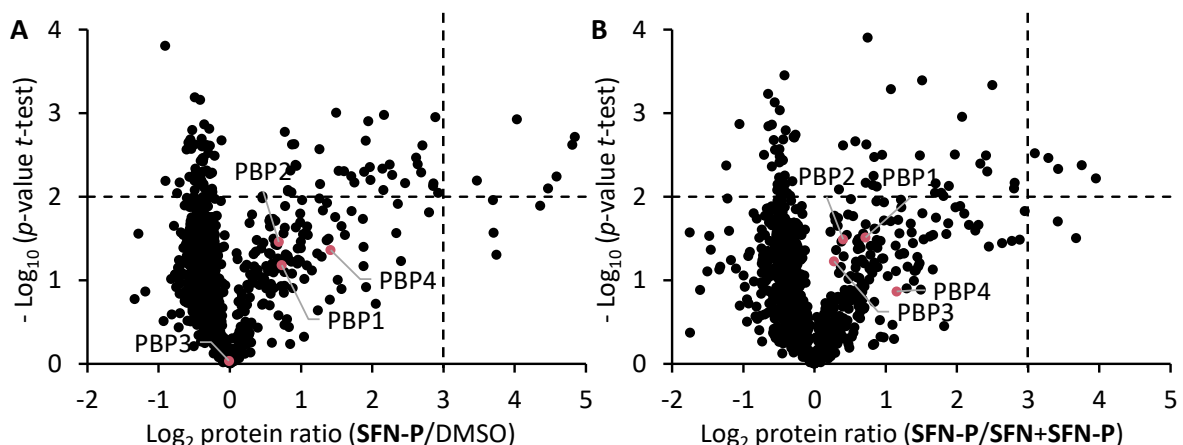


Figure 40: Volcano plots showing AfBPP target identification experiment. Depicted are the enrichments in the insoluble fraction fraction after treatment of *S. aureus* NCTC 8325 cells with SFN-P (50 µM) compared to DMSO (A) or to competition experiment with 500 µM SFN (B). Red dots represent penicillin-binding proteins. Data represent mean values; $n = 3$ independent experiments performed in triplicates.

2.2.7 SpsB and the Mode of Action

To obtain further insights into the mode of action and especially to elucidate the contribution of SpsB to the mechanism, a closer look into the secretome analyses was taken. As cell wall degradation and lysis were observed in electron micrographs, a deeper analysis was performed regarding a class of enzymes called autolysins. Autolysins are peptidoglycan (PG) hydrolases that break down the cell wall. Together with peptidoglycan synthases (i.e. penicillin-binding proteins) they play a major role in remodeling of the peptidoglycan network.^{234,235} Peptidoglycan hydrolase (PGH) domains catalyze different reactions and are thus classified according to their catalytic specificity. Major classes are *N*-acetylmuramidases and *N*-acetylglucosaminidases digesting the glycan backbone, *N*-acetylmuramoyl-L-alanine amidases, cleaving the bond between MurNAc and L-alanine, endo- and carboxypeptidases as well as lytic transglycosylases.^{222,236,237} Proteins measured in the secretomes were annotated as peptidoglycan hydrolases (PGHs) based on the presence of PGH-domains, as retrieved from the protein families (Pfam) database (see Table S13 for Pfam entries used for annotation).^{237,238} Table 12 gives an overview of the peptidoglycan hydrolases as identified in the secretomes.

Subsequently, annotation enrichment analysis was performed using Fisher's Exact test with proteins enriched in the secretome (\log_2 ratios higher than 0.5) against the whole secretome as background (Table 13 and Table S15). Proteins containing PGH-domains and signal peptides were significantly enriched in secretomes of **PK150**- and **SFN**-treated cells, whereas this was not the case for the control compounds **PK150-C** and **SFN-C**.

Regarding the destructive capacity of autolysins, their action requires a tight regulation, as their dysregulation and imbalance in relation to peptidoglycan-synthesizing proteins is known to cause cell lysis.^{226,239,240} One prominent example is the action of β -lactam antibiotics which inhibit penicillin-binding proteins, thus leading to lysis.²⁴¹ As the lytic activity of β -lactams can be suppressed by inactivation of some autolysins, it is assumed that proteins of this class are the cause for the disruption of cell walls.²²⁶ Their activities are regulated via several mechanisms. Most autolysins are synthesized as pre-proteins with Sec-type signal peptide sequences,²³⁴ thus requiring activation through SpsB-dependent cleavage. They are furthermore kept inactive by an acidic pH value at the *trans* side of the membrane maintained by the proton motive force,²³⁵ and are targeted to their sites of action via wall teichoic acids (WTAs)²⁴² and lipoteichoic acids (LTAs).²⁴³ Additionally, multienzyme complexes formed with PBPs coordinate the activities of synthesizing and hydrolyzing enzymes, thereby restricting the uncontrolled action of hydrolases.

Table 12: Peptidoglycan hydrolases, detected in the secretomes upon treatment with **PK150** and **SFN** compared to DMSO. Prediction of signal peptides by PrediSi is indicated in the column “SP” as “Y” or “N” for the presence or absence of a predicted signal peptide. The abbreviations of PGH classes can be found below the table. Furthermore enrichment ratios (PR = \log_2 protein ratio) and p -values (PV = $-\log_{10}$ p -value (t -test)) are given. Ratios with values > 0.5 are shaded in gray. For ratios retrieved from comparison of the inactive compounds **PK150-C** and **SFN-C** to DMSO see Table S14.

Protein IDs	Protein names	SP	PGH	PK150/ DMSO		SFN/ DMSO	
				PR	PV	PR	PV
O33599	Glycyl-glycine endopeptidase LytM	Y	P	0.98	1.08	0.99	1.46
Q2FV55	Staphylococcal secretory antigen SsaA	Y	CH	0.94	0.79	0.93	0.63
Q2G0D4	Secretory antigen SsaA-like protein	Y	CH; LM	0.74	1.94	0.93	2.20
Q2G222	N-acetylmuramoyl-L-alanine amidase domain-containing protein	Y	CH; GA	0.73	0.92	0.86	0.97
Q2G1W1	Secretory antigen SsaA, putative	Y	CH	0.66	0.70	0.86	0.81
Q2FWF8	Probable TG SceD	Y	TG	0.60	0.63	0.58	0.50
Q2G0U9	N-acetylmuramoyl-L-alanine amidase sle1	Y	CH; LM	0.56	0.54	0.64	0.65
Q2G190	Putative uncharacterized protein	Y	CH	0.55	1.72	0.57	1.53
Q2G2J2	Staphylococcal secretory antigen ssaA2	Y	CH	0.54	0.46	0.34	0.22
Q2FV52	Probable TG IsaA	Y	TG	0.53	0.78	0.77	1.29
Q2FX77	Autolysin	N	CH	0.42	0.77	0.48	0.87
Q9ZNI1	Probable cell wall hydrolase LytN	Y	CH; LM	0.42	0.41	-0.12	0.10
Q2FZK7	Bifunctional autolysin	Y	GA	0.42	0.83	0.03	0.03
Q2FV81	LM domain protein	N	CH	-0.13	0.11	0.01	0.01
Q2FYL3	Putative uncharacterized protein	N	PB	-0.57	0.38	0.67	0.29
Q2FVW2	N-acetylmuramoyl-L-alanine amidase, putative	N	GA	-0.70	0.92	0.29	0.12
Q2FXF4	Putative uncharacterized protein	N	GA	-1.75	0.67	-0.83	0.61

SP, Signal Peptide predicted (by PrediSi), Y=yes, N=no; PGH, peptide hydrolase domain; CH, CHAP; GA, Glucosaminidase; LM, LysM; P, Peptidase; TG, Transglycosylase; PB, Putative peptidoglycan binding; PR, \log_2 protein ratio; PV, $-\log_{10}$ p -value (t -test)

The observed changes in the secretome upon **PK150**- and **SFN**-treatments likely cause a dysregulation of the homeostatic protein balance. With respect to the multitude of mechanisms controlling PGH activities, it is possible that imbalances in levels of autolysins like glycyl-glycine endopeptidase LytM (O33599), staphylococcal secretory antigen SsaA (Q2FV55), secretory antigen SsaA-like protein (Q2G0D4) and N-acetylmuramoyl-L-alanine amidase domain-containing protein (Q2G222) (Table 12) are responsible for peptidoglycan degradation and lytic events observed in electron micrographs.

To directly investigate the changes in autolysin activities upon **SFN**- and **PK150**-treatments, zymography-based analysis was conducted (Figure 41). Polyacrylamide gels used for zymography-assays contain autoclaved *S. aureus* cells, giving the gels a turbid appearance. After separation of protein extracts using these gels, proteins are re-natured and enzymes with autolytic activities are re-activated. Active autolysins degrade peptidoglycan of embedded cells resulting in clear bands. For

zymographic analysis, *S. aureus* NCTC 8325 cells were treated for 1.5 h with 8-fold MIC concentrations of active and inactive compounds as well as penicillin G for comparison. Extracellular and cell wall-bound protein extracts were prepared by concentration of the supernatants and by the freeze-thaw method, respectively. The antibioticly active compounds **PK150** and **SFN** revealed a characteristic induction of several hydrolytic enzymes in the higher molecular weight (MW) range, whereas hydrolytically active enzymes in the lower molecular range showed a decrease in autolysis. In contrast to that, the inactive compounds **PK150-C** and **SFN-C** revealed the same band pattern as DMSO. Penicillin G resembled the activity of **PK150** and **SFN** in the higher molecular range, indicating that the autolytic response could be similar for this antibiotic class.

Table 13: Enrichment analysis of peptidoglycan hydrolase domain-containing proteins (Pfam annotations: CHAP domain, LysM domain, amidase, transglycolase, glucosaminidase and peptidase M23 domain) using Fisher's exact test. Proteins with a \log_2 -fold enrichment of > 0.5 for compound- vs. DMSO-treatment were tested against the whole secretome as the background. See Table S15 for **PK150/PK150-C** and **SFN/SFN-C** analyses.

Category	Proteins with \log_2 protein ratio > 0.5				Secretome
	PK150/ DMSO	SFN/ DMSO	PK150-C/ DMSO	SFN-C/ DMSO	
Total proteins	83	121	46	45	806
„PGH domain AND predicted signal peptide“ proteins	10	9	0	1	12
Not „PGH domain AND predicted signal peptide“ proteins	73	112	46	44	794
Fisher's Exact <i>p</i> -value (Secretome as background)	<0.0001	0.0006	1.0000	0.5091	

The regulation of autolysin-activity is a complex, multifaceted system. An involvement of the LytSR two-component system, for example, has been shown to have inhibitory functions via the operon *IrgAB*, whereas expression of the *cidAB* operon was found to act in the opposite way.^{244–246} Interestingly, in a previous work by Brunskill *et al.*, an insertional disruption of *lytS* has led to a similar zymographic pattern as observed for **PK150**- and **SFN**-treated cells,²⁴⁵ indicating similar outcomes for a genetic dysregulation of autolysin activities as well as the chemical one by **PK150** and **SFN**. Taken together, the results suggest that an imbalance of the fine-tuned homeostasis of autolysins might play a role in bactericidal effects of **PK150** and **SFN**.

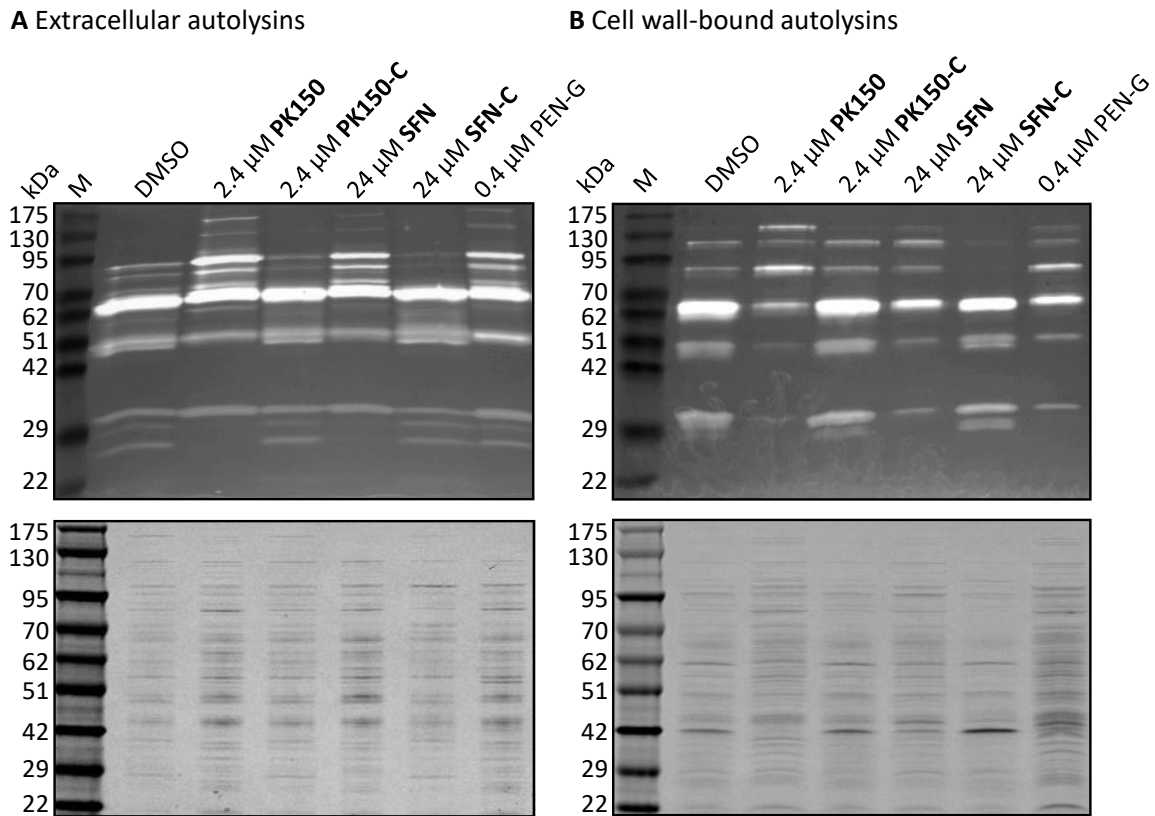


Figure 41: Zymography of protein extracts after treatment of *S. aureus* NCTC 8325 cells with **PK150** (2.4 μ M, 8 \times MIC), **SFN** (24 μ M, 8 \times MIC) and penicillin G (PEN-G, 0.4 μ M, 8 \times MIC) as well as with control compounds **PK150-C** (2.4 μ M), **SFN-C** (24 μ M) and DMSO. (A) Zymogram (upper panel) and coomassie-stained gel as loading control (lower panel) of extracellular protein extracts. (B) Zymogram (upper panel) and coomassie-stained gel as loading control (lower panel) of cell-wall bound protein extracts. Clear bands in zymograms indicate peptidoglycan hydrolase activity.

Briefly summarized, **PK150** causes rapid cell death, which is accompanied by the release of DNA, protrusion of EVs and lysis. These effects are most likely provoked by imbalances in protein secretion caused by a dysregulation of SpsB. Enrichment and zymography analyses indicate a role of autolysins in these processes. In the case of β -lactams, cell death is connected to the inhibition of peptidoglycan-synthesizing enzymes leading to imbalances in autolysin activities and ultimately to cell lysis.²²⁶ Similarly, the dysregulation of autolysin secretion might be the cause for cell death upon **PK150**-treatment.

3 Conclusions and Outlook

The imminent risk of losing effective antibiotic therapies, as resistances continue to rise rapidly, strongly demands the identification of novel chemical scaffolds addressing unprecedented and therefore resistance-free targets.^{2,4,247} Repurposing of available scaffolds to distinct indication areas is an attractive strategy for identification of lead structures addressing novel targets. In the present work, a panel of human kinase inhibitors was screened to evaluate the antibiotic potency of this drug class in the pathogen *Staphylococcus aureus*. Sorafenib and regorafenib, two structurally similar and approved multikinase inhibitors, exhibited good antibiotic activity with MIC values of 3 μ M. During the course of the presented work, other groups have corroborated this finding.^{141,176}

The optimization potential within the novel indication area as an antibiotic was analyzed using a library of 72 **SFN** derivatives. The chemical dissection of the scaffold via structure-activity relationship analysis revealed the 4-chloro-3-(trifluoromethyl) phenyl moiety as indispensable for antibiotic activity, whereas modifications in the heteroaryl ether were largely tolerable. One compound of the library, **PK150**, stood out in the phenotypic screen, exhibiting an MIC of 300 nM. The antibiotic potency of this compound was thus ten times higher than of the parent compound **SFN**. **PK150** was active against a panel of gram-positive bacteria, including multidrug-resistant *S. aureus* strains, *Mycobacterium tuberculosis* and vancomycin-resistant enterococci. In gram-negative bacteria, however, no growth inhibition could be observed. As discovery of new antibiotics against resistant pathogens of this class, especially *Acinetobacter baumannii* and *Pseudomonas aeruginosa*, is most urgently required,⁴ it should be further investigated in order to reveal both the cause of and the possibilities to overcome this lack of activity.

The fact that **PK150** was developed based on an already approved drug with optimized pharmacokinetic properties, turned out to be beneficial. Drug-like properties such as plasma stability and toxicity were in a similar range as for **SFN**. Although the optimization of **SFN** to **PK150** resulted in a loss of affinity to human kinases, cell toxicity only slightly changed. This result indicates that **PK150** addresses other off-targets in human cells. The elucidation of their identities is therefore an interesting future task. Despite the similar toxicity, **PK150** exhibited a stronger antibiotic potency than **SFN** and thus provided a suitable therapeutic window for the novel indication area as an antibiotic. *In vivo* pharmacokinetic and -dynamic analyses revealed that the small molecule exhibits good oral bioavailability and is furthermore effective in reducing bacterial loads in heart and lung in a mouse bloodstream infection model. This is especially interesting as *S. aureus* -induced endocarditis and pneumonia are two hard-to-treat infection variants. As VRE can cause even more severe endocarditis,

an investigation of *in vivo* efficacy regarding this pathogen is a highly desirable experiment for the future.

Strikingly, there was no *in vitro* resistance detected for **PK150** in contrast to **SFN**, which acquired resistance rapidly. Moreover, activity against several multi-drug resistant *S. aureus* isolates suggested the absence of cross-resistances to **PK150**, indicating a novel mechanism of action. **PK150** furthermore exhibited excellent activity in reducing clinically challenging persister cells.²⁴⁸ In addition, established biofilms, which are largely composed of persister cells,⁶⁸ could be successfully eradicated at concentrations that were in the same range as for best known biofilm eradicators to date.¹⁶⁴ Taken together, these are outstanding characteristics of **PK150**, considering the current antibiotic-resistance crisis and the difficulties in treatment of antibiotic-tolerant phenotypes.²⁴⁹

Although **PK150** already exhibits promising drug-like properties, further medicinal chemistry studies are required to optimize solubility and toxicity of the molecule to enable its further development as a drug candidate. The focus of the present work was set on *S. aureus*. However, as antibiotic activity could be shown for other clinically highly relevant pathogens, such as mycobacteria and VRE, the potential of **PK150** as a drug candidate should be further evaluated regarding these organisms.

As mentioned previously, the antibiotic activity of **SFN** has been recognized by other groups. Although Roberts *et al.*¹⁷⁶ suggested the protein DnaK as a target of **SFN** in bacteria, this assumption was mainly based on homology to a human target. No detailed analysis of the antibiotic mechanism of **SFN** had been performed to date. Thus, target identification using a gel-free quantitative affinity-based protein profiling strategy was the starting point for the elucidation of the antibiotic mechanism in the present work. A **SFN**-based photoprobe revealed binding to several proteins. For the most enriched target candidates, their corresponding transposon mutants were screened for MIC shifts. Only one mutant, that of the gene coding for a protein with unknown function (Lrp), revealed a slight MIC shift upon **SFN**-treatment. The strongest hit of the proteomic analysis was the essential protein SpsB. Therefore, this enzyme was chosen for a closer analysis as a putative target of **SFN** and **PK150**. Interestingly, although **SFN** is a multikinase inhibitor in human cells, no known bacterial protein kinase was identified as a significant target. SAR studies revealed that the pyridine moiety, important for kinase binding, is dispensable for antibiotic activity. This might be a hint that the bioactivity of **SFN**-related compounds in human and bacterial cells is resulting from addressing structurally different classes of proteins.

For validation of SpsB as a target, the enzyme was recombinantly overexpressed in *E. coli* and binding was confirmed in a gel-based *in situ* labeling as well as in competition experiments. Competitive labeling furthermore revealed that **PK150** was also binding to the same target site as **SFN** and the photoprobe, indicating that SpsB is a target of **PK150** as well. FRET-based activity assays with the purified protein showed concentration-dependent changes in substrate cleavage rates for both

compounds, **SFN** and **PK150**. Similar results were obtained with *S. aureus*- and *E. coli*-membranes containing endogenous and overexpressed SpsB, respectively. Interestingly, not an inhibition, but a stimulation of activity was observed. The maximum increase in activity was higher for **PK150** (2.9-fold) than for **SFN** (1.7-fold), reflecting the stronger antibiotic activity. Docking and molecular dynamics experiments corroborate a binding of **PK150** to the protein. The identified binding position adjacent to the substrate binding pocket, is in agreement with the observed stimulating effect, as **PK150** does not block the substrate binding site. The studies furthermore revealed a rigidification of the active site that might trap the protein in an active and uncontrollable state, which is likely responsible for the stimulation of proteolytic turnover.

As SpsB plays a major role in secretion of proteins by cleaving off signal peptides of translocated proteins, an analysis of the secretome was conducted. Treatment with **SFN** and **PK150** led to an accumulation of SpsB-substrate proteins in the extracellular medium. This observation suggests that the activation of SpsB by **SFN** and **PK150** *in vitro* is also true for the *in vivo* situation, supporting the target hypothesis. While inhibition of SpsB had been described previously,^{55,56} results presented in this work showed an activation mechanism for this enzyme for the first time.

Further analysis of the antibiotic mode of action revealed that **PK150** was bactericidal, rapidly killing exponentially growing bacteria as well as bacteria that had been arrested in growth by a second bacteriostatic antibiotic. A highlight of the bactericidal action was the above mentioned killing of persister cells. Previously, a stimulation of another protease, the caseinolytic peptidase ClpP, by acyldepsipeptides (ADEPs) has been shown to kill cells of this phenotype.¹⁶⁰ In contrast to the inhibition of enzymes in growing cells, a stimulation of enzymes in dormant cells might thus represent a generally applicable strategy to cause a dysregulation of cellular physiology, which is sufficient for cell death.

Tracking down the destructive effects of dysregulated secretion to single molecules, however, is a challenging task. For further clues about the killing mechanism, a closer inspection of the secretome was performed. Peptidoglycan-hydrolyzing enzymes were significantly enriched among secreted proteins. It is thus possible that a dysregulation of these proteins leads to an imbalance in the homeostasis between peptidoglycan-synthetizing and –degrading enzymes, resulting in cell death, similarly to the action of β -lactam antibiotics. In line with this, electron microscopic images revealed the protrusion of extracellular vesicles, ruptures in the cell wall, release of DNA and lysis of cells, processes that have been previously associated with the activity of autolysins.^{230,231,250–252} Zymography analyses revealed changed autolysin activities, supporting this hypothesis. Thus, in contrast to the SpsB inhibitor class of arylomycins that are believed to kill cells via an accumulation of unprocessed proteins in the membranes,¹⁸⁸ here the opposite mechanism, a stimulation-induced dysregulation of secretion, seems to be the cause of cell death. The exact mechanism and a detailed involvement of autolytic enzymes, however, remain to be deciphered in future studies.

As SpsB is essential and no knockout strain is available, the demonstration of a direct link between SpsB and the phenotypic effect was challenging. A strain that bypasses the essentiality of SpsB by overexpressing an ABC transporter, did not show a MIC-shift upon compound treatment. However, the strongly differing phenotype of this strain precluded final conclusions. With respect to this, it cannot be excluded that other targets might be responsible for the antibiotic effect. Therefore, further investigations regarding the involvement of SpsB in the antibiotic mechanism are required.

PK150 is very likely a polypharmacological compound. The involvement of other targets is indicated by a lack of resistance development against this compound. Multiple targeting strongly reduces the probability that a bacterium establishes protective mechanisms against several points of attack simultaneously. This strategy has recently started to gain more attention in the scientific community, as the problem of rapid resistance development for specific single-target drugs was recognized.^{253,254} The majority of drugs against human targets address several proteins, on average six per compound.²⁵⁵ It is thus likely that a compound derived from a human kinase inhibitor has several targets in bacteria as well. Correlation analysis of MIC values vs. stimulation of SpsB revealed that although some **SFN**-related derivatives showed low stimulatory effects on SpsB, they were nevertheless good inhibitors of antibiotic growth, supporting the existence of further targets for the class of **SFN**-related compounds. The phenomenon of multiple targeting might also be responsible for the higher antibiotic potency of **PK150** compared to **SFN**.

AfBPP experiments revealed a panel of other putative targets, which could be involved in the antibiotic mechanism. Foremost, lytic regulatory protein (Lrp) is an interesting candidate for further investigation as its respective transposon revealed a slight MIC shift. Additionally to the putative targets identified by AfBPP studies here, further target deconvolution experiments could be helpful to reveal other proteins that might play a role in the antibiotic mechanism. As the scope of identifiable targets is limited to the experimental methodology, variation in conditions could be applied to extend the search space. This can be conducted, for example, by designing probes with slightly modified scaffolds or variations in several steps of the identification workflow, including analysis of different growth phases. Additionally, alternative target identification strategies that do not rely on a probe could be applied, such as thermal proteome profiling.²⁵⁶ Finally, non-protein targets, such as peptidoglycan, should be taken into consideration for further analysis of the antibiotic mechanism.

In conclusion, the present work revealed **PK150** as a novel potent **SFN**-derived antibiotic compound. Its antibacterial scope and promising pharmacokinetic and –dynamic properties render the compound an ideal candidate for the further optimization towards a therapeutic drug against clinically challenging gram-positive pathogens. The current antimicrobial resistance crisis emphasizes the value of **PK150** even more as it is active against multi-drug resistant *S. aureus* and does not provoke *in vitro* resistance.

Further highlights of **PK150** potency are the eradication of persisters and biofilms. SpsB emerged as the most promising target candidate in this study. Mechanistic analyses suggest a hypothesis regarding the mode of action, in which **PK150** binds into a pocket of SpsB adjacent to the substrate binding pocket, thereby rigidifying the active site and constraining the enzyme in an active state. This leads to a stimulated cleavage activity of SpsB resulting in the triggered release of its substrates into the extracellular space. This dysregulation of secretion overwhelms the bacterial physiology and rapidly leads to bacterial cell death. Involvement of autolysins is likely responsible for the observed lytic events. The final validation of this mechanistic hypothesis, especially regarding the link between SpsB and the antibiotic activity, remains object to further investigation. Additionally, interesting aspects for future studies is the contribution of other targets to the antibiotic mode of action, as well as the roles of autolysins in the bactericidal mechanism.

4 Materials and Methods

4.1 Microbiology

4.1.1 Bacterial Strains and Media

Table 14: Bacterial strains, sources, and respective cultivation media.

Species/ Risk group	Strain	Source	Medium*
<i>Escherichia coli</i> / S1	BL21(DE3)pLysS		LB
<i>Bacillus subtilis</i> / S1	168	ATCC	LB
<i>Staphylococcus aureus</i> / S2	ATCC 33591	ATCC	
	ATCC 33592	ATCC	
	DSM-18827	DSMZ	B
	Newman	Prof. Olaf Schneewind ¹	B
	NCTC 8325	Institute Pasteur, France	B
	NCTC 8325	DSMZ	TSB
	NCTC 8325-4	Prof. Knut Ohlsen ¹	B
	Mu 50	Institute Pasteur, France	B
	SH1000		
	USA300		
	FPR3757	ATCC	B
	USA300-0114		TSB
	USA300 Transposon Library	NTML by NARSA	B + 5 µg/mL erythromycin
	N315	Prof. Floyd Romesberg ³	B
clinical isolates	BK95395		B
	BK97296		B
	IS050678		B
	IS050611		B
	VA417350	Prof. Markus Gerhard ⁴	B
	VA418879		B
	VA402923		B
	VA412350		B
	VA409044		B
<i>Enterococcus faecalis</i> / S2	ATCC 47077	ATCC	BHB
	ATCC 700802	ATCC	BHB
<i>Enterococcus faecium</i> / S2	DSM-17050	DSMZ	TSB
	DSM-20477	DSMZ	TSB
<i>Listeria monocytogenes</i> / S2	EGD-e	Institute Pasteur, France	BHB

	F2365	BCCM/LMG	BHB
<i>Mycobacterium bovis</i> / S2	BCG		7H9
<i>Mycobacterium smegmatis</i> / S2	mc ² 155	ATCC	7H9
<i>Mycobacterium tuberculosis</i> / S3	H37Rv	ATCC	7H9-OADC
<i>Acinetobacter baumannii</i> / S2	DSM-30007	DSMZ	BHB
<i>Enterobacter aerogenes</i> / S2	DSM-30053	DSMZ	BHB
<i>Enterobacter cloacae</i> subsp. <i>Cloacae</i> / S2	DSM-30054	DSMZ	BHB
<i>Escherichia coli</i> / S2	CFT073	Dr. Guiseppe Magistro ⁵	LB
<i>Klebsiella pneumoniae</i> / S2	DSM-30104	DSMZ	BHB
<i>Pseudomonas aeruginosa</i> / S2	DSM-19882	DSMZ	BHB
<i>Salmonella typhimurium</i> / S2	LT2	Chair of Biochemistry, Genetics and Microbiology ⁶	LB
	TA100		LB
<i>Salmonella enteritides</i> / S2	veterinary isolate (dog)		LB

ATCC, American Type Culture Collection, USA; DSMZ, Deutsche Sammlung von Mikroorganismen und Zellkulturen, Germany; NTML, Nebraska Transposon Mutant Library; NARSA, Network on Antimicrobial Resistance in *Staphylococcus aureus*; BCCM/LMG, Belgian Coordinated Collections of Microorganisms/Laboratory of microbiology, Belgium.

¹The University of Chicago, Chicago, IL, USA; ²Institut für Molekulare Infektionsbiologie, Würzburg, Germany; ³The Scripps Research Institute, La Jolla, CA, USA; ⁴Institute of Medical Microbiology and Immunology, Technische Universität München, Germany; ⁵Department of Urology, Hospital of the Ludwig-Maximilians-Universität München, Germany; ⁶University of Regensburg, Germany; *unless otherwise stated

Table 15: Composition of media for the cultivation of different bacterial strains.

Name of the medium	Composition
B	10 g/L casein peptone 5 g/L NaCl 5 g/L yeast extract 1 g/L K ₂ HPO ₄ pH 7.5
BM, Basic Medium	10 g/L casein peptone 5 g/L NaCl 5 g/L yeast extract 1 g/L glucose 1 g/L K ₂ HPO ₄ pH 7.5
LB, Lysogeny Broth	10 g/L casein peptone 5 g/L NaCl 5 g/L yeast extract pH 7.5
BHB, Brain Heart Infusion Broth	7.5 g/L brain infusion 10 g/L heart infusion 10 g/L casein peptone 5 g/L NaCl 2.5 g/L Na ₂ HPO ₄ 2 g/L glucose pH 7.4

TSB, Tryptic Soy Broth	17 g/L casein peptone (pancreas hydrolysate) 3 g/L soy peptone (papain hydrolysate) 2.5 g/L K ₂ HPO ₄ 5 g/L NaCl 2.5 g/L glucose pH 7.3
7H9	4.7 g/L 7H9 (0.5 g/L ammonium sulfate, 2.5 g/L Na ₂ HPO ₄ , 1 g/L KH ₂ PO ₄ , 0.5 g/L L-glutamic acid, 0.1 g/L sodium citrate, 0.05 g/L MgSO ₄ , 0.04 g/L ferric ammonium citrate, 1 mg/L pyridoxine, 1 mg/L ZnSO ₄ , 1 mg/L CuSO ₄ , 0.5 mg/L CaCl ₂ , 0.5 mg/L biotin) 2 mL/L glycerol 2.5 mL/L 20% Tween 80 5 g/L BSA 2 g/L dextrose 0.85 g/L NaCl 3 mg/L catalase pH 6.8
7H9-OADCC	7H9-medium 25 mg/L oleic acid
MHB, Mueller-Hinton Broth	2 g/L beef infusion solids 17.5 g/L casein hydrolysate 1.5 g/L starch pH 7.4
SOC, Super Optimal broth with Catabolite repression	20 g/L yeast extract 5 g/L tryptone 0.5 g/L NaCl 0.2 g/L KCl 1 g/L MgCl ₂ 1.2 g/L MgSO ₄ 3.6 g/L glucose, pH 7.3

4.1.2 Cultivation Methods

All methods concerning bacteria were performed under sterile conditions with sterilized materials and equipment. Pathogenic bacteria of the biosafety/risk level two (S2) were handled in a specialized S2-laboratory in a safety workbench.

Cryostocks

Cryostocks were prepared by picking three single colonies from agar plates (prepared from master cryostocks) and cultivating them in the corresponding medium over night (16 h) at 37 °C and 200 rpm. Cells were harvested by centrifugation (6000 × g, 10 min, 4 °C) and pellets were resuspended in ¼ of the initial culture volume in 1:1 mixture of the respective buffer plus glycerol. The stocks were aliquoted and stored at -80 °C.

Overnight Cultures

Overnight cultures were prepared by inoculation of medium at a 1:1000 ratio with an aliquot of the cryostocks. The cultures were incubated for 16 h at 37 °C and 200 rpm. Once thawed, residual aliquot was discarded. Uninoculated medium was used as control.

4.1.3 Determination of Minimum Inhibitory Concentration (MIC)

The minimum inhibitory concentration (MIC) represents the lowest concentration of an antibiotic that will inhibit the visible growth of a microorganism after 24 h of incubation. Assays were performed in a 96-well plate-based format (transparent Nunc 96-well flat bottom, *Thermo Fisher Scientific*) with serial dilutions of the compounds tested. In case of *Staphylococcus aureus*, B medium was inoculated with a bacterial overnight culture (1:100) and incubated at 37 °C with gentle shaking (200 rpm) until the cultures reached an OD₆₀₀ of 0.4 – 0.6. Colony forming units (CFU)/mL were calculated according to the formula $CFU/mL = 4 \times 10^7 \times e^{(1.0958 \times OD_{600})}$ and bacteria were diluted to a concentration of 10⁵ CFU/mL in fresh medium. For all other bacterial species tested, medium was inoculated from corresponding bacterial overnight cultures (1:10000) and directly used for testing. Compounds at various concentrations were added to the diluted bacterial cultures (1:100, 100 µL/well final volume; final assay concentration of DMSO from compound stocks was 1%). All measurements were done in triplicates. A growth control containing DMSO only and a sterile control containing fresh medium were included. Plates were sealed with parafilm to avoid evaporation. After incubation at 37 °C with gentle shaking (200 rpm) for 16 - 24 hours, dilution series were analyzed for microbial growth, usually indicated by turbidity and/or a pellet of bacteria at the bottom of the well. The lowest concentration in the dilution series at which no growth of bacteria could be observed by eye was defined as the minimum inhibitory concentration (MIC) of the compound. MIC values were determined by three independent experiments.

For cultivation of transposon mutants, precultures were grown under addition of 5 µg/mL erythromycin, while the MIC assay was performed without the use of antibiotics to avoid interfering effects.

For *M. bovis* and *M. tuberculosis* strains, the MIC value was determined as follows: A culture of stationary phase growing bacteria was diluted to a final OD₆₀₀ = 0.001 in 7H9 media (7H9 media for *M. bovis* and 7H9-OADC for *M. tuberculosis*; note that for MIC determination media did not contain Tween 80). Diluted bacteria (100 µL/well) were added to the wells of a sterile 96-well microtitre plate containing two-fold serial dilutions of the respective compound in growth medium (100 µL/well). Control wells were prepared with culture medium and bacterial suspension only. The microtitre plates

were sealed with a water-impermeable membrane and incubated at 37 °C. To determine the growth of mycobacteria, a 0.02% resazurin solution (100 µL/well) was added (after 5 - 7 days for *M. tuberculosis*). A color change from purple to pink within 2 to 4 days indicated viable cells, while purple colored wells suggested no bacterial growth. MIC values were determined by three independent experiments.

4.1.4 Resistance Development Assay

The resistance development assay was based on a procedure previously published by Ling *et al.*⁷⁹. For resistance development by sequential passaging, exponentially growing *S. aureus* NCTC 8325 was diluted 1:100 in MHB medium (1 mL) containing various concentrations of **SFN**, PK150 or ofloxacin as positive control, as well as DMSO or 0.1 M NaOH as growth controls (final assay concentration of DMSO from compound stocks was 1%). Bacteria were incubated at 37 °C, 200 rpm, and passaged in 24 h intervals in the presence of **SFN**, **PK150** or ofloxacin at different concentrations (0.25 ×, 0.5 ×, 1 ×, 2 ×, 4 × MIC). Cultures from the second highest concentrations that allowed growth ($OD_{600} \geq 3$) were diluted 1:100 into fresh media (1 mL) containing again the different concentrations of the respective antimicrobial compound (0.25 ×, 0.5 ×, 1 ×, 2 ×, 4 × MIC). If a shift in MIC levels was observed, concentrations of the respective antimicrobial were adjusted accordingly for the following passaging. This serial passaging was repeated for 27 days and in two independent biological replicates. The MIC shifts were calculated by dividing the respective daily MICs by the initial MIC on day 1.

4.1.5 Persister Cell Assays

As the generation and treatment of persister cells is highly dependent on the conditions and there is no consistency in the scientific community⁶³, two assays using different conditions were performed.

Persister Cell Assay №1

Persister cell assay №1 was based on a procedure by Conlon *et al.*¹⁶⁰ and Kim W *et al.*¹⁵⁶, with modifications. *S. aureus* NCTC 8325 cells were inoculated from an exponentially growing culture ($OD_{600} = 0.4 - 0.5$, 1:1000) into tryptic soy broth and grown at 37 °C, 200 rpm for 15 h. Cells were serially diluted and plated on agar plates to determine cell numbers before treatment. Persisters were prepared by treatment with gentamicin (20 µg/mL, 40 × MIC in *S. aureus* NCTC 8325) at 37 °C, 200 rpm for 4 h. An H₂O-treated control culture was incubated in parallel. Persisters (and control cells) were washed three times with PBS (5,000 × g, 5 min) and diluted to $OD_{600} = 4$ in PBS. Serial dilutions were prepared for plating and determination of CFU/mL. **PK150** (2.4 µM, 8 × MIC), **SFN** (24 µM, 8 × MIC) or ciprofloxacin (5 µg/mL, 20 × MIC) as negative control were added to 10 mL aliquots of the diluted

persisters in 100 mL flasks (1:1000, final assay concentration of DMSO from compound stocks 1%) and incubated at 37 °C, 200 rpm for 70 h. At indicated time points, samples (1 mL) were withdrawn and corresponding bacteria harvested (10,000 × g, 3 min), washed with PBS (1 mL) and resuspended in PBS (1 or 0.1 mL) for the determination of CFU/mL by plating. Three biological replicates were prepared and means, standard deviations and *p*-values (unpaired parametric *t*-test) were determined with Prism (GraphPadPrism v6.05, GraphPad Software).

Persister Cell Assay №2

Persister cell assay №2 was based on a procedure by Springer *et al.*¹⁵⁵. Tryptic soy broth (50 mL in 250 mL culture flasks) was inoculated at a 1:1000 ratio with an overnight culture of *S. aureus* NCTC 8325 and grown at 37 °C, 200 rpm to OD₆₀₀ = 4 or for 20 h (OD₆₀₀ = 11). Serial dilutions were prepared and plated on agar plates to determine the cell numbers of the inoculum. The cultures were aliquoted (á 1 mL) and treated with ciprofloxacin (CIPRO, 5 µg/mL, 20 × MIC) or compounds to be tested (**PK150** or **PK150 -C**, 2.4 µM, 8 × MIC; **SFN** or **SFN-C**, 24 µM, 8 × MIC) with and without addition of oxacillin (30 µg/mL, 30 × MIC). for 20 or 70 h at 37 °C and 200 rpm. Cells were then harvested, washed two times with PBS (10,000 × g, 3 min), serially diluted, and plated for determination of surviving cell numbers.

4.1.6 Biofilm Assays

Minimum Biofilm Eradication Concentration (MBEC)

Overnight cultures of *S. aureus* NCTC 8325 (obtained from ATCC) and USA300-0114 in TSB were diluted 1:100 in fresh medium and added to each well (200 µL/well; flat-bottomed 96-well plate, *BD Biosciences*, BD 351172). Plates were incubated at 37 °C for 24 h to establish biofilms. After 24 h, the wells were emptied and a pre-mixed solution of media and compound stock solution was added to each well (maximum DMSO concentration 2% for single compounds and 4% for combination of **PK150** and oxacillin). Plates were incubated at 37 °C for 20 or 70 h, then the media from each well was removed and biofilms were washed three times with PBS (200 µL) to remove planktonic cells. Biofilm were regrown overnight at 37 °C in fresh media (200 µL). An aliquot of 100 µL of supernatant from each well was transferred to a fresh 96-well flat bottomed plate and the OD₆₀₀ at 595 nm was measured using a plate reader (POLARstar Omega, *BMG Labtech*). Concentrations of compound yielding a regrowth OD₆₀₀ of less than 0.1 correspond to the MBEC. Three biological replicates containing three technical replicates each (n = 9) were prepared for each concentration of compound as well as positive (cetyl pyridinium chloride and PQ-11,11)⁷⁸ and negative controls (DMSO). Cetylpyridinium chloride has shown full eradication of biofilms at 50 µM for NCTC 8325 (MSSA) and

USA300-0114 (MRSA) and PQ-11,11 at 50 μ M for NCTC 8325 (MSSA) and 200 μ M for USA300-0114 (MRSA). Means and standard deviations (SD) were calculated with GraphPadPrism (version (v.) 6.05, *GraphPad Software*) across the nine replicates.

Minimum Biofilm Inhibitory Concentration (MBIC)

Prior to MBIC determination, MIC values in tryptic soy broth were determined (in contrast to standard MIC conditions in B medium, as mentioned above). For this, overnight bacterial cultures were diluted to 10^6 CFU/mL in TSB and 100 μ L thereof added into each well of a U-bottom 96-well plate (BD Biosciences, BD 351177) containing 100 μ L compound in medium (maximum DMSO concentration 2% for single compounds and 4% for combination of **PK150** and oxacillin). Plates were incubated at 37 °C for 72 h and evaluated visually for bacterial growth. For **PK150**, MIC values were 0.78 μ M and 1.56 μ M for *S. aureus* NCTC 8325 and USA300-0114, respectively. For MBIC determination, sub-MIC concentrations of compounds were used. Overnight cultures of *S. aureus* NCTC 8325 and USA300-0114 in tryptic soy broth were diluted in fresh medium (1:100) and 100 μ L thereof were added to each well of a flat-bottomed 96-well plate (BD Biosciences, BD 351172) already containing different concentrations of compounds in 100 μ L of medium (maximum DMSO concentration 2%). Plates were incubated at 37 °C for 24 h. After emptying the wells, they were washed with 200 μ L of double-distilled water (ddH₂O) and subsequently dried (first for 3 h at 37 °C, then at room temperature overnight). Wells were then incubated at room temperature for 10 min with 1% w/v crystal violet. Excess crystal violet was removed by submerging plates in fresh tap water until the run off was colorless. Plates were then dried once more at room temperature. Crystal violet was redissolved in 95% ethanol, and 100 μ L were transferred to a new flat-bottom 96-well plate for absorbance measurements at 595 nm. Controls corresponding to each test concentration were performed. Three biological replicates were prepared. No biofilm inhibition could be observed for sub-MIC concentrations of **PK150**.

4.1.7 Time-Kill Assays

Time-kill experiments were performed as described previously by Smith and Romesberg.¹⁹¹ An overnight culture of *S. aureus* NCTC 8325 was diluted to an OD₆₀₀ of 0.025 and grown to mid-logarithmic phase (OD₆₀₀ = 0.4 - 0.5) at 37 °C, 200 rpm. Subsequently, cells were diluted to 1×10^6 CFU/mL in B-medium. Diluted cells were aliquoted à 3 mL in 15 mL culture tubes containing **SFN** (24, 6 and 3 μ M final concentration) or **PK150** (0.24, 0.6 and 0.3 μ M final concentration; corresponding to 8 \times , 2 \times and 1 \times MIC). Cells were incubated at 37 °C and 200 rpm, serially diluted, and plated on agar plates at indicated time points for the determination of numbers of viable cells (CFU/mL). Additionally, time-kill experiments were performed with stationary-phase bacteria in

presence of tetracycline (bacteriostatic translational inhibitor, 1 μ M, 2 \times MIC) to arrest growth of the cells.

4.1.8 Cell Membrane Permeability Assay

For the cell wall permeability assays,²⁵⁷ cells were grown to an OD₆₀₀ of 0.4 to 0.5, harvested and washed with 5 mM of HEPES-NaOH pH 7.2 and 5 mM glucose. Pellets were then resuspended in the same buffer to an OD₆₀₀ of 0.4, and 100 μ L aliquots were transferred to black 96-well-plates and incubated for 15 min at 37 °C with 10 μ M of propidium iodide. During incubation, fluorescence (535 nm excitation and 617 nm emission) was measured at 37 °C with a *TECAN* Infinite M200 Pro microplate reader to make sure that propidium iodide had been fully integrated into membranes in the defined period of time. After addition of the respective compounds, measurements were continued at the same wavelengths over the course of 1 h. 100 μ g/mL of benzalkonium chloride (BAC) and 16 μ g/mL of daptomycin together with 50 μ g/mL CaCl₂ were added as positive controls.

4.1.9 Zymography

Preparation of Extracellular and Cell Wall-Bound Autolysins

Preparation of extracts was based on procedures published previously by Mani *et al.*²⁵⁸ and Huff *et al.*²⁵⁹ B medium was inoculated at a 1:1000 ratio from an overnight-culture of *S. aureus* NCTC 8325 and incubated at 37 °C for 8 h to an OD₆₀₀ of 4 - 4.5. Cells were harvested (3,000 \times g, 15 min) and washed with PBS to remove secreted proteins. The cell density was adjusted to an OD₆₀₀ = 1.6 in B medium and treated with 8 \times MIC concentration of the compounds (**PK150** and **PK150-C**, 2.4 μ M; **SFN** and **SNF-C** 24 μ M; penicillin G, 0.4 μ M) at 37 °C for 1.5 h. Cells were harvested by centrifugation (3,000 \times g, 4 °C, 15 min) and saved for the extraction of cell wall-bound lytic proteins. Supernatants were filtrated (0.2 μ m), concentrated by factor 100 by ultrafiltration with 10 kDa filters (*Amicon* YM-10, *Merck*), and used for the analysis of extracellular proteins. Cell wall-bound enzymes were extracted by a freeze-thaw method. Here, harvested cells were washed with cold ddH₂O, then with potassium hydrogen phosphate buffer (0.01 M, pH 7) and resuspended in the same buffer. The cell suspension was frozen at -80 °C for 1 h and thawed at 37 °C for 10 min. This cycle was repeated and cells were stored overnight at -80 °C. After thawing at 37 °C, supernatants were collected by centrifugation (13,300 \times g, 4 °C, 10 min). Concentrations of all protein extracts were determined by Bradford assay (*Roti-Quant*, *Carl Roth*) and adjusted to equal protein concentrations.

Preparation of Zymogram Gels and SDS-PAGE

Zymogram assays for the analysis of lytic activities of protein extracts were based on SDS-PAGE²⁶⁰ using 10% gels containing *S. aureus* NCTC 8325 as substrate cells. The protocol for the preparation of gels and performing SDS-PAGE was adapted from Vaz *et al.*^{261,262} For the preparation of substrate cells, *S. aureus* NCTC 8325 was grown to an OD₆₀₀ = 1 in B medium at 37 °C, 200 rpm. Cells were harvested (6,000 × g, RT, 15 min), then washed and autoclaved (121°C, 15 min) in ddH₂O. The autoclaved cells were harvested by centrifugation (15,050 × g, RT, 15 min). Pellets were kept at -20 °C overnight, resuspended in ddH₂O and lyophilized at -80 °C. Substrate cells were then resuspended in ddH₂O and added to the resolving gel-buffer (0.2% (w/v) final concentration). Subsequently, gels were prepared based on the standard procedures by Laemmli.²⁶⁰ Samples of prepared extracellular (11 µg) and cell wall-bound protein extracts (3 µg) were loaded on zymogram gels. After SDS-PAGE (70 V per gel) in tris-glycine-SDS-buffer, gels were rinsed and washed three times with ddH₂O (RT, 15 min with gentle agitation) to remove SDS. Gels were subsequently incubated in renaturation buffer (50 mM Tris-HCl, pH 7.5, 0.1% (v/v) Triton X-100, 10 mM calcium chloride, 10 mM magnesium chloride) at 37 °C with gentle agitation overnight. Afterwards, gels were stained with methylene blue solution (0.1% (w/v) methylene blue in 0.01% potassium hydroxide) at RT for 1 h and de-stained in ddH₂O overnight. The same samples were also analyzed on 4 - 12% bis-tris gels with 1 × MOPS SDS Running Buffer (NuPAGE, Thermo Fisher Scientific). Pink Color Protein Standard II protein size marker (prestained, SERVA) was used.

4.2 Drug Candidate Development Assays

4.2.1 *In vitro* assays

4.2.1.1 Cytotoxicity

All cell culture procedures were performed under sterile conditions in a laminar airflow cabinet class I.

Cell Culture

A549, HeLa, HepG2 and NIH/3T3 cells were cultivated in Dulbecco's modified Eagle's medium (DMEM, Sigma Life Sciences), supplemented with 10% fetal bovine serum (FBS, Sigma Life Sciences) and 2 mM (4 mM for NIH/3T3) L-glutamine (GE Healthcare).

Cells were grown in cell culture flasks (for rapid cell propagation) using an incubator at 37 °C and 5% CO₂ supply. The status of cells was controlled daily by checking their density, morphology and adherence via light microscopy, and nutritional situation via the color of the containing pH indicator

(Phenol red), which is red at neutral pH and turns yellow at acidic pH, which is the case when the medium gets old or bacterial contamination takes place. Absence of contaminating organisms was also checked using light microscopy. As all of the cell lines were adherent, it was possible to decant the old medium in order to change the medium, then cells were washed with preheated PBS without Mg^{2+} and Ca^{2+} and new pre-warmed (37 °C) medium was added.

For passaging of cells, they were first washed with pre-warmed PBS without Mg^{2+} and Ca^{2+} and PBS was removed to completion. Accutase (Sigma Life Sciences, 37 °C) was then added and the cells incubated at 37 °C until complete detachment (5 – 10 min), which was controlled by light microscopy. Fresh, preheated (37 °C) medium was added and the cell-containing solution then splitted.

Freezing and Defrosting of Cells

Medium of those cells, which were going to be stored, was changed 24 h before freezing. Cells were washed with PBS (w/o Mg^{2+} and Ca^{2+}), detached using Accutase, transferred to a 50 mL tube and centrifuged at 1,000 rpm for 5 – 10 min. The supernatant was discarded and cells were washed with PBS (with Mg^{2+} and Ca^{2+}). After a new centrifugation step, the cell sediment was resuspended in 4 °C cold medium containing 10% glycerol (at a concentration of $1-2 \cdot 10^6$ cells/mL) and aliquoted into cryovials à 1 mL. Cryovials were then placed into a precooled (4 °C) freezing box, frozen at -80 °C overnight, and transferred into liquid nitrogen tanks for long-term storage.

Cell were counted using a Neubauer improved chamber after staining 1:1 with 0.1% trypan blue in PBS.

For defrosting, the cryovial with frozen cells was taken out of the -80 °C liquid nitrogen tank and thawed under cold water until only a small ice block was left. The cells were transferred to a tube containing 20 mL of 4 °C cold medium (without serum) and incubated 5 – 10 min at room temperature (RT). Cells were then centrifuged, resuspended in the appropriate medium, and transferred into T175 cell culture flasks according to the frozen cell amount. Medium was changed after 24 h.

MTT-Assay

IC_{50} values for cytotoxicity assessment were determined using the tetrazolium dye 3-(4,5-dimethylthiazol-2-yl)-2,5-diphenyltetrazolium bromide (MTT). MTT assay was performed in 96-well plates (transparent Nunc 96-well flat bottom, *Thermo Fisher Scientific*). A549, HeLa and HepG2 cells were seeded at a density of 4000 cells/well, while NIH/3T3 cells were seeded at a density of 2000 cells/well. Cells were grown to 30-40% confluency at 37 °C in a humidified 5% CO_2 atmosphere over a time span of 24 h. The medium was removed and the cells were treated with varying concentrations of the respective compound or DMSO in growth media (100 μ L/well, final assay

concentration of DMSO from compound stocks 0.1%) in triplicates. After incubation at 37 °C in a humidified 5% CO₂ atmosphere for 24 h, 20 µL thiazolyl blue tetrazolium bromide (5 mg/mL in PBS, *Sigma Aldrich*) were added to the cells, followed by incubation at 37 °C in a humidified 5% CO₂ atmosphere for 4 h until complete consumption was observed. After removal of the medium, the resulting formazan was dissolved in 200 µL DMSO. Optical density was measured at 570 nm (562 nm) with background subtraction at 630 nm (620 nm) by a *TECAN* Infinite M200 Pro. MTT data were obtained from at least three independent experiments with triplicate runs for each concentration. All measured values were normalized to values resulting from DMSO-treated samples (100% cell viability). IC₅₀ values and 95% confidence intervals were calculated with GraphPadPrism (v. 5.03, *GraphPad Software*) across all replicates with each measured value given equal weight. For calculation of IC₅₀ values, residual viabilities for the respective compound concentrations were fitted using the formula:

$$V = \frac{100}{1 + 10^{(\log(IC_{50}) - \log(c)) \cdot N}}; V, \text{ viability (\%)}, c, \text{ inhibitor concentration (M)}, N, \text{ hill slope.}$$

4.2.1.2 Hemolysis Assay

The hemolysis protocol was adapted from Blazysk *et al.*²⁶³ and Nüsslein *et al.*²⁶⁴. Hemolysis at different antibiotic concentrations was determined by the use of a suspension of erythrocytes collected from blood of an adult sheep (*elocin-lab GmbH*). Fresh sheep blood (containing heparin) was centrifuged (2,000 × g, 20 min), the supernatant removed, and erythrocytes washed five times in phosphate-buffered saline (PBS) (1:1). Subsequently, an erythrocyte suspension with 50% hematocrit was prepared and stored at 4 °C for further use. Hemolysis at different antibiotic concentrations was determined the use of a 5% suspension of erythrocytes in PBS (400 µL final volume; final assay concentration of DMSO from compound stocks 1%). 100% hemolysis was determined by adding 0.2% (v/v) Triton X-100 while DMSO served as the zero-hemolysis control. After incubation at 37 °C for 30 min, the suspension was centrifuged (10,000 × g, 10 min) and the absorbance of the supernatant (1:4 dilution with PBS; 100 µL) was measured at 414 nm at a *TECAN* Infinite M200 Pro. Hemolysis was determined in four independent experiments with triplicate runs for each concentration. Means and standard deviations were calculated across all four experiments after normalization to the negative control (DMSO; hemolysis 0%) and the positive control (Triton X-100, 0.2% v/v; hemolysis 100%).

4.2.1.3 Stability in Mouse Plasma

The *in vitro* stabilities of **SFN** and **PK150** were tested by a LC-MS based method. Murine blood plasma (*biowest*, mouse plasma w/ lithium heparin, sterile filtered; S2162-010) was used as a 1:1 dilution with potassium phosphate buffer (0.1 M, pH 7.4). **U1**, a β-lactone with known low plasma stability,¹⁷² was used as positive control. For the plasma stability testing, compounds were diluted 1:100 to a final concentration of 10 µM (50 µM in the case of **U1**, final assay concentration of DMSO from compound

stocks was 1%) into pre-warmed plasma at 37 °C. The initial sample was taken immediately after compound addition (time point 0 min). In the following, the mixture was incubated at 37 °C with gentle shaking at 600 rpm and additional samples were withdrawn at certain time points (5, 10, 20, 30, 60, 120, 240, 360 min). Directly after withdrawal, samples were quenched by the addition of pre-chilled acetonitrile (MeCN) (1:1 v/v) and stored at -20 °C. Prior to LC-MS analysis, samples were centrifuged to pellet proteins (17,000 × g, 5 min) and supernatants were filtered through modified nylon centrifugal filters (0.45 µM, VWR) for particle removal. Quantitative LC-MS analysis was performed using a LCQ-Fleet Ion Trap Mass Spectrometer (*Thermo Fisher Scientific*) equipped with an APCI ion source and a Ultimate3000 HPLC system using a *Waters Xbridge BEH130 C18*-reverse phase column (5 µM 4.6 x 100 mm). Data analysis was performed using XCalibur software (*Thermo Fisher Scientific*). Briefly, ion peaks from single ion monitoring mass detection were integrated and peak areas at the time point 0 min were set to 100%. The time-dependent peak decline was monitored relative to 100% at t = 0 min. Plasma stability was determined in at least three independent experiments

4.2.1.4 Colloidal Aggregation Determination by Dynamic Light Scattering (DLS)

The critical agglomeration concentration (CAC) represents the concentration at which small molecules begin to self-aggregate into a suspension of colloid-like aggregates. This transition point is observed by an abrupt increase in dynamic light scattering (DLS) intensity with an increasing compound concentration.

Here, DLS was used in order to detect the presence of soluble aggregates at different concentrations of **SFN** and **PK150** in 50 mM NaPPi buffer (pH 7). The compounds were diluted from concentrated DMSO stocks with freshly filtered 50 mM NaPPi buffer, pH 7, at room temperature (final assay concentration of DMSO from compound stocks was 1%). Optionally, Tween 80 (0.023% v/v) was added to the buffer prior to the addition of compounds. Measurements were performed using a DynaPro NanoStar Dynamic Light Scattering reader (*Wyatt Technology*) equipped with a 662.3 nm laser. All measurements were performed at 37 °C. Data were obtained from three measurements of the same sample, with a total measurement time of 50 s each (10 acquisitions à 5 s).

The lowest concentration in the dilution series at which the DLS intensity started to differ from the solvent background was defined as the critical agglomeration concentration (CAC).

4.2.2 *In vivo* animal studies

Mice

For pharmacokinetic and pharmacodynamic experiments, outbred male CD-1 mice (*Charles River*, Netherlands), 4 weeks old, were used. For efficacy experiments, pathogen-free 9-week old female C57BL/6J mice were purchased from Harlan-Winkelmann (*Envigo*, Netherlands). The animal studies were conducted in accordance with the recommendations of the European Community (Directive 86/609/EEC, 24 November 1986). All animal procedures were performed in strict accordance with the German regulations of the Society for Laboratory Animal Science (GV- SOLAS) and the European Health Law of the Federation of Laboratory Animal Science Associations (FELASA). Animals were excluded from further analysis if sacrifice was necessary according to the human endpoints established by the ethical board. All experiments were approved by the ethical board of the Niedersächsisches Landesamt für Verbraucherschutz und Lebensmittelsicherheit, Oldenburg, Germany (LAVES; permit No. 33.9-42502-04-13/1195 and 33.19-42502-04-15/1857).

Pharmacokinetic (PK) Study

PK150 was dissolved in 55% PEG-400, 15% *N*-methyl pyrrolidon, 20% dimethyl sulfoxide, and 10% ethanol. Mice were administered **PK150** by intragastric gavage at 10 and 20 mg/kg or intravenously at 10 mg/kg. About 20 µL of whole blood was collected serially from the lateral tail vein at time points 0.5, 1, 2, 4, 8 and 24 h post administration. Additionally, about 20 µL of whole blood was collected at time point 0.25 h after i.v. administration. After 48 h mice were sacrificed and blood was collected from the heart. Whole blood was collected into tubes coated with 0.5 M EDTA and immediately centrifuged (13,000 rpm, 4 °C, 10 min). Afterwards, plasma was transferred into new tube and then stored at -80 °C until analysis.

PK Sample Preparation and Analysis

All PK plasma samples were analyzed by HPLC-MS/MS using an *Agilent* 1290 HPLC system equipped with a diode array UV detector and coupled to an QTrap 6500 mass spectrometer (*AB Sciex*). First, a calibration curve was prepared by spiking different concentrations of **PK150** into mouse plasma. The lower limit of quantification was 25 ng/mL. The upper limit of quantification was 2000 ng/mL. The lower limit of qualification was 10 ng/mL. Caffeine was used as an internal standard. In addition, quality control samples (QCs) were prepared at 25, 100, 500 and 2000 ng/mL. 7.5 µL of plasma sample (calibration samples, QCs or PK samples) were extracted with 37.5 mL of MeCN containing 12.5 ng/mL of caffeine as internal standard for 5 min at 2000 rpm on an Eppendorf MixMate® vortex mixer. Then samples were centrifuged (13,000 rpm, 5 min). Supernatants were transferred to standard HPLC-glass

vials. HPLC conditions were as follows: column: *Agilent Zorbax Eclipse Plus C18*, 50 x 2.1 mm, 1.8 μm ; temperature: 30 $^{\circ}\text{C}$; injection volume: 1 μL ; flow rate: 700 $\mu\text{L}/\text{min}$; solvent A: ddH₂O + 0.1% FA; solvent B: ACN + 0.1% FA; gradient: 99% A at 0 min, 99% - 90% A from 0.1 min to 1.00 min, 90% - 50% A from 1.00 min to 1.50 min, 50% - 0% A from 1.50 min to 5.50 min, 0% A until 6.00 min, then 99% A post-run for 2 min; UV detection: 190 - 400 nm. Mass spectrometric parameters were as follows: Scan type: MRM, positive mode; Q1 and Q3 masses for caffeine and **PK150** can be found in Table 16. Peak areas of each sample and of the corresponding internal standard were analyzed using MultiQuant 3.0 software (*AB Sciex*). Peak areas of the respective samples of **PK150** were normalized to the internal standard peak area. For **PK150** m/z 394.898 \rightarrow 196.100 and m/z 394.898 \rightarrow 174.100 were used for qualification. For caffeine m/z 195.116 \rightarrow 138.100 and m/z 195.116 \rightarrow 110.100 were used for qualification. Peaks of PK samples were quantified using the calibration curve. The accuracy of the calibration curve was determined using QCs independently prepared on different days (accuracy: 98.77 - 114.60%). PK parameters were determined using a non-compartmental analysis with PKSolver.²⁶⁵

Table 16: Peak areas of each sample and of the corresponding internal standard.

ID	Q1 Mass (Da)	Q3 Mass (Da)	time (msec)	CE (volts)	CXP (volts)
PK150	394.898	196.100	50	31.000	6.000
PK150	394.898	174.100	50	31.000	4.000
caffeine	195.116	138.100	50	27.000	10.000
caffeine	195.116	110.100	50	31.000	6.000

Pharmacodynamic (PD) Efficacy Study Using a Neutropenic Thigh Infection Model

S. aureus ATCC 33591 (MRSA) was used to evaluate the antibiotic effect of **PK150** in a neutropenic thigh infection model. CD-1 mice were rendered neutropenic by intraperitoneal administration of cyclophosphamide of 150 mg/kg on day -4 and of 100 mg/kg on day -1 prior to infection. On the day of infection, mice were infected i.m. with 7.2×10^5 CFU/ml *S. aureus* strain ATCC 33591 (30 μL into each posterior thigh muscle). 20 mg/kg **PK150**, dissolved in 55% PEG-400, 15% *N*-methyl pyrrolidone, 20% dimethyl sulfoxide and 10% ethanol, and an equally prepared vehicle as sham treatment were administered p.o. 30 min, 4 h and 8 h post infection. In addition, 5 mg/kg of levofloxacin (as positive control) dissolved in PBS and an equally prepared vehicle as sham treatment were administered i.p. 2 h, 6 h and 10 h post infection. Mice were sacrificed 24 h post infection and the posterior thigh muscles were aseptically removed, weighted and homogenized in PBS (3 mL). The amount of viable bacteria was determined after plating 10-fold serial dilutions on BHI agar plates following overnight

incubation at 37 °C. Results were expressed as log₁₀ CFU/g of muscle. Tukey's test was performed to test for outliers and two-sided Student's t-test was used as significance test.

Efficacy Experiment Mimicking a *S. aureus* Bloodstream Infection

The antibiotic efficacy of **PK150** was determined in a murine model of *S. aureus* bloodstream infection. Mice were intravenously infected with 4 x 10⁷ CFU of *S. aureus* strain SH1000 and treated with 20 mg/kg **PK150** (dissolved in 55% PEG-400, 15% *N*-methyl pyrrolidone, 20% dimethyl sulfoxide and 10% ethanol) or vehicle (55% PEG-400, 15% *N*-methyl pyrrolidone, 20% dimethyl sulfoxide and 10% ethanol) starting at day 3 post inoculation. **PK150** and vehicle was administered p.o. twice on day 3 after infection (at 6 h interval), followed by a single oral dose on day 4, 6 and 8 after infection. Mice were sacrificed on day 9 and CFU of *S. aureus* were determined in liver, kidneys, and heart by plating in serial dilutions. A two-sided Student's t-test was used as significance test.

4.3 Proteomics

4.3.1 AfBPP with Sorafenib Photoprobe SFN-P in *E. coli* BL21(DE3)pLysS harboring pET-DEST-55-fl-SpsB

E. coli BL21(DE3)pLysS harboring the pET-55-DEST-fl-SpsB were grown at 37 °C, 200 rpm in LB medium to OD₆₀₀ = 0.5 - 0.6. To induce the overexpression, isopropyl β-D-1-thiogalactosidase (IPTG, 0.5 mM) was added. A non-induced culture was included and treated in the same way as the induced one for all subsequent steps. After incubation (22 °C, 200 rpm, 3 h) cells were harvested (5,000 × g, 4 °C, 10 min) and washed with PBS. For labeling, bacteria were resuspended in PBS and adjusted to OD₆₀₀ = 10 (0.1 mL aliquots for subsequent labeling experiments). Samples were preincubated with **SFN** or **PK150** (0.5 mM) for competition experiments or DMSO only (final concentration of DMSO 1%) at 25 °C, 700 rpm for 45 min. After preincubation, photoprobe (**SFN-P**, 50 μM) or DMSO as control (final total concentration of DMSO was 2%) were added and incubated at 25 °C, 700 rpm for 45 min. After compound treatment, samples were transferred to 96-well plates (transparent Nunc 96-well flat bottom, *Thermo Fisher Scientific*) and irradiated with UV light (360 nm) for 30 min on ice. Cells were lysed by bead beating (3 x 5500 rpm, 15 s, 2 min cooling breaks on ice after each run; Precellys Glass Kit VK05 0.5 mL tubes; Precellys 24 Homogenizer, *Bertin Technologies*) and the lysates were transferred to 1.5 mL microcentrifuge tubes. They were subsequently treated with lysozyme (1 mg/mL) at 37 °C for 20 min. For click chemistry, 50 μL of samples were treated with trifunctional linker (TFL, 60 μM)¹⁷, TCEP (1 mM), TBTA ligand (0.1 mM) and CuSO₄ (1 mM) for 1 h at room temperature in the dark. Recombinantly expressed and purified fl-SpsB (see section "*Expression and*

purification of full-length SpsB”) was included as control. Reactions were quenched by the addition of 50 μ L of 2 \times SDS loading buffer (125 mM Tris-HCl, 20% (v/v) glycerol, 4% (w/v) SDS, 0.005% (w/v) bromophenol blue, 10% (v/v) 2-mercaptoethanol)⁵⁵ and proteins resolved using SDS-PAGE. An ImageQuant Las-4000 image reader (*GE Healthcare*) equipped with a *Fujinon* VRF43LMD3 lens and a 575DF20 filter was used for visualization of fluorescence labeled proteins. Additionally, gels were stained with Coomassie brilliant blue.

4.3.2 AfBPP with Sorafenib Photoprobe SNF-P in *S. aureus* NCTC 8325

Culture, Labeling, Lysis and Click Reaction

B-medium (100 mL) was inoculated at a ratio of 1:10 from a bacterial overnight culture (37 °C, 200 rpm, 14 h). After 7 h of growth at 37 °C, 200 rpm an equivalent of OD₆₀₀ = 20 of the culture was harvested (6,000 \times g, 4 °C, 10 min), washed with PBS and cells were resuspended in PBS (0.5 mL). For competition experiments, samples were preincubated with **SFN** (0.5 mM) or DMSO only (concentration of DMSO 1% during preincubation) at 25 °C, 700 rpm for 45 min. After preincubation, photoprobe (**SFN-P**, 10 or 50 μ M), minimal photoprobes (**DA-1**, **DA-2** or **DA-3**, 50 μ M) or DMSO (final total concentration of DMSO 2%) were added and incubated at 25 °C, 700 rpm for 45 min. After compound treatment, samples were diluted with PBS (5 mL final volume), transferred to petri dishes (5 cm radius) and irradiated with UV light (360 nm) for 30 min with ice cooling. Subsequently, bacteria were harvested (6,000 \times g, 4 °C, 10 min) and washed with PBS. Cell pellets were resuspended in PBS (0.5 mL; 1 \times protease inhibitor cocktail (Complete, Mini, EDTA-free, *Roche Diagnostics*)) on ice and lysed (6 \times 5,500 rpm, 15 s, 2 min cooling breaks on ice after each run; Precellys Glass/Ceramic Kit SK38 2.0 mL tubes; Precellys 24 Homogenizer, *Bertin Technologies*). 300 μ L of the lysate were transferred to 1.5 mL microcentrifuge tubes and treated with 8 μ g/mL lysostaphin (from *S. staphylolyticus*, Sigma-Aldrich) at 37 °C, 700 rpm for 20 min. Separation of the soluble and insoluble fraction was performed by centrifugation (21,000 \times g, 4 °C, 1 h). The insoluble fraction was washed twice with PBS using an ultrasonic rod (10% intensity, 10 s; Sonopuls HD 2070, *Bandelin electronic GmbH*) for resuspension. Note that no separation of soluble and insoluble fractions was performed for the investigation of labeling before enrichment and LC-MS/MS analysis of the minimal photoprobes **DA-1**, **DA-2** and **DA-3**. Protein concentrations were determined using the Pierce BCA Protein assay kit (*Thermo Fisher Scientific, Pierce Biotechnology*) and samples normalized to equal protein amounts. For click chemistry, 300 μ L of the normalized soluble and insoluble fractions were treated with trifunctional linker (TFL, 60 μ M)¹⁷, TCEP (1 mM), TBTA ligand (0.1 mM) and CuSO₄ (1 mM). Samples were incubated at room temperature in the dark for 1 h. Subsequently, proteins were precipitated by adding cold acetone (4 times the sample volume) and incubated at -20 °C overnight. Precipitated

proteins were centrifuged ($16,900 \times g$, 4°C , 15 min) and protein pellets were washed two times with cold methanol (1 mL). Pellets were resuspended in 0.4% SDS in PBS (0.5 mL) at RT by sonication (10% intensity, 15 s; Sonopuls HD 2070 ultrasonic rod, *Bandelin electronic GmbH*). For enrichment 50 μL avidin-agarose beads (*Sigma-Aldrich*) were prepared by washing three times with 0.4% (w/v) SDS in PBS (1 mL). Protein solutions were added to the conditioned avidin-agarose beads and incubated under continuous inversion at 20 rpm and RT for 1 h. Beads were washed three times with 0.4% SDS in PBS (1 mL), two times with 6 M urea in ddH₂O (1 mL) and three times with PBS (1 mL). All centrifugation steps were conducted at $400 \times g$ for 2 min at RT.

Gel-based Analysis

For gel-based analysis, protein samples were mixed 1:1 with 2 \times SDS loading buffer (125 mM Tris-HCl, 20% (v/v) glycerol, 4% (w/v) SDS, 0.005% (w/v) bromphenol blue, 10% (v/v) 2-mercaptoethanol)⁵⁵ and separated by one-dimensional (1D) SDS-PAGE on a 4 - 12% Bis-Tris gel with 1 \times MOPS SDS Running Buffer (NuPAGE, *Thermo Fisher Scientific*). BenchMark Fluorescent Protein Standard (*Life Technologies*) and Pink Color Protein Standard II (prestained, *SERVA*) were used as size markers. An ImageQuant Las-4000 image reader (*GE Healthcare*) equipped with a *Fujinon* VRF43LMD3 lens and a 575DF20 filter was used for visualization of fluorescence labeled and enriched bands. Additionally, gels were stained with Coomassie brilliant blue.²⁶⁶

Preparation for Gel-free LC-MS/MS Analysis

For quantitative mass spectrometric analyses, beads with bound proteins were resuspended in 200 μL denaturation buffer (7 M urea, 2 M thiourea in 20 mM pH 7.5 HEPES buffer). Proteins were reduced on-bead with TCEP (5 mM) at 37°C for 1 h. Subsequent alkylation was performed with iodoacetamide (IAA, 10 mM) at 25°C for 30 min in the dark. Alkylation was quenched by the addition of dithiothreitol (DTT, 10 mM) and incubation at RT for 30 min. For digestion, the endoproteinase Lys-C (2.5 ng/ μL , *Wako*) was added to each sample and incubated at RT for 2 h. Afterwards, samples were diluted 1:4 with 50 mM TEAB buffer and digested with trypsin (3.75 ng/ μL ; sequencing grade, modified, *Promega*) at 37°C overnight. The reaction was stopped by adding formic acid (FA) to a final concentration of 0.5% (final pH 2 - 3). Peptides were desalted and labeled by stable isotope dimethyl labeling²¹ on-column using 50 mg SepPak C18 Vac cartridges (*Waters*). SepPak C18 cartridges were equilibrated with MeCN (1 mL), elution buffer (1 mL; 80% ACN, 0.5% FA) and three times aqueous 0.5% FA solution (1 mL). Subsequently, protein samples were loaded by gravity flow, washed with five times aqueous 0.5% FA solution (1 mL) and labeled with 5 mL of the respective dimethyl labeling solution. The following solutions were used: 30 mM NaBH₃CN, 0.2% CH₂O, 10 mM NaH₂PO₄, 35 mM Na₂HPO₄, pH 7.5 ("light" isotope (L)); 30 mM NaBH₃CN, 0.2% CD₂O, 10 mM NaH₂PO₄, 35 mM Na₂HPO₄, pH 7.5

("medium" isotope (M)) and 30 mM NaBHD₃CN, 0.2% ¹³CD₂O, 10 mM NaH₂PO₄, 35 mM Na₂HPO₄, pH 7.5 ("heavy" isotope (H)). For technical replicates, isotopic labels were permuted. Labeled peptides were washed three times with 0.5% FA (1 mL) and eluted with elution buffer (0.75 mL; 80% ACN, 0.5% FA). Differentially labeled peptides were mixed according to respective replicates for quantification and lyophilized using a vacuum centrifuge.

LC-MS/MS Analysis

Prior to mass spectrometry, peptides were reconstituted in 0.5% FA, filtered using centrifugal filter units (modified Nylon, 0.45 μm, low protein binding, *VWR International, LLC*), and transferred into LC-MS sample vials. Samples were analyzed via HPLC-MS/MS using an UltiMate 3000 nano HPLC system (*Thermo Fisher Scientific*) equipped with Acclaim C18 PepMap100 75 μm ID x 2 cm trap and Acclaim C18 PepMap RSLC, 75 μm ID x 15 cm (for **DA-1** and **DA-2** experiments: 75 μm ID x 50 cm) separation columns coupled to an Orbitrap Fusion (*Thermo Fisher Scientific*). Peptides were loaded onto the trap and washed for 10 min with 0.1% FA, then transferred to the analytical column, and separated using a 120 min gradient from 3% to 25 % ACN in 0.1% FA and 5% DMSO at 200 nL/min flow rate (for **DA-1** and **DA-2** experiments: 105 min gradient from 5% to 22% and a 10 min step from 22% to 32% ACN in 0.1% FA at 300 nL/min flow rate). LTQ Orbitrap Fusion was operated in a 3 second top speed data dependent mode. Full scan acquisition was performed in the orbitrap at a resolution of 120000 and an ion target of 4e5 (for **DA-1** and **DA-2** experiments: 2e5) in a scan range of 300 – 1700 m/z (for **DA-1** and **DA-2** experiments: 2e5 and 300 – 1500 m/z). Monoisotopic precursor selection as well as dynamic exclusion for 60 s were enabled. Precursors with charge states of 2 - 7 and intensities greater than 5e3 were selected for fragmentation. Isolation was performed in the quadrupole using a window of 1.6 m/z. Precursors were collected to a target of 1e2 for a maximum injection time of 250 with "inject ions for all available parallelizable time" enabled ("Universal" method)²⁶⁷ (for **DA-1** and **DA-2** experiments: 1e4 AGC target and 50 ms maximum injection time). Fragments were generated using higher-energy collisional dissociation (HCD) and detected in the ion trap at a rapid scan rate. Internal calibration was performed using the ion signal of fluoranthene cations (EASY-ETD/IC source).

Protein Identification and Quantification

Peptide and protein identifications were performed using MaxQuant (v. 1.5.1.2)⁵⁶ with Andromeda⁵⁷ as search engine with the following parameters: Carbamidomethylation of cysteines as fixed modification and oxidation of methionine as dynamic modification, trypsin/P as the proteolytic enzyme, 4.5 ppm for precursor mass tolerance (main search ppm) and 0.5 Da for fragment mass tolerance (ITMS MS/MS tolerance). Searches were performed against the Uniprot database for *S. aureus* NCTC 8325 (taxon identifier: 93061, downloaded on 02.12.2014). Quantification was

performed using the following settings: DimethLys0, DimethNter0 (“light” isotopes), DimethLys4, DimethNter4 (“medium” isotopes) and DimethLys8, DimethNter8 (“heavy” isotopes) with a maximum of four labeled amino acids. “l = L”, “requantify” and “match between runs” (default settings) options were used. Identification was done with at least 2 unique peptides and quantification was done only with unique peptides. For statistical analysis with Perseus (v. 1.5.3.2),⁵⁸ three biological replicates consisting of three technical replicates each were analyzed for **SFN-P** and competition experiments of **SFN** and **SFN-P** as well as for **DA-1** and **DA-2**. For **DA-3**, three biological replicates were prepared and analyzed. Putative contaminants, reverse hits and proteins, identified by side only, were removed. Normalized protein ratios were $\log_2(x)$ transformed and filtered to contain at least one valid value within technical replicates. Ratios were z-score normalized within replicates and mean values of technical replicates were calculated. Mean differences in enrichment and respective *p*-values were obtained by a two-sided one sample *t*-test over the three biological replicates.

4.3.3 Secretome and Surfaceome analyses

Preparation of the Secretome

Secretome analysis was based on a procedure published previously by Schallenberg *et al.*²²⁰ For the preparation of overnight cultures, 50 mL of B medium were inoculated with a cryostock (50 μ L, 1:100) and incubated at 37 °C, 200 rpm for 16 h. The overnight culture was diluted to $OD_{600} = 0.1$ into fresh B medium (40 mL per biological replicate). After 5 h of growth at 37 °C, OD_{600} was measured, cells harvested (3,000 \times g, 4 °C, 15 min), and washed with PBS. Cells were resuspended in fresh B medium to a cell density of 1.5×10^9 CFU/mL. 10 mL of the cells were incubated with **SFN** or **SFN-C** (1.5 μ M, 0.5 \times MIC), **PK150** or **PK150-C** (0.15 μ M, 0.5 \times MIC), or DMSO as control in 50 mL tubes at 37 °C, 200 rpm for 1.5 h. OD_{600} was measured, and serial dilutions were plated on agar plates for cell number determination. Cells were pelleted by centrifugation (3,000 \times g, 15 min and 6,000 \times g, 5 min). The resulting pellets were saved for surfaceome analysis (see below). The resulting supernatants were filtered (0.22 μ M filter) and proteins precipitated by overnight incubation with 10% (w/v) trichloroacetic acid at 4 °C. Proteins were harvested (9,000 \times g, 15 min), and washed two times with 90% acetone. Protein pellets were air dried and dissolved in 8 M urea in Tris buffer (50 mM, pH 8.0). Protein concentrations were measured using a Pierce BCA Protein assay kit (*Thermo Fisher Scientific, Pierce Biotechnology*). Protein concentrations were normalized according to the BCA assay (as determined by serial dilutions), as for 0.5 \times MIC no cell number reduction could be observed.

Preparation of the Surfaceome

Surfaceome analysis was based on a procedure published previously by Ventura *et al.*²⁶⁸ Cell pellets were washed three times with 50 mM Tris-HCl pH 7.4 (centrifugation at 3,000 × g, 4 °C, 15 min) and carefully resuspended in 0.4 mL of hydrolysis buffer (50 mM Tris-HCl pH 7.4, 0.6 M sucrose). The OD₆₀₀ values were adjusted to equal turbidity and volumes with hydrolysis buffer (50 mM Tris-HCl pH 7.4, 0.6 M sucrose). Surface proteins were shaved with trypsin (15 µg) at 37 °C for 25 min under continuous inversion at 20 rpm. The digestion was stopped by cooling on ice for 5 min. Supernatants were collected by centrifugation (1,000 × g, 4 °C, 15 min) and filtered (0.22 µm mesh) to eliminate residual cells. Resulting protein concentrations were determined using a Pierce BCA Protein assay kit (*Thermo Fisher Scientific, Pierce Biotechnology*) and adjusted to equal amounts.

Sample Preparation for LC-MS/MS

Proteins for both secretome and surfaceome analyses were reduced with TCEP (10 mM) at 37 °C, 1,200 rpm for 1 h. Subsequent alkylation was performed with iodoacetamide (IAA, 12.5 mM) at 25 °C, 1,200 rpm for 30 min in the dark. Alkylation was quenched by the addition of dithiothreitol (DTT, 12.5 mM) at RT, 1,200 rpm for 30 min. For digestion, LysC (0.5 µg/µL) was added to each sample and incubated at RT, 700 rpm for 2 h. Afterwards, samples were diluted 1:5 with 50 mM TEAB buffer and digested with trypsin (0.5 µg/µL) at 37 °C overnight. The reaction was stopped by adding FA to a final concentration of 0.5% (pH 2 - 3). Peptides were desalted on-column using 50 mg SepPak C18 Vac cartridges (*Waters*). For this, SepPak C18 cartridges were equilibrated with MeCN (1 mL), elution buffer (1 mL; 80% MeCN, 0.5% FA) and three times with aqueous 0.5% FA solution (1 mL). Subsequently, the samples were loaded by gravity flow, washed three times with aqueous 0.5% FA solution (1 mL), eluted with elution buffer (0.5 mL, 80% MeCN, 0.5% FA), and lyophilized using a vacuum centrifuge.

LC-MS/MS Analysis

Prior to mass spectrometry, peptides were reconstituted in 0.5% FA, filtered using centrifugal filter units (modified Nylon, 0.45 µm, low protein binding, *VWR International, LLC*) and transferred into LC-MS sample vials. Samples were analyzed via HPLC-MS/MS using an UltiMate 3000 nano HPLC system (*Thermo Fisher Scientific*) equipped with *Acclaim C18 PepMap100* 75 µm ID x 2 cm trap and *Acclaim C18 PepMap RSLC*, 75 µm ID x 50 cm separation columns coupled to an Orbitrap Fusion (*Thermo Fisher Scientific*). Peptides were loaded onto the trap and washed for 10 min with 0.1% FA, then transferred to the analytical column, and separated using a 105 min gradient from 5% to 22% and a final 10 min step from 22% to 32% ACN in 0.1% FA at a 300 nL/min flow rate. LTQ Orbitrap Fusion was operated in a 3 second top speed data dependent mode. Full scan acquisition was performed in the orbitrap at a

resolution of 120000 and an ion target of $2e5$ in a scan range of 300 – 1500 m/z . Monoisotopic precursor selection as well as dynamic exclusion for 60 s were enabled. Precursors with charge states of 2 - 7 and intensities greater than $5e3$ were selected for fragmentation. Isolation was performed in the quadrupole using a window of 1.6 m/z . Precursors were collected to a target of $1e4$ for a maximum injection time of 50 with “inject ions for all available parallelizable time”. Fragments were generated using higher-energy collisional dissociation (HCD) and detected in the ion trap at a rapid scan rate. Internal calibration was performed using the ion signal of fluoranthene cations (EASY-ETD/IC source).

Protein Identification and Quantification

Peptide and protein identifications were performed using MaxQuant (v. 1.5.1.2)¹²³ with Andromeda²⁶⁹ as search engine using the following parameters: Carbamidomethylation of cysteines as fixed and oxidation of methionine as dynamic modifications, trypsin/P as the proteolytic enzyme, 4.5 ppm for precursor mass tolerance (main search ppm) and 0.5 Da for fragment mass tolerance (ITMS MS/MS tolerance). Searches were performed against the Uniprot database for *S. aureus* NCTC 8325 (taxon identifier: 93061, downloaded on 8.5.2014). Quantification was performed using MaxQuant’s LFQ algorithm. The “I = L”, “requantify” and “match between runs” (default settings) options were used. Identification was done with at least 2 unique peptides and quantification was done only with unique peptides. For statistics with Perseus (v. 1.5.1.6),¹⁸¹ four biological replicates were analyzed. Putative contaminants, reverse hits and proteins, identified by side only, were removed. LFQ intensities were $\log_2(x)$ transformed and filtered to contain minimum three valid values in at least one condition. Missing values were imputed on the basis of a normal distribution (width = 0.3, down-shift = 1.8). *P*-values were obtained by a two sided two-sample *t*-test over the three biological replicates.

Autolysin Enrichment Analysis

Peptidoglycan hydrolase domain-containing proteins were annotated using Pfam for the entries PF05257 (CHAP domain), PF01520 (*N*-acetylmuramoyl-L-alanine amidase), PF01464 (transglycosylase SLT domain), PF06737 (transglycosylase-like domain), PF01832 (mannosyl-glycoprotein endo-beta-*N*-acetylglucosaminidase), PF01551 (peptidase family M23). Enrichment analyses were performed using the Fisher Exact test.

4.3.4 Kinobead Pull-downs

Kinase Inhibitor Profiling with Kinobeads

Kinobeads selectivity profiling of **SFN** and **PK150** was performed as described previously.¹⁷³ Briefly, 5 mg of a protein mixture of four cancer cell lines (K562, Colo205, SKNBE2 and MV4 11) were incubated

with compound dilutions in DMSO (3 nM, 10 nM, 30 nM, 100 nM, 300 nM, 1 μ M, 3 μ M, 30 μ M) at 4 °C for 45 min on an end over end shaker. DMSO without compound was used as control. After preincubation, the mixtures were incubated with Kinobeads (35 μ l settled beads) at 4 °C for 30 min on an end over end shaker. After washing, bound proteins were eluted with LDS sample buffer (NuPAGE, *Invitrogen*) containing 50 mM DTT. For the calculation of a correction factor, the flowthrough of the DMSO control was incubated with fresh beads for a second time (pull-down of pull-down).

LC-MS/MS Analysis

Reduced eluates were alkylated with chloroacetamide (55 mM) and the proteins were desalted and concentrated by a short electrophoresis on a 4 - 12% NuPAGE gel (*Invitrogen*). In-gel digestion was performed according to the standard protocol. Peptides generated by in-gel trypsin digestion were analyzed via LC-MS/MS on a Ultimate3000 nano HPLC coupled online to an Orbitrap HF (*Thermo Fisher Scientific*) mass spectrometer. Peptides were delivered to a trap column (100 μ m x 2 cm, packed in house with Reprosil-Gold C18 ODS-3 5 μ m resin, *Dr. Maisch HPLC GmbH*, Germany) at a flow rate of 5 μ L/min in solvent A₀ (0.1% FA in HPLC grade H₂O). Peptides were then separated on an analytical column (75 μ m x 40 cm, packed in house with Reprosil-Gold C18 3 μ m resin, *Dr. Maisch HPLC GmbH*, Germany) using a 52 min gradient ranging from 5 - 33% solvent B (0.1% FA, 5% DMSO in ACN) in solvent A₁ (0.1% FA, 5% DMSO in HPLC grade H₂O) at a flow rate of 300 nL/min. The mass spectrometer was operated in data dependent mode, automatically switching between MS and MS2 spectra. MS1 spectra were acquired at a resolution of 60,000 (at m/z 200) in the Orbitrap using a maximum injection time of 10 ms and an AGC target value of 3e6. Up to 12 peptide precursors were isolated (isolation width of 1.7 Th, maximum injection time of 75 ms, AGC value of 2e5) and fragmented by HCD using 25% CE and analyzed in the Orbitrap at a resolution of 15,000. The dynamic exclusion duration of fragmented precursor ions was set to 30 s.

Peptide and Protein Identification and Quantification

Peptide and protein quantification was performed using MaxQuant (v. 1.5.3.30)¹²³ by searching the tandem MS data against all canonical protein sequences as annotated in the Swissprot reference database (20193 entries, downloaded 22.03.2016, annotated in-house with Pfam domains) using the embedded search engine Andromeda.²⁶⁹ Carbamidomethylated cysteine was used as a fixed modification, phosphorylation of serine, threonine and tyrosine, oxidation of methionine, and N-terminal protein acetylation as variable modifications. Trypsin/P was specified as the proteolytic enzyme and up to two missed cleavage sites were allowed. Label-free quantification and match between runs were enabled within MaxQuant.¹²⁵ Search results were filtered for a minimal length of

seven amino acids, 1% peptide and protein FDR as well as common contaminants and reverse identifications.

Data Analysis

For competition binding assays, EC₅₀ values were determined based on the LFQ intensity ratio to the DMSO control for every single dose point by nonlinear regression with variable slope using an in-house pipeline.²⁷⁰ A K_d^{app} was then calculated by multiplying the EC₅₀ with a correction factor for each protein. The correction factor (r) for a protein is defined as the ratio of the amount of protein captured from two consecutive pull-downs of the same DMSO control lysate.²⁷¹ Targets of the inhibitors were annotated manually. A protein was considered as target if the resulting binding curve showed a sigmoidal curve shape with a dose dependent decrease of binding to the beads. Furthermore, unique peptides and MSMS-counts as well as peptide and MSMS behavior with increasing dosage were taken into account. Proteins that only showed an effect at the highest inhibitor concentration were not annotated as targets.

4.4 Molecular Biology and Protein Biochemistry

4.4.1 Cloning of Full-length SpsB (fl-SpsB)

Successful overexpression of the full-length SpsB in *E. coli* has been reported previously by Cregg *et al.*¹⁸⁴ and Rao *et al.*¹⁸⁵ For cloning the Invitrogen Gateway Technology^{272,273} was used. The native full-length SpsB gene (Note: the protein sequence of SpsB with the Uniprot ID Q2FZT7 is wrongly annotated, it lacks the catalytic serine and the transmembrane domain) (Figure S4) was amplified by PCR from *S. aureus* NCTC 8325 (taxid: 93061) using genomic DNA as template and Phusion High-Fidelity DNA Polymerase (*New England Biolabs*) according to the manufacturer's instructions. Genomic DNA was prepared using a peqGOLD Bacterial DNA Kit (*VWR Peqlab*) according to the provided protocol, but using lysostaphin (0.1 mg/mL, from *S. staphylolyticus*, *Sigma-Aldrich*) instead of lysozyme. Primers (*Eurofins Genomics*) were designed based on the GenBank entry CP000253.1, removing the first codon (as it is TTG, coding for a leucine and not appropriate as start codon), replacing the rare codon ATA (*ileY*) (5th codon) by TTA (coding the amino acid leucine) and expanding the sequence by a tobacco etch virus (TEV) cleavage site and the sequences for *attB1*- and *attB2*-sites for Gateway cloning (Table 17). The PCR product was integrated into the donor vector pDONR207 (*Invitrogen*) (Table 18) using BP Clonase II Enzyme Mix (*Thermo Fisher Scientific*) and subsequently transformed into TOP10 chemically competent *E. coli* (*Invitrogen*). Plasmid DNA was purified using E.Z.N.A Plasmid Mini Kit I (*Omega Bio-tek*). Fl-SpsB was cloned into the destination vector pET-55-DEST

(Novagen) by the LR Clonase II Enzyme Mix (*Thermo Fisher Scientific*) and transformed into chemically competent *E. coli* BL21(DE3)pLysS (*Promega*). Plasmid DNA was purified and the correct sequence was verified via Sanger sequencing (*GATC Biotech*). Upon translation, the sequence additionally gets an N-terminal *Strep*-tag II coded in the destination vector as well as some amino acids belonging to the *attB1* site required for the cloning strategy resulting in a protein sequence comprising 220 amino acids and having a molecular weight of 24951.4 Da (average mass) (Figure S4).

Table 17: Primer sequences used for cloning of SpsB in *E. coli* BL21(DE3)pLysS. AttB1- and attB2-sequences are underlined, the TEV cleavage site sequence is shown in italics and the replacement of the rare ATA- to TTA-codon is shown in bold letters. Capital letters indicate consensus sequences with the SpsB genetic code (with the exception of the replacement of the codon ATA to TTA).

Primer	Sequence (5'- to -3')
fl-SpsB-fw	<u>ggggacaagtttgtacaaaaagcaggctttgagaatctttattttcagggc</u> AAAAAAGAATTATTGGAATGGATTATT
fl-SpsB-rv	<u>ggggaccactttgtacaagaaagctgggtg</u> TAAATTTTAGTATTTTCAGGatt

Table 18: Plasmids used for cloning of SpsB in *E. coli* BL21(DE3)pLysS.

Plasmid	Description	Source
pDONR207	<i>rrnB</i> T2, <i>rrnB</i> T1, <i>attP1</i> , <i>ccdB</i> , Cm ^R , <i>attP2</i> , Gm ^R , pUC ori, Gateway donor vector	Invitrogen
pDONR207-fl-SpsB	<i>rrnB</i> T2, <i>rrnB</i> T1, <i>attL1</i> , <i>attL2</i> , Gm ^R , pUC ori, fl-SpsB cloned into <i>attP1</i> and <i>attP2</i> sites of pDONR207, entry clone	This study
pET-55-DEST	<i>attR1</i> , <i>ccdB</i> , Cm ^R , <i>attR2</i> , Amp ^R , <i>lacI</i> , pUC ori, T7 promotor, <i>Strep</i> -tag II sequence (N-terminal), Gateway Nova destination vector)	Novagen
pET-55-DEST-fl-SpsB	<i>attB1</i> , <i>attB2</i> , Amp ^R , <i>lacI</i> , pUC ori, T7 promotor, <i>Strep</i> -tag II sequence (N-terminal), fl-SpsB cloned into <i>attR1</i> and <i>attR2</i> sites of pET-55-DEST, expression clone	This study

4.4.2 Expression and Purification of Full-length SpsB

Expression and purification of fl-SpsB were based on a previously published procedure by Rao *et al.*¹⁸⁵ *E. coli* BL21(DE3)pLysS harboring the pET-55-DEST-fl-SpsB were grown at 37 °C, 200 rpm in LB medium to OD₆₀₀ = 0.5 - 0.6. To induce the overexpression, isopropyl β-D-1-thiogalactosidase (IPTG, 0.5 mM) was added. After incubation (22 °C, 200 rpm, 3 h), cells were harvested by centrifugation (5,000 × g, 4 °C, 10 min) and washed with PBS. For purification of the recombinant protein from the soluble

fraction, cells were resuspended in Tris-HCl (50 mM, pH 8; supplemented with 20% sucrose and 1 × protease inhibitor cocktail (Complete, Mini, EDTA-free, *Roche Diagnostics*)), treated with DNase I (5 µg/mL, *AppliChem*) and lysed using high-pressure homogenization (1.7 kbar), and additionally by ultrasonication (80% intensity, 5 min; Sonopuls HD 2070 ultrasonic rod, *Bandelin electronic GmbH*) on ice. Cell debris was removed by centrifugation (12,000 × g, 4 °C, 10 min) and the resulting supernatant transferred onto a StrepTrap HP column (*GE Healthcare Life Sciences*) for the purification on an ÄKTA protein purification system (*GE Healthcare Life Sciences*). The column was washed with eight column volumes of washing buffer (100 mM Tris, 150 mM NaCl, 1 mM EDTA) and eluted with washing buffer containing d-desthiobiotin (2.5 mM, *IBA*). The identity of the protein was verified by both western blotting using a Strep-Tactin-HRP conjugate and via intact protein mass spectrometry.

4.4.3 Western Blot Analysis

Western Blots were performed using Strep-Tactin-HRP conjugate (*IBA*) following the manufacturer's protocol using semi-dry Trans-Blot SD Transfer Cell (*Bio-Rad*). Blotting filter paper was soaked in blotting buffer (48 mM Tris-base (Trizma), 39 mM glycine, 10% SDS, 20% MeOH). A PVDF membrane (immun-blot PVDF membrane, *Bio-Rad*), was wetted for 5 min in 100% methanol. The SDS-PA-gel was bathed shortly in blotting buffer and placed on the membrane between two blotting filters. Western blotting was carried out at 10 V for 50 min. After the transfer, the membrane was blocked for 1 h at RT on an orbital shaker in 3% BSA and 0.5% Tween 20 in PBS (PBS-T), washed 3 times for 5 min with 0.1% PBS-T and incubated with 10.000-fold dilution of the Strep-Tactin-Conjugate in 0.1% PBS-T for 1 h at RT on an orbital shaker. The membrane was then washed 2 times with 0.1% PBS-T and 2 times with PBS for 1 min each. Detection was carried out using ECL Prime Western Blotting Detection Reagent (*GE Amersham*) via chemoluminescence read-out on a LAS-4000 gel scanning station (*Fujifilm*).

4.4.4 Intact Protein Mass Spectrometry

Intact protein measurements were performed on a Ultimate 3000 HPLC system (*Thermo Fisher Scientific*) coupled to a linear trap quadrupole fourier transform LTQ-FT mass spectrometer (LTQ-FT Ultra, *Thermo Fisher Scientific*). Samples were desalted on-line using a Massprep desalting cartridge (*Waters*) and further analyzed in electrospray ionization (ESI) positive mode (spray voltage 4.0 kV, tube lens 110 V, capillary voltage 48 V, sheath gas 60 arb, aux gas 10 arb) with a resolution of 200,000 and a mass range of 600-2000 m/z. Deconvolution of collected data was performed using Xcalibur software (*Thermo Fisher Scientific*).

4.4.5 Preparation of Membrane Fractions from *E. coli* and *S. aureus* NCTC 8325

For preparation of *E. coli* membrane fractions, growth and induction of BL21(DE3)pLysS cells harboring the pET-55-DEST-fl-SpsB were performed as described above (Chapter 4.4.2). For preparation of *S. aureus* NCTC 8325 membrane fractions, cells were grown up to the stationary phase (B medium, 37 °C, 200 rpm) after inoculation from the respective overnight cultures (1:100). The preparation of membrane fractions was performed as previously described by Therien *et al.*¹⁸⁷ *E. coli* and *S. aureus* cells were harvested (12,000 × g, 10 min, 4 °C) and lysed using a bead beater homogenizer (6 × 5500 rpm, 15 s, 2 min cooling breaks on ice after each run; Precellys Ceramic Kit CK01L, 7.0 mL tubes; Precellys 24 Homogenizer, Bertin Technologies). The lysate was centrifuged (12,000 × g, 4 °C, 10 min) to remove intact cells and debris. Membranes were collected from the supernatant (39,000 × g, 4 °C, 75 min) and resuspended in cold sodium phosphate buffer (50 mM, pH 7.5). Protein concentrations were determined using the Pierce BCA Protein assay kit (Thermo Fisher Scientific).

4.4.6 FRET Assays

SpsB activities were measured using the Förster Resonance Energy Transfer (FRET) assay, as described by Rao *et al.*¹⁸⁵ A synthetic peptide based on the known SpsB substrate SceD and modified by 4-(4-dimethylaminophenylazo)benzoic (DABCYL) acid and 5-((2-aminoethyl)amino)-1-naphthalenesulfonic (EDANS) acid was used as substrate (DABCYL-AGHDAHASET-EDANS, AnaSpec). Assays were performed with either purified fl-SpsB (0.2 μM protein concentration) or with membranes from both induced and not induced *E. coli* membranes (50 μg/mL total membrane protein concentration) or *S. aureus* NCTC 8325 membranes (200 μg/mL total membrane protein concentration) in 50 mM sodium phosphate buffer pH 7.5. Membranes containing endogenous SpsB or recombinant SpsB (100 μL/well final volume, 50 mM sodium phosphate buffer, 50 mM, pH 7.5) were treated with varying concentrations of the respective compound or DMSO (1:100, final assay concentration of DMSO from compound stocks 1%) at 37 °C for 5 min. After addition of the substrate (10 μM final substrate concentration, final DMF concentration from substrate stock 1%), fluorescence turnover was monitored by a Tecan infinite 200Pro plate reader (340 nm excitation and 510 nm emission wavelengths, fluorescence top reading mode) at 37 °C. Initial substrate cleavage velocities were determined (linear range), normalized to DMSO-treated samples (for *E. coli* data was normalized to DMSO-treated sample for induced membranes), and plotted against respective compound concentrations. Curves were fitted by the nonlinear Hill1 function ($y=START+(END-START)*x^n/(k^n+x^n)$, OriginPro 9.1G, OriginLab). *P*-values for the stimulation were determined for compound concentrations of 10 μM using an unpaired parametric *t*-test.

4.5 Other Methods

4.5.1 Computational methods - Molecular Docking and Dynamic Simulations

Preparation of the Systems

The nomenclature for residue numbers refers to the genomic sequence of *S. aureus* NCTC 8325 SpsB and is based on the entire extracellular region of the protein (residues index 26–191).

For the preparation of the systems, the signal peptidase crystal structure with the PDB code 4wvj was used for the simulations. The bound peptide was removed and the protein was solvated in a water box using tleap module of the Amber15²⁷⁴ program package by applying a 12 Å buffer region around protein atoms (yielding in a model consisting of ~30,000 atoms).

Molecular Dynamic Simulations

All simulations were performed using the ff03,²⁷⁵ GAFF²⁷⁶ and TIP3P²⁷⁷ force field parameters for the solute, **PK150**, and solvent, respectively. Missing bonded parameters for the probe were obtained using the antechamber package²⁷⁸ of Amber15, with the RESP charges calculated by the Gaussian09 software.²⁷⁹ Prior to the minimization of the models, the density of the systems was adjusted to 1 g/cm³ using an in-house python script. Hydrogens and heavy atoms were minimized consecutively, using the SANDER module of Amber15. Periodic boundary conditions were applied. Long-range electrostatic interactions were calculated using the particle mesh Ewald method.²⁸⁰ A non-bonded cutoff of 12 Å and a time step of 1 fs were used. The systems were heated up to 300 K in the NVT ensemble in a stepwise fashion as performed in previous works.^{281,282} The SHAKE algorithm was used to constraint all bonds involving hydrogens.²⁸³ The production runs were performed in the NPT ensemble for 150 ns and 100 ns for the **PK150** bound complex and the apo-protein, respectively. The cuda-enabled graphics processing units (GPUS) version of the pmemd module of Amber15 was used.^{284,285}

Docking and Binding Free Energy Calculations

A stepwise and comparative protocol was followed in order to find the binding site of the probe. Two plausible binding sites were detected using surface based analysis and analyzing their distances to the active site. The probe was docked to these two grooves separately, using the DynaDock approach of our in-house modeling program DynaCell.²⁰⁶ The docking was performed in two steps; broad sampling and the molecular dynamic based energy refinement of the selected poses. The energetically-highest ranked five poses (total of ten poses coming from two different binding sites) were further simulated up to 5 ns using the same simulation scheme introduced above. The Molecular Mechanics-Generalized

Born Surface Area approach (MMGBSA)²⁸⁶ was applied to calculate the binding free energies of these 10 complexes. The pose with the lowest binding free energy was chosen for further analysis. For the MMGBSA calculations, three distinct production runs (starting with different velocities) were performed on each equilibrated structure to yield 20 ns simulation time in total (time step 1 fs, a total of 225,000 complex frames (3 x 75,000)). The MMGBSA.py module²⁸⁷ of Amber15^{288,289} was used to combine these frames and calculate the binding free energy. The contribution of the solvent was computed with Generalized Born Surface Area (GBSA) with a probe radius of 1.4 Å and the 'mbondi2' radii set⁷³ using the modified GB model introduced by Case *et al.*^{290,291} The entropic contributions to the free energy of binding were not included in the calculation scheme as it has been shown that such costly computations do not significantly improve the results.^{292–294}

4.5.2 Electron Microscopy

Sample Preparation for Electron Microscopy

S. aureus strain NCTC8325 was grown in LB medium at 37 °C, 120 rpm overnight. The following day NCTC8325 was inoculated in fresh LB medium and diluted to OD₆₀₀ = 0.03. NCTC8325 was incubated at 37 °C, 120 rpm until it was grown to an OD₆₀₀ of around 0.5. Then DMSO, **PK150** (final concentration: 2.4 µM for TEM and 2.4 µM and 1.2 µM for FESEM), **PK150-C** (final concentration: 2.4 µM), **SFN** (final concentration: 24 µM), and **SFN-C** (final concentration: 24 µM) were added and incubated for 3 additional hours at 37 °C, 120 rpm. Then bacteria were fixed as described for FESEM or TEM procedures.

Field Emission Scanning Electron Microscopy (FESEM)

Bacteria were fixed with 5% formaldehyde and 2% glutaraldehyde in growth media and washed with TE buffer (10 mM Tris, 2 mM EDTA, pH 6.9). Samples were dehydrated in a graded series of acetone (10, 30, 50, 70, 90, 100%) on ice for 10 min for each step. Samples in the 100% acetone step were allowed to reach room temperature before another change in 100% acetone. Samples were then subjected to critical-point drying with liquid CO₂ (CPD 030, *Bal-Tec*). Dried samples were coated with a gold/palladium (80/20) film by sputter coating (SCD 500, *Bal-Tec*) before examination in a field emission scanning electron microscope *Zeiss Merlin* using the Everhart Thornley HESE2-detector and the inlens SE-detector in a 25:75 ratio at an acceleration voltage of 5 kV. Images were recorded with *Zeiss SEMSmart V 5.05* and contrast and brightness were adjusted with *Adobe Photoshop CS5*.

Embedding of *S. aureus* for Transmission Electron Microscopy (TEM)

First, bacteria were fixed with 5% formaldehyde and 2% glutaraldehyde in growth media, washed with TE buffer, and further fixed with 1% osmium tetroxide in TE buffer at room temperature for 1 h. After a washing step with TE buffer, samples were dehydrated with 10%, 30%, and 50% acetone on ice before incubation in 70% acetone with 2% uranyl acetate at 7 °C overnight. Samples were further dehydrated with 90% and 100% acetone on ice, allowed to reach room temperature, and further dehydrated with 100% acetone. Subsequently, samples were infiltrated with the epoxy resin Low Viscosity resin (*Agar Scientific*). After polymerisation at 75 °C for 2 days, ultrathin sections were cut with a diamond knife, collected onto butvar-coated 300 mesh grids, and counterstained with 4% aqueous uranyl acetate for 4 min. Samples were imaged in a *Zeiss* TEM 910 at an acceleration voltage of 80 kV and at calibrated magnifications. Images were recorded digitally at calibrated magnifications with a Slow-Scan CCD-Camera (*ProScan*, 1024x1024) with ITEM-Software (*Olympus Soft Imaging Solutions*). Contrast and brightness were adjusted with *Adobe* Photoshop CS5.

4.5.3 Next-Generation Sequencing

Library preparation and sequencing

Three replicates of each of the three biologically independent **SFN** mutants were sequenced. DNA extraction was performed using PowerSoil DNA extraction kit (*MOBIO Laboratories*) following manufacturer's instructions. DNA Quality of the libraries was validated using Agilent Bioanalyzer (*Agilent Technologies*) and Qbit (*Thermo Fisher Scientific*) following the manufacturer's instruction. Library preparation was performed by the use of the NEBNext Ultra DNA Library Prep Kit for Illumina. Samples were sequenced on MiSeq using MiSeq Reagent Kits v3 (2 × 300 bp).

Bioinformatic procedures

Each library generated approximately 2 M of reads. Sequences per samples were trimmed for quality and illumine adapters by the use of Trimmomatic,²⁹⁵ with the following parameters: Min. length: 200 bp, sliding window: 4:20, leading and trailing: 3. High quality reads per library were aligned using bowtie2,²⁹⁶ and BWA-SW²⁹⁷ for long-read alignment. Alignments were sorted and indexed by SAMtools. As reference, the genome of *S. aureus* NCTC 8325 (Taxon ID 93061, Genome ID 93061.5) was downloaded from Patric database v. 3.2.76 within the RefSeq repository.

Variant called format (VCF) were computed by the use of Freebayes²⁹⁸ and mpileup from SAMtools.²⁹⁹ SNIPs were recovered by the use of VarScan (v. 2.9.9), additional filters on the VCF files were performed with vcflib toolbox. Finally, filtered VCFs were annotated and characterized using snpEff software (v. 4.3i).³⁰⁰

5 Contributions

Philipp Kleiner (Chair of Organic chemistry II, Technische Universität München, Lichtenbergstraße 4, 85747, Garching, Germany) synthesized the compounds and probes. He also performed structure-activity relationship studies. The synthesis routes and analysis data will be published in his dissertation as well as in the publication by Elena Kunold, Philipp Kleiner, Katharina Rox, Megan C. Jennings, Ilke M. Ugur, Maria Reinecke, Bernhard Kuster, Iris Antes, Manfred Rohde, William M. Wuest, Eva Medina, Stephan A. Sieber entitled "Repurposing human kinase inhibitors to create an antibiotic active against drug-resistant *Staphylococcus aureus* (submitted). Furthermore, he performed hemolysis assays, cytotoxicity assays and colloidal aggregation measurements by DLS.

Gel- and mass spectrometry-based labeling as well as target deconvolution and validation experiments were performed jointly with Philipp Kleiner.

MIC testing of *Mycobacterium* species was performed by Dr. Johannes Lehmann (Chair of Organic chemistry II, Technische Universität München, Lichtenbergstraße 4, 85747, Garching, Germany) in the laboratories of Prof. Dr. Eric Ruben (Department of Immunology and Infectious Diseases, Harvard School of Public Health, Boston, USA).

Biofilm experiments were performed by Dr. Megan C. Jennings (Department of Chemistry, Temple University, 1901 N. 13th St., Philadelphia, PA, 19122, USA) and Prof. Bill M. Wuest (Department of Chemistry, Emory University, 1515 Dickey Dr, Atlanta, GA, 30322, USA)

Animal studies were carried out by Dr. Katharina Rox (Department of Chemical Biology (CBIO), Helmholtz Centre for Infection Research (HZI), Inhoffenstraße 7, 38124 Braunschweig, Germany; German Centre for Infection Research (DZIF), Partner Site Braunschweig-Hannover, Hannover, Germany) and Prof. Dr. Eva Medina (Infection Immunology Research Group, Helmholtz Centre for Infection Research, Inhoffenstrasse 7, 38124, Braunschweig, Germany).

Electron microscopy was carried out by Dr. Katharina Rox and Prof. Dr. Manfred Rohde (Central Facility for Microscopy (ZEIM), Helmholtz Centre for Infection Research (HZI), Inhoffenstraße 7, 38124, Braunschweig, Germany).

Molecular docking and dynamic simulations were performed by Dr. Ilke Ugur and Prof. Dr. Iris Antes (Center for Integrated Protein Science, Department für Biowissenschaften, Technische Universität München, Emil-Erlenmeyer-Forum 8, 85354, Freising, Germany).

Kinobead pull-downs were performed by Maria Reinecke and Prof. Dr. Bernhard Küster (Chair of Proteomics and Bioanalytics, Technische Universität München, Emil-Erlenmeyer-Forum 5, 85354,

Freising, Germany; Center for Integrated Protein Science Munich, Emil-Erlenmeyer-Forum 5, 85354, Freising, Germany).

Next-generation sequencing of sorafenib-resistant *S. aureus* was performed bei Dr. Diego Chaves-Moreno and Prof. Dr. Dietmar H. Pieper (Research Group Microbial Interactions and Processes, Helmholtz Centre for Infection Research, Inhoffenstr. 7, 38124, Braunschweig, Germany).

6 References

1. Ventola, C. L. The antibiotic resistance crisis: part 1: causes and threats. *P T* **40**, 277–83 (2015).
2. World Health Organization. Global action plan on antimicrobial resistance. *WHO Press* 1–28 (2015). doi:ISBN 978 92 4 150976 3
3. Antibacterial agents in clinical development: an analysis, of the antibacterial clinical development pipeline, including tuberculosis., Geneva: World Health Organization; 2017 (WHO/EMP/IAU/2017.12). Licence: & CC BY-NC-SA 3.0 IGO. Antibacterial Agents in Clinical Development. *Who/Emp/Iau/2017.12* 48 (2017).
4. Tacconelli, E., Magrini, N., Kahlmeter, G. & Singh, N. Global Priority List Of Antibiotic-Resistant Bacteria To Guide Research, Discovery, And Development Of New Antibiotics. *World Heal. Organ.* 1–7 (2017).
5. Alanis, A. J. Resistance to antibiotics: Are we in the post-antibiotic era? *Archives of Medical Research* **36**, 697–705 (2005).
6. Kåhrström, C. T. Entering a post-antibiotic era? *Nat. Rev. Microbiol.* **11**, 146–146 (2013).
7. Aminov, R. I. A brief history of the antibiotic era: lessons learned and challenges for the future. *Front. Microbiol.* **1**, 134 (2010).
8. Barlow, M. & Hall, B. G. Phylogenetic Analysis Shows That the OXA β -Lactamase Genes Have Been on Plasmids for Millions of Years. *J. Mol. Evol.* **55**, 314–321 (2002).
9. Fevre, C. *et al.* Six groups of the OXY β -Lactamase evolved over millions of years in *Klebsiella oxytoca*. *Antimicrob. Agents Chemother.* **49**, 3453–62 (2005).
10. Clardy, J., Fischbach, M. A. & Currie, C. R. The natural history of antibiotics. *Curr. Biol.* **19**, R437–41 (2009).
11. Kumbhar, C. & Watve, M. Why antibiotics: A comparative evaluation of different hypotheses for the natural role of antibiotics and an evolutionary synthesis. *Nat. Sci.* **5**, 26–40 (2013).
12. Berglund, B. Environmental dissemination of antibiotic resistance genes and correlation to anthropogenic contamination with antibiotics. *Infect. Ecol. Epidemiol.* **5**, 28564 (2015).
13. Goh, E.-B. *et al.* Transcriptional modulation of bacterial gene expression by subinhibitory concentrations of antibiotics. *Proc. Natl. Acad. Sci.* **99**, 17025–17030 (2002).
14. Tsui, W. H. W. *et al.* Dual Effects of MLS Antibiotics. *Chem. Biol.* **11**, 1307–1316 (2004).
15. Davies, J. Are antibiotics naturally antibiotics? *J. Ind. Microbiol. Biotechnol.* **33**, 496–499 (2006).
16. Fleming, A. On the Antibacterial Action of Cultures of a *Penicillium*, with Special Reference to their Use in the Isolation of *B. influenzae*. *Br. J. Exp. Pathol.* **10**, 226 (1929).
17. Waksman, S. A. *et al.* The Role of Antibiotics in Nature. *Perspect. Biol. Med.* **4**, 271–287 (1961).
18. Munita, J. M. & Arias, C. A. Mechanisms of Antibiotic Resistance. *Microbiol. Spectr.* **4**, (2016).
19. Fleming, A. Banquet Speech - The Nobel Prize in Physiology or Medicine. (1945). Available at: https://www.nobelprize.org/nobel_prizes/medicine/laureates/1945/fleming-speech.html. (Accessed: 4th October 2017)
20. von Wintersdorff, C. J. H. *et al.* Dissemination of Antimicrobial Resistance in Microbial Ecosystems through Horizontal Gene Transfer. *Front. Microbiol.* **7**, 173 (2016).
21. Blair, J. M. A., Webber, M. A., Baylay, A. J., Ogbolu, D. O. & Piddock, L. J. V. Molecular mechanisms of antibiotic resistance. *Nat. Rev. Microbiol.* **13**, 42–51 (2014).
22. Craney, A. & Romesberg, F. E. A Putative Cro-Like Repressor Contributes to Arylomycin Resistance in *Staphylococcus aureus*. *Antimicrob. Agents Chemother.* **59**, 3066–3074 (2015).
23. Chellat, M. F., Raguž, L. & Riedl, R. Targeting Antibiotic Resistance. *Angew. Chemie Int. Ed.* **55**, 6600–6626 (2016).
24. Lewis, K. Platforms for antibiotic discovery. *Nat. Rev. Drug Discov.* **12**, 371–87 (2013).
25. Wright, G. D. Q&A: Antibiotic resistance: where does it come from and what can we do about it? *BMC Biol.* **8**, 123 (2010).

26. Payne, D. J., Gwynn, M. N., Holmes, D. J. & Pompliano, D. L. Drugs for bad bugs: confronting the challenges of antibacterial discovery. *Nat. Rev. Drug Discov.* **6**, 29–40 (2007).
27. Fair, R. J. & Tor, Y. Antibiotics and bacterial resistance in the 21st century. *Perspect. Medicin. Chem.* 25–64 (2014). doi:10.4137/PMC.S14459
28. Katz, M. L., Mueller, L. V., Polyakov, M. & Weinstock, S. F. Where have all the antibiotic patents gone? *Nat. Biotechnol.* **24**, 1529–1531 (2006).
29. Bartlett, J. G., Gilbert, D. N. & Spellberg, B. Seven Ways to Preserve the Miracle of Antibiotics. *Clin. Infect. Dis.* **56**, 1445–1450 (2013).
30. Kirbis, A. & Krizman, M. Spread of Antibiotic Resistant Bacteria from Food of Animal Origin to Humans and Vice Versa. *Procedia Food Sci.* **5**, 148–151 (2015).
31. Lowy, F. D. Antimicrobial resistance: the example of *Staphylococcus aureus*. *J. Clin. Invest.* **111**, 1265–1273 (2003).
32. Peacock, S. J., de Silva, I. & Lowy, F. D. What determines nasal carriage of *Staphylococcus aureus*? *Trends Microbiol.* **9**, 605–10 (2001).
33. Wertheim, H. F. *et al.* The role of nasal carriage in *Staphylococcus aureus* infections. *Lancet Infect. Dis.* **5**, 751–762 (2005).
34. Acton, D. S., Tempelmans Plat-Sinnige, M. J., Wamel, W., Groot, N. & Belkum, A. Intestinal carriage of *Staphylococcus aureus*: how does its frequency compare with that of nasal carriage and what is its clinical impact? *Eur. J. Clin. Microbiol. Infect. Dis.* **28**, 115–127 (2009).
35. Kluytmans, J., van Belkum, A. & Verbrugh, H. Nasal carriage of *Staphylococcus aureus*: epidemiology, underlying mechanisms, and associated risks. *Clin. Microbiol. Rev.* **10**, 505–20 (1997).
36. Tong, S. Y. C., Davis, J. S., Eichenberger, E., Holland, T. L. & Fowler, V. G. *Staphylococcus aureus* Infections: Epidemiology, Pathophysiology, Clinical Manifestations, and Management. *Clin. Microbiol. Rev.* **28**, 603–661 (2015).
37. Thomer, L., Schneewind, O. & Missiakas, D. Pathogenesis of *Staphylococcus aureus* Bloodstream Infections. *Annu. Rev. Pathol. Mech. Dis.* **11**, 343–364 (2016).
38. Fitzpatrick, F., Humphreys, H. & O’Gara, J. P. The genetics of staphylococcal biofilm formation—will a greater understanding of pathogenesis lead to better management of device-related infection? *Clin. Microbiol. Infect.* **11**, 967–973 (2005).
39. Foster, T. J. Immune evasion by staphylococci. *Nat. Rev. Microbiol.* **3**, 948–958 (2005).
40. Lowy, F. D. *Staphylococcus aureus* Infections. *N. Engl. J. Med.* **339**, 520–532 (1998).
41. Conlon, B. P. *Staphylococcus aureus* chronic and relapsing infections: Evidence of a role for persister cells. *BioEssays* **36**, 991–996 (2014).
42. Tzagoloff, H. & Novick, R. Geometry of cell division in *Staphylococcus aureus*. *J. Bacteriol.* **129**, 343–50 (1977).
43. Monteiro, J. M. *et al.* Cell shape dynamics during the staphylococcal cell cycle. *Nat. Commun.* **6**, 8055 (2015).
44. Lan, L., Cheng, A., Dunman, P. M., Missiakas, D. & He, C. Golden Pigment Production and Virulence Gene Expression Are Affected by Metabolisms in *Staphylococcus aureus*. *J. Bacteriol.* **192**, 3068–3077 (2010).
45. Clauditz, A., Resch, A., Wieland, K.-P., Peschel, A. & Götz, F. Staphyloxanthin plays a role in the fitness of *Staphylococcus aureus* and its ability to cope with oxidative stress. *Infect. Immun.* **74**, 4950–3 (2006).
46. Plata, K., Rosato, A. E. & Wegrzyn, G. *Staphylococcus aureus* as an infectious agent: overview of biochemistry and molecular genetics of its pathogenicity. *Acta Biochim. Pol.* **56**, 597–612 (2009).
47. Liu, G. Y. *et al.* *Staphylococcus aureus* golden pigment impairs neutrophil killing and promotes virulence through its antioxidant activity. *J. Exp. Med.* **202**, 209–15 (2005).
48. Chua, K. Y. L., Stinear, T. P. & Howden, B. P. Functional genomics of *Staphylococcus aureus*. *Brief. Funct. Genomics* **12**, 305–315 (2013).

49. Gillaspay, A. F. *et al.* The *Staphylococcus aureus* NCTC 8325 Genome. in *Gram-Positive Pathogens, Second Edition* 381–412 (American Society of Microbiology, 2006). doi:10.1128/9781555816513.ch32
50. Rasmussen, G., Monecke, S., Ehricht, R. & Söderquist, B. Prevalence of clonal complexes and virulence genes among commensal and invasive *Staphylococcus aureus* isolates in Sweden. *PLoS One* **8**, e77477 (2013).
51. Bonar, E., Wójcik, I. & Wladyka, B. Proteomics in studies of *Staphylococcus aureus* virulence. *Acta Biochim. Pol.* **62**, 367–381 (2015).
52. Costa, A. R. *et al.* *Staphylococcus aureus* virulence factors and disease. *Microb. Pathog. Strateg. Combat. them Sci. Technol. Educ.* 702–710 (2013).
53. Sibbald, M. J. J. B. *et al.* Mapping the Pathways to Staphylococcal Pathogenesis by Comparative Secretomics. *Microbiol. Mol. Biol. Rev.* **70**, 755–788 (2006).
54. Tsirigotaki, A., De Geyter, J., Šoštarić, N., Economou, A. & Karamanou, S. Protein export through the bacterial Sec pathway. *Nat. Rev. Microbiol.* **15**, 21–36 (2016).
55. Rao C.V., S., De Waelheyns, E., Economou, A. & Anné, J. Antibiotic targeting of the bacterial secretory pathway. *Biochim. Biophys. Acta - Mol. Cell Res.* **1843**, 1762–1783 (2014).
56. Rao CV, S. & Anné, J. Bacterial type I signal peptidases as antibiotic targets. *Future Microbiol.* **6**, 1279–1296 (2011).
57. Culp, E. & Wright, G. D. Bacterial proteases, untapped antimicrobial drug targets. *Journal of Antibiotics* **70**, 366–377 (2017).
58. Lobanovska, M. & Pilla, G. Penicillin's discovery and antibiotic resistance: Lessons for the future? *Yale J. Biol. Med.* **90**, 135–145 (2017).
59. Enright, M. C. *et al.* The evolutionary history of methicillin-resistant *Staphylococcus aureus* (MRSA). *Proc. Natl. Acad. Sci. U. S. A.* **99**, 7687–92 (2002).
60. Chambers, H. F. & DeLeo, F. R. Waves of resistance: *Staphylococcus aureus* in the antibiotic era. *Nat. Rev. Microbiol.* **7**, 629–641 (2009).
61. Gardete, S. & Tomasz, A. Mechanisms of vancomycin resistance in *Staphylococcus aureus*. *J. Clin. Invest.* **124**, 2836–40 (2014).
62. Cameron, D. R. *et al.* Impact of daptomycin resistance on *Staphylococcus aureus* virulence. *Virulence* **6**, 127–131 (2015).
63. Harms, A., Maisonneuve, E. & Gerdes, K. Mechanisms of bacterial persistence during stress and antibiotic exposure. *Science (80-)*. **354**, aaf4268 (2016).
64. Lechner, S., Lewis, K. & Bertram, R. *Staphylococcus aureus* Persists Tolerant to Bactericidal Antibiotics. *J. Mol. Microbiol. Biotechnol.* **22**, 235–244 (2012).
65. Maisonneuve, E. & Gerdes, K. Molecular mechanisms underlying bacterial persisters. *Cell* **157**, 539–548 (2014).
66. Fisher, R. A., Gollan, B. & Helaine, S. Persistent bacterial infections and persister cells. *Nat. Rev. Microbiol.* **15**, 453–464 (2017).
67. Conlon, B. P. *et al.* Persister formation in *Staphylococcus aureus* is associated with ATP depletion. *Nat. Microbiol.* **1**, (2016).
68. Waters, E. M., Rowe, S. E., O'Gara, J. P. & Conlon, B. P. Convergence of *Staphylococcus aureus* Persister and Biofilm Research: Can Biofilms Be Defined as Communities of Adherent Persister Cells? *PLoS Pathog.* **12**, e1006012 (2016).
69. Wohlleben, W., Mast, Y., Stegmann, E. & Ziemert, N. Antibiotic drug discovery. *Microb. Biotechnol.* **9**, 541–548 (2016).
70. Sakharkar, K. R., Sakharkar, M. K. & Chow, V. T. K. Biocomputational Strategies for Microbial Drug Target Identification. in *Methods in Molecular Medicine, Vol. 142: New Antibiotic Targets* 1–10 (2008). doi:10.1007/978-1-59745-246-5_1
71. Rasko, D. A. & Sperandio, V. Anti-virulence strategies to combat bacteria-mediated disease. *Nat. Rev. Drug Discov.* **9**, 117–128 (2010).
72. Dickey, S. W., Cheung, G. Y. C. & Otto, M. Different drugs for bad bugs: antivirulence strategies in the age of antibiotic resistance. *Nat. Rev. Drug Discov.* **16**, 457–471 (2017).

73. Yarwood, J. M. & Schlievert, P. M. Quorum sensing in Staphylococcus infections. *J. Clin. Invest.* **112**, 1620–5 (2003).
74. Rangel-Vega, A., Bernstein, L. R., Mandujano-Tinoco, E. A., García-Contreras, S. J. & García-Contreras, R. Drug repurposing as an alternative for the treatment of recalcitrant bacterial infections. *Front. Microbiol.* **6**, (2015).
75. Hughes, C. C. & Fenical, W. Antibacterials from the sea. *Chemistry* **16**, 12512–25 (2010).
76. Rahman, H. *et al.* Novel Anti-Infective Compounds from Marine Bacteria. *Mar. Drugs* **8**, 498–518 (2010).
77. Zipperer, A. *et al.* Human commensals producing a novel antibiotic impair pathogen colonization. *Nature* **535**, 511–516 (2016).
78. Nichols, D. *et al.* Use of ichip for high-throughput in situ cultivation of "uncultivable microbial species". *Appl. Environ. Microbiol.* **76**, 2445–2450 (2010).
79. Ling, L. L. *et al.* A new antibiotic kills pathogens without detectable resistance. *Nature* **517**, 455–459 (2015).
80. Piddock, L. J. V. Teixobactin, the first of a new class of antibiotics discovered by iChip technology? *J. Antimicrob. Chemother.* **70**, 2679–80 (2015).
81. Rutledge, P. J. & Challis, G. L. Discovery of microbial natural products by activation of silent biosynthetic gene clusters. *Nat. Rev. Microbiol.* **13**, 509–23 (2015).
82. The PEW charitable Trusts. A Scientific Roadmap for Antibiotic Discovery. *Report May*, 1–47 (2016).
83. Nicola Nosengo. Can you teach old drugs new tricks? *Nature* **534**, 314–316 (2016).
84. Miller, J. R. *et al.* A class of selective antibacterials derived from a protein kinase inhibitor pharmacophore. *Proc. Natl Acad. Sci. USA* **106**, 1737–1742 (2009).
85. Ashburn, T. T. & Thor, K. B. Drug repositioning: identifying and developing new uses for existing drugs. *Nat. Rev. Drug Discov.* **3**, 673–683 (2004).
86. Chan, G., Hardej, D., Santoro, M., Lau-Cam, C. & Billack, B. Evaluation of the antimicrobial activity of ebselen: Role of the yeast plasma membrane H⁺-ATPase. *J. Biochem. Mol. Toxicol.* **21**, 252–264 (2007).
87. Younis, W., Thangamani, S. & Seleem, M. N. Repurposing Non-Antimicrobial Drugs and Clinical Molecules to Treat Bacterial Infections. *Curr. Pharm. Des.* **21**, 4106–11 (2015).
88. Perlmutter, J. I. *et al.* Repurposing the Antihistamine Terfenadine for Antimicrobial Activity against *Staphylococcus aureus*. *J. Med. Chem.* **57**, 8540–8562 (2014).
89. Lee, J. & Bogoyo, M. *Target deconvolution techniques in modern phenotypic profiling. Current Opinion in Chemical Biology* **17**, 118–126 (NIH Public Access, 2013).
90. Evans, M. J. & Cravatt, B. F. Mechanism-Based Profiling of Enzyme Families. *Chem. Rev.* **106**, 3279–3301 (2006).
91. Cravatt, B. F., Wright, A. T. & Kozarich, J. W. Activity-Based Protein Profiling: From Enzyme Chemistry to Proteomic Chemistry. *Annu. Rev. Biochem.* **77**, 383–414 (2008).
92. Fonović, M. & Bogoyo, M. Activity based probes for proteases: applications to biomarker discovery, molecular imaging and drug screening. *Curr. Pharm. Des.* **13**, 253–61 (2007).
93. Fonović, M. & Bogoyo, M. Activity-based probes as a tool for functional proteomic analysis of proteases. *Expert Rev. Proteomics* **5**, 721–730 (2008).
94. Li, N., Overkleeft, H. S. & Florea, B. I. Activity-based protein profiling: an enabling technology in chemical biology research. *Curr. Opin. Chem. Biol.* **16**, 227–233 (2012).
95. Patricelli, M. P. *et al.* Functional Interrogation of the Kinome Using Nucleotide Acyl Phosphates. *Biochemistry* **46**, 350–358 (2007).
96. Adachi, J. *et al.* Data for proteomic analysis of ATP-binding proteins and kinase inhibitor target proteins using an ATP probe. *Data Br.* **5**, 726–9 (2015).
97. Liu, Y., Patricelli, M. P. & Cravatt, B. F. Activity-based protein profiling: the serine hydrolases. *Proc. Natl. Acad. Sci. U. S. A.* **96**, 14694–9 (1999).

98. Jessani, N. *et al.* A streamlined platform for high-content functional proteomics of primary human specimens. *Nat. Methods* **2**, 691–697 (2005).
99. Nodwell, M. B. & Sieber, S. A. ABPP methodology: Introduction and overview. *Topics in Current Chemistry* **324**, 1–41 (2012).
100. Lapinsky, D. J. Tandem photoaffinity labeling–bioorthogonal conjugation in medicinal chemistry. *Bioorg. Med. Chem.* **20**, 6237–6247 (2012).
101. Kleiner, P., Heydenreuter, W., Stahl, M., Korotkov, V. S. & Sieber, S. A. A Whole Proteome Inventory of Background Photocrosslinker Binding. *Angew. Chemie Int. Ed.* **56**, 1396–1401 (2017).
102. Sieber, S. A., Niessen, S., Hoover, H. S. & Cravatt, B. F. Proteomic profiling of metalloprotease activities with cocktails of active-site probes. *Nat. Chem. Biol.* **2**, 274–81 (2006).
103. Balakrishnan, A. *et al.* Metalloprotease Inhibitors GM6001 and TAPI-0 Inhibit the Obligate Intracellular Human Pathogen *Chlamydia trachomatis* by Targeting Peptide Deformylase of the Bacterium. *J. Biol. Chem.* **281**, 16691–16699 (2006).
104. Salisbury, C. M. & Cravatt, B. F. Optimization of Activity-Based Probes for Proteomic Profiling of Histone Deacetylase Complexes. *J. Am. Chem. Soc.* **130**, 2184–2194 (2008).
105. Salisbury, C. M. & Cravatt, B. F. Click Chemistry-Led Advances in High Content Functional Proteomics. *QSAR Comb. Sci.* **26**, 1229–1238 (2007).
106. Sumranjit, J. & Chung, S. Recent Advances in Target Characterization and Identification by Photoaffinity Probes. *Molecules* **18**, 10425–10451 (2013).
107. Best, M. D. Click Chemistry and Bioorthogonal Reactions: Unprecedented Selectivity in the Labeling of Biological Molecules. *Biochemistry* **48**, 6571–6584 (2009).
108. Sletten, E. M. & Bertozzi, C. R. Bioorthogonal chemistry: fishing for selectivity in a sea of functionality. *Angew. Chem. Int. Ed. Engl.* **48**, 6974–98 (2009).
109. Rostovtsev, V. V., Green, L. G., Fokin, V. V. & Sharpless, K. B. A stepwise Huisgen cycloaddition process: copper(I)-catalyzed regioselective “ligation” of azides and terminal alkynes. *Angew. Chem. Int. Ed. Engl.* **41**, 2596–9 (2002).
110. Kolb, H. C. & Sharpless, K. B. The growing impact of click chemistry on drug discovery. *Drug Discov. Today* **8**, 1128–37 (2003).
111. Meldal, M. & Tornøe, C. W. Cu-Catalyzed Azide–Alkyne Cycloaddition. *Chem. Rev.* **108**, 2952–3015 (2008).
112. Eirich, J. *et al.* Pretubulysin derived probes as novel tools for monitoring the microtubule network via activity-based protein profiling and fluorescence microscopy. *Mol. Biosyst.* **8**, 2067–75 (2012).
113. Shevchenko, A., Tomas, H., Havli[š], J., Olsen, J. V. & Mann, M. In-gel digestion for mass spectrometric characterization of proteins and proteomes. *Nat. Protoc.* **1**, 2856–2860 (2007).
114. Nguyen, T. T., Sly, K. L. & Conboy, J. C. Comparison of the Energetics of Avidin, Streptavidin, NeutrAvidin, and Anti-Biotin Antibody Binding to Biotinylated Lipid Bilayer Examined by Second-Harmonic Generation. *Anal. Chem.* **84**, 201–208 (2012).
115. Yates, J. R., Ruse, C. I. & Nakorchevsky, A. Proteomics by Mass Spectrometry: Approaches, Advances, and Applications. *Annu. Rev. Biomed. Eng.* **11**, 49–79 (2009).
116. Aebersold, R. & Mann, M. Mass spectrometry-based proteomics. *Nature* **422**, 198–207 (2003).
117. Aebersold, R. & Mann, M. Mass-spectrometric exploration of proteome structure and function. *Nature* **537**, 347–55 (2016).
118. Rix, U. & Superti-Furga, G. Target profiling of small molecules by chemical proteomics. *Nat. Chem. Biol.* **5**, 616–624 (2009).
119. Zhang, Y. *et al.* Protein analysis by shotgun/bottom-up proteomics. *Chem. Rev.* **113**, 2343–94 (2013).
120. Ong, S.-E. & Mann, M. Mass spectrometry–based proteomics turns quantitative. *Nat. Chem. Biol.* **1**, 252–262 (2005).
121. Elliott, M. H., Smith, D. S., Parker, C. E. & Borchers, C. Current trends in quantitative proteomics. *Journal of Mass Spectrometry* **44**, 1637–1660 (2009).

122. Boersema, P. J., Raijmakers, R., Lemeer, S., Mohammed, S. & Heck, A. J. R. Multiplex peptide stable isotope dimethyl labeling for quantitative proteomics. *Nat. Protoc.* **4**, 484–494 (2009).
123. Cox, J. & Mann, M. MaxQuant enables high peptide identification rates, individualized p.p.b.-range mass accuracies and proteome-wide protein quantification. *Nat. Biotechnol.* **26**, 1367–1372 (2008).
124. Tyanova, S., Temu, T. & Cox, J. The MaxQuant computational platform for mass spectrometry-based shotgun proteomics. *Nat. Protoc.* **11**, 2301–2319 (2016).
125. Cox, J. *et al.* Accurate Proteome-wide Label-free Quantification by Delayed Normalization and Maximal Peptide Ratio Extraction, Termed MaxLFQ. *Mol. Cell. Proteomics* **13**, 2513–2526 (2014).
126. Dinges, M. M., Orwin, P. M. & Schlievert, P. M. Exotoxins of *Staphylococcus aureus*. *Clin. Microbiol. Rev.* **13**, 16–34 (2000).
127. George, E. A. & Muir, T. W. Molecular mechanisms of agr quorum sensing in virulent staphylococci. *ChemBioChem* **8**, 847–855 (2007).
128. Gotoh, Y. *et al.* Two-component signal transduction as potential drug targets in pathogenic bacteria. *Current Opinion in Microbiology* **13**, 232–239 (2010).
129. Kurosu, M. & Begari, E. Bacterial protein kinase inhibitors. *Drug Development Research* **71**, 168–187 (2010).
130. Ohlsen, K. & Donat, S. The impact of serine/threonine phosphorylation in *Staphylococcus aureus*. *International Journal of Medical Microbiology* **300**, 137–141 (2010).
131. Wu, P., Nielsen, T. E. & Clausen, M. H. Small-molecule kinase inhibitors: An analysis of FDA-approved drugs. *Drug Discovery Today* **21**, 5–10 (2016).
132. Cohen, M. H. *et al.* Approval Summary for Imatinib Mesylate Capsules in the Treatment of Chronic Myelogenous Leukemia. *Clin. Cancer Res.* **8**, (2002).
133. Scott, L. J. Lenvatinib: First Global Approval.: UGA Libraries Multi-Search. *Drugs* **75**, 553–560 (2015).
134. Meulenbeld, H. J. *et al.* Randomized phase II study of danusertib in patients with metastatic castration-resistant prostate cancer after docetaxel failure. *BJU Int.* **111**, 44–52 (2013).
135. Papp, K. A. *et al.* Tofacitinib, an oral Janus kinase inhibitor, for the treatment of chronic plaque psoriasis: results from two randomized, placebo-controlled, phase III trials. *Br. J. Dermatol.* **173**, 949–961 (2015).
136. Wilhelm, S. *et al.* Discovery and development of sorafenib: a multikinase inhibitor for treating cancer. *Nat. Rev. Drug Discov.* **5**, 835–844 (2006).
137. Mullard, A. 2012 FDA drug approvals. *Nat. Rev. Drug Discov.* **12**, 87–90 (2013).
138. Augustine, C. K. *et al.* Sorafenib, a Multikinase Inhibitor, Enhances the Response of Melanoma to Regional Chemotherapy. *Mol. Cancer Ther.* **9**, 2090–2101 (2010).
139. Wilhelm, S. M. *et al.* Regorafenib (BAY 73-4506): A new oral multikinase inhibitor of angiogenic, stromal and oncogenic receptor tyrosine kinases with potent preclinical antitumor activity. *Int. J. Cancer* **129**, 245–255 (2011).
140. Roskoski, R. Classification of small molecule protein kinase inhibitors based upon the structures of their drug-enzyme complexes. *Pharmacological Research* **103**, 26–48 (2016).
141. Chang, H.-C. *et al.* *In vitro* and *in vivo* activity of a novel sorafenib derivative SC5005 against MRSA. *J. Antimicrob. Chemother.* **71**, 449–459 (2016).
142. Masi, M., Réfregiers, M., Pos, K. M. & Pagès, J.-M. Mechanisms of envelope permeability and antibiotic influx and efflux in Gram-negative bacteria. *Nat. Microbiol.* **2**, 17001 (2017).
143. Li, X.-Z., Plésiat, P. & Nikaido, H. The Challenge of Efflux-Mediated Antibiotic Resistance in Gram-Negative Bacteria. *Clin. Microbiol. Rev.* **28**, 337–418 (2015).
144. Diep, B. A. *et al.* Complete genome sequence of USA300, an epidemic clone of community-acquired methicillin-resistant *Staphylococcus aureus*. *Lancet (London, England)* **367**, 731–9 (2006).
145. Hiramatsu, K., Cui, L., Kuroda, M. & Ito, T. The emergence and evolution of methicillin-resistant *Staphylococcus aureus*. *Trends Microbiol.* **9**, 486–93 (2001).

146. Zhou, W. *et al.* Molecular characterization of rifampicin-resistant *Staphylococcus aureus* isolates in a Chinese teaching hospital from Anhui, China. *BMC Microbiol.* **12**, 240 (2012).
147. Jansen van Rensburg, M. J., Whitelaw, A. C. & Elisha, B. G. Genetic basis of rifampicin resistance in methicillin-resistant *Staphylococcus aureus* suggests clonal expansion in hospitals in Cape Town, South Africa. *BMC Microbiol.* **12**, 46 (2012).
148. Sekiguchi, J. *et al.* Emergence of rifampicin resistance in methicillin-resistant *Staphylococcus aureus* in tuberculosis wards. *J. Infect. Chemother.* **12**, 47–50 (2006).
149. Pai, M. *et al.* Tuberculosis. *Nat. Rev. Dis. Prim.* **2**, 16076 (2016).
150. Kristich, C. J., Rice, L. B. & Arias, C. A. Enterococcal Infection—Treatment and Antibiotic Resistance. in *Enterococci: From Commensals to Leading Causes of Drug Resistant Infection* 1–63 (2014).
151. Hamilton-Miller, J. M. T. & Shah, S. Effect of antibiotic concentration on the killing of *Staphylococcus aureus* and *Enterococcus faecalis*: Comparison of the novel penem, Men 10700, with other β -lactam antibiotics [3]. *Journal of Antimicrobial Chemotherapy* **44**, 418–420 (1999).
152. Gullberg, E. *et al.* Selection of resistant bacteria at very low antibiotic concentrations. *PLoS Pathog.* **7**, e1002158 (2011).
153. Silver, L. L. Multi-targeting by monotherapeutic antibacterials. *Nat. Rev. Drug Discov.* **6**, 41–55 (2007).
154. Talevi, A. Multi-target pharmacology: possibilities and limitations of the “skeleton key approach” from a medicinal chemist perspective. *Front. Pharmacol.* **6**, 205 (2015).
155. Springer, M. T., Singh, V. K., Cheung, A. L., Donegan, N. P. & Chamberlain, N. R. Effect of clpP and clpC deletion on persister cell number in *Staphylococcus aureus*. *J. Med. Microbiol.* **65**, 848–857 (2016).
156. Kim, W. *et al.* Identification of an Antimicrobial Agent Effective against Methicillin-Resistant *Staphylococcus aureus* Persisters Using a Fluorescence-Based Screening Strategy. *PLoS One* **10**, e0127640 (2015).
157. Cañas-Duarte, S. J., Restrepo, S. & Pedraza, J. M. Novel protocol for persister cells isolation. *PLoS One* **9**, e88660 (2014).
158. Kussell, E., Kishony, R., Balaban, N. Q. & Leibler, S. Bacterial persistence: a model of survival in changing environments. *Genetics* **169**, 1807–14 (2005).
159. Lewis, K. Persister Cells: Molecular Mechanisms Related to Antibiotic Tolerance. in *Handbook of experimental pharmacology* 121–133 (2012). doi:10.1007/978-3-642-28951-4_8
160. Conlon, B. P. *et al.* Activated ClpP kills persisters and eradicates a chronic biofilm infection. *Nature* **503**, 365–370 (2013).
161. Keren, I., Kaldalu, N., Spoering, A., Wang, Y. & Lewis, K. Persister cells and tolerance to antimicrobials. *FEMS Microbiol. Lett.* **230**, 13–8 (2004).
162. Allison, K. R., Brynildsen, M. P. & Collins, J. J. Metabolite-enabled eradication of bacterial persisters by aminoglycosides. *Nature* **473**, 216–220 (2011).
163. Hall-Stoodley, L., Costerton, J. W. & Stoodley, P. Bacterial biofilms: from the Natural environment to infectious diseases. *Nat. Rev. Microbiol.* **2**, 95–108 (2004).
164. Jennings, M. C., Ator, L. E., Paniak, T. J., Minbiole, K. P. C. & Wuest, W. M. Biofilm-eradicating properties of quaternary ammonium amphiphiles: simple mimics of antimicrobial peptides. *Chembiochem* **15**, (2014).
165. Rabin, N. *et al.* Agents that inhibit bacterial biofilm formation. *Future Med. Chem.* **7**, 647–671 (2015).
166. Koo, H., Allan, R. N., Howlin, R. P., Stoodley, P. & Hall-Stoodley, L. Targeting microbial biofilms: current and prospective therapeutic strategies. *Nat. Rev. Microbiol.* (2017). doi:10.1038/nrmicro.2017.99
167. Ceri, H. *et al.* The MBEC Assay System: multiple equivalent biofilms for antibiotic and biocide susceptibility testing. *Methods Enzymol.* **337**, 377–85 (2001).

168. Li, A. P. Preclinical in vitro screening assays for drug-like properties. *Drug Discov. Today Technol.* **2**, 179–185 (2005).
169. Dausset, J. & Contu, L. Drug-Induced Hemolysis. *Annu. Rev. Med.* **18**, 55–70 (1967).
170. Food and Drug Administration. Guidance for Industry Nonclinical Studies for the Safety Evaluation of Pharmaceutical Excipients. *Pharmacol. Toxicol.* **12** (2005).
171. Di, L., Kerns, E. H., Hong, Y. & Chen, H. Development and application of high throughput plasma stability assay for drug discovery. *Int. J. Pharm.* **297**, 110–119 (2005).
172. Weinandy, F. *et al.* A β -Lactone-Based Antivirulence Drug Ameliorates *Staphylococcus aureus* Skin Infections in Mice. *ChemMedChem* **9**, 710–713 (2014).
173. Médard, G. *et al.* Optimized Chemical Proteomics Assay for Kinase Inhibitor Profiling. *J. Proteome Res.* **14**, 1574–1586 (2015).
174. Wu, P., Nielsen, T. E. & Clausen, M. H. FDA-approved small-molecule kinase inhibitors. *Trends Pharmacol. Sci.* **36**, 422–439 (2015).
175. Wan, P. T. C. *et al.* Mechanism of activation of the RAF-ERK signaling pathway by oncogenic mutations of B-RAF. *Cell* **116**, 855–67 (2004).
176. Roberts, J. L. *et al.* GRP78/Dna K Is a Target for Nexavar/Stivarga/Votrient in the Treatment of Human Malignancies, Viral Infections and Bacterial Diseases. *J. Cell. Physiol.* **230**, 2552–2578 (2015).
177. Booth, L. *et al.* GRP78/BiP/HSPA5/Dna K is a universal therapeutic target for human disease. *J. Cell. Physiol.* **230**, 1661–1676 (2015).
178. Bush, J. T. *et al.* The Ugi four-component reaction enables expedient synthesis and comparison of photoaffinity probes. *Chem. Sci.* **4**, 4115 (2013).
179. Sakurai, K., Ozawa, S., Yamada, R., Yasui, T. & Mizuno, S. Comparison of the Reactivity of Carbohydrate Photoaffinity Probes with Different Photoreactive Groups. *ChemBioChem* **15**, 1399–1403 (2014).
180. Marraffini, L. A., DeDent, A. C. & Schneewind, O. Sortases and the Art of Anchoring Proteins to the Envelopes of Gram-Positive Bacteria. *Microbiol. Mol. Biol. Rev.* **70**, 192–221 (2006).
181. Tyanova, S. *et al.* The Perseus computational platform for comprehensive analysis of (prote)omics data. *Nat. Methods* **13**, 731–740 (2016).
182. Débarbouillé, M. *et al.* Characterization of a serine/threonine kinase involved in virulence of *Staphylococcus aureus*. *J. Bacteriol.* **191**, 4070–81 (2009).
183. Auclair, S. M., Bhanu, M. K. & Kendall, D. A. Signal peptidase I: cleaving the way to mature proteins. *Protein Sci.* **21**, 13–25 (2012).
184. Cregg, K. M., Wilding, I. & Black, M. T. Molecular cloning and expression of the *spsB* gene encoding an essential type I signal peptidase from *Staphylococcus aureus*. *J. Bacteriol.* **178**, 5712–8 (1996).
185. Rao, S. *et al.* Enzymatic investigation of the *Staphylococcus aureus* type I signal peptidase SpsB - implications for the search for novel antibiotics. *FEBS J.* **276**, 3222–3234 (2009).
186. Paetzel, M., Karla, A., Strynadka, N. C. J. & Dalbey, R. E. Signal Peptidases. *Chem. Rev.* **102**, 4549–4580 (2002).
187. Therien, A. G. *et al.* Broadening the Spectrum of β -Lactam Antibiotics through Inhibition of Signal Peptidase Type I. *Antimicrob. Agents Chemother.* **56**, 4662–4670 (2012).
188. Craney, A. & Romesberg, F. E. The inhibition of type I bacterial signal peptidase: Biological consequences and therapeutic potential. *Bioorg. Med. Chem. Lett.* **25**, 4761–6 (2015).
189. Jin, X. *et al.* Biosynthesis of new lipopentapeptides by an engineered strain of *Streptomyces* sp. *Biotechnol. Lett.* **34**, 2283–2289 (2012).
190. Höltzel, A. *et al.* Arylomycins A and B, new biaryl-bridged lipopeptide antibiotics produced by *Streptomyces* sp. Tü 6075. II. Structure elucidation. *J. Antibiot. (Tokyo)*. **55**, 571–577 (2002).
191. Smith, P. A. & Romesberg, F. E. Mechanism of Action of the Arylomycin Antibiotics and Effects of Signal Peptidase I Inhibition. *Antimicrob. Agents Chemother.* **56**, 5054–5060 (2012).
192. Strynadka, N. C. J., Paetzel, M. & Dalbey, R. E. Crystal structure of a bacterial signal peptidase in complex with a beta-lactam inhibitor. *Nature* **396**, 186–190 (1998).

193. Wang, Y., Bruckner, R. & Stein, R. L. Regulation of signal peptidase by phospholipids in membrane: characterization of phospholipid bilayer incorporated Escherichia coli signal peptidase. *Biochemistry* **43**, 265–270 (2004).
194. Clarke, S. The size and detergent binding of membrane proteins. *J. Biol. Chem.* **250**, 5459–69 (1975).
195. Ting, Y. T. *et al.* Peptide binding to a bacterial signal peptidase visualized by peptide tethering and carrier-driven crystallization. *IUCr* **3**, 10–9 (2016).
196. Feng, B. Y. *et al.* A High-Throughput Screen for Aggregation-Based Inhibition in a Large Compound Library. *J. Med. Chem.* **50**, 2385–2390 (2007).
197. Blevitt, J. M. *et al.* Structural Basis of Small-Molecule Aggregate Induced Inhibition of a Protein–Protein Interaction. *J. Med. Chem.* **60**, 3511–3517 (2017).
198. Thorne, N., Auld, D. S. & Inglese, J. Apparent activity in high-throughput screening: origins of compound-dependent assay interference. *Curr. Opin. Chem. Biol.* **14**, 315–324 (2010).
199. Coan, K. E. D., Maltby, D. A., Burlingame, A. L. & Shoichet, B. K. Promiscuous Aggregate-Based Inhibitors Promote Enzyme Unfolding. *J. Med. Chem.* **52**, 2067–2075 (2009).
200. McGovern, S. L., Helfand, B. T., Feng, B. & Shoichet, B. K. A Specific Mechanism of Nonspecific Inhibition. *J. Med. Chem.* **46**, 4265–4272 (2003).
201. Feng, B. Y. & Shoichet, B. K. A detergent-based assay for the detection of promiscuous inhibitors. *Nat. Protoc.* **1**, 550–553 (2006).
202. Seidler, J., McGovern, S. L., Doman, T. N. & Shoichet, B. K. Identification and Prediction of Promiscuous Aggregating Inhibitors among Known Drugs. *J. Med. Chem.* **46**, 4477–4486 (2003).
203. Goode, D. R., Totten, R. K., Heeres, J. T. & Hergenrother, P. J. Identification of Promiscuous Small Molecule Activators in High-Throughput Enzyme Activation Screens. *J. Med. Chem.* **51**, 2346–2349 (2008).
204. Wolan, D. W., Zorn, J. A., Gray, D. C. & Wells, J. A. Small-molecule activators of a proenzyme. *Science* **326**, 853–8 (2009).
205. Owen, S. C., Doak, A. K., Wassam, P., Shoichet, M. S. & Shoichet, B. K. Colloidal Aggregation Affects the Efficacy of Anticancer Drugs in Cell Culture. *ACS Chem. Biol.* **7**, 1429–1435 (2012).
206. Antes, I. DynaDock: A new molecular dynamics-based algorithm for protein-peptide docking including receptor flexibility. *Proteins Struct. Funct. Bioinforma.* **78**, 1084–1104 (2010).
207. Eisenmesser, E. Z. *et al.* Intrinsic dynamics of an enzyme underlies catalysis. *Nature* **438**, 117–121 (2005).
208. McAuley, M. & Timson, D. J. Modulating Mobility: a Paradigm for Protein Engineering? *Appl. Biochem. Biotechnol.* **181**, 83–90 (2017).
209. Gersch, M. *et al.* AAA+ chaperones and acyldepsipeptides activate the ClpP protease via conformational control. *Nat. Commun.* **6**, 6320 (2015).
210. Ting, Y. T., Batot, G., Baker, E. N. & Young, P. G. Expression, purification and crystallization of a membrane-associated, catalytically active type I signal peptidase from *Staphylococcus aureus*. *Acta Crystallogr. Sect. F Struct. Biol. Commun.* **71**, 61–65 (2015).
211. Hazenbos, W. L., Skippington, E. & Tan, M.-W. *Staphylococcus aureus* type I signal peptidase: essential or not essential, that’s the question. *Microb. cell (Graz, Austria)* **4**, 108–111 (2017).
212. Morisaki, J. H. *et al.* A Putative Bacterial ABC Transporter Circumvents the Essentiality of Signal Peptidase. *MBio* **7**, e00412-16 (2016).
213. Craney, A., Dix, M. M., Adhikary, R., Cravatt, B. F. & Romesberg, F. E. An alternative terminal step of the general secretory pathway in *Staphylococcus aureus*. *MBio* **6**, (2015).
214. Lambert, P. A. Bacterial resistance to antibiotics: Modified target sites. *Advanced Drug Delivery Reviews* **57**, 1471–1485 (2005).
215. Andrä, J., Goldmann, T., Ernst, C. M., Peschel, A. & Gutschmann, T. Multiple Peptide Resistance Factor (MprF)-mediated Resistance of *Staphylococcus aureus* against Antimicrobial Peptides Coincides with a Modulated Peptide Interaction with Artificial Membranes Comprising Lysyl-Phosphatidylglycerol. *J. Biol. Chem.* **286**, 18692–18700 (2011).

216. Mishra, N. N. *et al.* Phenotypic and Genotypic Characterization of Daptomycin-Resistant Methicillin-Resistant Staphylococcus aureus Strains: Relative Roles of mprF and dlt Operons. *PLoS One* **9**, e107426 (2014).
217. Kang, K.-M. *et al.* Phenotypic and genotypic correlates of daptomycin-resistant methicillin-susceptible Staphylococcus aureus clinical isolates. *J. Microbiol.* **55**, 153–159 (2017).
218. Hoang, C. & Ferré-D'Amaré, A. R. Cocystal structure of a tRNA^{Psi55} pseudouridine synthase: nucleotide flipping by an RNA-modifying enzyme. *Cell* **107**, 929–39 (2001).
219. Hamma, T. & Ferré-D'Amaré, A. R. Pseudouridine Synthases. *Chem. Biol.* **13**, 1125–1135 (2006).
220. Schallenberger, M. A., Niessen, S., Shao, C., Fowler, B. J. & Romesberg, F. E. Type I signal peptidase and protein secretion in Staphylococcus aureus. *J. Bacteriol.* **194**, 2677–86 (2012).
221. Hiller, K., Grote, A., Scheer, M., Münch, R. & Jahn, D. PrediSi: prediction of signal peptides and their cleavage positions. *Nucleic Acids Res.* **32**, W375-9 (2004).
222. Hempel, K. *et al.* Quantitative Cell Surface Proteome Profiling for SigB-Dependent Protein Expression in the Human Pathogen *Staphylococcus aureus* via Biotinylation Approach. *J. Proteome Res.* **9**, 1579–1590 (2010).
223. Dreisbach, A., van Dijk, J. M. & Buist, G. The cell surface proteome of Staphylococcus aureus. *Proteomics* **11**, 3154–3168 (2011).
224. Gatlin, C. L. *et al.* Proteomic profiling of cell envelope-associated proteins from Staphylococcus aureus. *Proteomics* **6**, 1530–1549 (2006).
225. Pankey, G. A. & Sabath, L. D. Clinical Relevance of Bacteriostatic versus Bactericidal Mechanisms of Action in the Treatment of Gram-Positive Bacterial Infections. *Clin. Infect. Dis.* **38**, 864–870 (2004).
226. Kohanski, M. A., Dwyer, D. J. & Collins, J. J. How antibiotics kill bacteria: from targets to networks. *Nat. Rev. Microbiol.* **8**, 423–35 (2010).
227. Cotroneo, N., Harris, R., Perlmutter, N., Beveridge, T. & Silverman, J. A. Daptomycin exerts bactericidal activity without lysis of Staphylococcus aureus. *Antimicrob. Agents Chemother.* **52**, 2223–5 (2008).
228. Tomasz, A. The mechanism of the irreversible antimicrobial effects of penicillins: how the beta-lactam antibiotics kill and lyse bacteria. *Annu. Rev. Microbiol.* **33**, 113–137 (1979).
229. Chopra, I. & Roberts, M. Tetracycline Antibiotics: Mode of Action, Applications, Molecular Biology, and Epidemiology of Bacterial Resistance. *Microbiol. Mol. Biol. Rev.* **65**, 232–260 (2001).
230. Brown, L., Wolf, J. M., Prados-Rosales, R. & Casadevall, A. Through the wall: extracellular vesicles in Gram-positive bacteria, mycobacteria and fungi. *Nat. Rev. Microbiol.* **13**, 620–30 (2015).
231. Chen, C. *et al.* Secreted proteases control autolysin-mediated biofilm growth of staphylococcus aureus. *J. Biol. Chem.* **288**, 29440–29452 (2013).
232. Mann, E. E. *et al.* Modulation of eDNA release and degradation affects Staphylococcus aureus biofilm maturation. *PLoS One* **4**, (2009).
233. Nazari, M., Kurdi, M. & Heerklotz, H. Classifying surfactants with respect to their effect on lipid membrane order. *Biophys. J.* **102**, 498–506 (2012).
234. Vollmer, W., Joris, B., Charlier, P. & Foster, S. Bacterial peptidoglycan (murein) hydrolases. *FEMS Microbiol. Rev.* **32**, 259–286 (2008).
235. Forster, B. M. & Marquis, H. Protein transport across the cell wall of monoderm Gram-positive bacteria. *Mol. Microbiol.* **84**, 405–13 (2012).
236. Humann, J. & Lenz, L. L. Bacterial peptidoglycan degrading enzymes and their impact on host muropeptide detection. *J. Innate Immun.* **1**, 88–97 (2009).
237. Pasztor, L. *et al.* Staphylococcal major autolysin (Atl) is involved in excretion of cytoplasmic proteins. *J. Biol. Chem.* **285**, 36794–803 (2010).
238. Sharma, A. K., Kumar, S., K, H., Dhakan, D. B. & Sharma, V. K. Prediction of peptidoglycan hydrolases- a new class of antibacterial proteins. *BMC Genomics* **17**, 411 (2016).

239. Chao, M. C. *et al.* Protein Complexes and Proteolytic Activation of the Cell Wall Hydrolase RipA Regulate Septal Resolution in Mycobacteria. *PLoS Pathog.* **9**, e1003197 (2013).
240. Meisel, U., Höltje, J.-V. & Vollmer, W. Overproduction of inactive variants of the murein synthase PBP1B causes lysis in *Escherichia coli*. *J. Bacteriol.* **185**, 5342–8 (2003).
241. Tomasz, A., Albino, A. & Zanati, E. Multiple Antibiotic Resistance in a Bacterium with Suppressed Autolytic System. *Nature* **225**, 563–564 (1970).
242. Brown, S., Santa Maria, J. P., Walker, S. & Walker, S. Wall teichoic acids of gram-positive bacteria. *Annu. Rev. Microbiol.* **67**, 313–36 (2013).
243. Höltje, J. V & Tomasz, A. Lipoteichoic acid: a specific inhibitor of autolysin activity in *Pneumococcus*. *Proc. Natl. Acad. Sci. U. S. A.* **72**, 1690–4 (1975).
244. Rice, K. C. *et al.* The *Staphylococcus aureus* cidAB operon: evaluation of its role in regulation of murein hydrolase activity and penicillin tolerance. *J. Bacteriol.* **185**, 2635–43 (2003).
245. Brunskill, E. W. & Bayles, K. W. Identification and molecular characterization of a putative regulatory locus that affects autolysis in *Staphylococcus aureus*. *J. Bacteriol.* **178**, 611–8 (1996).
246. Bayles, K. W. The biological role of death and lysis in biofilm development. *Nat. Rev. Microbiol.* **5**, 721–726 (2007).
247. O’Neill, J. Tackling drug-resistant infections globally: final report and recommendations. *Rev. Antimicrob. Resist.* **84** (2016). doi:10.1016/j.jpha.2015.11.005
248. Lewis, K. Persister cells, dormancy and infectious disease. *Nat. Rev. Microbiol.* **5**, 48–56 (2007).
249. Wood, T. K., Knabel, S. J. & Kwan, B. W. Bacterial persister cell formation and dormancy. *Applied and Environmental Microbiology* **79**, 7116–7121 (2013).
250. Lee, E.-Y. *et al.* Gram-positive bacteria produce membrane vesicles: Proteomics-based characterization of *Staphylococcus aureus*-derived membrane vesicles. *Proteomics* **9**, 5425–5436 (2009).
251. Giesbrecht, P., Kersten, T., Maidhof, H. & Wecke, J. Staphylococcal cell wall: morphogenesis and fatal variations in the presence of penicillin. *Microbiol. Mol. Biol. Rev.* **62**, 1371–414 (1998).
252. Yamada, S. *et al.* An autolysin ring associated with cell separation of *Staphylococcus aureus*. *J. Bacteriol.* **178**, 1565–71 (1996).
253. Silver, L. L. Challenges of antibacterial discovery. *Clin. Microbiol. Rev.* (2011). doi:10.1128/CMR.00030-10
254. Singh, S. B., Young, K. & Silver, L. L. What is an ‘ideal’ antibiotic? Discovery challenges and path forward. *Biochem. Pharmacol.* **133**, 63–73 (2017).
255. Mestres, J., Gregori-Puigjané, E., Valverde, S. & Solé, R. V. The topology of drug–target interaction networks: implicit dependence on drug properties and target families. *Mol. Biosyst.* **5**, 1051 (2009).
256. Savitski, M. F. M. *et al.* Tracking cancer drugs in living cells by thermal profiling of the proteome. *Science (80-.).* **346**, 1255784–1255784 (2014).
257. Okano, A., Isley, N. A. & Boger, D. L. Peripheral modifications of [Ψ [CH₂NH]Tpg⁴]vancomycin with added synergistic mechanisms of action provide durable and potent antibiotics. *Proc. Natl. Acad. Sci.* **114**, 201704125 (2017).
258. Mani, N., Tobin, P. & Jayaswal, R. K. Isolation and characterization of autolysis-defective mutants of *Staphylococcus aureus* created by Tn917-lacZ mutagenesis. *J. Bacteriol.* **175**, 1493–9 (1993).
259. Huff, E., Silverman, C. S., Adams, N. J. & Awkard, W. S. Extracellular cell wall lytic enzyme from *Staphylococcus aureus*: purification and partial characterization. *J. Bacteriol.* **103**, 761–9 (1970).
260. Laemmli, U. K. Cleavage of structural proteins during the assembly of the head of bacteriophage T4. *Nature* **227**, 680–5 (1970).
261. Atilano, M. L. *et al.* Bacterial autolysins trim cell surface peptidoglycan to prevent detection by the *Drosophila* innate immune system. *Elife* **3**, e02277 (2014).
262. Vaz, F. & Filipe, S. Preparation and Analysis of Crude Autolytic Enzyme Extracts from *Staphylococcus aureus*. *BIO-PROTOCOL* **5**, (2015).

263. Blazyk, J. *et al.* A Novel Linear Amphipathic β -Sheet Cationic Antimicrobial Peptide with Enhanced Selectivity for Bacterial Lipids. *J. Biol. Chem.* **276**, 27899–27906 (2001).
264. Nüsslein, K., Arnt, L., Rennie, J., Owens, C. & Tew, G. N. Broad-spectrum antibacterial activity by a novel abiogenic peptide mimic. *Microbiology* **152**, 1913–1918 (2006).
265. Zhang, Y., Huo, M., Zhou, J. & Xie, S. PKSolver: An add-in program for pharmacokinetic and pharmacodynamic data analysis in Microsoft Excel. *Comput. Methods Programs Biomed.* **99**, 306–314 (2010).
266. Syrový, I. & Hodný, Z. Staining and quantification of proteins separated by polyacrylamide gel electrophoresis. *Journal of Chromatography B: Biomedical Sciences and Applications* **569**, 175–196 (1991).
267. Eliuk, S. *et al.* "Universal" Data-dependent Mass Spectrometry Method That Eliminates Time-Consuming Method Optimization for Achieving Maximal Identifications from Each Sample. (2016).
268. Ventura, C. L. *et al.* Identification of a Novel *Staphylococcus aureus* Two-Component Leukotoxin Using Cell Surface Proteomics. *PLoS One* **5**, e11634 (2010).
269. Cox, J. *et al.* Andromeda: A Peptide Search Engine Integrated into the MaxQuant Environment. *J. Proteome Res.* **10**, 1794–1805 (2011).
270. Bantscheff, M. *et al.* Quantitative chemical proteomics reveals mechanisms of action of clinical ABL kinase inhibitors. *Nat. Biotechnol.* **25**, 1035–44 (2007).
271. Lemeer, S., Zörgiebel, C., Ruprecht, B., Kohl, K. & Kuster, B. Comparing immobilized kinase inhibitors and covalent ATP probes for proteomic profiling of kinase expression and drug selectivity. *J. Proteome Res.* **12**, 1723–31 (2013).
272. Katzen, F. Gateway[®] recombinational cloning: a biological operating system. *Expert Opin. Drug Discov.* **2**, 571–589 (2007).
273. Invitrogen. Gateway recombination cloning technology. *Integr. Vlsi J.* 1–15 (2011).
274. Case, D. A. *et al.* AMBER 2017. (2017).
275. Duan, Y. *et al.* A point-charge force field for molecular mechanics simulations of proteins based on condensed-phase quantum mechanical calculations. *J. Comput. Chem.* **24**, 1999–2012 (2003).
276. Wang, J., Wolf, R. M., Caldwell, J. W., Kollman, P. A. & Case, D. A. Development and testing of a general amber force field. *J. Comput. Chem.* **25**, 1157–1174 (2004).
277. Jorgensen, W. L., Chandrasekhar, J., Madura, J. D., Impey, R. W. & Klein, M. L. Comparison of simple potential functions for simulating liquid water. *J. Chem. Phys.* **79**, 926–935 (1983).
278. Wang, J., Wang, W., Kollman, P. A. & Case, D. A. Automatic atom type and bond type perception in molecular mechanical calculations. *J. Mol. Graph. Model.* **25**, 247–260 (2006).
279. Frisch, M. J. *et al.* Gaussian 09. *Gaussian, Inc. Wallingford CT* 2–3 (2009). doi:111
280. Essmann, U. *et al.* A smooth particle mesh Ewald method. *J. Chem. Phys.* **103**, 8577–8593 (1995).
281. Marcinowski, M. *et al.* Conformational Selection in Substrate Recognition by Hsp70 Chaperones. *J. Mol. Biol.* **425**, 466–474 (2013).
282. Schneider, M. *et al.* BiPPred: Combined sequence- and structure-based prediction of peptide binding to the Hsp70 chaperone BiP. *Proteins Struct. Funct. Bioinforma.* **84**, 1390–1407 (2016).
283. Ryckaert, J. P., Ciccotti, G. & Berendsen, H. J. C. Numerical integration of the cartesian equations of motion of a system with constraints: molecular dynamics of n-alkanes. *J. Comput. Phys.* **23**, 327–341 (1977).
284. Götz, A. W. *et al.* Routine Microsecond Molecular Dynamics Simulations with AMBER on GPUs. 1. Generalized Born. *J. Chem. Theory Comput.* **8**, 1542–1555 (2012).
285. Salomon-Ferrer, R., Götz, A. W., Poole, D., Le Grand, S. & Walker, R. C. Routine Microsecond Molecular Dynamics Simulations with AMBER on GPUs. 2. Explicit Solvent Particle Mesh Ewald. *J. Chem. Theory Comput.* **9**, 3878–3888 (2013).
286. Srinivasan, J., Miller, J., Kollman, P. A. & Case, D. A. Continuum Solvent Studies of the Stability of RNA Hairpin Loops and Helices. *J. Biomol. Struct. Dyn.* **16**, 671–682 (1998).

287. Miller, B. R. *et al.* MMPBSA.py : An Efficient Program for End-State Free Energy Calculations. *J. Chem. Theory Comput.* **8**, 3314–3321 (2012).
288. Hornak, V. *et al.* Comparison of multiple Amber force fields and development of improved protein backbone parameters. *Proteins Struct. Funct. Bioinforma.* **65**, 712–725 (2006).
289. Srinivasan, J., Trevathan, M. W., Beroza, P. & Case, D. A. Application of a pairwise generalized Born model to proteins and nucleic acids: inclusion of salt effects. *Theor. Chem. Accounts Theory, Comput. Model. (Theoretica Chim. Acta)* **101**, 426–434 (1999).
290. Onufriev, A., Donald Bashford & Case, D. A. Modification of the Generalized Born Model Suitable for Macromolecules. (2000). doi:10.1021/JP994072S
291. Onufriev, A., Bashford, D. & Case, D. A. Exploring protein native states and large-scale conformational changes with a modified generalized born model. *Proteins Struct. Funct. Bioinforma.* **55**, 383–394 (2004).
292. Hou, T., Wang, J., Li, Y. & Wang, W. Assessing the Performance of the MM/PBSA and MM/GBSA Methods. 1. The Accuracy of Binding Free Energy Calculations Based on Molecular Dynamics Simulations. *J. Chem. Inf. Model.* **51**, 69–82 (2011).
293. Genheden, S. MM/GBSA and LIE estimates of host–guest affinities: dependence on charges and solvation model. *J. Comput. Aided. Mol. Des.* **25**, 1085–1093 (2011).
294. Genheden, S. & Ryde, U. Comparison of the Efficiency of the LIE and MM/GBSA Methods to Calculate Ligand-Binding Energies. *J. Chem. Theory Comput.* **7**, 3768–3778 (2011).
295. Bolger, A. M., Lohse, M. & Usadel, B. Trimmomatic: A flexible trimmer for Illumina sequence data. *Bioinformatics* **30**, 2114–2120 (2014).
296. Langmead, B. & Salzberg, S. L. Fast gapped-read alignment with Bowtie 2. *Nat. Methods* **9**, 357–359 (2012).
297. Li, H. & Durbin, R. Fast and accurate long-read alignment with Burrows-Wheeler transform. *Bioinformatics* **26**, 589–595 (2010).
298. Garrison, E. & Marth, G. Haplotype-based variant detection from short-read sequencing. (2012).
299. Li, H. *et al.* The Sequence Alignment/Map format and SAMtools. *Bioinformatics* **25**, 2078–2079 (2009).
300. Cingolani, P. *et al.* A program for annotating and predicting the effects of single nucleotide polymorphisms, SnpEff: SNPs in the genome of *Drosophila melanogaster* strain w1118; iso-2; iso-3. *Fly (Austin)*. **6**, 80–92 (2012).

7 Abbreviations, Units and Symbols

ABP	Activity-based probe
ABPP	Activity-based protein profiling
AfBPP	Affinity-based protein profiling
AfBP	Affinity-based probe
AMP	Antimicrobial peptide
ATCC	American Type Culture Collection
BAC	Benzalkonium chloride
BCCM/LMG	Belgian Coordinated Collections of Microorganisms/Laboratory of microbiology
BGC	Biosynthetic Gene Cluster
BH	Benjamini-Hochberg method
BHB	Brain Heart Infusion Broth
BM	Basic medium
BSA	Bovine serum albumin
C18	Octadecyl carbon chain bonded silica
CA-MRSA	Community-acquired MRSA
CAC	Critical aggregation concentration
CETSA	Cellular thermal shift assay
CIPRO	Ciprofloxacin
CMC	Critical micelle concentration
CuAAC	Copper(I)-catalyzed alkyne-azide cycloaddition
DAP	Daptomycin
ddH ₂ O	Double-distilled water
DLS	Dynamic light scattering
DMEM	Dulbecco's Modified Eagle Medium
DMF	Dimethylformamide
DMSO	Dimethyl sulfoxide
DNA	Desoxyribonucleic acid
DSMZ	Deutsche Sammlung von Mikroorganismen und Zellkulturen
e.g.	<i>Exempli gratia</i> , for example
EM	Electron microscopy
EPS	Extracellular polymeric matrix
EV	Extracellular vesicle
FA	Formic acid
FCS	Fetal calf serum
FDR	False discovery rate
FESEM	Field emission scanning electron micrographs
Fl-SpsB	Full-length SpsB
FRET	Förster resonance energy transfer
FT-ICR	Fourier transform ion cyclotron resonance
GENTA	Gentamicin
HPLC	High performance liquid chromatography
HTS	High-throughput screening
i.e.	<i>Id est</i> , that is
IAA	2-Iodoacetamide
IPTG	Isopropyl- β -D-1-thiogalactopyranoside
LB	Lysogeny Broth

LC	Liquid chromatography
LFQ	Label free quantification
Lrp	Lytic regulatory protein (Uniprot ID: Q2FWA8)
LTA	Lipoteichoic acid
LTQ	Linear trap quadrupol
m/z	Mass to charge ratio
MBEC	Minimum biofilm eradication concentration
MBIC	Minimum biofilm inhibitory concentration
MD	Molecular dynamics
MeCN	Acetonitrile
MHB	Mueller-Hinton broth
MIC	Minimum inhibitory concentration
MRSA	Methicillin-resistant <i>Staphylococcus aureus</i>
MS	Mass spectrometry
MS/MS	Tandem mass spectrometry
MSCRAMM	Microbial surface components recognizing adhesive matrix molecule
MSSA	Methicillin-sensitive <i>Staphylococcus aureus</i>
MTT	3-(4,5-dimethylthiazol-2-yl)-2,5-diphenyltetrazolium bromide
MW	Molecular weight
n. a.	Not available
n. d.	Not detected
n. m.	Not measured
NARSA	Network on Antimicrobial Resistance in <i>Staphylococcus aureus</i>
NMR	Nuclear magnetic resonance
NTML	Nebraska Transposon Mutant Library
OD	Optical density
OFLOX	Ofloxacin
OXA	Oxacillin
PBP	Penicillin-binding protein
PBS	Phosphate-buffered saline
PCR	Polymerase chain reaction
PD	Pharmacodynamic(s)
PEN-G	Penicillin G
Pfam	Protein families (database)
PG	Peptidoglycan
PGH	Peptidoglycan hydrolysis
pH	<i>Pondus Hydrogenii</i>
PK	Pharmacokinetic(s)
PTM	Post-translational modification
QAC	Quaternary ammonium cation
ROS	Reactive oxygen species
RT	Room temperature
SAR	Structure-activity relationship
SCV	Small colony variants
SD	Standard deviation
SDS-PAGE	Sodium dodecyl sulfate polyacrylamide gel electrophoresis
SFN	Sorafenib
SFN-P	Sorafenib photoprobe
SOC	Super optimal broth with catabolite repression

SPase	Signal peptidase
SPR	Surface plasmon resonance
SpsB	Signal peptidase IB
SSC _{mec}	Staphylococcal cassette chromosome <i>mec</i>
TBTA	Tris(benzyltriazolylmethyl)amine
TCEP	Tris-(2-carboxyethyl)-phosphine
TEAB	Tetraethylammonium bromide
TEM	Transmission electron microscopy
TEV	Tobacco etch virus
TFA	Trifluoroacetic acid
TFL	Tri-functional linker
TMS	Transmembrane domain
TPP	Thermal proteome profiling
TRIS	Tris(hydroxymethyl)aminomethane
TSB	Tryptic soy broth
UV	Ultraviolet
v.	Version
VISA	Vancomycin-intermediate <i>Staphylococcus aureus</i>
VRE	Vancomycin-resistant <i>Enterococcus faecalis</i>
VRSA	Vancomycin-resistant <i>Staphylococcus aureus</i>
vs.	<i>Versus</i> , against
w/o	Without
WHO	World Health Organization
WT	Wild type
WTA	Wall teichoic acid

%	Percent
Ω	Ohm(s)
μ	Micro (10 ⁻⁶)
AU	Absorbance unit(s)
c	Centi (10 ⁻²)
CFU	Colony forming unit(s)
d	Day(s)
Da	Dalton [1 Da = 1 g/mol]
F	Farad(s)
g	Gram(s)
h	Hour(s)
k	Kilo (10 ³)
L	Litre(s)
m	Milli (10 ⁻³)/Meter(s)
M	Molar [1 M = 1 g/L]
m/z	Mass to charge ratio
min	Minute(s)
mol	Mole(s)
n	Nano (10 ⁻⁹)
p	Pico (10 ⁻¹²)
rpm	Rotations per minute
s	Second(s)
V	Volt(s)

8 Supporting Information

8.1 Supporting Figures

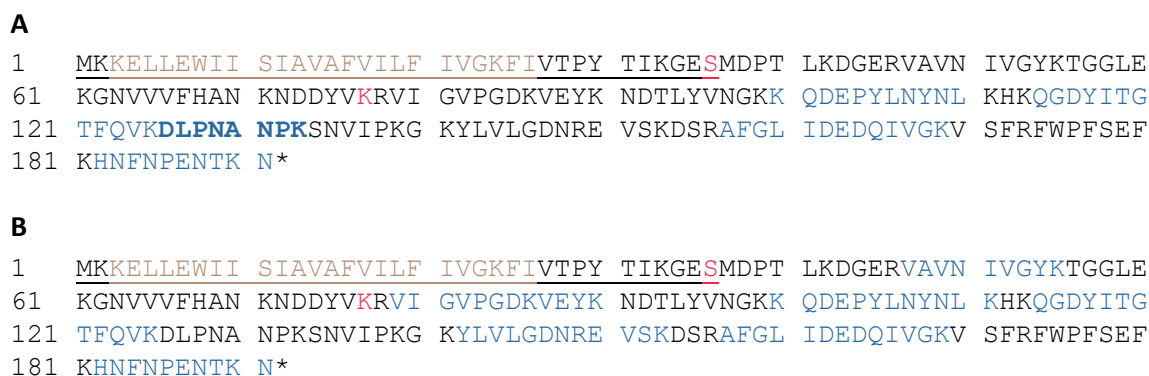


Figure S1: Unique peptides of SpsB, identified by MS/MS in the soluble (A) and insoluble (B) fractions are highlighted in blue. In red the active site amino acids Ser and Lys are highlighted. It is important to mention that the protein sequence of SpsB with the Uniprot ID Q2FZT7 is wrongly annotated; it lacks the sequence part which is underlined, comprising the catalytic serine (red) and the transmembrane domain (beige). Thus, this part of the sequence was absent in the fasta-file used for the initial identification of targets.

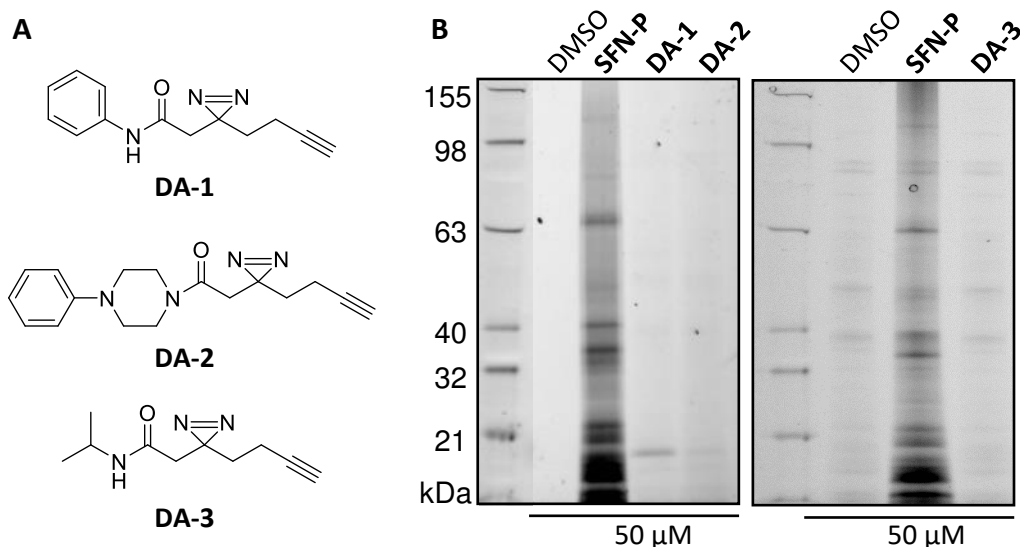


Figure S2: Panel of minimal photocrosslinker probes. (A) Structures of the probes **DA-1**, **DA-2** and **DA-3**. (B) Fluorescence SDS-PAGE shows labeling of *S. aureus* NCTC 8325 cells with sorafenib-photoprobe (**SFN-P**, 50 μM) or minimal photocrosslinker probes **DA-1**, **DA-2**, **DA-3** (50 μM)¹⁰¹ after enrichment on avidin beads. Note: No separation of soluble and insoluble fractions was conducted here.

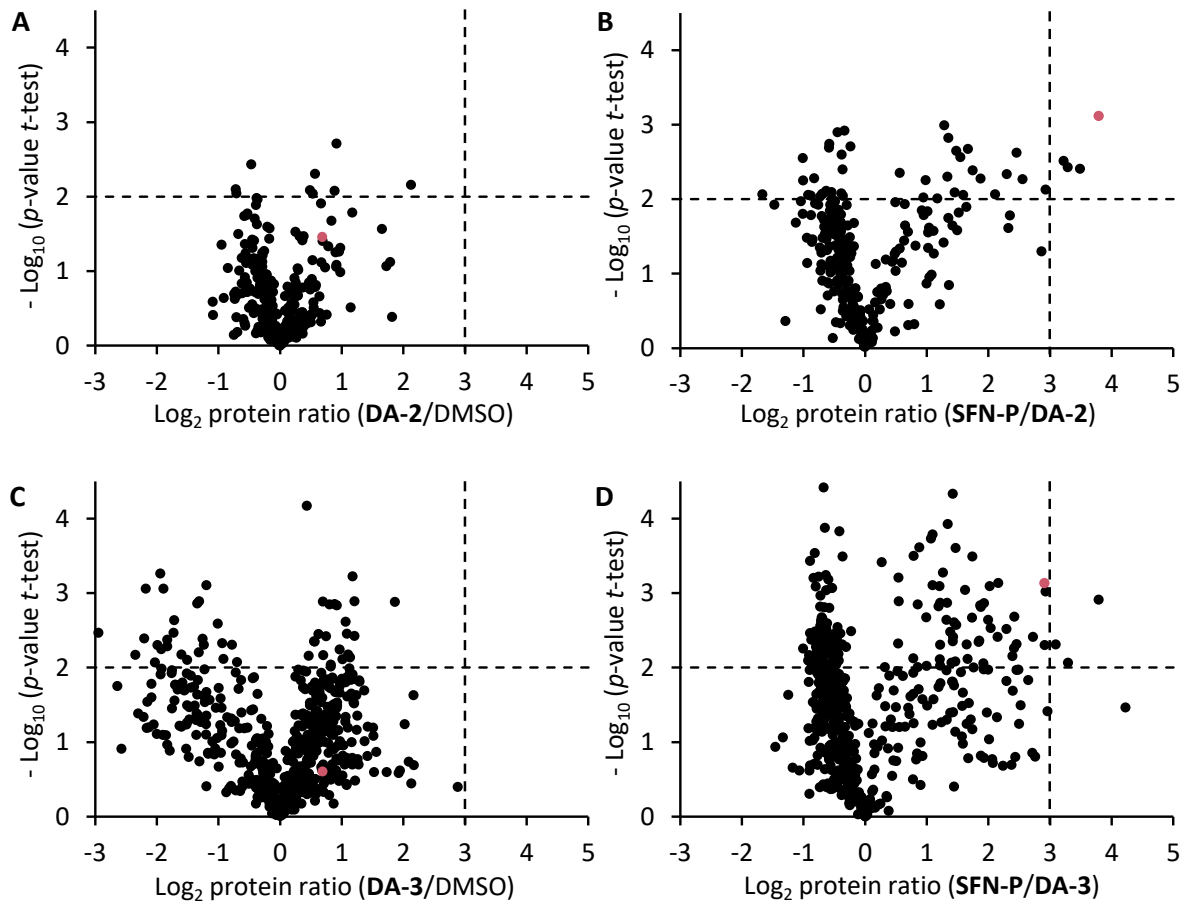


Figure S3: Photocrosslinker background binding. Volcano plots show \log_2 fold enrichment of proteins after treatment of *S. aureus* NCTC 8325 cells with minimal photocrosslinker probes **DA-2** and **DA-3** ($50 \mu\text{M}$)¹⁰¹ compared to treatment with DMSO (A, C) or **SFN-P** ($50 \mu\text{M}$, B, D). Dashed lines represent \log_2 enrichment ratio of 3 and a $-\log_{10}$ p-value of 2. The red dot represents SpsB. Data represent mean values; $n = 3$ independent experiments performed in triplicates for DA-2 and $n = 3$ independent experiments for DA-3. For structures, see Figure S2. Note: No separation of soluble and insoluble fractions was conducted here.

A

```

1   TTGAAAAAAG AAATATTGGA ATGGATTATT TCAATTGCAG TCGCTTTTGT CATTTTATTT
61  ATAGTAGGTA AATTTATTGT TACGCCATAT ACAATTAAAG GTGAATCAAT GGATCCAAC
121 TTGAAAGATG GCGAGCGAGT AGCTGTAAAC ATTGTTGGAT ATAAAACAGG TGGTTTGGAA
181 AAAGGTAATG TAGTTGTCTT CCATGCAAAAC AAAAATGATG ACTATGTAA ACCTGTCATC
241 GGTGTTCCCTG GTGATAAAGT AGAATACAAA AATGATACAT TATATGTCAA TGGTAAAAAA
301 CAAGATGAAC CATATTTAAA CTACAATTTA AACATAAAC AAGGTGATTA CATTACTGGG
361 ACTTTCCAAG TTAAAGATTT ACCGAATGCG AATCCTAAAT CAAATGTCAT TCCAAAAGGT
421 AAATATTTAG TGCTTGGAGA TAATCGTGAA GTAAGTAAAG ATAGCCGTGC GTTTGGCCTC
481 ATTGATGAAG ACCAAATTGT TGGTAAAGTT TCATTTAGGT TCTGGCCATT TAGTGAATTT
541 AACATAATT TCAATCCTGA AAATACTAAA AATTAA

```

B

```

1   LKKEILEWII SIAVAFVILF IVGKFIVTPY TIKGESMDPT LKDGERVAVN IVGYKTGGLE
61  KGNVVVFHAN KNDDYVKRVI GVPDKVEYK NDTLYVNGKK QDEPYLNYNL KHKQGDYITG
121 TFQVKDLPNA NPKSNVIPKG KYLVLGDNRE VSKDSRAFGL IDEDQIVGKV SFRFWPFSEF
181 KHNFNPENTK N*

```

C

```

1   MASWSHPQFE KGAVTSLYKK AGFENLYFQG KKELLEWII S IAVAFVILFI VGKFIVTPYT
61  IKGESMDPTL KDGERVAVNI VGYKTGGLEK GNVVVFHANK NDDYVKRVIG VPGDKVEYKN
121 DTLYVNGKKQ DEPYLNYNL HKQGDYITGT FQVKDLPNAN PKSNVIPKGK YLVLGDNREV
181 SKDSRAFGLI DEDQIVGKVS FRFWPFSEFK HNFNPENTKN*

```

D

Figure S4: SpsB sequences. (A) Native SpsB nucleotide sequence in *S. aureus* NCTC 8325. For cloning of fl-SpsB into pET-55-Dest cloning vector, TTG codon (underlined) was removed and codon for isoleucine (*ileY*) (bold and underlined) replaced by a leucine (ATA to TTA). (B) Native SpsB amino acid sequence in *S. aureus* NCTC 8325. Active amino acids Ser36 and Lys77 are highlighted in red, predicted transmembrane domain (TMS) is highlighted in beige. (C) Amino acid sequence of the cloned and expressed fl-SpsB, comprising 220 amino acids in total. Molecular weight of fl-SpsB is 24951.4 Da (average mass). Additionally to active site amino acids, highlighted in red, and TMS, highlighted in beige, sequences for Strep-tag II and TEV cleavage site are highlighted in green and blue, respectively. (D) Schematic representation of the SpsB-construct.

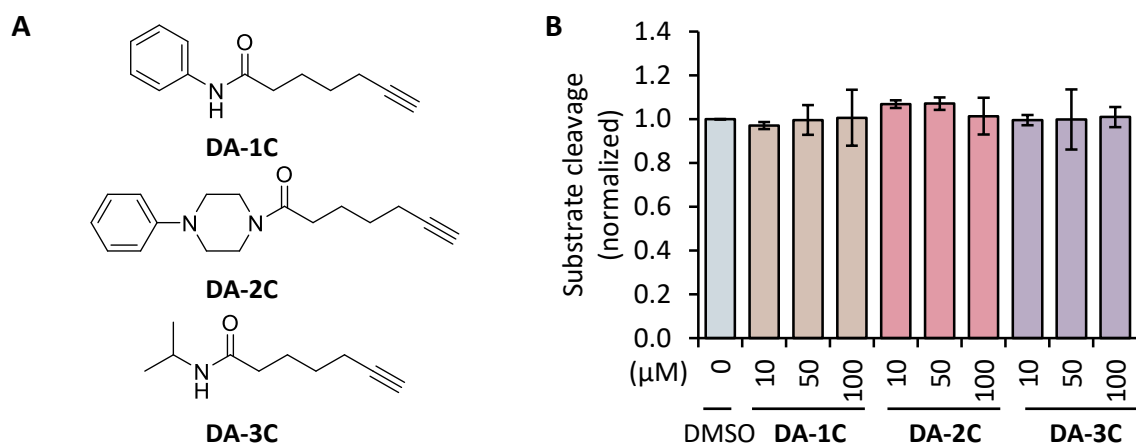


Figure S5: FRET-based activity assay with *S. aureus* NCTC 8325 membranes and minimal photocrosslinker-related control compounds, lacking the diazirine-photocrosslinker moiety to facilitate UV measurement. (A) Structures of the control compounds. (B) Membranes containing endogenous SpsB (0.2 mg/mL total membrane protein concentration) were tested using control compounds **DA-1C**, **DA-2C** and **DA-3C**, based on the respective minimal photocrosslinker probes **DA1**, **DA2** and **DA-3** (Figure S2 A). Substrate cleavage rates are normalized to DMSO-treated samples. Data represent mean values \pm SD; $n = 3$ independent experiments in triplicates.

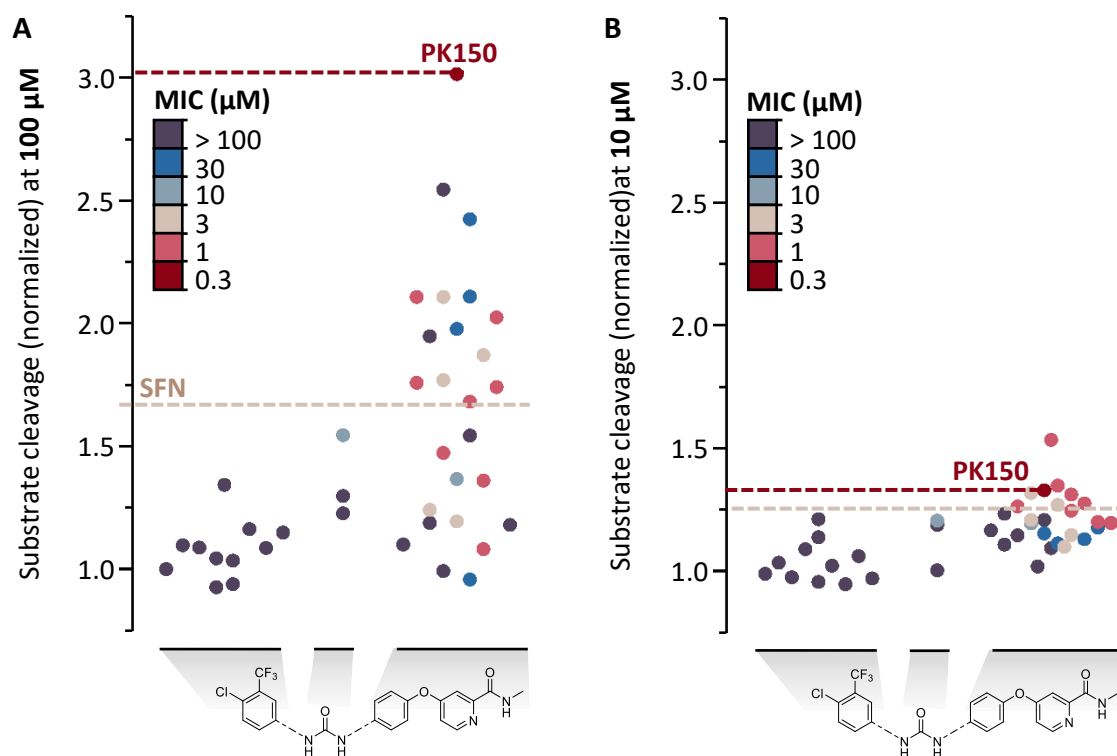


Figure S6: Correlation between modifications of the SFN scaffold, MIC (color code) and SpsB activity at (A) 100 μM and (B) 10 μM compound concentration.

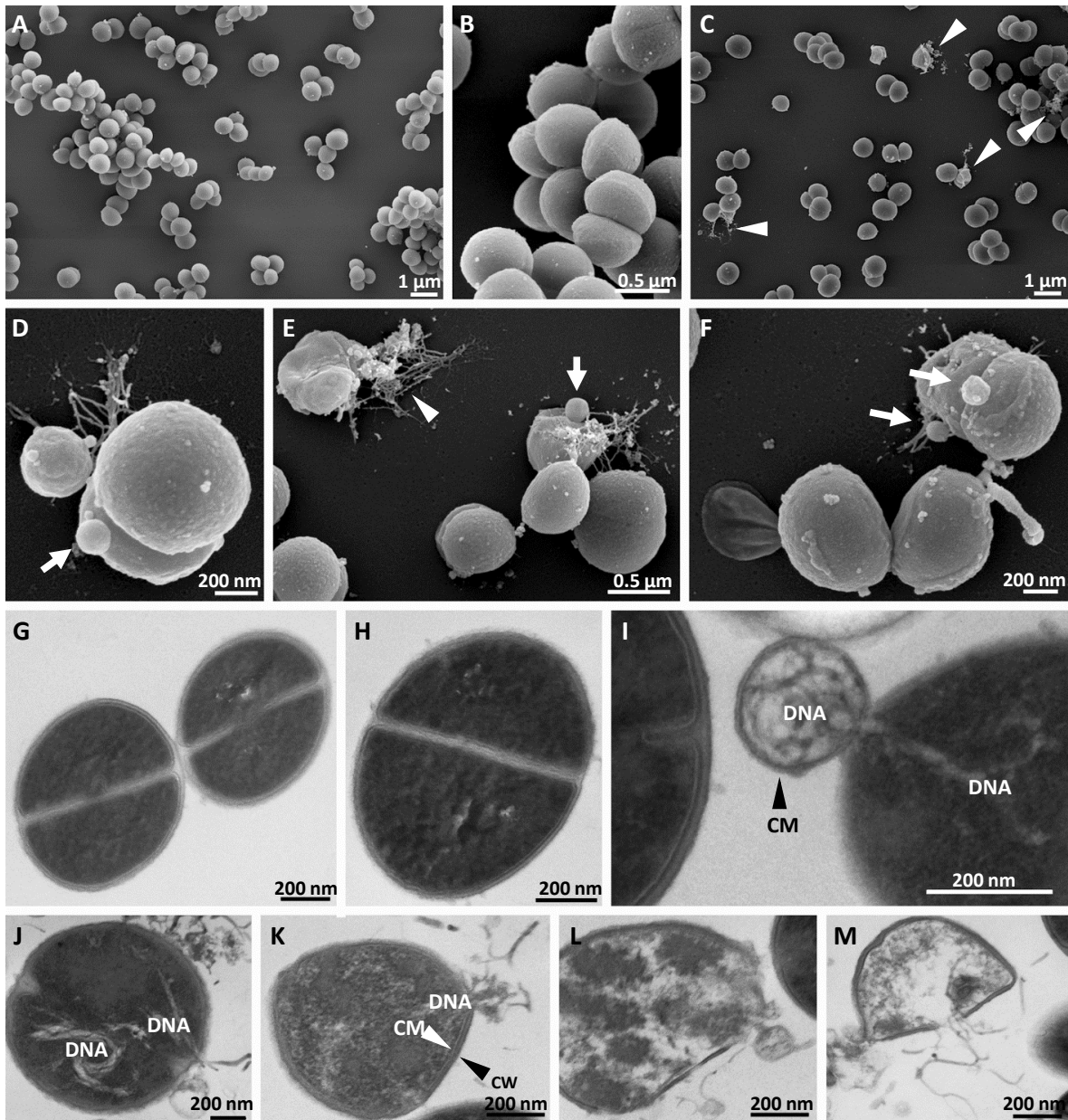


Figure S7: Electron microscopy. (A - F) FESEM micrographs of *S. aureus* NCTC 8325 treated with DMSO (A, B), 1.2 μM **PK150** (D) and 2.4 μM **PK150** (C, E, F). White arrow heads point to damaged cells and arrows point to vesicles. (G - M) TEM micrographs of *S. aureus* NCTC 8325 treated with DMSO (G), 2.4 μM **PK150-C** (H) and 2.4 μM **PK150** (I - M). DNA, Deoxyribonucleic acid; CM, cytoplasmic membrane; CW, cell wall.

8.2 Supporting Tables

Table S1: Overview of human kinase inhibitors screened for growth inhibition in *S. aureus* NCTC 8325.

Kinase Inhibitor	MIC (μ M)	Molecular Weight	Cas Number	Supplier/Manufacturer*
Sorafenib Tosylate (Bay 43-9006)	3	637.03	475207-59-1	SC
Regorafenib (Bay 73-4506)	3	482.82	755037-03-7	SC
Degrasyn (WP1130)	10	384.27	856243-80-6	SC
TAK-285	30	547.96	871026-44-7	SC
RAF265 (CHIR-265)	30	518.41	927880-90-8	SC
MK-2461	30	495.55	917879-39-1	SC
Gandotinib (LY2784544)	30	469.94	1229236-86-5	SC
Brivanib alaninate (BMS-582664)	30	441.46	649735-63-7	SC
AZ 960	30	354.36	905586-69-8	SC
AX20017	> 30	264.34	329221-38-7	SA/VM
Bisindolylmaleimid III	> 30	384.43	137592-43-9	SA/EL
Fasudil (HA-1077)	> 30	327.83	105628-07-7	SA/EL
GSK690693	> 30	425.48	37174-76-0	SA/SC
H-89	> 30	519.28	130964-39-5	SA/EL
Mitoxantrone	> 30	444.48	65271-80-9	SA/SC
Orantinib (SU6668, TSU-68)	> 30	310.35	252916-29-3	SA/SC
SB202190 (FHPI)	> 30	331.34	152121-30-7	SA/SA
Tozasertib (VX-680, MK-0457)	> 30	464.59	639089-54-6	SA/VM
Tyrphostin 23	> 30	186.17	118409-57-7	SA/SA
Wortmannin	> 30	428.43	19545-26-7	SA/SC
Temsirolimus	> 30	1030.29	162635-04-3	SC
Deforolimus (MK-8669)	> 30	990.21	572924-54-0	SC
Everolimus (RAD001)	> 30	958.22	159351-69-6	SC
Lapatinib Ditosylate	> 30	925.46	388082-77-7	SC
Rapamycin (Sirolimus)	> 30	914.17	53123-88-9	SC
Vinorelbine (Navelbine)	> 30	778.93	71486-22-1	SC
XL880 (GSK1363089)	> 30	632.65	849217-64-7	SC
R406	> 30	628.63	841290-81-1	SC
R935788	> 30	624.42	1025687-58-4	SC
BI6727	> 30	618.81	755038-65-4	SC
PF-05212384	> 30	615.73	1197160-78-3	SC
GSK1120212	> 30	615.39	871700-17-3	SC
NVP-TAE684	> 30	614.20	761439-42-3	SC
LY2228820	> 30	612.74	862507-23-1	SC
XL765	> 30	599.66	1123889-87-1	SC
Imatinib Mesylate	> 30	589.71	220127-57-1	SC
Aurora A Inhibitor I	> 30	588.07	1158838-45-9	SC

Motesanib Diphosphate	> 30	569.44	857876-30-3	SC
SU11274 (PKI-SU11274)	> 30	568.09	658084-23-2	SC
BMS-599626	> 30	567.01	8173837-23-1	SC
NVP-BSK805 dihydrochloride	> 30	563.47	1092499-93-8	SC
Tandutinib (MLN518)	> 30	562.70	387867-13-2	SC
PD318088	> 30	561.09	391210-00-7	SC
Quizartinib	> 30	560.67	950769-58-1	SC
Neratinib	> 30	557.04	698387-09-6	SC
DCC-2036	> 30	553.59	1020172-07-9	SC
KU-60019	> 30	547.67	925701-49-1	SC
GSK461364	> 30	543.60	929095-18-1	SC
Saracatinib (AZD0530)	> 30	542.03	379231-04-6	SC
Vargatef (BIBF1120)	> 30	539.62	928326-83-4	SC
GSK1838705A	> 30	532.57	1116235-97-2	SC
Sunitinib Malate	> 30	532.56	341031-54-7	SC
AP24534	> 30	532.56	943319-70-8	SC
Bosutinib (SKI-606)	> 30	530.45	380843-75-4	SC
Nilotinib	> 30	529.52	641571-10-0	SC
WYE-687	> 30	528.61	1062161-90-3	SC
BIRB 796	> 30	527.66	285983-48-4	SC
SNS-314 Mesylate	> 30	527.04	1057249-41-8	SC
ENMD-2076	> 30	525.56	934353-76-1	SC
BI 2536	> 30	521.65	755038-02-9	SC
WYE-125132	> 30	519.60	1144068-46-1	SC
MLN8237	> 30	518.92	1028486-01-2	SC
MGCD-265	> 30	517.60	875337-44-3	SC
Hesperadin	> 30	516.65	422513-13-1	SC
Enzastaurin	> 30	515.60	170364-57-5	SC
GDC-0941	> 30	513.64	957054-30-7	SC
ZM-447439	> 30	513.59	331771-20-1	SC
BMS 777607	> 30	512.89	1196681-44-3	SC
TG101209	> 30	509.67	936091-14-4	SC
Barasertib	> 30	507.56	722544-51-6	SC
PF-00562271 (PF-562271)	> 30	507.49	717907-75-0	SC
GSK2126458	> 30	505.50	1086062-66-9	SC
TAK-901	> 30	504.64	934541-31-8	SC
Raf265 derivative	> 30	504.39	n. a.	SC
TAK-733	> 30	504.23	1035555-63-5	SC
AMG 900	> 30	503.58	945595-80-2	SC
NVP-BHG712	> 30	503.48	940310-85-0	SC
PHA-680632	> 30	501.62	398493-79-3	SC
XL184	> 30	501.51	849217-68-1	SC
Masitinib (AB1010)	> 30	498.64	790299-79-5	SC

GDC-0980	> 30	498.60	1032754-93-0	SC
CCT129202	> 30	497.02	942947-93-5	SC
WYE-354	> 30	495.53	1062169-56-5	SC
WZ4002	> 30	494.97	1213269-23-8	SC
WAY-600	> 30	494.59	1062159-35-6	SC
Imatinib (STI571)	> 30	493.60	152459-95-5	SC
Apatinib	> 30	493.58	811803-05-1	SC
PIK-294	> 30	489.53	900185-02-6	SC
PIK-75 Hydrochloride	> 30	488.74	372196-77-5	SC
Dasatinib	> 30	488.01	302962-49-8	SC
Afatinib	> 30	485.94	439081-18-2	SC
Canertinib (CI-1033)	> 30	485.94	267243-28-7	SC
PD0325901	> 30	482.19	391210-10-9	SC
WZ8040	> 30	481.01	1214265-57-2	SC
MK-2206	> 30	480.39	1032350-13-2	SC
CI-1040 (PD184352)	> 30	478.66	212631-79-3	SC
PH-797804	> 30	477.30	586379-66-0	SC
Vandetanib	> 30	475.35	443913-73-3	SC
Danusertib (PHA-739358)	> 30	474.55	827318-97-8	SC
Pazopanib Hydrochloride	> 30	473.98	635702-64-6	SC
AZD8931	> 30	473.93	848942-61-0	SC
ON-01910	> 30	473.47	1225497-78-8	SC
R406 (free base)	> 30	470.45	841290-80-0	SC
BEZ235	> 30	469.54	915019-65-7	SC
CP-724714	> 30	469.53	537705-08-1	SC
Ki8751	> 30	469.41	228559-41-9	SC
BMS 794833	> 30	468.84	1174046-72-0	SC
Mubritinib	> 30	468.47	366017-09-6	SC
Pelitinib	> 30	467.92	257933-82-7	SC
AZD8055	> 30	465.54	1009298-09-2	SC
KU-0063794	> 30	465.54	938440-64-3	SC
CHIR-99021	> 30	465.34	252917-06-9	SC
WZ3146	> 30	464.95	1214265-56-1	SC
VX-680	> 30	464.59	639089-54-6	SC
AZD8330	> 30	461.23	869357-68-6	SC
Selumetinib (AZD6244)	> 30	457.68	606143-52-6	SC
Tivozanib (AV-951)	> 30	454.86	475108-18-0	SC
NVP-ADW742	> 30	453.58	475488-23-4	SC
Cediranib (AZD2171)	> 30	450.51	288383-20-0	SC
Crizotinib (PF-02341066)	> 30	450.34	877399-52-5	SC
XL147	> 30	448.52	956958-53-5	SC
PD0332991	> 30	447.53	571190-30-2	SC
Amuvatinib	> 30	447.51	850879-09-3	SC

Gefitinib (Iressa)	> 30	446.90	184475-35-2	SC
Crenolanib (CP-868569)	> 30	443.54	670220-88-9	SC
OSI-930	> 30	443.44	728033-96-3	SC
AEE788	> 30	440.58	497839-62-0	SC
BIX 02189	> 30	440.54	1094614-85-3	SC
PCI-32765	> 30	440.50	936563-96-1	SC
Flavopiridol hydrochloride	> 30	438.30	131740-09-5	SC
LY2603618	> 30	436.30	911222-45-2	SC
VX-745	> 30	436.26	209410-46-8	SC
KX2-391	> 30	431.53	897016-82-9	SC
AS703026	> 30	431.20	1236699-92-5	SC
Erlotinib Hydrochloride	> 30	429.90	183319-69-9	SC
U0126-EtOH	> 30	426.56	1173097-76-1	SC
BIX 02188	> 30	426.51	1094614-84-2	SC
PF-04691502	> 30	425.48	1013101-36-4	SC
HMN-214	> 30	424.47	173529-46-9	SC
Vatalanib	> 30	419.73	212141-51-0	SC
ZSTK474	> 30	417.41	475110-96-4	SC
BS-181 hydrochloride	> 30	416.99	n. a.	SC
KRN 633	> 30	416.86	286370-15-8	SC
OSI-420	> 30	415.87	183320-51-6	SC
CAL-101	> 30	415.42	870281-82-6	SC
Cyt387	> 30	414.46	1056634-68-4	SC
PLX-4720	> 30	413.83	918505-84-7	SC
Danusertib (PHA-739358)	> 30	413.49	503468-95-9	SC
BKM-120	> 30	410.39	1202777-78-3	SC
Telatinib	> 30	409.83	332012-40-5	SC
LDN193189	> 30	406.48	1062368-24-4	SC
OSI027	> 30	406.44	936890-98-1	SC
VX-702	> 30	404.32	479543-46-9	SC
Flavopiridol (Alvocidib)	> 30	401.84	146426-40-6	SC
IC-87114 (PIK-293)	> 30	397.43	371242-69-2	SC
PIK-293	> 30	397.43	900185-01-5	SC
PD153035 hydrochloride	> 30	396.67	183322-45-4	SC
KU-55933	> 30	395.49	587871-26-9	SC
JNJ-7706621	> 30	394.36	443797-96-4	SC
A66	> 30	393.53	1166227-08-2	SC
PIK-93	> 30	389.88	593960-11-3	SC
ZM 336372	> 30	389.45	208260-29-1	SC
Axitinib	> 30	386.47	319460-85-0	SC
SB 431542	> 30	384.39	301836-41-9	SC
AT7519	> 30	382.24	844442-38-2	SC
AT9283	> 30	381.43	896466-04-9	SC

SNS-032 (BMS-387032)	> 30	380.53	345627-80-7	SC
SB 203580	> 30	377.43	152121-47-6	SC
JNJ-38877605	> 30	377.35	943540-75-8	SC
Linifanib (ABT-869)	> 30	375.40	796967-16-3	SC
PF-04217903	> 30	372.38	956905-27-4	SC
AZD5438	> 30	371.46	602306-29-6	SC
SB 216763	> 30	371.22	280744-09-4	SC
CYC116	> 30	368.46	693228-63-6	SC
TGX-221	> 30	364.44	663619-89-4	SC
AZD7762	> 30	362.42	860352-01-8	SC
PHA-793887	> 30	361.48	718630-59-2	SC
A-769662	> 30	360.39	844499-71-4	SC
SGX-523	> 30	359.41	1022150-57-7	SC
A-674563	> 30	358.44	552325-73-2	SC
Roscovitine (CYC202)	> 30	354.45	186692-46-6	SC
PIK-90	> 30	351.36	677338-12-4	SC
CX-4945	> 30	349.77	1009820-21-6	SC
AZD1480	> 30	348.77	935666-88-9	SC
PI-103	> 30	348.36	371935-74-9	SC
TG100-115	> 30	346.34	677297-51-7	SC
SB 525334	> 30	343.42	356559-20-1	SC
CCT128930	> 30	341.84	885499-61-6	SC
AT7867	> 30	337.85	857531-00-1	SC
GDC-0879	> 30	334.37	905281-76-7	SC
GSK1059615	> 30	333.36	958852-01-1	SC
KW 2449	> 30	332.40	1000669-72-6	SC
SB 202190	> 30	331.34	152121-30-7	SC
PP121	> 30	319.36	1092788-83-4	SC
Tofacitinib citrate (CP-690550 citrate)	> 30	312.37	540737-29-9	SC
TSU-68	> 30	310.35	252916-29-3	SC
PP242	> 30	308.34	1092351-67-1	SC
LY294002	> 30	307.34	154447-36-6	SC
AS252424	> 30	305.28	900515-16-4	SC
Quercetin (Sophoretin)	> 30	302.24	117-39-5	SC
AG-490	> 30	294.30	133550-30-8	SC
AS604850	> 30	285.22	648449-76-7	SC
PD98059	> 30	267.28	167869-21-8	SC
Indirubin	> 30	262.26	479-41-4	SC
AS-605240	> 30	257.27	648450-29-7	SC
Phenformin hydrochloride	> 30	241.72	834-28-6	SC
SP600125	> 30	220.23	129-56-6	SC
AMG-208	> 30	383.40	1002304-34-8	SC
Tivantinib (ARQ-197)	> 30	369.42	905854-02-6	SC

Irbinitinib (ONT-380, ARRY-380)	> 30	480.52	937263-43-9	SC
Dovitinib (BGJ-398, CHIR-258, TKI-258,)	> 30	392.43	405169-16-6	SC
BGT226 (NVP-BGT226)	> 30	650.60	1245537-68-1	SC
Brivanib (BMS-540215)	> 30	370.38	649735-46-6	SC
CUDC-101	> 30	434.49	1012054-59-9	SC
Lenvatinib (E7080)	> 30	426.85	417716-92-8	SC
GSK1070916	> 30	507.63	942918-07-2	SC
Ruxolitinib (INCB018424)	> 30	306.37	941678-49-5	SC
Galunisertib (LY-2157299)	> 30	369.42	700874-72-2	SC
MK-5108 (VX-689)	> 30	461.94	1010085-13-8	SC
MLN-0128 (INK-128)	> 30	309.33	1224844-38-5	SC
MLN-8054	> 30	476.86	869363-13-3	SC
Sotrastaurin (NVP-AEB071)	> 30	438.48	425637-18-9	SC
Linsitinib (OSI-906)	> 30	421.49	867160-71-2	SC
Dacomitinib (PF-00299804)	> 30	469.94	1110813-31-4	SC
PF-04691502	> 30	425.48	1013101-36-4	SC
PF-03814735	> 30	474.48	942487-16-3	SC
PH-797804	> 30	477.30	586379-66-0	SC
Milciclib (PHA-848125)	> 30	460.57	802539-81-7	SC
Vemurafenib (PLX-4032, R-7204)	> 30	489.92	918504-65-1	SC
Dinaciclib (SCH-727965)	> 30	396.49	779353-01-4	SC
SGI-1776	> 30	405.42	1025065-69-3	SC
TG-101348 (SAR-302503)	> 30	524.68	936091-26-8	SC

n. a., not available; SC, Selleck Chemicals; SA, Sigma-Aldrich; VM, Vitas-M Laboratory; EL, Enzo Lifesciences International.

Table S2: Antibacterial activities of **SFN** and **PK150** in non-pathogenic and pathogenic bacteria, determined as MIC values; The highest tested concentration was 100 μ M.

Species	Strain	Resistance	MIC (μ M)	
			SFN	PK150
Gram-positive bacteria				
<i>Staphylococcus aureus</i>	ATCC 33591	MRSA	n. m.	0.76 - 1.58 ¹
	ATCC 33592	MRSA	10	0.3
	DSM-18827	MRSA	3	0.3 - 1
	Newman		3	0.3
	NCTC 8325 [#]		3	0.3
	NCTC 8325 (DSM-4910)*		n. m.	0.78 ²
	NCTC 8325-4		3	0.3
	Mu 50	MRSA, VISA	3	0.3
	SH1000		n. m.	0.76 - 1.58 ¹
	USA300 FPR3757	MRSA	3 - 10	0.3
	USA300-0114	MRSA	n. m.	1.56 ²
	N315	MRSA	3 - 10	0.3
	ARC0001 Δ spsB		3 - 10	0.3
	clinical isolates	BK95395	MRSA	3 - 10

	BK97296	MRSA	3 - 10	0.3
	IS050678	MRSA	3 - 10	0.3
	IS050611	MRSA	3 - 10	0.3
	VA417350	MRSA	3 - 10	0.3
	VA418879	MRSA	3 - 10	0.3
	VA402923	MRSA	3 - 10	0.3
	VA412350	MRSA	3 - 10	0.3
	VA409044	MRSA	3 - 10	0.3
<i>Bacillus subtilis</i>	168		5	1
<i>Enterococcus faecalis</i>	ATCC 47077		> 100	3
	ATCC 700802	VRE	> 100	3
<i>Enterococcus faecium</i>	DSM-17050	VRE	> 100	1
	DSM-20477		> 100	1
<i>Listeria monocytogenes</i>	EGD-e		3	0.3
	F2365		3	0.3
<i>Mycobacterium bovis</i>	BCG		12.5 ³	3 ³
<i>Mycobacterium smegmatis</i>	mc ² 155		50 ³	6 ³
<i>Mycobacterium tuberculosis</i>	H37Rv		25 ³	2 ³
Gram-negative bacteria				
<i>Acinetobacter baumannii</i>	DSM-30007		>100	>100
<i>Enterobacter aerogenes</i>	DSM-30053		>100	>100
<i>Enterobacter cloacae subsp. Cloacae</i>	DSM-30054		>100	>100
<i>Escherichia coli</i>	CFT073		>100	>100
<i>Klebsiella pneumoniae</i>	DSM-30104		>100	>100
<i>Pseudomonas aeruginosa</i>	DSM-19882		>100	>100
<i>Salmonella typhimurium</i>	LT2		>100	>100
	TA100		>100	>100
<i>Salmonella enteritides</i>	Veterinary isolate (dog)		>100	>100

¹Experiment was performed by Dr. Katharina Rox (Helmholtz-Zentrum für Infektionsforschung, Braunschweig, Germany); ²Experiments were performed by Dr. Megan C. Jennings (Department of Chemistry, Temple University, Philadelphia, USA); ³Experiments were performed by Dr. Johannes Lehmann in the laboratories of Prof. Eric Ruben (Department of Immunology and Infectious Diseases, Harvard School of Public Health, Boston, USA). #Strain was obtained from Institute Pasteur, France; *Strain was obtained from Deutsche Sammlung von Mikroorganismen und Zellkulturen (DSMZ); n m., not measured

Table S3: Resistance spectrum of the clinical MRSA isolates. MIC, Minimum inhibitory concentration ($\mu\text{g}/\text{mL}$); CL, Classification; S, Susceptible I, Intermediate; R, Resistant.

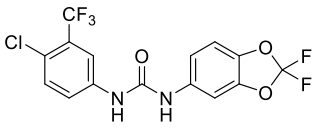
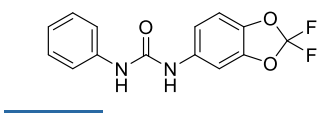
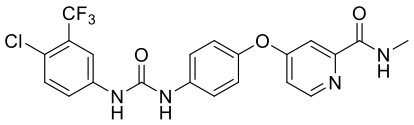
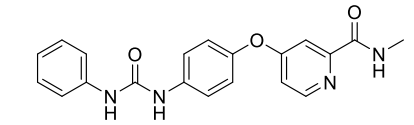
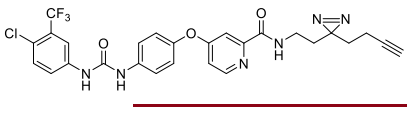
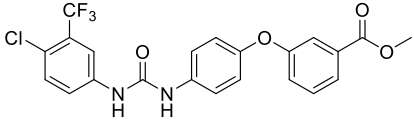
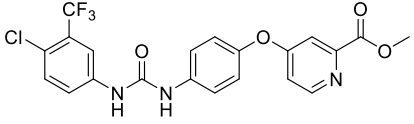
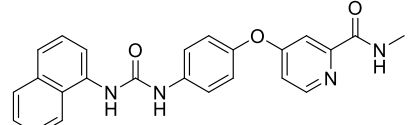
	VA402525		VA409044		VA412350		VA402923		VA418879	
	MIC	CL	MIC	CL	MIC	CL	MIC	CL	MIC	CL
Penicillin-G	≥ 0.5	R	≥ 0.5	R	≥ 0.5	R	≥ 0.5	R	≥ 0.5	R
Ampicillin/Amoxicillin		R		R		R		R		R
Oxacillin	≥ 4	R	≥ 4	R	≥ 4	R	≥ 4	R	≥ 4	R
Ampicillin+Sulbactam		R		R		R		R		R
Piperacillin		R		R		R		R		R
Piperacillin+Tazobactam		R		R		R		R		R
Cefazolin		R		R		R		R		R
Cefuroxim		R		R		R		R		R

8 - Supporting Information

Imipenem		R		R		R		R		R
Erythromycin	≥ 8	R	≤0.25	S	≤0.25	S	≤0.25	S	≥ 8	R
Clindamycin	≤0.25	S	≤0.25	S	≤0.25	S	≤0.25	S	≥ 8	R
Cotrimoxazol	≤ 10	S	≤ 10	S	≤ 10	S	≤ 10	S	≤ 10	S
Gentamicin	≤ 0.5	S	≤ 0.5	S	≤ 0.5	S	≤ 0.5	S	≤ 0.5	S
Tobramycin	≤ 1	S	≤ 1	S	≤ 1	S	≤ 1	S	≤ 1	S
Teicoplanin	≤ 0.5	S	≤ 0.5	S	≤ 0.5	S	≤ 0.5	S	≤ 0.5	S
Vancomycin	1	S	≤ 0.5	S	≤ 0.5	S	1	S	≤ 0.5	S
Ciprofloxacin		R		S		S		R		R
Levofloxacin	4	R	0.3	S	0.3	S	≥ 8	R	≥ 8	R
Moxifloxacin	2	R	≤0.25	S	≤0.25	S	≥ 8	R	4	R
Tetracycline	≤ 1	S	≤ 1	S	≤ 1	S	≤ 1	S	≤ 1	S
Rifampicin	≤ 0.5	S	≤ 0.5	S	≤ 0.5	S	≤ 0.5	S	≤ 0.5	S
Fosfomycin	≤ 8	S	≤ 8	S	≤ 8	S	≤ 8	S	≤ 8	S
Linezolid	2	S	2	S	2	S	2	S	2	S
Mupirocin	≤ 2	S	≤ 2	S	≤ 2	S	≤ 2	S	≤ 2	S
Fusidinsäure	≤ 0.5	S	≤ 0.5	S	16	I	≤ 0.5	S	≤ 0.5	S

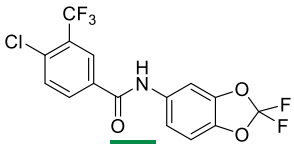
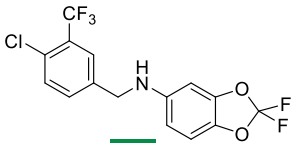
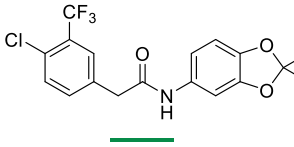
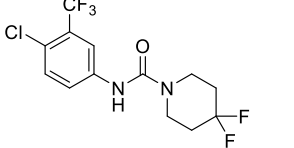
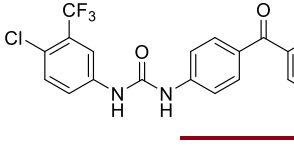
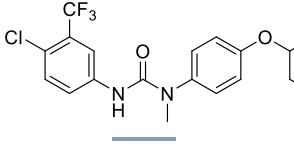
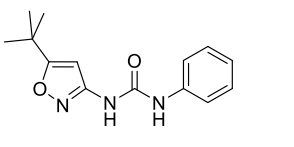
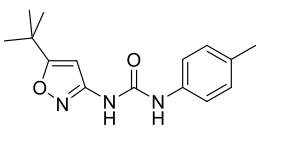
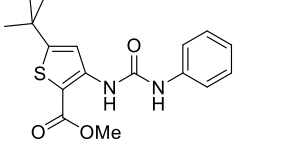
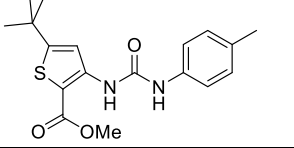
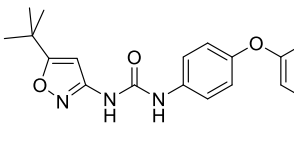
	VA417350		IS050611		BK097296		IS050678		BK095395	
	MIC	CL	MIC	CL	MIC	CL	MIC	CL	MIC	CL
Penicillin-G	≥ 0.5	R	≥ 0.5	R	≥ 0.5	R	≥ 0.5	R	≥ 0.5	R
Ampicillin/Amoxicillin		R		R		R		R		R
Oxacillin	≥ 4	R	≥ 4	R	≥ 4	R	≥ 4	R	≥ 4	R
Ampicillin+Sulbactam		R		R		R		R		R
Piperacillin		R		R		R		R		R
Piperacillin+Tazobactam		R		R		R		R		R
Cefazolin		R		R		R		R		R
Cefuroxim		R		R		R		R		R
Imipenem		R		R		R		R		R
Erythromycin	≥ 8	R	≥ 8	R	≥ 8	R	≥ 8	R	≥ 8	R
Clindamycin	≤0.25	S	≥ 8	R	≤0.25	S	≤0.25	R	≥ 8	R
Cotrimoxazol	≤ 10	S	≤ 10	S	≤ 10	S	≤ 10	S	≤ 10	S
Gentamicin	8	R	≤ 0.5	S	4	R	≤ 0.5	S	≤ 0.5	S
Tobramycin	2	R	≥ 16	R	2	R	≤ 1	S	≤ 1	S
Teicoplanin	≤ 0.5	S	≤ 0.5	S	≤ 0.5	S	≤ 0.5	S	≤ 0.5	S
Vancomycin	1	S	1	S	1	S	≤ 0.5	S	≤ 0.5	S
Ciprofloxacin		R		R		R		S		R
Levofloxacin	4	R	≥ 8	R	4	R	0.3	S	≥ 8	R
Moxifloxacin	2	R	4	R	2	R	≤0.25	S	4	R
Tetracycline	≥ 16	R	≤ 1	S	≥ 16	R	≥ 16	R	≤ 1	S
Rifampicin	≤ 0.5	S	≤ 0.5	S	≤ 0.5	S	≤ 0.5	S	≤ 0.5	S
Fosfomycin	≤ 8	S	≤ 8	S	≤ 8	S	≤ 8	S	≤ 8	S
Linezolid	2	S	2	S	4	S	2	S	2	S
Mupirocin	≤ 2	S	≤ 2	S	≤ 2	S	≤ 2	S	≤ 2	S
Fusidinsäure	≥ 32	R	≤ 0.5	S	≥ 32	R	≤ 0.5	S	≤ 0.5	S

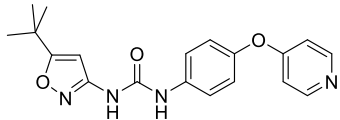
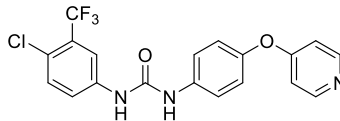
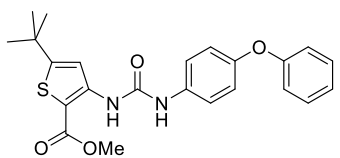
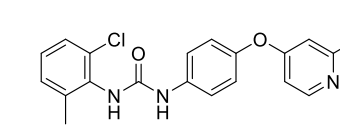
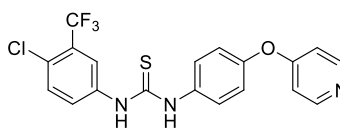
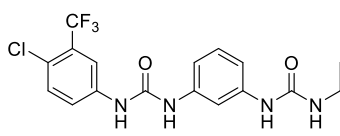
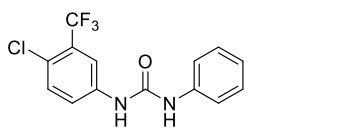
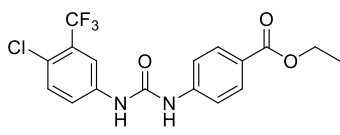
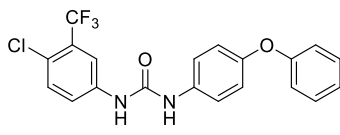
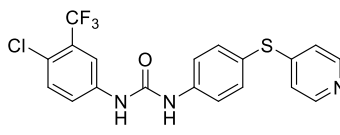
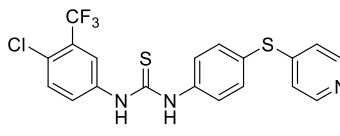
Table S4: Overview of the 72 SFN derivatives with respective structures, MICs in *S. aureus* NCTC 8325 (SA), *M. tuberculosis* H37Rv (MT), *E. faecalis* V582 (EF) and SpsB activities (normalized to DMSO) at different compound concentrations. M, mean; SD, standard Deviation); n. a., values not available due to interference with assay conditions). *Compounds, used for systematic SAR studies as depicted in Figure 9.

Name	Structure	MIC (μM)	SpsB activity (μM)								
			100			50		10			
			SA	MT	EF	M	SD	M	SD	M	SD
PK150*		5.18	0.3	5	3	3.01	0.80	2.54	0.39	1.33	0.12
PK150-C		3.7	> 100	> 40		1.25	0.17	1.15	0.01	0.99	0.05
SFN		3.76	3	40		1.69	0.22	1.64	0.12	1.25	0.07
SFN-C*		2.28	> 100	> 40		1.10	0.08	1.18	0.16	0.99	0.08
SFN-P		6.15	10			n. a.	n. a.	n. a.	n. a.	n. a.	n. a.
1-052*		5.35	0.5			1.68	0.03	1.58	0.13	1.35	0.03
1-056*		4.44	3			1.77	0.11	1.43	0.13	1.27	0.03
1-105*		3.28	> 100			1.03	0.02	0.99	0.09	1.02	0.04

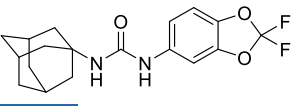
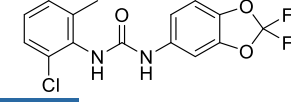
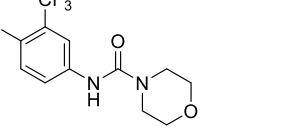
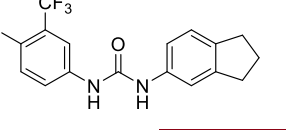
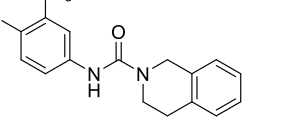
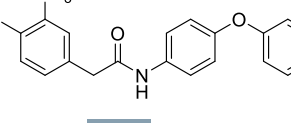
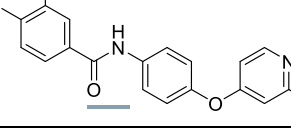
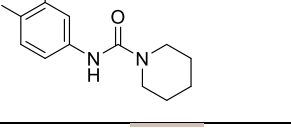
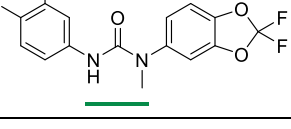
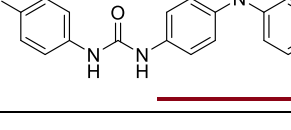
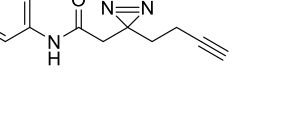
1-106*	Chemical structure of 1-106* showing a pyridine ring connected via an ether linkage to a benzamide group, which is further connected to another benzamide group with a p-tolyl substituent.	2.77	> 100			0.94	0.13	0.89	0.10	1.09	0.14
1-108*	Chemical structure of 1-108* showing a pyridine ring connected via an ether linkage to a benzamide group, which is further connected to another benzamide group with a tert-butyl substituent.	1.49	> 100			1.05	0.04	0.99	0.07	0.96	0.03
1-109*	Chemical structure of 1-109* showing a pyridine ring connected via an ether linkage to a benzamide group, which is further connected to another benzamide group with a phenoxy substituent.	3.82	> 100			1.16	0.10	1.24	0.14	1.14	0.11
1-110*	Chemical structure of 1-110* showing a pyridine ring connected via an ether linkage to a benzamide group, which is further connected to another benzamide group with a heptyl substituent.	3.53	> 100			0.93	0.22	1.05	0.22	0.98	0.04
1-112*	Chemical structure of 1-112* showing a pyridine ring connected via an ether linkage to a benzamide group, which is further connected to another benzamide group with a 2,4,6-trimethylphenyl substituent.	3.74	> 100			1.09	0.08	1.07	0.20	0.95	0.05
1-134*	Chemical structure of 1-134* showing a pyridine ring connected via an ether linkage to a benzamide group, which is further connected to another benzamide group with a 3-chloro-4-methylphenyl substituent.	3.32	> 100			1.09	0.05	1.12	0.08	1.06	0.08
1-141	Chemical structure of 1-141 showing a pyridine ring connected via an ether linkage to a benzamide group, which is further connected to another benzamide group with a 3-chloro-4-(trifluoromethyl)phenyl substituent.	4.32	1	40	10*	n. a.	n. a.	n. a.	n. a.	n. a.	n. a.
1-142	Chemical structure of 1-142 showing a pyridine ring connected via an ether linkage to a benzamide group, which is further connected to another benzamide group with a 3-chloro-4-(trifluoromethyl)phenyl substituent.	5.47	3	> 40	10*	1.39	0.06	1.22	0.03	1.19	0.02
1-144	Chemical structure of 1-144 showing a pyridine ring connected via an ether linkage to a benzamide group, which is further connected to another benzamide group with a 3-chloro-4-(trifluoromethyl)phenyl substituent.	5.2	1	20	100	n. a.	n. a.	n. a.	n. a.	n. a.	n. a.
1-145*	Chemical structure of 1-145* showing a pyridine ring connected via an ether linkage to a benzamide group, which is further connected to another benzamide group with a 3-chloro-4-(trifluoromethyl)phenyl substituent.	3.13	30			1.98	0.09	1.70	0.16	1.11	0.08
1-149*	Chemical structure of 1-149* showing a pyridine ring connected via an ether linkage to a benzamide group, which is further connected to another benzamide group with a 3-chloro-4-(trifluoromethyl)phenyl substituent.	3.3	30			0.96	0.05	1.15	0.21	1.15	0.06

1-152*	<p>Chemical structure of 1-152*: A benzamide derivative with a 3-chloro-4-(trifluoromethyl)phenyl group on the amide nitrogen and a 4-(propylamino)phenyl group on the carbonyl nitrogen.</p>	4.38	> 100		1.54	0.18	1.28	0.17	1.21	0.12
1-153*	<p>Chemical structure of 1-153*: A benzamide derivative with a 3-chloro-4-(trifluoromethyl)phenyl group on the amide nitrogen and a phenyl group on the carbonyl nitrogen.</p>	4.8	> 100		0.99	0.10	1.11	0.22	1.09	0.06
1-154*	<p>Chemical structure of 1-154*: A benzamide derivative with a 3-chloro-4-(trifluoromethyl)phenyl group on the amide nitrogen and a morpholine ring on the carbonyl nitrogen.</p>	3.88	> 100		1.95	0.12	1.28	0.16	1.02	0.05
1-155*	<p>Chemical structure of 1-155*: A benzamide derivative with a 3-chloro-4-(trifluoromethyl)phenyl group on the amide nitrogen and a 4-methoxyphenyl group on the carbonyl nitrogen.</p>	3.87	3		1.19	0.05	1.34	0.29	1.15	0.10
1-159*	<p>Chemical structure of 1-159*: A benzamide derivative with a 3-chloro-4-(trifluoromethyl)phenyl group on the amide nitrogen and a 2,3-dihydrobenzofuran ring system on the carbonyl nitrogen.</p>	3.77	10 40		1.37	0.08	1.40	0.01	1.19	0.01
1-160*	<p>Chemical structure of 1-160*: A benzamide derivative with a 3-chloro-4-(trifluoromethyl)phenyl group on the amide nitrogen and a 2,4,6-trimethoxyphenyl group on the carbonyl nitrogen.</p>	3.74	30 100		2.11	0.21	1.64	0.16	1.13	0.08
1-161*	<p>Chemical structure of 1-161*: A benzamide derivative with a 3-chloro-4-(trifluoromethyl)phenyl group on the amide nitrogen and a 2,3-dihydrobenzofuran ring system on the carbonyl nitrogen.</p>	3.5	> 100		1.19	0.06	1.28	0.13	1.15	0.08
1-162*	<p>Chemical structure of 1-162*: A benzamide derivative with a 3-chloro-4-(trifluoromethyl)phenyl group on the amide nitrogen and a 2,4,6-trimethoxyphenyl group on the carbonyl nitrogen.</p>	3.61	30		2.42	0.21	1.70	0.24	1.18	0.05
1-163*	<p>Chemical structure of 1-163*: A benzamide derivative with a 3-(trifluoromethyl)phenyl group on the amide nitrogen and a 4-(2-(dimethylamino)nicotin-5-yl)phenyl group on the carbonyl nitrogen.</p>	3.2	> 100		1.34	0.10	1.33	0.20	1.21	0.10
1-164*	<p>Chemical structure of 1-164*: A benzamide derivative with a 3-chloro-4-(trifluoromethyl)phenyl group on the amide nitrogen and a 2-(2-fluoroethoxy)phenyl group on the carbonyl nitrogen.</p>	5.18	0.5 > 40		1.08	0.17	1.42	0.08	1.25	0.05
1-166	<p>Chemical structure of 1-166: A benzamide derivative with a 3-chloro-4-(trifluoromethyl)phenyl group on the amide nitrogen and a 2-(2,2-difluoroethoxy)phenyl group on the carbonyl nitrogen.</p>	6.32	0.5 10		2.55	0.26	1.85	0.44	1.21	0.06

1-168		5.5	3	40	10*	n. a.	n. a.	n. a.	n. a.	n. a.
1-169		5.93	30	100	2.04	0.26	1.83	0.41	1.17	0.17
1-170		5.45	> 100	1.30	0.01	1.43	0.10	1.08	0.07	
1-171		3.48	10	100	1.19	0.07	1.25	0.39	1.05	0.06
1-175		4.91	30.0	n. a.	n. a.	n. a.	n. a.	n. a.	n. a.	n. a.
1-182*		3.99	> 100	1.30	0.10	1.17	0.03	1.00	0.17	
2-002		3.16	> 100	1.07	0.14	1.15	0.27	0.89	0.03	
2-003		3.65	> 100	1.06	0.07	1.16	0.15	0.98	0.02	
2-004		4.08	> 100	n. a.	n. a.	n. a.	n. a.	n. a.	n. a.	
2-005		4.56	> 100	n. a.	n. a.	n. a.	n. a.	n. a.	n. a.	
2-006		4.7	> 100	1.11	0.11	1.20	0.10	1.06	0.10	

2-012		3.36		100		1.16	0.10	1.19	0.14	1.05	0.07	
2-013*		4.19		3	100	2.11	0.07	1.91	0.25	1.21	0.09	
2-014		5.61		> 100		n. a.	n. a.	n. a.	n. a.	n. a.	n. a.	
2-015*		3.32		> 100		1.15	0.15	1.00	0.06	0.97	0.14	
3-001*		4.9		10	100	1.55	0.12	1.58	0.28	1.21	0.02	
3-003*		5.95		1	> 40	1.74	0.07	1.77	0.19	1.53	0.05	
3-004*		3.99		3	40	1.24	0.19	1.49	0.16	1.10	0.02	
3-005*		5.05		0.6	40	100	2.03	0.09	2.12	0.25	1.28	0.11
3-006*		5.53		0.5	20	100	2.11	0.14	2.10	0.14	1.31	0.04
3-008		5		3		n. a.	n. a.	n. a.	n. a.	n. a.	n. a.	
3-009		6.15		> 100		n. a.	n. a.	n. a.	n. a.	n. a.	n. a.	

4-001*	<chem>Clc1ccc(cc1C(F)(F)F)NC(=O)Nc2ccc(O)cc2</chem>	3.6		100		100	2.55	0.30	1.90	0.13	1.11	0.09
4-002*	<chem>Clc1ccc(cc1C(F)(F)F)NC(=O)Nc2ccc3ccccc3c2</chem>	4.99		0.7	> 40		1.47	0.12	1.53	0.20	1.26	0.08
4-003*	<chem>Clc1ccc(cc1C(F)(F)F)NC(=O)Nc2ccc(cc2)Cc3ccccc3</chem>	6.08		1	20		1.76	0.17	2.06	0.05	1.20	0.14
4-004*	<chem>Clc1ccc(cc1C(F)(F)F)NC(=O)Nc2ccc(CC)cc2</chem>	4.9		0.7	20		1.36	0.13	1.79	0.14	1.20	0.14
4-008*	<chem>Clc1ccc(cc1C(F)(F)F)NC(=O)Nc2ccc(C)cc2</chem>	4.97		> 100			1.10	0.01	1.06	0.03	1.17	0.14
4-013	<chem>Cc1ccc(NC(=O)Nc2ccc3c(c2)oc(F)(F)F)cc1</chem>	4.19		> 100			1.09	0.12	1.09	0.10	1.02	0.03
4-014	<chem>Cc1cc(C)c(NC(=O)Nc2ccc3c(c2)oc(F)(F)F)cc1C</chem>	5.16		> 100			1.21	0.23	0.99	0.13	1.01	0.22
4-017	<chem>Clc1ccc(NC(=O)Nc2ccc3c(c2)oc(F)(F)F)cc1C</chem>	4.74		0.5	20		1.17	0.15	1.23	0.05	1.15	0.07
4-018	<chem>Cc1ccc(NC(=O)Nc2ccc3c(c2)oc(F)(F)F)cc1C(F)(F)F</chem>	4.62		0.7	10	10*	1.72	0.14	2.39	0.23	1.27	0.14
4-020	<chem>CCCCCCCCNC(=O)Nc1ccc2c(c1)oc(F)(F)F2</chem>	4.95		> 100			1.16	0.12	1.13	0.18	1.24	0.05
5-002*	<chem>Cc1ccc(NC(=O)Nc2ccc3c(c2)oc(F)(F)F3)cc1Oc4ccc5c(c4)nc(C)nc5</chem>	2.44		> 100			1.00	0.10	1.13	0.14	1.03	0.11

5-003		3.86	> 100		1.38	0.16	1.39	0.18	1.10	0.15
5-004		4.74	> 100		0.95	0.05	1.01	0.14	0.97	0.04
5-005		2.16	> 100		1.14	0.17	1.06	0.10	1.00	0.08
5-006*		4.89	> 100		1.18	0.08	1.34	0.21	1.23	0.15
5-007		4.28	30		1.48	0.22	1.56	0.07	1.16	0.11
5-009*		4.03	> 100		1.23	0.05	1.31	0.13	1.19	0.21
5-010		4.08	> 100		n. a.	n. a.	n. a.	n. a.	n. a.	n. a.
5-015		3.3	30	100	1.29	0.21	1.15	0.20	1.09	0.10
5-016		5.41	> 100	> 40	1.41	0.24	1.39	0.11	1.12	0.11
6-015*		5.46	3		1.87	0.12	1.86	0.06	1.32	0.10
DA-1		3.17	> 100		n. a.	n. a.	n. a.	n. a.	n. a.	n. a.

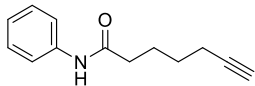
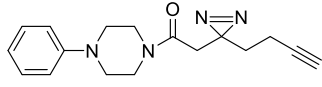
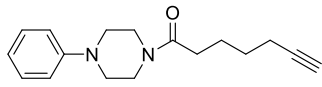
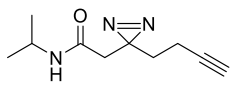
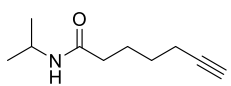
DA-1C		2.52	> 100						
DA-2		3.57	> 100	n. a.	n. a.	n. a.	n. a.	n. a.	n. a.
DA-2C		2.92	> 100						
DA-3		2.16	> 100	n. a.	n. a.	n. a.	n. a.	n. a.	n. a.
DA-3C		1.51	> 100						

Table S5: Numbers of identified and quantified proteins and protein kinases in the kinobead pull-down experiment.

	Category	Compound	
		SFN	PK150
Number of	Identified proteins	3557	3673
	Identified protein kinases	264	267
	Quantified proteins	1943	226
	Quantified protein kinases	2140	230
	Proteins interacting with the compound	8	0

Table S6: Target identification (50 μ M SFN-P/DMSO) in the soluble fraction. PR, \log_2 protein ratio; PV, $-\log_{10}$ *p*-value (*t*-test); MW, Molecular weight (kDa); UP, unique peptides; USC, Unique sequence coverage (%).

Uniprot ID	Protein name	Gene name	PR	LP	MW	UP	USC
Q2FZT7	Signal peptidase IB, putative	SAOUHSC_00903	3.93	2.48	17.60	5	35.5
Q2FWA8	Lytic regulatory protein, putative	SAOUHSC_02390	3.11	1.89	40.67	5	11.8
Q2FVS2	Putative uncharacterized protein	SAOUHSC_02620	3.10	1.87	24.96	2	10.2
Q2FVZ5	Putative uncharacterized protein	SAOUHSC_02525	2.79	1.70	114.70	10	13.3
Q2G193	Putative uncharacterized protein	SAOUHSC_00253	2.60	1.62	57.92	10	18.5
Q2FZG5	Putative uncharacterized protein	SAOUHSC_01039	2.57	1.14	23.88	3	18.3
Q2FVN6	Putative uncharacterized protein	SAOUHSC_02666	2.38	2.66	13.34	3	26.3
Q2G1G5	PTS system EIIBC component	SAOUHSC_00158	2.38	2.02	50.66	4	8.9
Q2FZJ9	Probable quinol oxidase subunit 2	qoxA	2.14	2.62	41.78	16	35.5
Q2FZV7	NADH dehydrogenase-like protein	SAOUHSC_00878	1.54	2.31	44.10	11	33.8
Q2G2D8	ABC transporter, substrate-binding protein, putative	SAOUHSC_00634	1.51	1.91	35.07	11	27.9
Q2FW66	Alkaline shock protein 23	asp23	1.16	1.10	19.19	5	30.2
Q2FXA0	UPF0342 protein	SAOUHSC_01977	0.98	0.81	13.31	5	43.9
Q2FZY9;Q2FXV1	UPF0337 protein	SAOUHSC_00845	0.85	0.32	7.02	4	53.1
Q2FYZ4	Aerobic glycerol-3-phosphate dehydrogenase	glpD	0.78	0.97	62.39	10	21
Q2FV52	Probable transglycosylase IsaA	isaA	0.52	0.94	24.20	2	15
Q2FVV9	Putative formate dehydrogenase	SAOUHSC_02582	0.51	3.76	111.24	7	8.3
Q2FXL6	Putative universal stress protein	SAOUHSC_01819	0.42	2.19	18.48	9	38
Q2FZ51	Acyl carrier protein	acpP	0.37	0.48	8.55	4	39
Q2FWE8	ATP synthase subunit alpha	atpA	0.17	0.94	54.58	5	12.9
Q2FV16	Probable malate:quinone oxidoreductase	mqr	0.17	0.93	56.00	11	24.1
Q2G2A5	Pyruvate dehydrogenase complex, E1 component, pyruvate dehydrogenase beta subunit, putative	SAOUHSC_01041	0.11	0.45	35.25	9	30.5
Q2FV17	Fructose-bisphosphate aldolase class 1	fda	0.08	0.17	33.05	13	41.9
Q2G032	Glyceraldehyde-3-phosphate dehydrogenase	SAOUHSC_00795	0.08	0.22	36.28	8	21.7
Q2G1J0	Putative aldehyde dehydrogenase AldA	aldA	0.03	0.33	53.66	11	25.7
Q2FYY6	Glutamine synthetase	SAOUHSC_01287	0.02	0.02	50.84	8	20.4
Q2FZ23	Elongation factor Ts	tsf	0.02	0.07	32.49	8	25.3
Q2G2A3	Dihydropolyl dehydrogenase	SAOUHSC_01043	-0.05	0.42	49.48	19	37.4
Q2G028	Enolase	eno	-0.06	0.38	47.12	12	38.9
Q2G0Q8	Cysteine synthase	SAOUHSC_00488	-0.09	0.38	32.98	8	37.7
Q2G115	Ribosome-binding ATPase YchF	ychF	-0.10	1.22	40.59	5	14.8
Q2FZG4	Pyruvate dehydrogenase complex, E1 component, alpha subunit, putative	SAOUHSC_01040	-0.12	1.09	41.38	7	26.2
Q2FZU0	Glucose-6-phosphate isomerase	pgi	-0.14	0.46	49.82	14	32.1
Q2FXP2	Glyceraldehyde-3-phosphate dehydrogenase	SAOUHSC_01794	-0.17	0.99	36.98	5	12
Q2FWB8	Purine nucleoside phosphorylase DeoD-type	deoD	-0.19	1.52	25.91	4	10.6
Q2G0G1	Alcohol dehydrogenase	adh	-0.20	1.20	36.05	18	39.6
Q2FXZ2	Chaperone protein DnaK	dnaK	-0.20	1.55	66.36	17	23.9
Q2G1C8	Putative uncharacterized protein	SAOUHSC_00197	-0.21	0.28	44.73	8	19.4
Q2FX94	Fumarate hydratase class II	fumC	-0.23	0.62	51.11	4	6.5
O05204	Alkyl hydroperoxide reductase subunit F	ahpF	-0.24	1.77	54.72	5	11.4
Q2FYP9	30S ribosomal protein S1, putative	SAOUHSC_01493	-0.24	0.19	43.29	3	11.5
Q2G227	Phosphopentomutase	deoB	-0.25	0.47	43.80	4	14.3
Q2G0Q1	Pyridoxal biosynthesis lyase PdxS	pdxS	-0.27	1.13	31.99	9	36.3
Q2G1Y5	L-lactate dehydrogenase 2	ldh2	-0.27	0.87	34.42	11	41.4
Q2FXI0	D-alanine aminotransferase	SAOUHSC_01867	-0.27	1.20	31.89	4	24.1
Q2FZ53	3-oxoacyl-(Acyl-carrier-protein) reductase, putative	SAOUHSC_01199	-0.28	1.60	25.89	16	58.2
Q2G0Y7	Inosine-5'-monophosphate dehydrogenase	guaB	-0.29	0.95	52.85	16	35.7
Q2G218	L-lactate dehydrogenase 1	ldh1	-0.30	1.62	34.58	10	29.7
Q2FY08	Glycine--tRNA ligase	glyQS	-0.30	3.00	53.62	8	14.5
POA0B7	Alkyl hydroperoxide reductase subunit C	ahpC	-0.30	1.56	20.98	10	55.6
Q2FWD3	Putative uncharacterized protein	SAOUHSC_02366	-0.31	1.12	30.84	14	48.6
Q2FXR4	Glutamate-1-semialdehyde 2,1-aminomutase 1	hemL1	-0.32	1.44	46.39	12	33.4
Q2FWZ8	Bacterial non-heme ferritin	ftnA	-0.32	1.64	19.59	4	21.1
Q2FZ37	Succinyl-CoA ligase [ADP-forming] subunit beta	sucC	-0.33	2.06	42.06	14	33.5
Q2FYZ5	Glycerol kinase	glpK	-0.33	1.17	55.63	10	24.9
Q2FXM9	Pyruvate kinase	pyk	-0.33	1.36	63.10	15	27.9
Q2FY60	6-phosphogluconate dehydrogenase, decarboxylating	SAOUHSC_01605	-0.33	1.80	51.80	9	17.3
Q2G248	Putative uncharacterized protein	SAOUHSC_01852	-0.34	1.74	40.62	9	29.8
Q2G0N0	Elongation factor Tu	tuf	-0.34	1.82	43.10	20	61.7

8 - Supporting Information

Q2G1W2	Phosphoenolpyruvate carboxykinase [ATP]	pckA	-0.34	1.38	59.38	12	25.8
Q2FZH5	Phosphoenolpyruvate-protein phosphotransferase	SAOUHSC_01029	-0.34	1.40	63.22	7	13.1
Q2FXQ1	50S ribosomal protein L20	rplT	-0.35	1.01	13.69	3	22.9
Q2FYT8	Transketolase	SAOUHSC_01337	-0.35	1.53	68.36	19	38.4
Q2FY71	Putative uncharacterized protein	SAOUHSC_01594	-0.36	1.38	33.51	2	6.3
Q2FXX0	Acetyl-CoA carboxylase, biotin carboxyl carrier protein, putative	SAOUHSC_01710	-0.36	1.29	16.79	7	40.3
Q2FWM1	Sucrose-6-phosphate dehydrogenase, putative	SAOUHSC_02268	-0.36	0.71	57.93	4	8.7
Q2G1K9	Aldehyde-alcohol dehydrogenase	SAOUHSC_00113	-0.37	2.07	94.94	21	24.3
Q2FZU6	Ornithine aminotransferase	rocD	-0.38	3.33	43.42	8	30.1
Q2FXR8	Valine--tRNA ligase	valS	-0.38	1.43	101.72	11	13.4
Q2FZ82	Isoleucine--tRNA ligase	ileS	-0.39	1.59	104.88	7	7.7
P60430	50S ribosomal protein L2	rplB	-0.39	1.87	30.16	8	31.4
Q2FZU5	Glutamate dehydrogenase	SAOUHSC_00895	-0.40	1.22	45.76	9	27.1
Q2FYU7	Catalase	katA	-0.40	2.06	58.38	15	30.1
Q2FXL5	Acetate kinase	ackA	-0.43	1.51	44.04	11	33.5
Q2FY42	Acetyl-CoA carboxylase, biotin carboxyl carrier protein	SAOUHSC_01624	-0.43	1.59	17.12	6	34.4
Q2FY35	Probable glycine dehydrogenase (decarboxylating) subunit 2	gcvPB	-0.43	2.01	54.78	4	12.9
Q2G0P5	ATP-dependent Clp protease ATP-binding subunit ClpC	clpC	-0.43	1.35	91.04	15	24
Q2FWE5	Serine hydroxymethyltransferase	glyA	-0.43	2.89	45.17	9	21.6
Q2G0M8	Putative uncharacterized protein	SAOUHSC_00532	-0.43	4.04	42.89	16	51.6
Q2FWY9	Glutamyl-tRNA(Gln) amidotransferase subunit A	gatA	-0.44	2.45	52.82	12	22.1
Q2FZ75	Aspartate carbamoyltransferase	pyrB	-0.44	1.20	33.26	3	10.6
Q2FWA0	Glutamine--fructose-6-phosphate aminotransferase [isomerizing]	glmS	-0.44	2.53	65.85	14	29
Q2FZ74	Dihydroorotase	pyrC	-0.45	2.94	46.37	7	18.2
Q2G030	Triosephosphate isomerase	tpiA	-0.46	1.50	27.29	11	38.3
Q2G1M1	3-ketoacyl-acyl carrier protein reductase, putative	SAOUHSC_00086	-0.46	2.68	27.22	3	16.7
Q2FV67	1-pyrroline-5-carboxylate dehydrogenase	rocA	-0.46	1.97	56.87	13	27.4
Q2FVT5	Urocanate hydratase	hutU	-0.48	3.32	60.63	7	11.4
Q2FXP7	Threonine--tRNA ligase	thrS	-0.50	1.41	74.49	22	25.6
Q2FVB2	Fructose-1,6-bisphosphatase class 3	fbp	-0.50	1.96	76.17	6	9.9
Q2FY66	Glucose-6-phosphate 1-dehydrogenase	zwf	-0.50	1.28	56.97	6	11.5
Q2G296	Formate--tetrahydrofolate ligase	fhs	-0.51	3.40	59.86	13	28.8
Q2G1H0	Indolepyruvate decarboxylase, putative	SAOUHSC_00153	-0.51	2.18	60.54	7	8.1
Q2FXH2	Leucine--tRNA ligase	leuS	-0.52	2.55	91.79	12	13.9
Q2G1E6	Putative uncharacterized protein	SAOUHSC_00179	-0.53	2.16	39.18	3	13.4
Q2G1U3	Oligoendopeptidase F	SAOUHSC_00937	-0.53	1.74	69.82	12	22.8
P0A0F4	50S ribosomal protein L11	rplK	-0.54	1.00	14.87	5	29.3
Q2G0N1	Elongation factor G	fusA	-0.54	2.15	76.61	21	32.5
Q2FZ36	Succinyl-CoA ligase [ADP-forming] subunit alpha	SAOUHSC_01218	-0.55	1.83	31.54	14	51.7
Q2G1C9	Putative uncharacterized protein	SAOUHSC_00196	-0.57	1.55	84.61	20	29
Q2G1D8	Formate acetyltransferase	pflB	-0.57	3.19	84.86	31	36.4
Q2G0N5	DNA-directed RNA polymerase subunit beta'	rpoC	-0.59	2.47	135.41	27	24.6
Q2FYS9	Aconitate hydratase 1	SAOUHSC_01347	-0.61	2.72	98.97	14	16.2
P47768	DNA-directed RNA polymerase subunit beta	rpoB	-0.61	3.53	133.22	16	14.9
Q2FYM1	2-oxoglutarate dehydrogenase E1 component	odhA	-0.61	2.30	105.34	25	30.3
Q2FWD1	CTP synthase	pyrG	-0.65	1.13	59.98	6	10.3
Q2G1C0	2-C-methyl-D-erythritol 4-phosphate cytidyltransferase	ispD	-0.70	0.71	26.66	3	14.3
Q2FZK7	Bifunctional autolysin	atl	-0.71	1.01	137.38	9	10.2
Q2G2C1	Pyruvate carboxylase	SAOUHSC_01064	-0.83	1.80	128.55	54	48.1

Table S7: Target identification (50 μ M SFN-P/DMSO) in the insoluble fraction. PR, \log_2 protein ratio; PV, $-\log_{10}$ p -value (t -test); MW, Molecular weight (kDa); UP, unique peptides; USC, Unique sequence coverage (%).

Uniprot ID	Protein name	Gene name	PR	LP	MW	UP	USC
Q2FZT7	Signal peptidase IB, putative	SAOUHSC_00903	4.84	2.72	17.60	7	51.6
Q2G2W2	Putative uncharacterized protein	SAOUHSC_02628	4.81	2.62	24.29	3	16
Q2FVZ5	Putative uncharacterized protein	SAOUHSC_02525	4.59	2.24	114.70	23	27.4
Q2G117	Putative uncharacterized protein	SAOUHSC_00344	4.47	2.10	32.19	4	18.1
Q2G193	Putative uncharacterized protein	SAOUHSC_00253	4.36	1.89	57.92	15	34.3
Q2G1C5	Membrane protein, putative	SAOUHSC_00200	4.03	2.93	42.18	2	6.8
Q2G2N2	Putative uncharacterized protein	SAOUHSC_01358	3.74	1.31	45.07	4	11.4
Q2FZQ2	Putative uncharacterized protein	SAOUHSC_00948	3.71	1.57	40.15	4	8.6
Q2FVS2	Putative uncharacterized protein	SAOUHSC_02620	3.70	1.96	24.96	3	18.6
Q2FV70	Putative uncharacterized protein	SAOUHSC_02866	3.47	2.19	90.41	15	20.6
Q2FYG5	Menaquinone biosynthesis methyltransferase, putative	SAOUHSC_01487	2.93	2.05	22.37	4	27
O08387	Protein translocase subunit SecY	secY	2.88	2.95	47.15	4	10
Q2G245	Putative uncharacterized protein	SAOUHSC_01854	2.86	2.16	55.09	30	50.1
Q2FXT8	Protein-export membrane protein SecDF	SAOUHSC_01746	2.86	2.13	82.05	17	25.4
Q2G0D7	ABC transporter permease, putative	SAOUHSC_00668	2.80	1.81	71.73	5	7.9
Q2FVN6	Putative uncharacterized protein	SAOUHSC_02666	2.70	2.61	13.34	3	23.7
Q2FVS4	Putative uncharacterized protein	SAOUHSC_02618	2.69	2.29	45.93	3	10.5
Q2G1P4	Putative uncharacterized protein	SAOUHSC_00060	2.64	2.39	60.65	7	17.5
Q93Q23	Monofunctional glycosyltransferase	mgt	2.62	2.47	31.46	3	19.3
Q2G1M2	Putative uncharacterized protein	SAOUHSC_00085	2.46	2.16	22.98	4	19.2
Q2FWG4	Membrane protein insertase YidC	yidC	2.41	1.23	33.58	4	12.8
Q2FVQ4	L-lactate permease	SAOUHSC_02648	2.36	1.92	56.64	2	4.5
Q2FVI6	Putative uncharacterized protein	SAOUHSC_02724	2.34	1.57	25.80	5	21.5
Q2G2N5	Sodium:alanine symporter family protein, putative	SAOUHSC_01354	2.28	2.26	52.14	4	11.3
Q2FVT1	Lysostaphin resistance protein A	lyrA	2.25	2.38	46.79	3	14.3
Q2FY00	Putative uncharacterized protein	SAOUHSC_01675	2.17	2.98	27.26	3	9.9
Q2G044	Prolipoprotein diacylglycerol transferase	lgt	2.16	2.08	31.57	2	3.6
Q2FWY7	Sodium/proline symporter	putP	2.14	2.34	55.98	2	5.1
Q2G2V9	Putative uncharacterized protein	SAOUHSC_02006	2.05	0.72	37.08	3	9.5
Q2FYZ6	Putative uncharacterized protein	SAOUHSC_01275	1.97	2.20	28.12	3	11
Q2G1Z5	Putative uncharacterized protein	SAOUHSC_01239	1.97	2.36	44.28	3	9.4
Q2FWY4	Sodium-dependent dicarboxylate transporter SdcS	sdcS	1.95	2.90	57.17	2	5.2
Q2FY84	Phi PVL ORF 30-like protein	SAOUHSC_01580	1.91	0.92	23.83	3	18.1
Q2G247	UPF0478 protein	SAOUHSC_01855	1.91	2.67	18.00	12	67.5
Q2FV29	Putative uncharacterized protein	SAOUHSC_02910	1.89	2.30	10.71	3	31.9
Q7BHL7	Regulatory protein MsrR	msrR	1.88	1.40	36.97	6	22.6
Q2FYT7	UPF0154 protein	SAOUHSC_01338	1.88	1.17	11.02	6	36.8
Q2FY80	Sensor protein SrrB	srrB	1.87	1.73	66.08	13	26.2
Q2FZK3	Protein FmtA	fmtA	1.75	2.17	46.07	4	10.1
Q2FW64	Putative uncharacterized protein	SAOUHSC_02443	1.71	1.83	20.80	4	29.8
Q2FZJ9	Probable quinol oxidase subunit 2	qoxA	1.70	2.25	41.78	16	36.9
Q2FVF5	Putative uncharacterized protein	SAOUHSC_02759	1.62	1.54	17.31	4	21.2
Q2FWX6	Putative uncharacterized protein	SAOUHSC_02145	1.61	2.30	6.56	2	19.3
Q2G1E0	Uncharacterized sensor-like histidine kinase	SAOUHSC_00185	1.57	0.90	61.05	5	10.2
Q2G242	Putative uncharacterized protein	SAOUHSC_00508	1.57	1.65	38.89	3	8.5
Q2FXG3	Putative uncharacterized protein	SAOUHSC_01884	1.53	2.31	38.03	9	39.9
Q2G1C1	Teichoic acid biosynthesis protein F, putative	SAOUHSC_00223	1.52	1.01	45.96	7	19.5
Q2FWM5	Accessory gene regulator protein C	SAOUHSC_02264	1.49	3.01	47.98	2	4.1
Q2FZQ5	Magnesium transporter	SAOUHSC_00945	1.48	1.76	51.44	4	9.8
Q2G2X6	Penicillin-binding protein 4, putative	SAOUHSC_00646	1.42	1.36	48.26	4	12.1
Q2FUU5	Lipase 1	lipA	1.40	0.77	76.68	10	18.4
Q2G1F2	FMN-dependent NADH-azoreductase	azoR	1.39	1.50	23.35	4	22.1
Q2G0Z4	Putative uncharacterized protein	SAOUHSC_00367	1.36	1.93	49.41	6	16
Q2G2T0	Putative uncharacterized protein	SAOUHSC_01969	1.36	1.48	13.21	6	56.2
Q2G0P9	Putative uncharacterized protein	SAOUHSC_00501	1.31	1.84	43.80	3	5.4
Q2G2U1	Histidine protein kinase SaeS	saeS	1.29	1.28	39.74	6	21.7
Q2G2E0	Putative uncharacterized protein	SAOUHSC_00633	1.27	2.15	74.93	4	9.1
Q2FUX2	Putative uncharacterized protein	SAOUHSC_02973	1.26	1.98	16.36	2	34.9
Q2FV90	Putative uncharacterized protein	SAOUHSC_02844	1.26	2.57	36.85	9	33.2

8 - Supporting Information

Q2FW13	50S ribosomal protein L16	rplP	1.24	0.64	16.24	5	31.9
Q2G0C7	Putative uncharacterized protein	SAOUHSC_00678	1.23	1.32	25.42	2	7.9
Q2G2M2	Phosphatidylglycerol lysyltransferase	mprF	1.15	1.12	96.87	6	6.4
Q2FVK5	Immunoglobulin-binding protein sbi	sbi	1.10	1.54	50.07	13	29.1
Q2FV54	O-acetyltransferase OatA	oatA	1.09	1.64	69.10	6	9.8
Q2FXJ7	1-acyl-sn-glycerol-3-phosphate acyltransferases domain protein	SAOUHSC_01837	1.08	1.18	23.07	8	32.7
Q2G0I1	Putative uncharacterized protein	SAOUHSC_00584	1.07	1.57	51.67	8	22.8
Q2FVL7	Putative uncharacterized protein	SAOUHSC_02694	1.05	1.02	23.06	2	11.6
Q2FWM8	Delta-hemolysin	hld	1.04	0.32	2.98	3	84.6
Q2FVV8	Transcriptional regulator, putative	SAOUHSC_02583	1.03	1.55	33.80	7	26.4
Q2FZA8	Putative uncharacterized protein	SAOUHSC_01130	1.02	1.96	54.07	4	9.1
Q2FWB6	Putative uncharacterized protein	SAOUHSC_02382	1.00	1.46	16.25	6	34.3
Q2FYF1	Elastin-binding protein EbpS	ebpS	1.00	1.38	53.22	13	45.3
Q2FZK0	Probable quinol oxidase subunit 1	qoxB	0.99	1.69	75.24	4	6.5
Q2FZW4	D-alanine--poly(phosphoribitol) ligase subunit 2	dlcC	0.99	1.80	9.06	2	33.3
Q2FXF4	Putative uncharacterized protein	SAOUHSC_01895	0.99	1.23	32.51	7	19.7
Q2G2W5	Putative uncharacterized protein	SAOUHSC_02630	0.96	1.25	23.02	4	28.4
Q2FZ18	Putative uncharacterized protein	SAOUHSC_01253	0.96	1.38	83.40	12	19.5
Q2G2G6	Putative uncharacterized protein	SAOUHSC_01050	0.95	1.20	40.06	3	11.2
Q2FYT0	Glycine betaine transporter, putative	SAOUHSC_01346	0.94	2.37	60.47	4	6.2
Q2FZF9	Glycerophosphoryl diester phosphodiesterase, putative	SAOUHSC_01071	0.93	1.63	34.73	9	26.9
Q2FZ91	Cell division protein DivIB	divIB	0.93	2.38	50.21	9	25.5
Q2G019	Putative uncharacterized protein	SAOUHSC_00808	0.91	2.63	28.42	9	33.1
Q2G035	Epimerase family protein	SAOUHSC_00792	0.88	0.91	34.23	5	21
Q2FWY6	Putative uncharacterized protein	SAOUHSC_02121	0.88	2.62	45.38	11	37.3
Q2G155	Lipase 2	lip2	0.87	1.08	76.39	10	21.9
Q2FVI3	Putative uncharacterized protein	SAOUHSC_02727	0.87	1.22	22.28	3	18
Q2G0Z9	Putative uncharacterized protein	SAOUHSC_00362	0.87	2.05	23.66	6	28.8
Q2FYL3	Putative uncharacterized protein	SAOUHSC_01427	0.85	2.31	55.26	12	24.6
Q2G222	N-acetylmuramoyl-L-alanine amidase domain-containing protein	SAOUHSC_02979	0.85	0.24	69.25	10	24.4
Q2G0F2	Putative uncharacterized protein	SAOUHSC_00617	0.83	0.44	18.59	5	30.4
Q2G221	Phage infection protein, putative	SAOUHSC_02978	0.83	1.25	108.71	25	29.7
Q2FXJ6	Putative uncharacterized protein	SAOUHSC_01838	0.82	2.07	45.80	12	25.9
Q2FXZ9	UPF0365 protein	SAOUHSC_01676	0.82	2.08	35.18	14	49.5
Q2FY36	Putative uncharacterized protein	SAOUHSC_01630	0.81	1.29	14.80	4	24.2
Q2FYW4	Cardiolipin synthetase, putative	SAOUHSC_01310	0.80	0.53	56.37	3	7.3
Q2FXN7	Histidine kinase-, DNA gyrase B-, and HSP90-like ATPase domain protein	SAOUHSC_01799	0.79	1.31	63.77	6	10.7
Q2FVE7	Peptide ABC transporter, peptide-binding protein, putative	SAOUHSC_02767	0.78	1.89	60.08	11	22
Q2G2J2	Staphylococcal secretory antigen ssaA2	ssaA2	0.77	1.63	29.33	6	47.9
Q2FY81;Q2FYE2;Q2FYE3;Q2FYE5	Putative uncharacterized protein	SAOUHSC_01584	0.77	2.78	33.58	6	22.8
Q2FVU4	PTS system component, putative	SAOUHSC_02597	0.77	0.93	59.33	3	6.6
Q2G1D9	Lipoprotein, putative	SAOUHSC_00186	0.77	1.10	36.93	4	14.3
Q2FZD3	Endonuclease MutS2	mutS2	0.77	0.47	88.66	11	14.3
Q2G2U4	Sensor protein kinase Walk	walk	0.76	0.85	69.92	7	11.5
Q2FV30	Dihydroorotate dehydrogenase	SAOUHSC_02909	0.75	1.56	39.54	9	33.1
Q2FZ94	Penicillin-binding protein 1	SAOUHSC_01145	0.73	1.18	82.71	18	34.8
Q2G0U0	Putative uncharacterized protein	SAOUHSC_00437	0.72	0.93	50.94	8	20
Q2FV87	PTS system glucoside-specific EIICBA component	glcB	0.71	1.23	74.42	9	19.8
Q2FYI0	Penicillin-binding protein 2	SAOUHSC_01467	0.69	1.46	80.43	21	35.1
Q2FYZ3	Hydrolase, alpha/beta fold family domain protein	SAOUHSC_01279	0.68	0.58	35.26	3	11.2
Q2FZV7	NADH dehydrogenase-like protein	SAOUHSC_00878	0.67	1.26	44.10	13	31.8
Q2FVW3	Putative uncharacterized protein	SAOUHSC_02579	0.67	1.14	41.89	9	28.1
Q2FWP0	Uncharacterized leukocidin-like protein 1	SAOUHSC_02241	0.67	1.42	38.69	4	17.8
Q2FXT7	Preprotein translocase, YajC subunit	SAOUHSC_01747	0.64	1.19	9.67	2	22.1
Q2G2E5	Putative uncharacterized protein	SAOUHSC_00647	0.64	1.43	64.05	12	26.6
Q2FZ64	Putative uncharacterized protein	SAOUHSC_01187	0.64	1.71	74.36	18	26.2
Q2FZP2	Serine protease HtrA-like	SAOUHSC_00958	0.62	0.91	86.46	10	20
Q2G105	Putative uncharacterized protein	SAOUHSC_00356	0.61	1.10	21.31	3	18.4
Q2FUS2	Sodium, sulfate symporter, putative	SAOUHSC_03030	0.61	1.50	51.34	2	4.7
Q2G1W5	Putative uncharacterized protein	SAOUHSC_01908	0.61	1.73	35.05	9	38.4
Q2FZ59	Putative uncharacterized protein	SAOUHSC_01192	0.60	1.20	13.39	4	41.9
Q2FZW3	Extramembranal protein	SAOUHSC_00872	0.59	0.25	44.95	4	12

P52078	Uncharacterized protein	SAOUHSC_00997	0.59	0.92	45.69	8	19.3
Q2FV64	Copper-exporting P-type ATPase A	copA	0.58	0.96	86.74	12	20.2
Q2FWN9	Uncharacterized leukocidin-like protein 2	SAOUHSC_02243	0.57	1.31	40.43	9	28.5
Q2FYK5	Thymidylate synthase	thyA	0.57	0.84	36.84	7	17.9
Q2FYR1	Aminoacyltransferase FemB	femB	0.57	1.73	49.68	5	10.7
Q2FXH8	Putative uncharacterized protein	SAOUHSC_01869	0.57	1.64	15.73	5	43.6
Q2G0P6	Protein-arginine kinase	mcsB	0.56	0.70	38.61	2	7.8
Q2G0F6	Iron compound ABC transporter, substrate-binding protein, putative	SAOUHSC_00613	0.55	1.71	31.09	8	32
Q2FXS6	Cell shape-determining protein MreC	SAOUHSC_01759	0.55	1.32	31.01	10	43.6
Q2FVN2	Putative uncharacterized protein	SAOUHSC_02670	0.54	1.11	16.31	2	17.6
Q2G188	Putative uncharacterized protein	SAOUHSC_00258	0.51	0.90	114.82	15	18.2
Q2G2L2	Putative uncharacterized protein	SAOUHSC_00637	0.51	1.17	28.02	5	22.3
Q2FVB4	Putative uncharacterized protein	SAOUHSC_02820	0.51	0.95	25.80	8	35.1
Q2FYV7	Putative uncharacterized protein	SAOUHSC_01317	0.48	1.01	32.85	5	20.1
Q2G264	Putative uncharacterized protein	SAOUHSC_01180	0.48	0.72	35.91	9	37.2
Q2G1G8	PTS system glucose-specific EIICBA component	ptsG	0.47	0.99	73.92	10	22.9
Q2G2G0	Putative uncharacterized protein	SAOUHSC_00717	0.47	1.45	16.05	6	34.2
Q2FYZ4	Aerobic glycerol-3-phosphate dehydrogenase	glpD	0.46	2.00	62.39	24	43.8
Q2FWW9	ABC transporter, ATP-binding protein, putative	SAOUHSC_02152	0.46	1.98	32.95	6	18.3
Q2G2T6	Putative uncharacterized protein	SAOUHSC_00015	0.45	0.71	73.78	9	14.8
Q2FY39	Putative uncharacterized protein	SAOUHSC_01627	0.44	1.38	21.47	4	28.5
Q2G1G5	PTS system EIIBC component	SAOUHSC_00158	0.44	1.04	50.66	7	24.6
Q2FW93	Putative uncharacterized protein	SAOUHSC_02406	0.41	0.94	34.62	11	40
Q2G1C2	TagB protein, putative	SAOUHSC_00222	0.39	0.43	60.18	7	13.8
Q2FYL5	UDP-N-acetylglucosamine--N-acetylmuramyl-(pentapeptide) pyrophosphoryl-undecaprenol N-acetylglucosamine transferase	murG	0.39	1.13	39.70	9	35.1
Q2FVL2	Putative uncharacterized protein	SAOUHSC_02699	0.38	1.48	28.90	7	23.2
Q2FUX0	PTS system, fructose-specific IIABC component, putative	SAOUHSC_02975	0.36	1.34	69.88	7	16.6
Q2FV86	Pyruvate oxidase, putative	SAOUHSC_02849	0.35	1.17	63.76	9	21.4
Q2FYR2	Aminoacyltransferase FemA	femA	0.34	1.31	49.12	8	18.1
Q2FYK7	Putative uncharacterized protein	SAOUHSC_01433	0.33	1.06	30.64	8	31.5
Q2FW75	ABC transporter periplasmic binding protein, putative	SAOUHSC_02430	0.33	0.97	36.59	6	15.3
Q2G1B8	Putative uncharacterized protein	SAOUHSC_00227	0.32	1.02	66.07	2	2.8
Q2FWZ9	UDP-N-acetylmuramyl tripeptide synthetase, putative	SAOUHSC_02107	0.32	1.79	49.27	7	19.5
Q2G239	Fructose specific permease, putative	SAOUHSC_00708	0.30	0.49	68.71	10	19
Q2FZH7	Putative uncharacterized protein	SAOUHSC_01027	0.30	0.26	20.09	3	18.9
Q2G260	Uncharacterized protein	SAOUHSC_00094	0.29	0.14	21.85	5	38.7
Q2FVN7	Putative uncharacterized protein	SAOUHSC_02665	0.29	1.07	15.91	4	42.1
Q2G067	Putative uncharacterized protein	SAOUHSC_00754	0.28	0.80	34.08	3	10.6
Q2G0I8	Mevalonate kinase, putative	SAOUHSC_00577	0.28	0.37	32.92	4	19.6
Q2G0W9;Q2G0X1	Uncharacterized lipoprotein	SAOUHSC_00405	0.28	1.69	31.47	9	28.5
Q2FZR3	Oligopeptide ABC transporter, substrate-binding protein, putative	SAOUHSC_00927	0.27	0.35	61.57	3	7.1
Q2FXL6	Putative universal stress protein	SAOUHSC_01819	0.27	0.90	18.48	9	66.9
Q2FVW0	Putative uncharacterized protein	SAOUHSC_02581	0.25	0.43	17.48	5	28.7
Q2G2L1	Teichoic acids export ATP-binding protein TagH	tagH	0.25	0.94	29.76	5	21.2
Q2G039	UPF0042 nucleotide-binding protein	SAOUHSC_00787	0.24	0.71	34.81	4	16.5
Q2FWL2	tRNA N6-adenosine threonylcarbamoyltransferase	tsaD	0.24	0.24	36.82	5	17.3
Q2G0U9	N-acetylmuramoyl-L-alanine amidase sle1	sle1	0.24	0.47	35.84	5	19.5
Q2FVQ2	Uncharacterized lipoprotein	SAOUHSC_02650	0.24	1.18	23.36	6	55
Q2FZC7	Iron-sulphur subunit of succinate dehydrogenase, putative	SAOUHSC_01105	0.22	0.51	30.58	7	29.9
Q2FV11	Oxygen-dependent choline dehydrogenase	betA	0.21	0.63	63.61	6	16.5
Q9KJN4	Response regulator ArlR	arlR	0.21	0.12	25.50	2	11.9
Q2G2S6	Foldase protein PrsA	prsA	0.21	1.15	35.64	8	23.8
Q2FYH5	Probable ATP-dependent helicase DinG homolog	dinG	0.21	0.38	104.22	7	8.7
Q2G0M6	Ribulokinase	araB	0.20	0.23	61.01	5	11.9
Q2G2F8	ATP synthase subunit b	atpF	0.20	0.30	19.54	7	43.9
Q2G170	5'-nucleotidase, lipoprotein e(P4) family	SAOUHSC_00284	0.19	0.71	33.35	4	22.3
Q2FZ86	Cell division protein SepF	sepF	0.19	0.34	21.02	2	17.1
Q2FYG0	GTPase Der	der	0.18	0.36	48.98	5	17.4
Q2FVS3	Putative uncharacterized protein	SAOUHSC_02619	0.18	0.29	33.72	7	31.1
Q2FWY8	Aspartyl/glutamyl-tRNA(Asn/Gln) amidotransferase subunit C	gatC	0.17	0.81	11.27	2	27
Q2FVW9	Putative uncharacterized protein	SAOUHSC_02554	0.17	0.69	34.01	12	39.4

8 - Supporting Information

Q2FZ08	Ribonuclease Y	rny	0.17	0.84	58.51	8	19.8
Q2FYF3	Putative uncharacterized protein	SAOUHSC_01290	0.15	0.16	7.86	2	36.8
Q2G012	Extracellular matrix protein-binding protein emp	emp	0.15	0.45	38.48	8	23.2
Q2FXK8	Septation ring formation regulator EzrA	ezrA	0.15	0.31	66.25	12	25
Q2FWK4	Ketol-acid reductoisomerase	ilvC	0.14	0.16	36.96	7	29
Q2G2U3	Putative uncharacterized protein	SAOUHSC_00022	0.14	0.30	49.01	9	25.5
Q2FVX4	Molybdenum ABC transporter, periplasmic molybdate-binding protein	SAOUHSC_02549	0.14	0.39	29.05	9	30
Q2FV52	Probable transglycosylase IsaA	isaA	0.13	0.35	24.20	5	39.9
Q2FY64	Alpha-amylase	SAOUHSC_01601	0.13	0.07	63.91	8	15.8
Q2FWW1	MHC class II analog protein	SAOUHSC_02161	0.13	0.89	65.57	19	35.8
Q2G111	30S ribosomal protein S18	rpsR	0.13	0.60	9.31	3	25
Q2G1V4	ABC transporter, ATP-binding protein, putative	SAOUHSC_00333	0.13	0.29	31.59	3	11.4
Q2G1U8	Putative uncharacterized protein	SAOUHSC_02690	0.12	0.74	59.19	12	28.1
Q2FW03	DNA topoisomerase 3	topB	0.12	0.13	81.55	11	17.4
O07325	Cell division protein FtsA	ftsA	0.11	0.29	52.93	14	35.5
Q2FW10	30S ribosomal protein S19	rpsS	0.11	1.25	10.62	4	35.9
Q2G2D8	ABC transporter, substrate-binding protein, putative	SAOUHSC_00634	0.11	0.34	35.07	15	44.2
Q2FZV8	Putative uncharacterized protein	SAOUHSC_00877	0.10	0.59	12.49	2	19.3
Q2FZX4	Lipoyl synthase	lipA	0.10	1.32	34.89	7	22.3
Q2G0Z0	Putative uncharacterized protein	SAOUHSC_00371	0.10	0.20	15.12	7	49.6
Q2FV62	D-lactate dehydrogenase, putative	SAOUHSC_02875	0.09	0.09	37.22	3	10.2
Q2FY78	Pseudouridine synthase	SAOUHSC_01587	0.07	0.10	27.97	4	21.2
Q2G2H3	Putative uncharacterized protein	SAOUHSC_02009	0.07	0.04	58.25	3	7.7
Q2G2R8	Staphopain A	sspP	0.06	0.09	44.26	6	19.3
Q2FVG8	Amino acid ABC transporter, ATP-binding protein, putative	SAOUHSC_02744	0.06	0.08	46.17	4	10.8
Q2G293	Putative uncharacterized protein	SAOUHSC_01847	0.06	0.08	24.78	5	28.6
Q2FYZ7	Glycerol uptake operon antiterminator regulatory protein	SAOUHSC_01274	0.05	0.08	20.45	4	30.6
Q2FWR2	Conserved hypothetical phage protein	SAOUHSC_02218	0.05	0.08	11.10	3	33.3
Q2G1Y7	Putative uncharacterized protein	SAOUHSC_01061	0.05	0.03	18.58	3	16.2
Q2FVH3	2-dehydropantoate 2-reductase	SAOUHSC_02739	0.05	0.07	34.44	3	13.2
Q2FWX9	Aldehyde dehydrogenase	SAOUHSC_02142	0.04	0.08	51.74	7	19.4
Q2FXA5	Protoporphyrinogen oxidase	SAOUHSC_01960	0.03	0.31	51.98	16	42.9
Q2FYP3	Conserved virulence factor B	cvfB	0.03	0.18	34.20	4	17.7
Q2G0F3	Putative uncharacterized protein	SAOUHSC_00616	0.03	0.07	30.93	2	8.3
Q2FYZ9	DNA mismatch repair protein MutS	mutS	0.02	0.03	99.90	11	12.6
Q2FYK4	UPF0403 protein	SAOUHSC_01436	0.02	0.01	16.01	5	40
Q2FVZ4	Lipid II:glycine glycytransferase	femX	0.01	0.03	48.52	10	29.5
Q2FZY5	Aminotransferase, class V superfamily, putative	SAOUHSC_00849	0.01	0.01	46.62	7	19
Q2FW22	50S ribosomal protein L18	rplR	0.01	0.01	13.10	6	51.3
Q2G0D1	HTH-type transcriptional regulator SarX	sarX	0.01	0.01	14.18	6	44.5
Q2FZZ0	Lipoprotein	SAOUHSC_00844	0.01	0.01	30.35	8	34.1
Q2FXL0	Putative uncharacterized protein	SAOUHSC_01825	0.00	0.01	42.37	3	9.7
Q2FW11	50S ribosomal protein L22	rplV	0.00	0.00	12.84	7	58.1
Q2FZT1	Putative uncharacterized protein	SAOUHSC_00909	-0.01	0.01	31.67	3	15
Q2FZC8	Succinate dehydrogenase, flavoprotein chain TC0881, putative	SAOUHSC_01104	-0.01	0.01	65.50	14	23.3
Q2FZK7	Bifunctional autolysin	atl	-0.01	0.07	137.38	42	40.6
Q2FY21	Penicillin-binding protein 3	SAOUHSC_01652	-0.01	0.03	77.24	19	33.3
Q2FY71	Putative uncharacterized protein	SAOUHSC_01594	-0.01	0.01	33.51	4	12.6
Q2FZ92	UDP-N-acetylmuramoylalanine--D-glutamate ligase	murD	-0.02	0.06	49.84	8	17.6
Q2G2T8	Putative uncharacterized protein	SAOUHSC_00712	-0.02	0.04	32.36	2	7.2
Q2G266	Primosomal protein N	SAOUHSC_01179	-0.03	0.04	92.52	10	12
Q2FYM7	TelA-like protein	SAOUHSC_01408	-0.03	0.13	43.41	13	42.1
Q2G2G9	Regulatory protein RecX	recX	-0.04	0.04	32.24	4	14.3
Q2G0Y9	Xanthine phosphoribosyltransferase	xpt	-0.04	0.06	20.88	4	25
P60430	50S ribosomal protein L2	rplB	-0.04	0.04	30.16	12	51.6
Q2FVL8	Assimilatory nitrite reductase [NAD(P)H], large subunit, putative	SAOUHSC_02684	-0.04	0.22	88.66	15	23.5
Q2FZQ3	Enoyl-[acyl-carrier-protein] reductase [NADPH] FabI	fabI	-0.05	0.29	28.02	4	14.8
Q2FW17	50S ribosomal protein L24	rplX	-0.05	0.17	11.54	5	20
Q2FXB7	ABC transporter domain protein	SAOUHSC_01948	-0.06	0.05	25.89	3	21.7
Q2FX19	Conserved hypothetical phage protein	SAOUHSC_02087	-0.06	0.07	35.63	5	15.6
Q2FWZ8	Bacterial non-heme ferritin	ftnA	-0.06	0.18	19.59	5	33.7
Q2FWC6	Putative uncharacterized protein	SAOUHSC_02372	-0.06	0.09	25.86	4	17.5
Q2FY46	Exodeoxyribonuclease 7 large subunit	xseA	-0.06	0.94	50.89	5	12.6

Q2FYZ0	Glutathione peroxidase	SAOUHSC_01282	-0.07	0.30	18.12	5	34.8
P0A0H0	30S ribosomal protein S12	rpsL	-0.07	0.16	15.29	3	13.1
Q2G0S2	Ribose-phosphate pyrophosphokinase	prs	-0.07	1.54	35.28	9	29
Q2FVK2	Gamma-hemolysin component C	hlgC	-0.07	0.02	35.61	5	18.7
Q2FWH5	DEAD-box ATP-dependent RNA helicase CshA	cshA	-0.08	0.18	56.94	16	40.1
Q2G1S4	Replicative DNA helicase	SAOUHSC_00018	-0.08	0.08	52.57	4	8.2
Q2G0M5	Uncharacterized epimerase/dehydratase	SAOUHSC_00535	-0.08	1.40	36.05	9	33.6
Q2FWE9	ATP synthase gamma chain	atpG	-0.08	0.28	29.47	10	46
Q2FZ78	Pseudouridine synthase	SAOUHSC_01163	-0.08	0.15	34.60	5	16.1
Q2FY01	Putative uncharacterized protein	SAOUHSC_01673	-0.09	0.26	34.91	6	22.9
Q2FXZ3	Chaperone protein DnaJ	dnaJ	-0.09	0.86	41.76	8	30.3
Q2G0D6	Putative uncharacterized protein	SAOUHSC_00669	-0.09	0.15	23.74	5	22.4
Q2FY88	Exonuclease family	SAOUHSC_01576	-0.09	0.20	35.90	9	28.1
Q2FVG5	Putative uncharacterized protein	SAOUHSC_02747	-0.09	0.11	23.80	3	15.6
Q2G093	Lipoteichoic acid synthase	ltaS	-0.09	0.02	74.40	11	24.3
Q2FXV8	Putative uncharacterized protein	SAOUHSC_01723	-0.09	0.11	93.05	6	10.7
Q2FY55	DNA topoisomerase 4 subunit B	parE	-0.10	0.32	74.36	8	13.6
Q2FZC6	Glutamate racemase	murI	-0.10	0.67	29.70	5	26.3
Q2FW08	50S ribosomal protein L23	rplW	-0.10	0.97	10.61	6	51.6
Q2FW31	30S ribosomal protein S11	rpsK	-0.10	0.21	13.88	5	40.3
Q2G0W8	Putative uncharacterized protein	SAOUHSC_00406	-0.10	0.31	49.26	8	31.7
Q2FX90	Putative uncharacterized protein	SAOUHSC_01987	-0.10	0.46	22.34	6	33.7
Q2FZM6	Glycosyl transferase, group 1	SAOUHSC_00974	-0.10	0.11	29.78	4	17.7
Q2FY06	GTPase Era	era	-0.11	0.16	34.27	6	17.4
Q2FXM8	ATP-dependent 6-phosphofructokinase	pfkA	-0.11	0.57	34.84	9	30.1
Q2G0R0	ATP-dependent zinc metalloprotease FtsH	ftsH	-0.11	0.23	77.81	18	31.7
Q2G1C0	2-C-methyl-D-erythritol 4-phosphate cytidyltransferase	ispD	-0.11	0.29	26.66	7	38.7
Q2FXQ1	50S ribosomal protein L20	rplT	-0.11	0.13	13.69	2	16.1
Q2FZ28	ATP-dependent protease ATPase subunit HslU	hslU	-0.11	0.51	52.31	11	31
Q2FZ42	50S ribosomal protein L19	rplS	-0.12	0.27	13.36	6	37.9
Q2G0L5	Serine-aspartate repeat-containing protein C	sdrC	-0.12	2.68	107.79	22	28.9
P0A0J0	RNA polymerase sigma factor SigA	sigA	-0.12	0.14	42.17	7	22.8
Q2FY27	Glucokinase, putative	SAOUHSC_01646	-0.12	1.19	35.08	7	32.3
Q2FYJ6	Extracellular matrix-binding protein ebh	ebh	-0.12	0.21	1029.9010		1.4
Q2G2S8	Putative uncharacterized protein	SAOUHSC_01974	-0.12	0.34	114.42	21	29
Q2G0L4	Serine-aspartate repeat-containing protein D	sdrD	-0.12	1.95	146.09	33	40
Q2G1B7	Putative uncharacterized protein	SAOUHSC_00228	-0.13	0.53	66.31	15	26.5
Q2G0S7	Pur operon repressor	SAOUHSC_00467	-0.13	1.39	30.40	9	37.6
Q2FZW9	D-isomer specific 2-hydroxyacid dehydrogenase, NAD binding domain protein	SAOUHSC_00866	-0.13	0.25	32.48	6	23.1
Q2G163	Pseudouridine-5'-phosphate glycosidase	psuG	-0.13	0.68	32.87	6	20.5
Q2G0S0	50S ribosomal protein L25	rplY	-0.13	0.39	23.79	7	30
Q05615	3-phosphoshikimate 1-carboxyvinyltransferase	aroA	-0.14	0.34	47.00	6	20.4
Q93T05	DNA mismatch repair protein MutL	mutL	-0.14	0.23	76.85	6	10.5
Q2FZP4	Peptide chain release factor 3	prfC	-0.14	0.86	59.60	4	7.9
Q2FVQ5	Probable malate:quinone oxidoreductase	mqo	-0.14	0.70	54.81	12	27
Q2G2Q4	Ribosome-binding factor A	rbfA	-0.15	0.19	13.52	4	41.4
Q2FZW0	Putative uncharacterized protein	SAOUHSC_00875	-0.15	0.74	39.40	8	27.7
Q2FZ22	Uridylate kinase	pyrH	-0.15	1.02	26.15	5	22.5
Q2FXW4	Putative uncharacterized protein	SAOUHSC_01717	-0.15	0.24	35.96	4	15.6
Q2G2C9	Putative uncharacterized protein	SAOUHSC_01245	-0.15	0.56	11.54	2	24.8
Q2FW79	UPF0457 protein	SAOUHSC_02425	-0.15	0.35	10.01	3	41.9
Q2FXM1	Putative uncharacterized protein	SAOUHSC_01814	-0.15	0.66	15.23	5	39.4
Q2G1U6	Regulatory protein Spx	spxA	-0.15	0.08	15.44	3	22.1
Q2FV16	Probable malate:quinone oxidoreductase	mqo	-0.16	0.70	56.00	17	34.9
Q2FUY2	Clumping factor B	clfB	-0.16	0.79	93.59	13	24.4
Q2G2F3	Signal transduction protein TRAP	traP	-0.16	0.53	19.55	5	22.2
Q2FYG6	Heptaprenyl diphosphate syntase component II, putative	SAOUHSC_01486	-0.16	0.39	35.59	2	7
Q2FZE9	Iron-regulated surface determinant protein A	isdA	-0.16	0.50	38.75	8	24
Q2G1W4	S-adenosylmethionine synthase	metK	-0.16	1.29	43.64	9	24.2
Q2G0N9	50S ribosomal protein L10	rplJ	-0.16	0.99	17.71	4	36.7
Q2FZY3	UPF0051 protein	SAOUHSC_00851	-0.17	1.30	52.53	11	23.7
Q9F0R1	HTH-type transcriptional regulator SarR	sarR	-0.17	0.27	13.67	6	34.8
Q2FZ39	Ribosome biogenesis GTPase A	SAOUHSC_01214	-0.17	0.99	33.38	6	17
Q2FVV2	Putative uncharacterized protein	SAOUHSC_02589	-0.17	0.23	33.00	6	29.7
Q2FZZ6	Putative uncharacterized protein	SAOUHSC_00838	-0.17	0.18	33.50	5	18.2

8 - Supporting Information

Q2FVI7	Glycerate kinase, putative	SAOUHSC_02723	-0.17	0.65	40.66	6	20.3
Q2FWW3	Putative uncharacterized protein	SAOUHSC_02158	-0.17	1.03	48.12	8	24.8
Q2G1Z4	Proline--tRNA ligase	proS	-0.17	0.27	63.86	7	16.9
Q2FZ51	Acyl carrier protein	acpP	-0.17	0.44	8.55	4	41.6
Q2FYZ1	Putative uncharacterized protein	SAOUHSC_01323	-0.18	1.19	29.82	5	26.6
Q7X2S2	Carbamate kinase 2	arcC2	-0.18	0.58	34.33	7	36.4
Q2G1Y0	DNA ligase	ligA	-0.18	0.55	75.08	13	21.3
Q2FY53	2-oxoisovalerate dehydrogenase, E1 component, beta subunit, putative	SAOUHSC_01612	-0.18	0.74	36.06	6	24.8
Q2FXT0	50S ribosomal protein L27	rpmA	-0.18	0.65	10.32	7	55.3
Q2FZ67	Ribosomal RNA small subunit methyltransferase B	SAOUHSC_01184	-0.18	1.77	50.11	8	18.9
Q2FWC9	Putative uncharacterized protein	SAOUHSC_02370	-0.18	0.23	33.11	4	15.7
Q2FZ77	Bifunctional protein PyrR	pyrR	-0.19	1.01	19.86	8	49.1
Q2FXI0	D-alanine aminotransferase	SAOUHSC_01867	-0.19	0.76	31.89	6	28.4
Q2FZM7	Putative uncharacterized protein	SAOUHSC_00973	-0.19	0.20	27.73	4	19.6
Q2FXY6	30S ribosomal protein S20	rpsT	-0.19	0.58	9.02	4	45.8
Q2FZB0	Ornithine carbamoyltransferase	argF	-0.19	1.65	37.52	9	31.2
Q2FZJ0	Phosphoribosylformylglycinamide synthase subunit PurL	purL	-0.19	0.90	79.54	10	17.3
Q2FWH4	UDP-N-acetylmuramoyl-tripeptide--D-alanyl-D-alanine ligase	SAOUHSC_02317	-0.20	1.34	50.05	8	14.6
Q2FWE8	ATP synthase subunit alpha	atpA	-0.20	1.32	54.58	15	30.3
Q2G1G0	Putative uncharacterized protein	SAOUHSC_00164	-0.20	1.12	35.55	4	15
Q2FX05	Methionine aminopeptidase	map	-0.20	0.35	27.50	5	22.2
Q2G1Z9	NAD kinase	nadK	-0.20	0.76	30.77	2	7.1
Q2FYV4	Homoserine dehydrogenase	SAOUHSC_01320	-0.20	0.35	46.87	11	34.5
Q2FY08	Glycine--tRNA ligase	glyQS	-0.20	0.81	53.62	13	27.6
Q2FWF4	UDP-N-acetylglucosamine 1-carboxyvinyltransferase	murA	-0.20	1.25	44.94	7	19
Q2G2B2	Surface protein G	sasG	-0.20	0.99	178.52	27	39.6
Q2FXP2	Glyceraldehyde-3-phosphate dehydrogenase	SAOUHSC_01794	-0.20	1.33	36.98	11	42.2
Q2FXQ7	ATP-dependent Clp protease ATP-binding subunit ClpX	clpX	-0.20	1.13	46.30	9	25
Q2G1G7	Putative uncharacterized protein	SAOUHSC_00156	-0.20	1.76	39.87	8	20.5
Q2FXL3	Probable thiol peroxidase	tpx	-0.21	1.12	18.01	6	49.4
Q2G078	Ribonucleoside-diphosphate reductase	SAOUHSC_00742	-0.21	1.97	82.60	15	23.2
Q2FY43	Acetyl-CoA carboxylase, biotin carboxylase	SAOUHSC_01623	-0.21	1.18	50.05	9	27.3
Q2FWE5	Serine hydroxymethyltransferase	glyA	-0.21	0.88	45.17	10	28.6
Q2FW81	Probable uridylyltransferase	SAOUHSC_02423	-0.21	1.55	44.89	12	33.2
Q2FV77	3-hydroxy-3-methylglutaryl coenzyme A reductase	SAOUHSC_02859	-0.21	0.90	46.24	7	23.5
Q2G015	Clumping factor A	clfA	-0.21	2.49	96.45	11	15.9
Q2FYU4	GMP reductase	guaC	-0.21	0.36	36.12	2	7.4
Q2FZA9	Carbamate kinase 1	arcC1	-0.21	1.47	33.60	10	37.1
Q2G295	Catabolite control protein A	SAOUHSC_01850	-0.22	1.18	36.06	13	48
Q2FYM3	Putative uncharacterized protein	SAOUHSC_01415	-0.22	1.52	30.08	5	21.6
Q2G1Y6	GTP-binding protein TypA, putative	SAOUHSC_01058	-0.22	1.08	69.20	14	26.3
Q2FZ58	Uncharacterized protein	SAOUHSC_01193	-0.22	1.38	60.52	12	30.8
Q2FXP9	Translation initiation factor IF-3	infC	-0.22	0.52	20.21	4	26.9
Q2G0R8	Transcription-repair-coupling factor	mfd	-0.22	0.35	134.22	6	6.7
Q2G0B1	HTH-type transcriptional regulator MgrA	mgrA	-0.22	1.25	17.09	9	42.9
Q2FWD7	Transcription termination factor Rho	rho	-0.22	1.45	49.97	12	28.8
Q2G2A3	Dihydropolyl dehydrogenase	SAOUHSC_01043	-0.22	1.28	49.48	17	46.6
Q2FXU7	Putative uncharacterized protein	SAOUHSC_01735	-0.22	0.60	28.64	4	15.6
Q2FZ55	Phosphate acyltransferase	plsX	-0.22	1.40	35.43	7	30.5
Q2G0X6;Q2FXD0	Type I restriction-modification system, M subunit	SAOUHSC_00397	-0.22	0.93	56.14	5	11.4
Q2FXK6	30S ribosomal protein S4	rpsD	-0.22	0.57	23.01	10	37.5
POA0F4	50S ribosomal protein L11	rplK	-0.22	0.64	14.87	7	45
Q2FXX2	UPF0271 protein	SAOUHSC_01708	-0.22	1.60	27.45	3	12.4
Q2FV28	Putative uncharacterized protein	SAOUHSC_02911	-0.23	0.30	27.79	2	10
Q2G1C6	Acetate CoA-transferase YdIF	SAOUHSC_00199	-0.23	0.13	58.88	6	14.1
Q2FWE7	ATP synthase subunit delta	atpH	-0.23	0.23	20.50	5	30.2
Q2FW06	50S ribosomal protein L3	rplC	-0.23	0.92	23.72	6	28.6
Q2FYY6	Glutamine synthetase	SAOUHSC_01287	-0.23	0.70	50.84	12	37.4
Q2FZ09	Protein RecA	recA	-0.23	1.23	34.88	11	48.1
Q2FXY7	Elongation factor 4	lepA	-0.23	1.73	68.17	8	18.9
P02976	Immunoglobulin G-binding protein A	spa	-0.23	1.08	56.44	28	57.4
Q2FWB5	Putative uncharacterized protein	SAOUHSC_02383	-0.23	0.48	52.95	7	23.2
Q2FYZ6	Asparagine--tRNA ligase	asnS	-0.23	1.33	49.16	11	28.4
Q9RFJ6	HTH-type transcriptional regulator rot	rot	-0.24	0.98	19.37	3	22.3
Q2G0T5	DNA polymerase III, gamma and tau subunits, putative	SAOUHSC_00442	-0.24	0.50	62.46	7	15.4

Q2FYG1	Glycerol-3-phosphate dehydrogenase [NAD(P)+]	gpsA	-0.24	0.98	36.07	8	36.7
Q2G1C7	Putative uncharacterized protein	SAOUHSC_00198	-0.24	0.63	56.21	13	35.1
Q2FY33	Aminomethyltransferase	gcvT	-0.24	0.85	40.46	9	30.6
Q2FV6	Putative uncharacterized protein	SAOUHSC_02585	-0.24	0.79	26.62	6	26.1
Q2G047	UvrABC system protein B	SAOUHSC_00779	-0.24	0.56	37.48	7	24.1
Q2FW21	50S ribosomal protein L6	rplF	-0.24	2.06	19.79	11	70.2
Q2G283	Glutamate-1-semialdehyde 2,1-aminomutase 2	hemL2	-0.24	0.54	46.76	10	31.5
Q2FXX0	Acetyl-CoA carboxylase, biotin carboxyl carrier protein, putative	SAOUHSC_01710	-0.24	0.70	16.79	3	27.5
Q2FZ50	Ribonuclease 3	rnc	-0.25	0.43	27.92	5	23.5
Q2FXM6	Acetyl-coenzyme A carboxylase carboxyl transferase subunit beta	accD	-0.25	1.58	31.87	8	33.7
Q2G077	Ribonucleotide-diphosphate reductase beta chain, putative	SAOUHSC_00743	-0.25	0.73	37.51	4	16.1
P60070	Anti-sigma-B factor antagonist	rsbV	-0.25	0.55	12.21	3	29.6
Q2FYT3	Nuclease SbcCD subunit C	sbcC	-0.25	0.79	117.27	7	8
Q2FWD6	Putative aldehyde dehydrogenase	SAOUHSC_02363	-0.25	2.10	51.97	14	32.4
Q2G1W0	Putative uncharacterized protein	SAOUHSC_02574	-0.25	1.29	40.74	5	20
Q2FW18	50S ribosomal protein L5	rplE	-0.25	2.29	20.27	14	63.7
Q2G1D0	Acetyl-CoA acetyltransferase, putative	SAOUHSC_00195	-0.25	1.76	41.84	8	35.8
Q2FYP2	ABC transporter, ATP-binding protein, putative	SAOUHSC_01392	-0.25	1.61	60.26	13	25.9
Q2FZL8	Putative uncharacterized protein	SAOUHSC_00982	-0.26	0.45	46.62	4	10.2
Q2FWY1	Probable manganese-dependent inorganic pyrophosphatase	ppaC	-0.26	1.26	34.07	12	31.4
Q2FY10	Putative pyruvate, phosphate dikinase regulatory protein	SAOUHSC_01664	-0.26	0.60	30.78	6	22.8
Q2G2G7	UPF0637 protein	SAOUHSC_01054	-0.26	1.04	24.02	4	21.1
Q2G045	HPr kinase/phosphorylase	hprK	-0.26	1.17	34.48	8	29.4
Q2FW12	30S ribosomal protein S3	rpsC	-0.26	0.86	24.10	12	48.8
O34090	Porphobilinogen deaminase	hemC	-0.26	1.20	34.35	8	31.8
Q2G243	DNA repair protein radA	SAOUHSC_00507	-0.26	0.71	48.68	4	11.9
Q2FY68	Pyrraline-5-carboxylate reductase	SAOUHSC_01597	-0.26	1.67	28.76	4	16.9
Q2FZ25	30S ribosomal protein S2	rpsB	-0.26	1.04	29.09	14	48.2
Q2FXM9	Pyruvate kinase	pyk	-0.26	1.16	63.10	29	66.3
Q2FXS8	50S ribosomal protein L21	rplU	-0.27	1.31	11.33	8	67.6
Q2FUX7	Arginine deiminase	arcA	-0.27	0.98	46.91	19	44.8
Q2FXJ0	UDP-N-acetylmuramate--L-alanine ligase	murC	-0.27	0.98	49.19	4	11.4
Q2FXN4	Isocitrate dehydrogenase [NADP]	SAOUHSC_01801	-0.27	1.61	46.42	7	22
Q2G0E8	Putative uncharacterized protein	SAOUHSC_00658	-0.27	1.27	12.79	2	25
Q2G0Z2	Putative uncharacterized protein	SAOUHSC_00369	-0.27	1.43	35.61	12	48.1
Q2G0L8	Putative uncharacterized protein	SAOUHSC_00542	-0.27	1.14	31.84	9	42.9
Q2FXT1	GTPase Obg	obg	-0.27	1.10	47.24	13	37
Q2FVK8	2,3-bisphosphoglycerate-dependent phosphoglycerate mutase	gpmA	-0.27	0.59	26.68	8	39
Q2FUW9	Putative uncharacterized protein	SAOUHSC_02982	-0.27	0.70	70.93	24	43.8
Q2FW66	Alkaline shock protein 23	asp23	-0.27	0.93	19.19	6	42.6
Q2FXI9	Putative uncharacterized protein	SAOUHSC_01857	-0.28	1.48	144.65	26	27.2
Q2FYG2	DNA-binding protein HU, putative	SAOUHSC_01490	-0.28	0.62	9.63	11	82.2
P60393	Ribosomal RNA small subunit methyltransferase H	rsmH	-0.28	0.73	35.68	5	19.3
Q2G0L0	Putative uncharacterized protein	SAOUHSC_00550	-0.28	0.84	24.92	4	18.1
Q2FZJ6	Bifunctional protein f0D	folD	-0.28	1.34	30.84	12	46.2
Q2FW32	DNA-directed RNA polymerase subunit alpha	rpoA	-0.28	1.18	35.01	12	38.9
Q2FZS8	ATP-dependent Clp protease, ATP-binding subunit ClpB	SAOUHSC_00912	-0.28	1.47	98.33	33	42.8
Q2FY79	Transcriptional regulatory protein SrrA	srrA	-0.28	2.27	28.16	3	13.3
Q2FV76	HMG-CoA synthase, putative	SAOUHSC_02860	-0.28	2.61	43.21	12	40.5
Q2FXU5	Aspartate--tRNA ligase	aspS	-0.28	1.56	66.63	11	23.5
Q2FYM2	Dihydrolypoyllysine-residue succinyltransferase component of 2-oxoglutarate dehydrogenase complex	odhB	-0.28	1.30	46.67	15	39.8
Q2G115	Ribosome-binding ATPase YchF	ychF	-0.28	1.64	40.59	11	41.4
Q2FZV6	Leucine aminopeptidase 2, chloroplastic	SAOUHSC_00879	-0.28	0.79	54.13	6	15.3
Q2FW28	Translation initiation factor IF-1	infA	-0.29	0.41	8.28	4	69.4
Q2FXA3	Uroporphyrinogen decarboxylase	hemE	-0.29	1.07	39.35	5	18.8
Q2G2S7	Putative uncharacterized protein	SAOUHSC_01975	-0.29	1.63	46.22	6	20.6
Q2FYI6	Putative uncharacterized protein	SAOUHSC_01460	-0.29	0.79	43.33	4	16.8
Q2FW33	50S ribosomal protein L17	rplQ	-0.29	2.81	13.75	5	42.6
Q2FZG8	UPF0356 protein	SAOUHSC_01036	-0.29	0.82	8.75	3	55.6
Q2G0N1	Elongation factor G	fusA	-0.29	1.70	76.61	25	49.4

8 - Supporting Information

Q2G0J8	Phosphomethylpyrimidine kinase	SAOUHSC_00562	-0.29	0.74	29.86	8	35.1
Q2G1G2	Type I site-specific deoxyribonuclease, HsdR family, putative	SAOUHSC_00162	-0.29	1.60	109.23	16	16.6
Q2FXT3	Holliday junction ATP-dependent DNA helicase RuvA	ruvA	-0.29	0.48	22.26	5	28.5
Q2FZ72	Carbamoyl-phosphate synthase large chain	carB	-0.29	1.65	117.18	27	30.3
Q2FW23	30S ribosomal protein S5	rpsE	-0.29	2.03	17.74	9	56.6
Q2FWM4	Accessory gene regulator protein A	SAOUHSC_02265	-0.29	1.39	24.25	3	9.6
Q2FVC3	Putative uncharacterized protein	SAOUHSC_02790	-0.29	0.35	109.90	14	19
Q2G1N7	HTH-type transcriptional regulator SarS	sarS	-0.29	0.46	29.89	4	18.8
Q2FY15	DEAD-box ATP-dependent RNA helicase CshB	cshB	-0.29	0.58	51.08	11	29.7
Q2G2T3	50S ribosomal protein L9	rplI	-0.29	1.65	16.64	7	43.3
Q2G1N4	Periplasmic binding protein, putative	SAOUHSC_00074	-0.29	0.47	36.74	5	18.2
Q2FYG7	Nucleoside diphosphate kinase	ndk	-0.30	0.45	16.58	5	40.9
Q2G0M7	Molecular chaperone Hsp31 and glyoxalase 3	hchA	-0.30	0.98	32.18	2	9.6
Q2FWJ5	S1 RNA binding domain protein	SAOUHSC_02297	-0.30	1.68	80.93	25	36.7
Q2FYJ3	L-threonine dehydratase catabolic TdcB	tdcB	-0.30	0.98	37.31	11	45.7
Q2FYZ5	Glycerol kinase	glpK	-0.30	2.06	55.63	16	31.9
Q2FWL6	Redox-sensing transcriptional repressor Rex	rex	-0.30	1.14	23.60	6	30.8
Q2G2U9	Transcriptional regulator SarA	sarA	-0.30	0.92	14.72	7	40.3
Q2FW16	50S ribosomal protein L14	rplN	-0.30	2.52	13.14	7	50.8
Q2G2G4	Inositol monophosphatase family protein, putative	SAOUHSC_01055	-0.30	1.24	30.47	3	13.8
Q2G069	UDP-N-acetylenolpyruvoylglucosamine reductase	murB	-0.30	0.67	33.80	3	11.7
Q2G113	30S ribosomal protein S6	rpsF	-0.30	1.65	11.60	4	40.8
Q2FY54	2-oxoisovalerate dehydrogenase, E2 component, dihydrolipoamide acetyltransferase, putative	SAOUHSC_01611	-0.30	1.76	46.73	7	17.7
Q2G2D0	Translation initiation factor IF-2	infB	-0.30	1.13	77.87	24	38.3
O06446	Protein translocase subunit SecA 1	secA1	-0.30	1.47	95.96	25	32.7
Q2G248	Putative uncharacterized protein	SAOUHSC_01852	-0.30	0.91	40.62	10	28.9
Q2G0C6	Putative uncharacterized protein	SAOUHSC_00679	-0.31	1.98	33.24	2	8.3
Q2G2H5	Chromosomal replication initiator protein DnaA	dnaA	-0.31	0.69	51.97	9	17.4
Q2G024	Ribonuclease R	rnr	-0.31	0.33	90.43	10	12.9
Q2G1T6	UTP--glucose-1-phosphate uridylyltransferase	gtaB	-0.31	0.67	32.45	6	17.7
Q2G2Q0	DNA gyrase subunit A	gyrA	-0.31	1.88	99.35	10	15.3
Q2FWF0	ATP synthase subunit beta	atpD	-0.31	1.58	51.40	16	43
Q2FV67	1-pyrroline-5-carboxylate dehydrogenase	rocA	-0.31	1.68	56.87	23	54.3
Q2FXV0	Putative uncharacterized protein	SAOUHSC_01732	-0.31	1.05	12.77	2	28.4
Q2FZG9	Ribonuclease J 1	rnj1	-0.31	1.56	62.67	15	32.4
Q2FZH8	Putative uncharacterized protein	SAOUHSC_01026	-0.32	1.13	44.77	6	19.2
Q2G0P5	ATP-dependent Clp protease ATP-binding subunit ClpC	clpC	-0.32	1.30	91.04	27	36.9
Q2FZ46	Signal recognition particle protein	ffh	-0.32	0.50	50.71	6	16.5
P0A088	Peptide methionine sulfoxide reductase MsrB	msrB	-0.32	0.62	16.28	3	29.6
Q2G234	Nitric oxide synthase oxygenase	SAOUHSC_02134	-0.32	1.63	41.71	5	18.4
Q2FWN3	10 kDa chaperonin	groS	-0.32	0.33	10.42	4	43.6
Q2G036	ATP-dependent Clp protease proteolytic subunit	clpP	-0.32	0.89	21.51	6	22.6
Q2G2P2	Globin domain protein	SAOUHSC_00204	-0.32	0.82	42.91	7	24.7
Q2G0Q1	Pyridoxal biosynthesis lyase PdxS	pdxS	-0.32	1.13	31.99	9	35.9
Q2FZ19	Ribonuclease J 2	rnj2	-0.32	2.62	62.60	13	20.1
Q2FXU4	Histidine--tRNA ligase	hisS	-0.32	0.75	48.28	5	14.8
Q2FWY9	Glutamyl-tRNA(Gln) amidotransferase subunit A	gatA	-0.32	2.31	52.82	15	36.1
Q2FW07	50S ribosomal protein L4	rplD	-0.32	0.73	22.46	6	40.6
Q2G2U6	Transcriptional regulatory protein WalR	walR	-0.32	1.18	27.19	6	27.9
Q2FZ48	Signal recognition particle receptor FtsY	ftsY	-0.33	1.29	46.59	9	28.6
Q2G0Q9	33 kDa chaperonin	hslO	-0.33	1.40	31.82	5	23.2
Q2FWE6	Uracil phosphoribosyltransferase	upp	-0.33	1.35	23.05	7	44.5
Q2FXV6	tRNA-specific 2-thiouridylase MnmA	mnmA	-0.33	1.41	42.15	7	20.4
Q2G1T9	DNA-directed RNA polymerase subunit omega	rpoZ	-0.33	0.64	8.15	3	50
Q2FUX3	Immunodominant staphylococcal antigen B	isaB	-0.33	0.97	19.37	6	28.6
Q2G2A4	Dihydrolipoamide S-acetyltransferase component of pyruvate dehydrogenase complex E2, putative	SAOUHSC_01042	-0.33	1.57	46.35	16	37.7
Q2FYI5	Cell cycle protein GpsB	gpsB	-0.33	0.66	13.15	3	27.2
Q2G055	Uncharacterized protein	SAOUHSC_00767	-0.33	1.24	22.21	6	29.5
Q2FZH5	Phosphoenolpyruvate-protein phosphotransferase	SAOUHSC_01029	-0.33	0.78	63.22	7	15.7
Q2FV39	Uncharacterized hydrolase	SAOUHSC_02900	-0.33	1.09	31.01	7	30.8
Q2G274	DNA gyrase subunit B	gyrB	-0.33	1.32	72.54	13	17.5
Q2G1Y5	L-lactate dehydrogenase 2	ldh2	-0.33	0.89	34.42	12	48.9
Q2G050	Excinuclease ABC, B subunit	SAOUHSC_00776	-0.34	1.36	39.82	7	23
Q2FYS0	Putative uncharacterized protein	SAOUHSC_01365	-0.34	0.94	37.86	6	19.5
Q2G1Q4	Putative uncharacterized protein	SAOUHSC_00049	-0.34	1.24	121.73	17	19

Q2G032	Glyceraldehyde-3-phosphate dehydrogenase	SAOUHSC_00795	-0.34	0.52	36.28	14	48.5
O52582	Coenzyme A disulfide reductase	cdr	-0.34	1.14	49.24	13	34
Q2FWC1	Pyrimidine-nucleoside phosphorylase	pdp	-0.34	1.42	46.31	15	43.4
Q2G0Y6	GMP synthase [glutamine-hydrolyzing]	guaA	-0.34	1.97	58.23	6	18.3
Q2G046	UvrABC system protein A	uvrA	-0.34	0.72	105.37	15	23.4
Q2G2Q3	tRNA pseudouridine synthase B	truB	-0.34	1.78	34.59	5	16.7
Q2FXU2	D-aminoacyl-tRNA deacylase	dtd	-0.34	1.60	16.70	2	10
Q2FXA4	Ferrochelatase	hemH	-0.34	0.66	35.07	7	32.9
Q2FW27	Adenylate kinase	adk	-0.35	0.78	23.97	9	39.5
Q2FXM0	UPF0173 metal-dependent hydrolase	SAOUHSC_01815	-0.35	0.76	25.25	3	17.5
Q2FY60	6-phosphogluconate dehydrogenase, decarboxylating	SAOUHSC_01605	-0.35	1.88	51.80	9	23.1
Q2FW30	30S ribosomal protein S13	rpsM	-0.35	1.11	13.72	9	37.2
Q2FY73	Transcriptional regulator, Fur, putative	SAOUHSC_01592	-0.35	0.25	17.24	3	20.8
Q2FXQ6	Trigger factor	tig	-0.35	0.97	48.61	22	44.3
Q2FWZ2	Diacylglycerol kinase	dagK	-0.35	1.03	34.89	6	21.6
Q2FVA3	D-lactate dehydrogenase, putative	SAOUHSC_02830	-0.35	1.47	34.80	7	24.4
Q2FXN9	DNA polymerase	SAOUHSC_01797	-0.35	1.56	99.19	17	27.3
Q2FZH6	Phosphocarrier protein hpr, putative	SAOUHSC_01028	-0.35	0.51	9.50	4	58
Q2FZ31	Methylenetetrahydrofolate--tRNA-(uracil-5)-methyltransferase TrmF	trmFO	-0.36	2.10	48.37	9	26
Q2FZZ8	Glycine cleavage system H protein	gcvH	-0.36	0.64	14.09	4	46
Q2G1C9	Putative uncharacterized protein	SAOUHSC_00196	-0.36	1.38	84.61	28	38.4
Q2G2H4	DNA polymerase III subunit beta	SAOUHSC_00002	-0.36	1.54	41.91	18	43.5
Q2G0Q8	Cysteine synthase	SAOUHSC_00488	-0.36	1.08	32.98	15	63.9
Q2G1D8	Formate acetyltransferase	pflB	-0.36	1.35	84.86	41	53.5
Q2FWD3	Putative uncharacterized protein	SAOUHSC_02366	-0.36	1.09	30.84	8	46.5
Q2FXA0	UPF0342 protein	SAOUHSC_01977	-0.36	0.31	13.31	6	58.8
Q2FZ45	30S ribosomal protein S16	rpsP	-0.36	2.87	10.24	5	60.4
Q2FXZ2	Chaperone protein DnaK	dnaK	-0.36	1.62	66.36	27	50.8
Q2FZT6	ATP-dependent helicase/deoxyribonuclease subunit B	addB	-0.36	1.24	134.50	7	6.6
Q2G252	Ribosomal RNA large subunit methyltransferase H	rlmH	-0.36	1.45	18.31	5	34.6
Q2G2D2	Transcription termination-antitermination factor, putative	SAOUHSC_01243	-0.36	1.54	43.74	9	25.8
Q2G0N0	Elongation factor Tu	tuf	-0.36	1.09	43.10	23	74.1
Q2G268	Phosphopantothenoylcysteine decarboxylase/phosphopantothenate--cysteine ligase	SAOUHSC_01178	-0.36	0.42	44.14	5	19
Q2FXI6	Putative uncharacterized protein	SAOUHSC_01860	-0.36	0.68	11.86	3	34
Q2FW62	Putative uncharacterized protein	SAOUHSC_02445	-0.36	0.83	37.27	5	18
Q2G0P0	50S ribosomal protein L1	rplA	-0.36	1.09	24.71	9	46.5
Q2FZ27	GTP-sensing transcriptional pleiotropic repressor CodY	codY	-0.36	0.65	28.76	14	48.2
Q2FVT2	Formimidoylglutamase	hutG	-0.37	0.63	34.51	4	14.5
Q2FW86	Putative uncharacterized protein	SAOUHSC_02417	-0.37	0.40	31.79	8	36.6
Q2FYPO	Aspartate-semialdehyde dehydrogenase	asd	-0.37	0.91	36.28	5	18.2
Q2FZY6	Putative uncharacterized protein	SAOUHSC_00848	-0.37	1.80	48.55	6	21.8
Q2FXM7	Acetyl-coenzyme A carboxylase carboxyl transferase subunit alpha	accA	-0.37	0.31	35.07	4	20.1
Q2FXV9	Alanine--tRNA ligase	alaS	-0.37	2.15	98.52	16	26.5
Q2G065	Putative uncharacterized protein	SAOUHSC_00756	-0.37	0.91	41.80	4	9.6
Q2FZ89	Cell division protein FtsZ	ftsZ	-0.37	1.16	41.04	15	43.6
Q2FZU5	Glutamate dehydrogenase	SAOUHSC_00895	-0.37	2.46	45.76	12	38.9
Q2G1M1	3-ketoacyl-acyl carrier protein reductase, putative	SAOUHSC_00086	-0.37	1.14	27.22	6	37.6
Q2FUQ5	Putative uncharacterized protein	SAOUHSC_03049	-0.37	0.77	32.20	4	22.2
Q2FZ53	3-oxoacyl-(Acyl-carrier-protein) reductase, putative	SAOUHSC_01199	-0.37	2.45	25.89	15	80.7
Q2FVV9	Putative formate dehydrogenase	SAOUHSC_02582	-0.37	1.90	111.24	14	18.8
P48940	30S ribosomal protein S7	rpsG	-0.37	0.76	17.79	7	40.4
Q2FX14	Aminopeptidase PepS, putative	SAOUHSC_02092	-0.37	0.89	47.12	9	28.2
Q2FYS9	Aconitate hydratase 1	SAOUHSC_01347	-0.38	2.42	98.97	20	28.6
Q2FXM5	NADP-dependent malic enzyme, putative	SAOUHSC_01810	-0.38	1.09	44.23	8	37.4
Q2G1K9	Aldehyde-alcohol dehydrogenase	SAOUHSC_00113	-0.38	1.96	94.94	28	40.3
Q2G124	Probable acetyl-CoA acyltransferase	SAOUHSC_00336	-0.38	1.63	41.70	8	32.6
Q2G0E9	Putative uncharacterized protein	SAOUHSC_00656	-0.38	1.18	21.26	5	27.8
Q2FV74	ATP-dependent Clp protease ATP-binding subunit ClpL	clpL	-0.38	1.66	77.84	22	35.4
Q2G0N5	DNA-directed RNA polymerase subunit beta'	rpoC	-0.38	2.30	135.41	42	38.1
Q2G218	L-lactate dehydrogenase 1	ldhI	-0.38	2.00	34.58	10	34.1
Q2FYF9	30S ribosomal protein S1, putative	SAOUHSC_01493	-0.38	2.13	43.29	17	51.4
Q2FZD9	Phenylalanine--tRNA ligase alpha subunit	pheS	-0.38	1.23	40.11	9	23.3
Q2G0F8	Arginine--tRNA ligase	argS	-0.38	1.83	62.38	22	46.8
POA0B7	Alkyl hydroperoxide reductase subunit C	ahpC	-0.38	2.46	20.98	11	58.2

8 - Supporting Information

Q2FXP7	Threonine--tRNA ligase	thrS	-0.38	1.50	74.49	16	24.5
Q2FZ21	Ribosome-recycling factor	frr	-0.38	1.05	20.35	8	57.6
Q2FXT6	Queuine tRNA-ribosyltransferase	tgt	-0.39	0.92	43.31	2	4.7
Q2FWA0	Glutamine--fructose-6-phosphate aminotransferase [isomerizing]	glmS	-0.39	1.51	65.85	16	29.5
Q2G2M6	Cysteine--tRNA ligase	cysS	-0.39	2.60	53.69	12	28.1
Q2FY49	Arginine repressor	argR	-0.39	0.37	17.10	2	22
Q2FY35	Probable glycine dehydrogenase (decarboxylating) subunit 2	gcvPB	-0.39	1.43	54.78	12	24.9
Q2FXL1	Probable tRNA sulfurtransferase	thiI	-0.39	1.44	46.21	6	17.4
O05204	Alkyl hydroperoxide reductase subunit F	ahpF	-0.39	1.39	54.72	11	25.2
Q2FZ36	Succinyl-CoA ligase [ADP-forming] subunit alpha	SAOUHSC_01218	-0.40	2.69	31.54	9	43.7
Q2G0V0	Lipoprotein	SAOUHSC_00426	-0.40	0.70	30.46	3	13.9
P95689	Serine--tRNA ligase	serS	-0.40	1.57	48.64	17	40.7
Q2FUX8	Ornithine carbamoyltransferase	argF	-0.40	1.15	37.76	6	21.4
P0A0F8	50S ribosomal protein L15	rplO	-0.40	2.20	15.60	6	48.6
Q2FZ32	DNA topoisomerase 1	topA	-0.40	1.21	79.11	7	16
Q2G1R9	Methionine--tRNA ligase	metG	-0.40	1.30	74.89	14	23.3
Q2FWB8	Purine nucleoside phosphorylase DeoD-type	deoD	-0.40	0.75	25.91	3	9.3
Q2G1Z8	DNA polymerase III PolC-type	polC	-0.40	0.86	162.46	7	6.5
Q2G2S0	Adenylosuccinate lyase	purB	-0.40	1.38	49.60	10	23.2
Q2G1C8	Putative uncharacterized protein	SAOUHSC_00197	-0.40	1.67	44.73	14	34.7
Q2G253	Putative uncharacterized protein	SAOUHSC_00025	-0.40	1.43	83.42	25	42.5
Q2FXZ7	30S ribosomal protein S21	rpsU	-0.40	1.00	6.97	5	34.5
Q2G1X0	Alpha-hemolysin	hly	-0.40	0.27	35.97	14	50.8
Q2FZW6	D-alanine--poly(phosphoribitol) ligase subunit 1	dltA	-0.40	1.14	54.67	9	26
Q2FZV4	Putative uncharacterized protein	SAOUHSC_00881	-0.40	0.54	13.55	2	14.5
Q2FY29	Putative uncharacterized protein	SAOUHSC_01644	-0.41	0.69	23.14	5	33.3
Q2G296	Formate--tetrahydrofolate ligase	fhs	-0.41	1.55	59.86	18	44
Q2FZM8	Putative uncharacterized protein	SAOUHSC_00972	-0.41	0.76	11.19	3	42.1
Q2FXY2	Putative uncharacterized protein	SAOUHSC_01698	-0.41	0.83	11.05	3	40.6
Q2FZ49	Chromosome partition protein Smc	smc	-0.41	0.65	136.75	14	15
Q2FXR4	Glutamate-1-semialdehyde 2,1-aminomutase 1	hemL1	-0.41	1.76	46.39	12	40.7
Q2FVB2	Fructose-1,6-bisphosphatase class 3	fbp	-0.41	2.27	76.17	14	26.8
Q2G041	Thioredoxin reductase	SAOUHSC_00785	-0.41	1.14	33.62	11	46.3
Q2FZ23	Elongation factor Ts	tsf	-0.41	2.43	32.49	15	60.8
Q2FW39	30S ribosomal protein S9	rpsI	-0.41	0.91	14.83	6	31.1
Q2FZQ7	Tryptophan--tRNA ligase	trpS	-0.41	1.08	36.91	10	35.3
Q2FZ20	Polyribonucleotide nucleotidyltransferase	pnp	-0.41	2.17	77.36	19	28.2
Q2G0G6	Putative uncharacterized protein	SAOUHSC_00603	-0.41	1.22	35.46	5	27.2
Q2FZ54	Malonyl CoA-acyl carrier protein transacylase	SAOUHSC_01198	-0.41	1.14	33.64	9	31.8
Q2FVC1	Phosphoglucomutase	pgcA	-0.41	1.20	62.38	11	23.4
Q2FZ68	Methionyl-tRNA formyltransferase	fmt	-0.41	1.28	34.21	9	34.7
Q2FZ37	Succinyl-CoA ligase [ADP-forming] subunit beta	sucC	-0.42	1.63	42.06	19	52.6
Q2FZR9	3-oxoacyl-[acyl-carrier-protein] synthase 2	SAOUHSC_00921	-0.42	3.16	43.74	11	37.7
Q2G2D7	Putative uncharacterized protein	SAOUHSC_02447	-0.42	1.87	36.27	7	26.7
Q2G0T9	Alpha amylase family protein, putative	SAOUHSC_00438	-0.42	0.83	63.51	3	6.8
Q2FY50	DNA repair protein RecN	SAOUHSC_01615	-0.42	1.23	64.32	5	10.6
Q2FW38	50S ribosomal protein L13	rplM	-0.42	0.77	16.33	8	39.3
Q2FV14	Acetyl-CoA synthetase, putative	SAOUHSC_02929	-0.42	2.29	59.75	10	21.6
Q2FXL5	Acetate kinase	ackA	-0.42	1.54	44.04	15	46.2
P0A0G2	50S ribosomal protein L30	rpmD	-0.42	0.67	6.55	7	72.9
Q2FYN4	Diaminopimelate decarboxylase	lysA	-0.43	0.91	47.03	4	13.8
Q2FY16	Probable endonuclease 4	nfo	-0.43	1.64	33.16	8	31.8
Q2G0P2	Transcription termination/antitermination protein NusG	nusG	-0.43	1.36	20.66	9	48.9
Q2FZ04	Putative uncharacterized protein	SAOUHSC_01267	-0.43	1.75	31.36	3	13.9
Q2G1W2	Phosphoenolpyruvate carboxykinase [ATP]	pckA	-0.43	1.17	59.38	16	37.4
Q2FXI8	Putative uncharacterized protein	SAOUHSC_01858	-0.43	1.02	21.69	5	25.3
Q2FWJ3	Serine-protein kinase RsbW	rsbW	-0.43	1.14	17.92	4	30.8
Q2FZS0	3-oxoacyl-[acyl-carrier-protein] synthase 3	fabH	-0.43	1.46	33.88	4	19.5
Q2FWD4	UDP-N-acetylglucosamine 1-carboxyvinyltransferase	murA	-0.43	1.71	45.07	8	26.3
Q2FZ83	Putative uncharacterized protein	SAOUHSC_01158	-0.43	0.83	23.51	4	21
Q2FZ74	Dihydroorotase	pyrC	-0.43	2.17	46.37	6	18.9
Q2FZ82	Isoleucine--tRNA ligase	ileS	-0.43	1.02	104.88	12	15.3
Q2FXR7	Putative uncharacterized protein	SAOUHSC_01768	-0.43	0.57	21.42	3	17.7
Q2FZ75	Aspartate carbamoyltransferase	pyrB	-0.43	1.09	33.26	5	19.8
Q2FVA6	Putative uncharacterized protein	SAOUHSC_02827	-0.43	0.66	10.55	3	38.3

Q2FZZ9	Putative uncharacterized protein	SAOUHSC_00835	-0.44	1.13	13.60	4	37.3
Q2FVQ0	Putative uncharacterized protein	SAOUHSC_02652	-0.44	0.66	32.87	6	26.3
Q2FVX8	Molybdopterin biosynthesis moaB, putative	SAOUHSC_02544	-0.44	0.34	18.50	2	15.5
Q2G1Z0	Putative uncharacterized protein	SAOUHSC_00655	-0.44	1.83	35.02	7	26.4
Q2FWB9;Q2G224	Deoxyribose-phosphate aldolase	deoC	-0.44	1.46	23.33	7	38.6
P72360	Iron-sulfur cluster repair protein ScdA	scdA	-0.44	1.91	25.49	5	21.4
Q2G2A5	Pyruvate dehydrogenase complex, E1 component, pyruvate dehydrogenase beta subunit, putative	SAOUHSC_01041	-0.44	1.82	35.25	12	48
Q2FWN4	60 kDa chaperonin	groL	-0.44	1.54	57.66	23	57.1
Q2G2U0	N-acetylglucosamine-6-phosphate deacetylase	SAOUHSC_00710	-0.44	0.77	43.13	7	22.6
P47768	DNA-directed RNA polymerase subunit beta	rpoB	-0.44	1.94	133.22	35	32.1
Q2FZG6	Peptide deformylase	def	-0.44	1.64	20.56	8	45.9
Q2FXL7	Alanine dehydrogenase 2	ald2	-0.44	0.74	40.11	18	56.2
Q2FZ16	Putative uncharacterized protein	SAOUHSC_01255	-0.44	1.51	48.62	5	11.4
Q2FXJ5	Tyrosine--tRNA ligase	tyrS	-0.44	2.27	47.60	9	26.2
Q2G0M4	Branched-chain-amino-acid aminotransferase	SAOUHSC_00536	-0.45	1.65	40.09	10	33
Q2FXU1	GTP pyrophosphokinase	SAOUHSC_01742	-0.45	0.95	83.69	9	15.8
Q2G0G1	Alcohol dehydrogenase	adh	-0.45	1.32	36.05	18	57.7
Q2FY41	Elongation factor P	efp	-0.45	1.22	20.55	7	36.8
Q2FYV3	Threonine synthase	SAOUHSC_01321	-0.45	1.17	37.87	8	27.2
Q2FYL0	Phosphotransferase system enzyme IIA, putative	SAOUHSC_01430	-0.46	1.06	17.96	8	63.3
Q2G031	Phosphoglycerate kinase	pgk	-0.46	1.25	42.60	14	32.1
Q2FZU0	Glucose-6-phosphate isomerase	pgi	-0.46	0.47	49.82	13	33.2
Q2G0Q3	Lysine--tRNA ligase	lysS	-0.46	1.65	56.72	16	35.6
Q2FV17	Fructose-bisphosphate aldolase class 1	fda	-0.46	0.91	33.05	21	65.5
Q2FZG4	Pyruvate dehydrogenase complex, E1 component, alpha subunit, putative	SAOUHSC_01040	-0.46	1.80	41.38	9	34.6
Q2G294	Acetyl-CoA synthetase, putative	SAOUHSC_01846	-0.46	1.86	64.36	11	23.4
Q2FZ29	ATP-dependent protease subunit HslV	hslV	-0.46	0.95	19.57	2	15.5
Q2G0J0	Phosphate acetyltransferase	SAOUHSC_00574	-0.46	1.52	34.95	13	56.4
Q2G280	Putative uncharacterized protein	SAOUHSC_01999	-0.47	1.00	17.26	4	26.5
Q2FVD5	Uncharacterized oxidoreductase	SAOUHSC_02778	-0.47	0.78	24.60	6	43.7
Q2FZX0	Protein NagD homolog	nagD	-0.47	1.39	27.95	6	25.9
Q2G0R1	Hypoxanthine phosphoribosyltransferase	SAOUHSC_00485	-0.47	0.72	20.15	4	20.1
Q2FWX1	Putative uncharacterized protein	SAOUHSC_02150	-0.47	1.31	21.92	9	49.7
Q53727	ATP-dependent DNA helicase PcrA	pcrA	-0.47	1.07	84.07	12	20.4
Q2FZP9	UPF0477 protein	SAOUHSC_00951	-0.48	1.45	19.33	11	56.8
Q2G241	Glutamate--tRNA ligase	gltX	-0.48	2.34	56.29	16	38.6
Q2FZU6	Ornithine aminotransferase	rocD	-0.48	1.94	43.42	9	29
Q2G1B9;Q2G1C4	Putative uncharacterized protein	SAOUHSC_00226	-0.48	1.86	38.45	6	16.4
Q2FVT5	Urocanate hydratase	hutU	-0.48	1.61	60.63	12	26.8
Q2FZL5	Enoyl-CoA hydratase/isomerase family protein, putative	SAOUHSC_00985	-0.48	1.40	30.43	10	48
Q2G1J0	Putative aldehyde dehydrogenase AldA	aldA	-0.48	1.00	53.66	20	54.7
Q2FX12	Low molecular weight protein-tyrosine-phosphatase PtpA	ptpA	-0.49	1.39	17.49	2	16.9
Q2FYT8	Transketolase	SAOUHSC_01337	-0.49	1.18	68.36	25	46.1
Q2G2M3	Putative uncharacterized protein	SAOUHSC_00513	-0.49	0.63	27.21	7	29.4
Q2G220	Putative uncharacterized protein	SAOUHSC_02980	-0.49	2.27	20.73	4	40.9
Q2FZT4	Uncharacterized protein	SAOUHSC_00906	-0.49	1.75	33.11	11	55.7
Q2FW91	Arginase	SAOUHSC_02409	-0.49	2.08	33.26	10	29.1
Q2FWE0	Peptide chain release factor 1	prfA	-0.49	1.57	40.35	10	32.7
Q2FWX8	Uncharacterized protein	SAOUHSC_02143	-0.49	3.19	38.55	5	16.1
POCOV7	Phosphoglucosamine mutase	glmM	-0.49	1.15	49.27	14	35.3
Q2FWZ0	Aspartyl/glutamyl-tRNA(Asn/Gln) amidotransferase subunit B	gatB	-0.49	2.19	53.66	25	50.5
Q2FY89	Helix-turn-helix domain protein	SAOUHSC_01575	-0.49	2.62	27.02	5	24.9
Q2FYS4	DNA topoisomerase 4 subunit A	parC	-0.50	1.67	91.00	16	22.6
Q2FX94	Fumarate hydratase class II	fumC	-0.50	2.24	51.11	11	27.8
Q2G0S5	Putative septation protein SpoVG	spoVG	-0.50	1.33	11.28	4	48
Q2FVT8	Putative uncharacterized protein	SAOUHSC_02604	-0.50	0.57	31.73	3	13
Q2FXE8	Putative uncharacterized protein	SAOUHSC_01901	-0.50	1.08	25.71	11	51.9
Q2G235	Nicotinate phosphoribosyltransferase	SAOUHSC_02133	-0.50	2.24	54.80	14	34.6
Q2FV21	3-methyl-2-oxobutanoate hydroxymethyltransferase	panB	-0.50	0.99	29.26	11	53.3
Q2FYU7	Catalase	katA	-0.50	2.00	58.38	15	33.9
Q2FVY0	Molybdopterin biosynthesis protein moeA, putative	SAOUHSC_02542	-0.50	1.20	45.02	9	31.3
Q2FXK7	GAF domain protein	SAOUHSC_01828	-0.50	1.59	17.11	4	19.5
Q2FXQ3	Putative uncharacterized protein	SAOUHSC_01782	-0.50	0.21	22.95	5	26.7

8 - Supporting Information

Q2FZY7	ABC transporter, ATP-binding protein, putative	SAOUHSC_00847	-0.51	1.42	28.28	6	30.4
Q2FXR8	Valine--tRNA ligase	valS	-0.52	1.38	101.72	19	24.5
Q2FZD2	Thioredoxin	trxA	-0.52	0.86	11.44	5	52.9
Q2FXW7	Transcription elongation factor GreA	greA	-0.52	1.15	17.74	7	69.6
Q2FUR8	Putative uncharacterized protein	SAOUHSC_03034	-0.52	1.29	30.44	3	11.4
Q2FXH9	Putative dipeptidase	SAOUHSC_01868	-0.52	1.41	52.82	13	31.6
Q2FXH2	Leucine--tRNA ligase	leuS	-0.52	1.49	91.79	12	22.9
Q2G0Y7	Inosine-5'-monophosphate dehydrogenase	guaB	-0.52	1.36	52.85	26	52.3
Q2G0L2	Putative uncharacterized protein	SAOUHSC_00548	-0.52	0.62	58.42	3	6.5
Q2FZP6	UDP-N-acetylmuramoyl-L-alanyl-D-glutamate--L-lysine ligase	murE	-0.52	0.66	54.10	12	25.4
Q2FVX0	Putative uncharacterized protein	SAOUHSC_02553	-0.53	2.80	35.36	4	16.3
Q2FWA2	Putative uncharacterized protein	SAOUHSC_02396	-0.53	1.12	32.30	4	18.6
Q2FXQ4	Putative uncharacterized protein	SAOUHSC_01781	-0.53	0.80	36.43	4	15.2
Q2FW14	50S ribosomal protein L29	rpmC	-0.53	1.13	8.09	5	55.1
Q2FWD0	Probable DNA-directed RNA polymerase subunit delta	rpoE	-0.53	1.03	20.88	4	30.1
Q2G1H0	Indolepyruvate decarboxylase, putative	SAOUHSC_00153	-0.53	1.10	60.54	6	14.1
Q2FVT6	Imidazolonepropionase	hutI	-0.53	1.36	45.04	12	36.2
Q2FUS9	UPF0312 protein	SAOUHSC_03022	-0.53	0.71	18.66	2	14.6
Q2FZU7	FMN oxidoreductase, putative	SAOUHSC_00893	-0.54	1.75	42.11	7	27.7
Q2G0M8	Putative uncharacterized protein	SAOUHSC_00532	-0.54	2.57	42.89	12	43.3
Q2G029	2,3-bisphosphoglycerate-independent phosphoglycerate mutase	gpml	-0.54	1.30	56.42	8	20.6
Q2G028	Enolase	eno	-0.54	1.36	47.12	19	55.8
Q2G0K7	3-hexulose-6-phosphate synthase	SAOUHSC_00553	-0.54	1.61	22.44	5	41
P0A0J3	Superoxide dismutase [Mn] 1	sodA	-0.54	0.92	22.71	3	22.6
Q2G112	Single-stranded DNA-binding protein	SAOUHSC_00349	-0.54	1.54	18.54	4	47.9
Q2G1U3	Oligoendopeptidase F	SAOUHSC_00937	-0.54	1.57	69.82	15	27.2
Q2G0M2	Haloacid dehalogenase-like hydrolase, putative	SAOUHSC_00538	-0.55	0.73	24.99	4	22.5
Q2G000	Thioredoxin, putative	SAOUHSC_00834	-0.55	0.51	12.14	2	24.5
Q2G030	Triosephosphate isomerase	tpiA	-0.55	1.30	27.29	11	50.2
Q2FYJ2	Alanine dehydrogenase 1	ald1	-0.55	1.71	40.22	10	30.4
Q2FVW4	Putative 2-hydroxyacid dehydrogenase	SAOUHSC_02577	-0.55	1.34	34.67	14	59.6
Q2FY34	Probable glycine dehydrogenase (decarboxylating) subunit 1	gcvPA	-0.56	2.68	49.72	10	26.6
Q2FWD1	CTP synthase	pyrG	-0.56	1.67	59.98	13	27.6
Q2G1X1	Putative uncharacterized protein	SAOUHSC_01120	-0.56	1.62	8.90	2	40.3
P48860	50S ribosomal protein L7/L12	rplL	-0.56	1.54	12.71	8	74.6
Q2FW20	30S ribosomal protein S8	rpsH	-0.56	1.88	14.83	8	57.6
Q2G0J1	Putative heme-dependent peroxidase	SAOUHSC_00573	-0.57	1.18	29.39	3	14.4
Q2G1E4	Putative uncharacterized protein	SAOUHSC_00181	-0.57	1.60	36.67	3	10.9
Q2FY52	2-oxoisovalerate dehydrogenase, E1 component, alpha subunit, putative	SAOUHSC_01613	-0.57	1.38	36.23	4	19.7
Q2FY40	Proline dipeptidase, putative	SAOUHSC_01626	-0.57	1.92	39.34	9	27.8
Q2G1S3	Adenylosuccinate synthetase	purA	-0.57	1.97	47.58	9	31.4
Q2FY59	Peptidase T, putative	SAOUHSC_01606	-0.57	2.24	40.26	6	22.8
Q9ZAH5	Alanine racemase 1	alr1	-0.57	0.79	42.82	3	7.9
Q2G0T4	Nucleoid-associated protein	SAOUHSC_00444	-0.57	1.57	11.60	2	26.7
Q2FZ16	Bifunctional purine biosynthesis protein PurH	purH	-0.58	1.20	54.35	8	16.5
Q2FXR3	Delta-aminolevulinic acid dehydratase	hemB	-0.58	2.65	36.58	7	26.9
Q2FXP3	Transcriptional repressor NrdR	nrdR	-0.58	0.76	18.20	2	17.3
Q2FWC3	S-ribosylhomocysteine lyase	luxS	-0.59	0.96	17.51	4	27.6
Q2FXV4	Putative uncharacterized protein	SAOUHSC_01727	-0.59	0.97	42.48	4	13.7
Q2FXQ8	Probable GTP-binding protein EngB	engB	-0.59	0.52	22.69	4	30.6
Q2G227	Phosphopentomutase	deoB	-0.60	1.45	43.80	8	22.2
Q2FZ10	Putative competence-damage inducible protein	cinA	-0.60	0.73	43.27	5	14.6
Q2FWF5	3-hydroxyacyl-[acyl-carrier-protein] dehydratase FabZ	fabZ	-0.60	1.48	16.08	3	19.2
Q2FWL5	ABC transporter, ATP-binding protein, putative	SAOUHSC_02274	-0.60	1.99	74.46	5	10.6
Q2G1A6	Ribokinase, putative	SAOUHSC_00239	-0.60	1.30	32.45	5	22
Q2FYQ2	Putative uncharacterized protein	SAOUHSC_01383	-0.61	2.57	69.28	8	20
Q2FYJ0	Putative uncharacterized protein	SAOUHSC_01455	-0.61	1.23	133.11	12	13
Q2FY66	Glucose-6-phosphate 1-dehydrogenase	zwf	-0.61	1.42	56.97	10	21.9
Q2FUT8	Histidinol dehydrogenase	hisD	-0.61	0.85	46.18	2	6
Q2FWH3	D-alanine--D-alanine ligase	ddl	-0.62	1.43	40.23	8	32.3
Q2FWM1	Sucrose-6-phosphate dehydrogenase, putative	SAOUHSC_02268	-0.62	1.07	57.93	6	15.2
Q2FXZ1	Protein GrpE	grpE	-0.62	0.75	24.01	7	52.9
Q2G2F0	Putative uncharacterized protein	SAOUHSC_01968	-0.63	1.07	15.95	6	39.3
Q2FWB7	Putative uncharacterized protein	SAOUHSC_02381	-0.63	0.77	16.69	5	66

Q2FXU0	Adenine phosphoribosyltransferase	apt	-0.63	0.86	19.12	4	35.5
Q2FYM1	2-oxoglutarate dehydrogenase E1 component	odhA	-0.63	1.90	105.34	14	21.2
Q2FVN3	HTH-type transcriptional regulator SarZ	sarZ	-0.63	0.75	17.44	4	29.7
Q2FZU9	Putative peptidyl-prolyl cis-trans isomerase	SAOUHSC_00891	-0.65	1.39	21.62	6	44.2
Q2G0L1	GTP cyclohydrolase FolE2	folE2	-0.65	1.54	33.48	6	25.7
Q2FVC2	Pyrophosphohydrolase, putative	SAOUHSC_02791	-0.67	1.20	14.89	2	16.9
Q2G0Q0	Glutamine amidotransferase subunit PdxT	pdxT	-0.69	1.57	20.63	3	16.1
Q2FZD8	Phenylalanine--tRNA ligase beta subunit	pheT	-0.69	1.10	88.92	12	17.8
Q2FX95	Ribosomal large subunit pseudouridine synthase, RluD subfamily, putative	SAOUHSC_01982	-0.70	0.61	31.44	4	17.2
Q2G0Q7	Dihydropteroate synthase	SAOUHSC_00489	-0.70	0.96	29.52	3	15.4
Q2FY42	Acetyl-CoA carboxylase, biotin carboxyl carrier protein	SAOUHSC_01624	-0.70	2.17	17.12	5	46.8
Q2G189	Putative uncharacterized protein	SAOUHSC_00257	-0.70	0.84	11.04	5	70.1
Q2G091	ABC transporter, ATP-binding protein	SAOUHSC_00729	-0.71	0.99	72.60	7	14.5
Q2FWD8	50S ribosomal protein L31 type B	rpmE2	-0.71	1.24	9.72	2	31
Q2G1G6	N-acetylmuramic acid 6-phosphate etherase	murQ	-0.72	0.44	32.38	4	13.4
Q2FXU8	Putative uncharacterized protein	SAOUHSC_01734	-0.73	1.15	46.28	7	20.5
Q2FV34	Putative uncharacterized protein	SAOUHSC_02905	-0.74	2.04	11.58	2	25.5
Q2G236	NH(3)-dependent NAD(+) synthetase	nadE	-0.74	1.04	30.70	9	41.4
Q2FZA1	Uncharacterized N-acetyltransferase	SAOUHSC_01138	-0.75	0.92	17.00	2	12.3
Q2G0S3	Bifunctional protein GlmU	glmU	-0.76	1.07	48.50	5	14.2
P0A086	Peptide methionine sulfoxide reductase MsrA 2	msrA2	-0.77	1.07	20.59	4	19.2
Q2FVM1	Nitrate reductase, alpha subunit	SAOUHSC_02681	-0.78	1.65	139.83	23	22.1
Q2FXI5	Putative uncharacterized protein	SAOUHSC_01861	-0.81	0.59	39.78	5	13.1
Q2G1U1	Fibronectin-binding protein A-related	SAOUHSC_01175	-0.82	1.02	65.78	14	29.4
Q2FVR9	Isopentenyl-diphosphate delta-isomerase	fni	-0.90	2.19	38.77	5	12
Q2G2C1	Pyruvate carboxylase	SAOUHSC_01064	-0.91	3.81	128.55	41	46.2
Q2FWI8	mRNA interferase MazF	mazF	-0.93	0.51	13.44	4	20.8
Q2FZ73	Carbamoyl-phosphate synthase small chain	carA	-1.19	0.86	40.39	4	13.1
Q2G270	Putative uncharacterized protein	SAOUHSC_02568	-1.28	1.56	12.53	2	23.1
Q2FVG3	Putative uncharacterized protein	SAOUHSC_02751	-1.34	0.78	51.97	5	10.2

Table S8: Target identification (50 μ M SFN-P/500 μ M SFN+50 μ M SFN-P) in the soluble fraction. PR, log₂ protein ratio; PV, -log₁₀ p-value (t-test); MW, Molecular weight (kDa); UP, unique peptides; USC, Unique sequence coverage (%).

Uniprot ID	Protein name	Gene name	PR	LP	MW	UP	USC
Q2FZT7	Signal peptidase IB, putative	SAOUHSC_00903	3.96	2.32	17.60	5	35.5
Q2FWA8	Lytic regulatory protein, putative	SAOUHSC_02390	3.10	2.38	40.67	5	11.8
Q2FVS2	Putative uncharacterized protein	SAOUHSC_02620	2.33	2.34	24.96	2	10.2
Q2FZV7	NADH dehydrogenase-like protein	SAOUHSC_00878	2.17	2.81	44.10	11	33.8
Q2FVZ5	Putative uncharacterized protein	SAOUHSC_02525	2.11	1.76	114.70	10	13.3
Q2FVN6	Putative uncharacterized protein	SAOUHSC_02666	2.09	1.64	13.34	3	26.3
Q2FZG5	Putative uncharacterized protein	SAOUHSC_01039	1.84	1.06	23.88	3	18.3
Q2FZJ9	Probable quinol oxidase subunit 2	SAOUHSC_01002	1.83	1.69	41.78	16	35.5
Q2G2D8	ABC transporter, substrate-binding protein, putative	SAOUHSC_00634	1.77	2.06	35.07	11	27.9
Q2G1G5	PTS system EIIBC component	SAOUHSC_00158	1.63	2.30	50.66	4	8.9
Q2FYZ4	Aerobic glycerol-3-phosphate dehydrogenase	SAOUHSC_01278	1.34	1.59	62.39	10	21
Q2G193	Putative uncharacterized protein	SAOUHSC_00253	1.30	0.72	57.92	10	18.5
Q2FVV9	Putative formate dehydrogenase	SAOUHSC_02582	1.24	1.48	111.24	7	8.3
P60430	50S ribosomal protein L2	SAOUHSC_02509	1.00	1.93	30.16	8	31.4
Q2FW66	Alkaline shock protein 23	SAOUHSC_02441	0.81	1.09	19.19	5	30.2
P0A0F4	50S ribosomal protein L11	SAOUHSC_00518	0.58	1.40	14.87	5	29.3
Q2FXL6	Putative universal stress protein	SAOUHSC_01819	0.47	0.90	18.48	9	38
Q2FV16	Probable malate:quinone oxidoreductase	SAOUHSC_02927	0.41	0.52	56.00	11	24.1
Q2FYY6	Glutamine synthetase	SAOUHSC_01287	0.41	0.17	50.84	8	20.4
Q2FXA0	UPF0342 protein	SAOUHSC_01977	0.36	1.12	13.31	5	43.9
Q2G1C0	2-C-methyl-D-erythritol 4-phosphate cytidyllyltransferase	SAOUHSC_00225	0.35	0.32	26.66	3	14.3
Q2FZ51	Acyl carrier protein	SAOUHSC_01201	0.34	0.56	8.55	4	39
Q2G1Y5	L-lactate dehydrogenase 2	SAOUHSC_02922	0.33	0.41	34.42	11	41.4
Q2FZ53	3-oxoacyl-(Acyl-carrier-protein) reductase, putative	SAOUHSC_01199	0.26	0.65	25.89	16	58.2
Q2FV52	Probable transglycosylase IsaA	SAOUHSC_02887	0.23	0.60	24.20	2	15
Q2FZ36	Succinyl-CoA ligase [ADP-forming] subunit alpha	SAOUHSC_01218	0.18	1.39	31.54	14	51.7
Q2FZ37	Succinyl-CoA ligase [ADP-forming] subunit beta	SAOUHSC_01216	0.13	0.51	42.06	14	33.5
Q2G248	Putative uncharacterized protein	SAOUHSC_01852	0.12	0.35	40.62	9	29.8

8 - Supporting Information

Q2FV67	1-pyrroline-5-carboxylate dehydrogenase	SAOUHSC_02869	0.11	0.61	56.87	13	27.4
Q2G1C8	Putative uncharacterized protein	SAOUHSC_00197	0.10	0.07	44.73	8	19.4
Q2G2A3	Dihydrolipoyl dehydrogenase	SAOUHSC_01043	0.06	0.26	49.48	19	37.4
Q2G115	Ribosome-binding ATPase YchF	SAOUHSC_00346	0.06	0.10	40.59	5	14.8
Q2G227	Phosphopentomutase	SAOUHSC_00101	-0.01	0.01	43.80	4	14.3
Q2FXI0	D-alanine aminotransferase	SAOUHSC_01867	-0.01	0.02	31.89	4	24.1
Q2G1W2	Phosphoenolpyruvate carboxykinase [ATP]	SAOUHSC_01910	-0.02	0.10	59.38	12	25.8
Q2FZH5	Phosphoenolpyruvate-protein phosphotransferase	SAOUHSC_01029	-0.04	0.13	63.22	7	13.1
Q2G1K9	Aldehyde-alcohol dehydrogenase	SAOUHSC_00113	-0.06	0.29	94.94	21	24.3
Q2FXQ1	50S ribosomal protein L20	SAOUHSC_01784	-0.07	0.04	13.69	3	22.9
Q2G1C9	Putative uncharacterized protein	SAOUHSC_00196	-0.09	0.17	84.61	20	29
O05204	Alkyl hydroperoxide reductase subunit F	SAOUHSC_00364	-0.10	1.89	54.72	5	11.4
Q2FXP7	Threonine--tRNA ligase	SAOUHSC_01788	-0.10	0.29	74.49	22	25.6
Q2FYZ5	Glycerol kinase	SAOUHSC_01276	-0.11	0.52	55.63	10	24.9
Q2FY60	6-phosphogluconate dehydrogenase, decarboxylating	SAOUHSC_01605	-0.12	0.48	51.80	9	17.3
Q2G028	Enolase	SAOUHSC_00799	-0.16	0.55	47.12	12	38.9
Q2FXM9	Pyruvate kinase	SAOUHSC_01806	-0.18	1.00	63.10	15	27.9
Q2FYU7	Catalase	SAOUHSC_01327	-0.18	1.12	58.38	15	30.1
Q2G1J0	Putative aldehyde dehydrogenase AldA	SAOUHSC_00132	-0.21	0.63	53.66	11	25.7
Q2G0N5	DNA-directed RNA polymerase subunit beta'	SAOUHSC_00525	-0.21	1.84	135.41	27	24.6
Q2FWE8	ATP synthase subunit alpha	SAOUHSC_02345	-0.21	0.16	54.58	5	12.9
Q2G0P5	ATP-dependent Clp protease ATP-binding subunit ClpC	SAOUHSC_00505	-0.21	0.86	91.04	15	24
Q2FZU0	Glucose-6-phosphate isomerase	SAOUHSC_00900	-0.23	0.61	49.82	14	32.1
Q2FY71	Putative uncharacterized protein	SAOUHSC_01594	-0.23	0.57	33.51	2	6.3
Q2G0G1	Alcohol dehydrogenase	SAOUHSC_00608	-0.27	0.51	36.05	18	39.6
Q2FWD3	Putative uncharacterized protein	SAOUHSC_02366	-0.27	1.29	30.84	14	48.6
Q2G0Q1	Pyridoxal biosynthesis lyase PdxS	SAOUHSC_00499	-0.27	0.78	31.99	9	36.3
Q2FWB8	Purine nucleoside phosphorylase DeoD-type	SAOUHSC_02380	-0.27	0.33	25.91	4	10.6
Q2FY08	Glycine--tRNA ligase	SAOUHSC_01666	-0.28	2.15	53.62	8	14.5
Q2FZ74	Dihydroorotase	SAOUHSC_01168	-0.28	2.52	46.37	7	18.2
Q2FYT8	Transketolase	SAOUHSC_01337	-0.29	1.12	68.36	19	38.4
Q2FXZ2	Chaperone protein DnaK	SAOUHSC_01683	-0.30	1.39	66.36	17	23.9
Q2G030	Triosephosphate isomerase	SAOUHSC_00797	-0.32	0.66	27.29	11	38.3
Q2FZU6	Ornithine aminotransferase	SAOUHSC_00894	-0.32	1.07	43.42	8	30.1
Q2G218	L-lactate dehydrogenase 1	SAOUHSC_00206	-0.32	1.03	34.58	10	29.7
Q2FXR8	Valine--tRNA ligase	SAOUHSC_01767	-0.32	1.40	101.72	11	13.4
Q2FY66	Glucose-6-phosphate 1-dehydrogenase	SAOUHSC_01599	-0.34	0.23	56.97	6	11.5
Q2FY35	Probable glycine dehydrogenase (decarboxylating) subunit 2	SAOUHSC_01632	-0.34	0.68	54.78	4	12.9
Q2FZ82	Isoleucine--tRNA ligase	SAOUHSC_01159	-0.35	1.88	104.88	7	7.7
Q2FZU5	Glutamate dehydrogenase	SAOUHSC_00895	-0.35	0.89	45.76	9	27.1
Q2FX94	Fumarate hydratase class II	SAOUHSC_01983	-0.36	0.31	51.11	4	6.5
Q2G0N0	Elongation factor Tu	SAOUHSC_00530	-0.36	1.46	43.10	20	61.7
P47768	DNA-directed RNA polymerase subunit beta	SAOUHSC_00524	-0.37	1.06	133.22	16	14.9
Q2G0M8	Putative uncharacterized protein	SAOUHSC_00532	-0.37	0.80	42.89	16	51.6
Q2G0N1	Elongation factor G	SAOUHSC_00529	-0.38	1.33	76.61	21	32.5
Q2G0Q8	Cysteine synthase	SAOUHSC_00488	-0.41	1.12	32.98	8	37.7
Q2FWD1	CTP synthase	SAOUHSC_02368	-0.42	0.78	59.98	6	10.3
Q2FXP2	Glyceraldehyde-3-phosphate dehydrogenase	SAOUHSC_01794	-0.44	0.57	36.98	5	12
Q2FV17	Fructose-bisphosphate aldolase class 1	SAOUHSC_02926	-0.44	0.64	33.05	13	41.9
Q2G1M1	3-ketoacyl-acyl carrier protein reductase, putative	SAOUHSC_00086	-0.45	1.86	27.22	3	16.7
Q2FZ75	Aspartate carbamoyltransferase	SAOUHSC_01166	-0.46	0.97	33.26	3	10.6
Q2G296	Formate--tetrahydrofolate ligase	SAOUHSC_01845	-0.46	1.07	59.86	13	28.8
Q2G1D8	Formate acetyltransferase	SAOUHSC_00187	-0.48	1.68	84.86	31	36.4
Q2FYF9	30S ribosomal protein S1, putative	SAOUHSC_01493	-0.52	4.04	43.29	3	11.5
Q2FXX0	Acetyl-CoA carboxylase, biotin carboxyl carrier protein, putative	SAOUHSC_01710	-0.53	0.62	16.79	7	40.3
Q2FZ23	Elongation factor Ts	SAOUHSC_01234	-0.54	1.02	32.49	8	25.3
Q2FY42	Acetyl-CoA carboxylase, biotin carboxyl carrier protein	SAOUHSC_01624	-0.55	1.95	17.12	6	34.4
Q2G2A5	Pyruvate dehydrogenase complex, E1 component, pyruvate dehydrogenase beta subunit, putative	SAOUHSC_01041	-0.55	1.22	35.25	9	30.5
Q2G0Y7	Inosine-5'-monophosphate dehydrogenase	SAOUHSC_00374	-0.55	1.49	52.85	16	35.7
Q2FYS9	Aconitate hydratase 1	SAOUHSC_01347	-0.56	2.69	98.97	14	16.2
Q2FXL5	Acetate kinase	SAOUHSC_01820	-0.57	1.44	44.04	11	33.5
P0A0B7	Alkyl hydroperoxide reductase subunit C	SAOUHSC_00365	-0.58	1.26	20.98	10	55.6
Q2G1H0	Indolepyruvate decarboxylase, putative	SAOUHSC_00153	-0.59	1.62	60.54	7	8.1
Q2FZG4	Pyruvate dehydrogenase complex, E1 component, alpha subunit, putative	SAOUHSC_01040	-0.60	1.05	41.38	7	26.2

Q2FWZ8	Bacterial non-heme ferritin	SAOUHSC_02108	-0.62	1.43	19.59	4	21.1
Q2FVT5	Urocanate hydratase	SAOUHSC_02607	-0.67	2.18	60.63	7	11.4
Q2FWA0	Glutamine--fructose-6-phosphate aminotransferase [isomerizing]	SAOUHSC_02399	-0.68	1.90	65.85	14	29
Q2FWE5	Serine hydroxymethyltransferase	SAOUHSC_02354	-0.68	1.22	45.17	9	21.6
Q2G032	Glyceraldehyde-3-phosphate dehydrogenase	SAOUHSC_00795	-0.70	1.46	36.28	8	21.7
Q2FXH2	Leucine--tRNA ligase	SAOUHSC_01875	-0.77	1.66	91.79	12	13.9
Q2G1U3	Oligoendopeptidase F	SAOUHSC_00937	-0.77	1.94	69.82	12	22.8
Q2FWY9	Glutamyl-tRNA(Gln) amidotransferase subunit A	SAOUHSC_02117	-0.78	1.42	52.82	12	22.1
Q2FWM1	Sucrose-6-phosphate dehydrogenase, putative	SAOUHSC_02268	-0.79	1.21	57.93	4	8.7
Q2G2C1	Pyruvate carboxylase	SAOUHSC_01064	-0.79	2.03	128.55	54	48.1
Q2FZK7	Bifunctional autolysin	SAOUHSC_00994	-0.80	1.16	137.38	9	10.2
Q2FXR4	Glutamate-1-semialdehyde 2,1-aminomutase 1	SAOUHSC_01771	-0.81	3.25	46.39	12	33.4
Q2G1E6	Putative uncharacterized protein	SAOUHSC_00179	-0.86	2.10	39.18	3	13.4
Q2FYM1	2-oxoglutarate dehydrogenase E1 component	SAOUHSC_01418	-0.86	2.24	105.34	25	30.3
Q2FZY9;Q2FXV1	UPF0337 protein	SAOUHSC_00845	-0.97	0.58	7.02	4	53.1
Q2FVB2	Fructose-1,6-bisphosphatase class 3	SAOUHSC_02822	-1.03	1.61	76.17	6	9.9

Table S9: Target identification (50 μ M SFN-P/500 μ M SFN+50 μ M SFN-P) in the soluble fraction. PR, \log_2 protein ratio; PV, $-\log_{10}$ p -value (t -test); MW, Molecular weight (kDa); UP, unique peptides; USC, Unique sequence coverage (%).

Uniprot ID	Protein name	Gene name	PR	LP	MW	UP	USC
Q2FZT7	Signal peptidase IB, putative	SAOUHSC_00903	3.96	2.22	17.60	7	51.6
Q2G117	Putative uncharacterized protein	SAOUHSC_00344	3.75	2.38	32.19	4	18.1
Q2G2N2	Putative uncharacterized protein	SAOUHSC_01358	3.67	1.51	45.07	4	11.4
Q2G2W2	Putative uncharacterized protein	SAOUHSC_02628	3.42	2.33	24.29	3	16
Q2FWD0	Probable DNA-directed RNA polymerase subunit delta	rpoE	3.42	1.71	20.88	4	30.1
Q2G1C5	Membrane protein, putative	SAOUHSC_00200	3.29	2.46	42.18	2	6.8
Q2G193	Putative uncharacterized protein	SAOUHSC_00253	3.10	2.52	57.92	15	34.3
Q2FVZ5	Putative uncharacterized protein	SAOUHSC_02525	2.96	1.83	114.70	23	27.4
Q2FZQ2	Putative uncharacterized protein	SAOUHSC_00948	2.88	1.49	40.15	4	8.6
Q2FYG5	Menquinone biosynthesis methyltransferase, putative	SAOUHSC_01487	2.81	2.17	22.37	4	27
Q2FVS2	Putative uncharacterized protein	SAOUHSC_02620	2.80	2.10	24.96	3	18.6
Q2G1P4	Putative uncharacterized protein	SAOUHSC_00060	2.77	1.47	60.65	7	17.5
Q2FWY7	Sodium/proline symporter	putP	2.63	1.45	55.98	2	5.1
Q2G245	Putative uncharacterized protein	SAOUHSC_01854	2.50	3.34	55.09	30	50.1
O08387	Protein translocase subunit SecY	secY	2.45	1.40	47.15	4	10
Q2G0D7	ABC transporter permease, putative	SAOUHSC_00668	2.43	2.30	71.73	5	7.9
Q2FXT8	Protein-export membrane protein SecDF	SAOUHSC_01746	2.41	2.50	82.05	17	25.4
Q2FVS4	Putative uncharacterized protein	SAOUHSC_02618	2.33	2.40	45.93	3	10.5
Q2FV70	Putative uncharacterized protein	SAOUHSC_02866	2.31	1.66	90.41	15	20.6
Q93Q23	Monofunctional glycosyltransferase	mgt	2.26	1.60	31.46	3	19.3
Q2G2N5	Sodium:alanine symporter family protein, putative	SAOUHSC_01354	2.17	1.66	52.14	4	11.3
Q2G2V9	Putative uncharacterized protein	SAOUHSC_02006	2.11	1.80	37.08	3	9.5
Q2FY00	Putative uncharacterized protein	SAOUHSC_01675	2.07	2.96	27.26	3	9.9
Q2G044	Prolipoprotein diacylglycerol transferase	lgt	2.05	1.89	31.57	2	3.6
Q2FVN6	Putative uncharacterized protein	SAOUHSC_02666	1.98	1.87	13.34	3	23.7
Q2FVT1	Lysostaphin resistance protein A	lyrA	1.97	2.51	46.79	3	14.3
Q2FW64	Putative uncharacterized protein	SAOUHSC_02443	1.89	2.13	20.80	4	29.8
Q2G1M2	Putative uncharacterized protein	SAOUHSC_00085	1.88	1.68	22.98	4	19.2
Q2FY26	Putative uncharacterized protein	SAOUHSC_01275	1.85	1.56	28.12	3	11
Q9KJN4	Response regulator ArlR	arlR	1.82	0.45	25.50	2	11.9
Q2FWG4	Membrane protein insertase YidC	yidC	1.81	2.01	33.58	4	12.8
Q2FWY4	Sodium-dependent dicarboxylate transporter SdcS	sdcS	1.78	2.05	57.17	2	5.2
Q2FVI6	Putative uncharacterized protein	SAOUHSC_02724	1.71	1.75	25.80	5	21.5
Q2G1Z5	Putative uncharacterized protein	SAOUHSC_01239	1.70	2.16	44.28	3	9.4
Q2FY80	Sensor protein SrrB	srrB	1.69	2.05	66.08	13	26.2
Q2FZK3	Protein FmtA	fmtA	1.67	1.54	46.07	4	10.1
Q2FYT7	UPF0154 protein	SAOUHSC_01338	1.66	1.13	11.02	6	36.8
Q2FZQ5	Magnesium transporter	SAOUHSC_00945	1.62	1.52	51.44	4	9.8
Q2G1F2	FMN-dependent NADH-azoreductase	azoR	1.54	1.49	23.35	4	22.1
Q2G247	UPF0478 protein	SAOUHSC_01855	1.52	1.80	18.00	12	67.5
Q9RFJ6	HTH-type transcriptional regulator rot	rot	1.51	3.39	19.37	3	22.3
Q2FUX2	Putative uncharacterized protein	SAOUHSC_02973	1.50	0.89	16.36	2	34.9

8 - Supporting Information

Q2FZJ9	Probable quinol oxidase subunit 2	qoxA	1.48	2.50	41.78	16	36.9
Q2G1E0	Uncharacterized sensor-like histidine kinase	SAOUHSC_00185	1.48	1.20	61.05	5	10.2
Q2FY84	Phi PVL ORF 30-like protein	SAOUHSC_01580	1.46	1.17	23.83	3	18.1
Q2FWM5	Accessory gene regulator protein C	SAOUHSC_02264	1.45	1.28	47.98	2	4.1
Q2FWX6	Putative uncharacterized protein	SAOUHSC_02145	1.42	1.12	6.56	2	19.3
Q2FZ51	Acyl carrier protein	acpP	1.41	1.11	8.55	4	41.6
Q2FZW4	D-alanine--poly(phosphoribitol) ligase subunit 2	dltC	1.40	0.99	9.06	2	33.3
Q2G2G6	Putative uncharacterized protein	SAOUHSC_01050	1.39	1.45	40.06	3	11.2
Q2G2E0	Putative uncharacterized protein	SAOUHSC_00633	1.37	1.57	74.93	4	9.1
Q2G242	Putative uncharacterized protein	SAOUHSC_00508	1.35	1.68	38.89	3	8.5
Q2G0P9	Putative uncharacterized protein	SAOUHSC_00501	1.31	1.16	43.80	3	5.4
Q7BHL7	Regulatory protein MsrR	msrR	1.30	0.90	36.97	6	22.6
Q2FXG3	Putative uncharacterized protein	SAOUHSC_01884	1.26	1.32	38.03	9	39.9
Q2FV29	Putative uncharacterized protein	SAOUHSC_02910	1.25	1.33	10.71	3	31.9
Q2FXS6	Cell shape-determining protein MreC	SAOUHSC_01759	1.22	1.87	31.01	10	43.6
Q2FV8	Transcriptional regulator, putative	SAOUHSC_02583	1.22	1.96	33.80	7	26.4
Q2G0Z4	Putative uncharacterized protein	SAOUHSC_00367	1.20	1.31	49.41	6	16
Q2G2T3	50S ribosomal protein L9	rplI	1.20	1.56	16.64	7	43.3
Q2FV90	Putative uncharacterized protein	SAOUHSC_02844	1.18	1.72	36.85	9	33.2
Q2G2X6	Penicillin-binding protein 4, putative	SAOUHSC_00646	1.16	0.87	48.26	4	12.1
Q2G2M2	Phosphatidylglycerol lysyltransferase	mprF	1.14	1.11	96.87	6	6.4
Q2FZA8	Putative uncharacterized protein	SAOUHSC_01130	1.14	1.41	54.07	4	9.1
Q2FXW4	Putative uncharacterized protein	SAOUHSC_01717	1.12	0.30	35.96	4	15.6
Q2FXU0	Adenine phosphoribosyltransferase	apt	1.10	0.47	19.12	4	35.5
Q2G019	Putative uncharacterized protein	SAOUHSC_00808	1.08	3.29	28.42	9	33.1
Q2FV54	O-acetyltransferase OatA	oatA	1.07	1.71	69.10	6	9.8
Q2FUU5	Lipase 1	lipA	1.03	1.05	76.68	10	18.4
Q2G2U1	Histidine protein kinase SaeS	saeS	0.98	1.93	39.74	6	21.7
Q2FZF9	Glycerophosphoryl diester phosphodiesterase, putative	SAOUHSC_01071	0.98	1.72	34.73	9	26.9
Q2FXI5	Putative uncharacterized protein	SAOUHSC_01861	0.97	0.31	39.78	5	13.1
Q2G035	Epimerase family protein	SAOUHSC_00792	0.97	1.26	34.23	5	21
Q2FYF1	Elastin-binding protein EbpS	ebpS	0.95	2.50	53.22	13	45.3
Q2FZK0	Probable quinol oxidase subunit 1	qoxB	0.95	1.26	75.24	4	6.5
Q2FVI3	Putative uncharacterized protein	SAOUHSC_02727	0.93	1.47	22.28	3	18
Q2FVQ4	L-lactate permease	SAOUHSC_02648	0.93	0.32	56.64	2	4.5
Q2FW13	50S ribosomal protein L16	rplP	0.92	0.52	16.24	5	31.9
Q2G105	Putative uncharacterized protein	SAOUHSC_00356	0.89	1.16	21.31	3	18.4
Q2G2E5	Putative uncharacterized protein	SAOUHSC_00647	0.89	1.39	64.05	12	26.6
Q2FWB6	Putative uncharacterized protein	SAOUHSC_02382	0.88	1.48	16.25	6	34.3
Q2FV87	PTS system glucoside-specific EIICBA component	glcB	0.88	2.12	74.42	9	19.8
Q2FYT0	Glycine betaine transporter, putative	SAOUHSC_01346	0.87	1.95	60.47	4	6.2
Q2FYL3	Putative uncharacterized protein	SAOUHSC_01427	0.85	1.61	55.26	12	24.6
Q2FY36	Putative uncharacterized protein	SAOUHSC_01630	0.84	1.62	14.80	4	24.2
Q2FZ18	Putative uncharacterized protein	SAOUHSC_01253	0.84	2.48	83.40	12	19.5
Q2FY42	Acetyl-CoA carboxylase, biotin carboxyl carrier protein	SAOUHSC_01624	0.84	1.21	17.12	5	46.8
Q2G239	Fructose specific permease, putative	SAOUHSC_00708	0.84	0.74	68.71	10	19
Q2FVF5	Putative uncharacterized protein	SAOUHSC_02759	0.84	0.24	17.31	4	21.2
Q2G0Z9	Putative uncharacterized protein	SAOUHSC_00362	0.83	2.25	23.66	6	28.8
Q2G155	Lipase 2	lip2	0.82	0.22	76.39	10	21.9
Q2FVE7	Peptide ABC transporter, peptide-binding protein, putative	SAOUHSC_02767	0.82	2.14	60.08	11	22
Q2FXJ7	1-acyl-sn-glycerol-3-phosphate acyltransferases domain protein	SAOUHSC_01837	0.81	1.09	23.07	8	32.7
Q2G0U0	Putative uncharacterized protein	SAOUHSC_00437	0.79	1.41	50.94	8	20
Q2G2T0	Putative uncharacterized protein	SAOUHSC_01969	0.79	1.15	13.21	6	56.2
Q2FV30	Dihydroorotate dehydrogenase	SAOUHSC_02909	0.79	1.30	39.54	9	33.1
Q2FV64	Copper-exporting P-type ATPase A	copA	0.77	1.14	86.74	12	20.2
Q2G1C1	Teichoic acid biosynthesis protein F, putative	SAOUHSC_00223	0.77	1.01	45.96	7	19.5
Q2FWY6	Putative uncharacterized protein	SAOUHSC_02121	0.75	3.90	45.38	11	37.3
Q2FZ91	Cell division protein DivIB	divIB	0.73	2.63	50.21	9	25.5
Q2G2U4	Sensor protein kinase Walk	walK	0.72	1.67	69.92	7	11.5
Q2FZ64	Putative uncharacterized protein	SAOUHSC_01187	0.72	2.17	74.36	18	26.2
Q2FZ94	Penicillin-binding protein 1	SAOUHSC_01145	0.72	1.51	82.71	18	34.8
Q2FXX0	Acetyl-CoA carboxylase, biotin carboxyl carrier protein, putative	SAOUHSC_01710	0.70	0.93	16.79	3	27.5
Q2G2H3	Putative uncharacterized protein	SAOUHSC_02009	0.70	0.67	58.25	3	7.7
P52078	Uncharacterized protein	SAOUHSC_00997	0.70	1.21	45.69	8	19.3

Q2G2W5	Putative uncharacterized protein	SAOUHSC_02630	0.69	0.66	23.02	4	28.4
Q2FXF4	Putative uncharacterized protein	SAOUHSC_01895	0.68	1.56	32.51	7	19.7
Q2FXQ6	Trigger factor	tig	0.67	0.77	48.61	22	44.3
Q2G248	Putative uncharacterized protein	SAOUHSC_01852	0.67	0.86	40.62	10	28.9
Q2FVU4	PTS system component, putative	SAOUHSC_02597	0.67	0.96	59.33	3	6.6
Q2FYV4	Homoserine dehydrogenase	SAOUHSC_01320	0.67	1.25	46.87	11	34.5
Q2FZZ8	Glycine cleavage system H protein	gcvH	0.65	1.39	14.09	4	46
Q2FXY6	30S ribosomal protein S20	rpsT	0.64	0.55	9.02	4	45.8
Q2FVL7	Putative uncharacterized protein	SAOUHSC_02694	0.64	0.62	23.06	2	11.6
Q2G2S6	Foldase protein PrsA	prsA	0.63	1.03	35.64	8	23.8
Q2FYK7	Putative uncharacterized protein	SAOUHSC_01433	0.63	1.42	30.64	8	31.5
Q2FWE0	Peptide chain release factor 1	prfA	0.62	0.69	40.35	10	32.7
Q2FZ59	Putative uncharacterized protein	SAOUHSC_01192	0.62	1.49	13.39	4	41.9
Q2G1G5	PTS system EIIBC component	SAOUHSC_00158	0.61	1.03	50.66	7	24.6
Q2FUX0	PTS system, fructose-specific IIABC component, putative	SAOUHSC_02975	0.61	0.81	69.88	7	16.6
Q2FXJ6	Putative uncharacterized protein	SAOUHSC_01838	0.61	1.37	45.80	12	25.9
Q2G1C2	TagB protein, putative	SAOUHSC_00222	0.61	0.57	60.18	7	13.8
Q2FUX3	Immunodominant staphylococcal antigen B	isaB	0.60	1.46	19.37	6	28.6
Q2FXZ9	UPF0365 protein	SAOUHSC_01676	0.60	0.89	35.18	14	49.5
Q2FVW3	Putative uncharacterized protein	SAOUHSC_02579	0.60	1.04	41.89	9	28.1
Q2G0W9;Q2G0X1	Uncharacterized lipoprotein	SAOUHSC_00405	0.58	1.22	31.47	9	28.5
Q2FZV7	NADH dehydrogenase-like protein	SAOUHSC_00878	0.58	1.15	44.10	13	31.8
Q2FVN2	Putative uncharacterized protein	SAOUHSC_02670	0.58	2.66	16.31	2	17.6
Q2FYW4	Cardiolipin synthetase, putative	SAOUHSC_01310	0.56	0.44	56.37	3	7.3
Q2FXT7	Preprotein translocase, YajC subunit	SAOUHSC_01747	0.55	0.83	9.67	2	22.1
Q2FYZ3	Hydrolase, alpha/beta fold family domain protein	SAOUHSC_01279	0.55	0.37	35.26	3	11.2
Q2G0R1	Hypoxanthine phosphoribosyltransferase	SAOUHSC_00485	0.55	0.77	20.15	4	20.1
Q2G0Z2	Putative uncharacterized protein	SAOUHSC_00369	0.54	1.77	35.61	12	48.1
Q2G0L2	Putative uncharacterized protein	SAOUHSC_00548	0.53	0.32	58.42	3	6.5
Q2FXH8	Putative uncharacterized protein	SAOUHSC_01869	0.51	1.97	15.73	5	43.6
Q2G1G8	PTS system glucose-specific EIICBA component	ptsG	0.51	0.76	73.92	10	22.9
Q2FYR1	Aminoacyltransferase FemB	femB	0.51	1.05	49.68	5	10.7
Q2FVX0	Putative uncharacterized protein	SAOUHSC_02553	0.50	0.89	35.36	4	16.3
Q2FY78	Pseudouridine synthase	SAOUHSC_01587	0.49	0.19	27.97	4	21.2
Q2FYI5	Cell cycle protein GpsB	gpsB	0.48	0.66	13.15	3	27.2
Q2G2L2	Putative uncharacterized protein	SAOUHSC_00637	0.48	1.02	28.02	5	22.3
Q2FY64	Alpha-amylase	SAOUHSC_01601	0.48	0.24	63.91	8	15.8
Q2G0I1	Putative uncharacterized protein	SAOUHSC_00584	0.47	1.79	51.67	8	22.8
Q2G2L1	Teichoic acids export ATP-binding protein TagH	tagH	0.46	0.52	29.76	5	21.2
Q2G243	DNA repair protein radA	SAOUHSC_00507	0.46	0.30	48.68	4	11.9
Q2G1W5	Putative uncharacterized protein	SAOUHSC_01908	0.45	1.54	35.05	9	38.4
Q2FZY5	Aminotransferase, class V superfamily, putative	SAOUHSC_00849	0.45	0.45	46.62	7	19
Q2G2G0	Putative uncharacterized protein	SAOUHSC_00717	0.44	0.72	16.05	6	34.2
Q2FXT0	50S ribosomal protein L27	rpmA	0.43	0.83	10.32	7	55.3
Q2FVG3	Putative uncharacterized protein	SAOUHSC_02751	0.43	0.89	51.97	5	10.2
Q2FV21	3-methyl-2-oxobutanoate hydroxymethyltransferase	panB	0.41	0.81	29.26	11	53.3
Q2FW93	Putative uncharacterized protein	SAOUHSC_02406	0.41	1.29	34.62	11	40
Q2FZZ6	Putative uncharacterized protein	SAOUHSC_00838	0.41	0.30	33.50	5	18.2
Q2G1D9	Lipoprotein, putative	SAOUHSC_00186	0.41	0.55	36.93	4	14.3
Q2G221	Phage infection protein, putative	SAOUHSC_02978	0.40	2.61	108.71	25	29.7
Q2FYI0	Penicillin-binding protein 2	SAOUHSC_01467	0.40	1.49	80.43	21	35.1
Q2FW17	50S ribosomal protein L24	rplX	0.40	0.69	11.54	5	20
Q2FXZ1	Protein GrpE	grpE	0.39	0.46	24.01	7	52.9
Q2G0S5	Putative septation protein SpoVG	spoVG	0.39	0.33	11.28	4	48
O07325	Cell division protein FtsA	ftsA	0.38	1.46	52.93	14	35.5
Q2FXK7	GAF domain protein	SAOUHSC_01828	0.37	1.16	17.11	4	19.5
Q2FYS0	Putative uncharacterized protein	SAOUHSC_01365	0.37	0.38	37.86	6	19.5
Q2FY39	Putative uncharacterized protein	SAOUHSC_01627	0.37	0.76	21.47	4	28.5
Q2FYK5	Thymidylate synthase	thyA	0.35	0.57	36.84	7	17.9
Q2G1B8	Putative uncharacterized protein	SAOUHSC_00227	0.34	0.51	66.07	2	2.8
Q2FZP2	Serine protease HtrA-like	SAOUHSC_00958	0.34	1.09	86.46	10	20
Q2FWZ9	UDP-N-acetylmuramyl tripeptide synthetase, putative	SAOUHSC_02107	0.34	2.09	49.27	7	19.5
Q2G220	Putative uncharacterized protein	SAOUHSC_02980	0.33	1.75	20.73	4	40.9
Q2FZ27	GTP-sensing transcriptional pleiotropic repressor CodY	codY	0.33	0.80	28.76	14	48.2
Q2G0F6	Iron compound ABC transporter, substrate-binding protein, putative	SAOUHSC_00613	0.33	1.65	31.09	8	32
Q2FYV7	Putative uncharacterized protein	SAOUHSC_01317	0.33	0.33	32.85	5	20.1

8 - Supporting Information

Q2FW28	Translation initiation factor IF-1	infA	0.32	0.24	8.28	4	69.4
Q2G0K7	3-hexulose-6-phosphate synthase	SAOUHSC_00553	0.32	0.42	22.44	5	41
Q2G0Z0	Putative uncharacterized protein	SAOUHSC_00371	0.31	0.79	15.12	7	49.6
P0A0J0	RNA polymerase sigma factor SigA	sigA	0.31	0.56	42.17	7	22.8
Q2G2F3	Signal transduction protein TRAP	traP	0.31	1.36	19.55	5	22.2
Q2G241	Glutamate--tRNA ligase	gltX	0.30	0.36	56.29	16	38.6
Q2FWK4	Ketol-acid reductoisomerase	ilvC	0.30	0.29	36.96	7	29
Q2G2U3	Putative uncharacterized protein	SAOUHSC_00022	0.30	0.79	49.01	9	25.5
Q2FXH9	Putative dipeptidase	SAOUHSC_01868	0.30	1.72	52.82	13	31.6
Q2G260	Uncharacterized protein	SAOUHSC_00094	0.29	0.13	21.85	5	38.7
Q2G0C7	Putative uncharacterized protein	SAOUHSC_00678	0.29	0.23	25.42	2	7.9
Q2G1V4	ABC transporter, ATP-binding protein, putative	SAOUHSC_00333	0.29	0.57	31.59	3	11.4
Q2FXK8	Septation ring formation regulator EzrA	ezrA	0.29	0.79	66.25	12	25
Q2FWB7	Putative uncharacterized protein	SAOUHSC_02381	0.28	0.75	16.69	5	66
Q2FWW9	ABC transporter, ATP-binding protein, putative	SAOUHSC_02152	0.28	0.52	32.95	6	18.3
Q2G0F3	Putative uncharacterized protein	SAOUHSC_00616	0.28	1.77	30.93	2	8.3
Q2FVG8	Amino acid ABC transporter, ATP-binding protein, putative	SAOUHSC_02744	0.28	0.24	46.17	4	10.8
Q2FYR2	Aminoacyltransferase FemA	femA	0.28	0.77	49.12	8	18.1
Q2FY21	Penicillin-binding protein 3	SAOUHSC_01652	0.27	1.23	77.24	19	33.3
Q2FYZ0	Glutathione peroxidase	SAOUHSC_01282	0.27	0.67	18.12	5	34.8
Q2G0S0	50S ribosomal protein L25	rplY	0.27	0.26	23.79	7	30
Q2FZ45	30S ribosomal protein S16	rpsP	0.26	0.38	10.24	5	60.4
Q2FY81;Q2FYE2;Q2FYE3;Q2FYE5	Putative uncharacterized protein	SAOUHSC_01584	0.26	0.38	33.58	6	22.8
Q2FVL2	Putative uncharacterized protein	SAOUHSC_02699	0.26	0.67	28.90	7	23.2
Q2FYT3	Nuclease SbcCD subunit C	sbcC	0.25	0.29	117.27	7	8
Q2G1Y7	Putative uncharacterized protein	SAOUHSC_01061	0.25	0.15	18.58	3	16.2
Q2FYZ4	Aerobic glycerol-3-phosphate dehydrogenase	glpD	0.24	0.47	62.39	24	43.8
P0C0V7	Phosphoglucosamine mutase	glmM	0.24	0.33	49.27	14	35.3
Q2G0M2	Haloacid dehalogenase-like hydrolase, putative	SAOUHSC_00538	0.24	0.15	24.99	4	22.5
Q2G1J0	Putative aldehyde dehydrogenase AldA	aldA	0.24	0.81	53.66	20	54.7
Q2FV62	D-lactate dehydrogenase, putative	SAOUHSC_02875	0.23	0.09	37.22	3	10.2
Q2FZV6	Leucine aminopeptidase 2, chloroplastic	SAOUHSC_00879	0.23	0.17	54.13	6	15.3
Q2G264	Putative uncharacterized protein	SAOUHSC_01180	0.23	1.58	35.91	9	37.2
Q2G039	UPF0042 nucleotide-binding protein	SAOUHSC_00787	0.22	0.17	34.81	4	16.5
Q2FVW9	Putative uncharacterized protein	SAOUHSC_02554	0.22	0.69	34.01	12	39.4
Q2G1G0	Putative uncharacterized protein	SAOUHSC_00164	0.22	0.62	35.55	4	15
Q2G1N4	Periplasmic binding protein, putative	SAOUHSC_00074	0.22	0.33	36.74	5	18.2
Q2FZC7	Iron-sulphur subunit of succinate dehydrogenase, putative	SAOUHSC_01105	0.22	0.43	30.58	7	29.9
Q2G112	Single-stranded DNA-binding protein	SAOUHSC_00349	0.22	0.20	18.54	4	47.9
Q2FVN7	Putative uncharacterized protein	SAOUHSC_02665	0.21	0.38	15.91	4	42.1
Q2G222	N-acetylmuramoyl-L-alanine amidase domain-containing protein	SAOUHSC_02979	0.19	0.07	69.25	10	24.4
Q2FXP3	Transcriptional repressor NrdR	nrdR	0.19	0.38	18.20	2	17.3
Q2FX14	Aminopeptidase PepS, putative	SAOUHSC_02092	0.19	0.25	47.12	9	28.2
Q2FZV8	Putative uncharacterized protein	SAOUHSC_00877	0.19	0.26	12.49	2	19.3
Q2FZW3	Extramembranal protein	SAOUHSC_00872	0.19	0.08	44.95	4	12
Q2G188	Putative uncharacterized protein	SAOUHSC_00258	0.19	0.51	114.82	15	18.2
Q2FY29	Putative uncharacterized protein	SAOUHSC_01644	0.18	0.38	23.14	5	33.3
Q2FWX8	Uncharacterized protein	SAOUHSC_02143	0.18	0.18	38.55	5	16.1
Q2FW33	50S ribosomal protein L17	rplQ	0.17	0.28	13.75	5	42.6
Q2FXN7	Histidine kinase-, DNA gyrase B-, and HSP90-like ATPase domain protein	SAOUHSC_01799	0.16	0.14	63.77	6	10.7
Q2FUS2	Sodium, sulfate symporter, putative	SAOUHSC_03030	0.16	0.12	51.34	2	4.7
Q2FW75	ABC transporter periplasmic binding protein, putative	SAOUHSC_02430	0.16	0.39	36.59	6	15.3
Q2FWF5	3-hydroxyacyl-[acyl-carrier-protein] dehydratase FabZ	fabZ	0.16	0.15	16.08	3	19.2
Q2FY60	6-phosphogluconate dehydrogenase, decarboxylating	SAOUHSC_01605	0.15	0.66	51.80	9	23.1
Q2G1U8	Putative uncharacterized protein	SAOUHSC_02690	0.15	0.73	59.19	12	28.1
Q2G0R0	ATP-dependent zinc metalloprotease FtsH	ftsH	0.15	0.30	77.81	18	31.7
Q2G0L1	GTP cyclohydrolase FolE2	folE2	0.15	0.34	33.48	6	25.7
Q2FXR3	Delta-aminolevulinic acid dehydratase	hemB	0.15	0.25	36.58	7	26.9
Q2FWD3	Putative uncharacterized protein	SAOUHSC_02366	0.14	0.20	30.84	8	46.5
Q2G0D6	Putative uncharacterized protein	SAOUHSC_00669	0.14	0.30	23.74	5	22.4
Q2G1Z0	Putative uncharacterized protein	SAOUHSC_00655	0.14	0.42	35.02	7	26.4
Q2FUX8	Ornithine carbamoyltransferase	argF	0.14	0.60	37.76	6	21.4
Q2G055	Uncharacterized protein	SAOUHSC_00767	0.13	0.38	22.21	6	29.5

Q2G0P2	Transcription termination/antitermination protein NusG	nusG	0.13	0.25	20.66	9	48.9
Q2FYF9	30S ribosomal protein S1, putative	SAOUHSC_01493	0.13	0.26	43.29	17	51.4
Q2G2Z7	Phosphopentomutase	deoB	0.13	0.31	43.80	8	22.2
Q2FZC8	Succinate dehydrogenase, flavoprotein chain TC0881, putative	SAOUHSC_01104	0.12	0.37	65.50	14	23.3
Q2FYH5	Probable ATP-dependent helicase DinG homolog	dinG	0.12	0.14	104.22	7	8.7
Q2G1H0	Indolepyruvate decarboxylase, putative	SAOUHSC_00153	0.12	0.31	60.54	6	14.1
Q2FZ29	ATP-dependent protease subunit HslV	hslV	0.12	0.53	19.57	2	15.5
Q2FUR8	Putative uncharacterized protein	SAOUHSC_03034	0.12	0.12	30.44	3	11.4
Q2FVT2	Formimidoylglutamase	hutG	0.11	0.43	34.51	4	14.5
Q2G0P6	Protein-arginine kinase	mcsB	0.11	0.19	38.61	2	7.8
Q2FXL0	Putative uncharacterized protein	SAOUHSC_01825	0.10	0.20	42.37	3	9.7
Q2FWR2	Conserved hypothetical phage protein	SAOUHSC_02218	0.10	0.15	11.10	3	33.3
Q2FVX4	Molybdenum ABC transporter, periplasmic molybdate-binding protein	SAOUHSC_02549	0.09	0.27	29.05	9	30
Q2G0Q9	33 kDa chaperonin	hslO	0.09	0.12	31.82	5	23.2
Q2FVA6	Putative uncharacterized protein	SAOUHSC_02827	0.09	0.36	10.55	3	38.3
Q2FZ73	Carbamoyl-phosphate synthase small chain	carA	0.09	0.02	40.39	4	13.1
Q2FW21	50S ribosomal protein L6	rplF	0.09	0.18	19.79	11	70.2
Q2FZG6	Peptide deformylase	def	0.09	0.17	20.56	8	45.9
Q2FV11	Oxygen-dependent choline dehydrogenase	betA	0.08	0.08	63.61	6	16.5
Q2FW86	Putative uncharacterized protein	SAOUHSC_02417	0.08	0.19	31.79	8	36.6
POA0F8	50S ribosomal protein L15	rplO	0.08	0.13	15.60	6	48.6
Q2FXU5	Aspartate--tRNA ligase	aspS	0.07	0.35	66.63	11	23.5
Q2FV16	Probable malate:quinone oxidoreductase	mqq	0.07	0.48	56.00	17	34.9
Q2FUW9	Putative uncharacterized protein	SAOUHSC_02982	0.07	0.08	70.93	24	43.8
Q2FY40	Proline dipeptidase, putative	SAOUHSC_01626	0.06	0.52	39.34	9	27.8
Q2FXL6	Putative universal stress protein	SAOUHSC_01819	0.06	0.42	18.48	9	66.9
Q2FVV9	Putative formate dehydrogenase	SAOUHSC_02582	0.05	0.27	111.24	14	18.8
POA088	Peptide methionine sulfoxide reductase MsrB	msrB	0.05	0.08	16.28	3	29.6
Q2G253	Putative uncharacterized protein	SAOUHSC_00025	0.05	0.07	83.42	25	42.5
Q2FZU6	Ornithine aminotransferase	rocD	0.05	0.17	43.42	9	29
Q2FWZ2	Diacylglycerol kinase	dagK	0.04	0.09	34.89	6	21.6
Q2FWX9	Aldehyde dehydrogenase	SAOUHSC_02142	0.04	0.08	51.74	7	19.4
Q2FXM5	NADP-dependent malic enzyme, putative	SAOUHSC_01810	0.04	0.07	44.23	8	37.4
Q2FXZ3	Chaperone protein DnaJ	dnaJ	0.04	0.11	41.76	8	30.3
Q2FY73	Transcriptional regulator, Fur, putative	SAOUHSC_01592	0.04	0.04	17.24	3	20.8
Q2G041	Thioredoxin reductase	SAOUHSC_00785	0.04	0.13	33.62	11	46.3
Q2FXU2	D-aminoacyl-tRNA deacylase	dtd	0.04	0.56	16.70	2	10
Q2FXI0	D-alanine aminotransferase	SAOUHSC_01867	0.03	0.12	31.89	6	28.4
Q2G2H4	DNA polymerase III subunit beta	SAOUHSC_00002	0.03	0.11	41.91	18	43.5
Q2FYU7	Catalase	katA	0.03	0.15	58.38	15	33.9
Q2FV39	Uncharacterized hydrolase	SAOUHSC_02900	0.03	0.05	31.01	7	30.8
Q2FV86	Pyruvate oxidase, putative	SAOUHSC_02849	0.03	0.09	63.76	9	21.4
Q2G000	Thioredoxin, putative	SAOUHSC_00834	0.03	0.01	12.14	2	24.5
Q2FVB4	Putative uncharacterized protein	SAOUHSC_02820	0.02	0.02	25.80	8	35.1
POA0B7	Alkyl hydroperoxide reductase subunit C	ahpC	0.02	0.32	20.98	11	58.2
Q2FZZ0	Lipoprotein	SAOUHSC_00844	0.02	0.03	30.35	8	34.1
Q2G0J1	Putative heme-dependent peroxidase	SAOUHSC_00573	0.02	0.04	29.39	3	14.4
Q2G0M4	Branched-chain-amino-acid aminotransferase	SAOUHSC_00536	0.01	0.04	40.09	10	33
Q2G124	Probable acetyl-CoA acyltransferase	SAOUHSC_00336	0.01	0.02	41.70	8	32.6
Q2FVD5	Uncharacterized oxidoreductase	SAOUHSC_02778	0.01	0.01	24.60	6	43.7
Q2FVQ5	Probable malate:quinone oxidoreductase	mqq	0.01	0.06	54.81	12	27
O52582	Coenzyme A disulfide reductase	cdr	0.01	0.02	49.24	13	34
Q2G2D8	ABC transporter, substrate-binding protein, putative	SAOUHSC_00634	0.01	0.02	35.07	15	44.2
Q2G0M7	Molecular chaperone Hsp31 and glyoxalase 3	hchA	0.01	0.00	32.18	2	9.6
Q2FZM8	Putative uncharacterized protein	SAOUHSC_00972	0.00	0.00	11.19	3	42.1
Q2FVM1	Nitrate reductase, alpha subunit	SAOUHSC_02681	-0.01	0.08	139.83	23	22.1
Q2FW27	Adenylate kinase	adk	-0.01	0.01	23.97	9	39.5
Q2FZL5	Enoyl-CoA hydratase/isomerase family protein, putative	SAOUHSC_00985	-0.01	0.03	30.43	10	48
Q2FVT6	Imidazolonepropionase	hutI	-0.02	0.02	45.04	12	36.2
Q2FVS3	Putative uncharacterized protein	SAOUHSC_02619	-0.02	0.04	33.72	7	31.1
Q2FXV4	Putative uncharacterized protein	SAOUHSC_01727	-0.02	0.02	42.48	4	13.7
Q2FWA2	Putative uncharacterized protein	SAOUHSC_02396	-0.02	0.01	32.30	4	18.6
Q2FZ83	Putative uncharacterized protein	SAOUHSC_01158	-0.02	0.03	23.51	4	21
Q2G2S8	Putative uncharacterized protein	SAOUHSC_01974	-0.02	0.04	114.42	21	29

8 - Supporting Information

Q2FWX1	Putative uncharacterized protein	SAOUHSC_02150	-0.02	0.06	21.92	9	49.7
Q2FXZ7	30S ribosomal protein S21	rpsU	-0.03	0.07	6.97	5	34.5
Q2FVT5	Urocanate hydratase	hutU	-0.03	0.05	60.63	12	26.8
P60070	Anti-sigma-B factor antagonist	rsbV	-0.03	0.02	12.21	3	29.6
Q2FXL3	Probable thiol peroxidase	tpx	-0.03	0.05	18.01	6	49.4
Q2FZ08	Ribonuclease Y	rny	-0.04	0.09	58.51	8	19.8
Q2FVW0	Putative uncharacterized protein	SAOUHSC_02581	-0.04	0.05	17.48	5	28.7
Q2G0Y7	Inosine-5'-monophosphate dehydrogenase	guaB	-0.04	0.08	52.85	26	52.3
Q2FYJ6	Extracellular matrix-binding protein ebh	ebh	-0.04	0.06	1029.9010		1.4
Q2G0I8	Mevalonate kinase, putative	SAOUHSC_00577	-0.04	0.03	32.92	4	19.6
Q2G0R8	Transcription-repair-coupling factor	mfd	-0.04	0.03	134.22	6	6.7
Q2FYZ7	Glycerol uptake operon antiterminator regulatory protein	SAOUHSC_01274	-0.04	0.03	20.45	4	30.6
Q2FUT8	Histidinol dehydrogenase	hisD	-0.04	0.06	46.18	2	6
Q2FYL5	UDP-N-acetylglucosamine--N-acetylmuramyl-(pentapeptide) pyrophosphoryl-undecaprenol N-acetylglucosamine transferase	murG	-0.04	0.10	39.70	9	35.1
Q2FXM0	UPF0173 metal-dependent hydrolase	SAOUHSC_01815	-0.05	0.08	25.25	3	17.5
Q2G067	Putative uncharacterized protein	SAOUHSC_00754	-0.05	0.13	34.08	3	10.6
Q2FY71	Putative uncharacterized protein	SAOUHSC_01594	-0.06	0.02	33.51	4	12.6
Q2G283	Glutamate-1-semialdehyde 2,1-aminomutase 2	hemL2	-0.06	0.46	46.76	10	31.5
Q2G045	HPr kinase/phosphorylase	hprK	-0.06	0.13	34.48	8	29.4
Q2FXB7	ABC transporter domain protein	SAOUHSC_01948	-0.06	0.02	25.89	3	21.7
Q2FZW9	D-isomer specific 2-hydroxyacid dehydrogenase, NAD binding domain protein	SAOUHSC_00866	-0.06	0.12	32.48	6	23.1
Q2G1E4	Putative uncharacterized protein	SAOUHSC_00181	-0.07	0.04	36.67	3	10.9
Q2G1C6	Acetate CoA-transferase YdiF	SAOUHSC_00199	-0.07	0.04	58.88	6	14.1
Q2FY55	DNA topoisomerase 4 subunit B	parE	-0.07	0.16	74.36	8	13.6
Q2G0M8	Putative uncharacterized protein	SAOUHSC_00532	-0.08	0.29	42.89	12	43.3
Q2FYP3	Conserved virulence factor B	cvfB	-0.09	0.08	34.20	4	17.7
Q2FZ31	Methylenetetrahydrofolate--tRNA-(uracil-5)-methyltransferase TrmF	trmFO	-0.09	0.54	48.37	9	26
Q2FX05	Methionine aminopeptidase	map	-0.09	0.41	27.50	5	22.2
Q2G1B7	Putative uncharacterized protein	SAOUHSC_00228	-0.09	0.32	66.31	15	26.5
Q2FZE9	Iron-regulated surface determinant protein A	isdA	-0.09	0.29	38.75	8	24
Q2FXA5	Protoporphyrinogen oxidase	SAOUHSC_01960	-0.10	0.58	51.98	16	42.9
Q2FWD1	CTP synthase	pyrG	-0.10	0.33	59.98	13	27.6
Q2G1U3	Oligoendopeptidase F	SAOUHSC_00937	-0.10	0.69	69.82	15	27.2
P72360	Iron-sulfur cluster repair protein ScdA	scdA	-0.10	0.25	25.49	5	21.4
Q2FZM6	Glycosyl transferase, group 1	SAOUHSC_00974	-0.11	0.12	29.78	4	17.7
Q2FZ74	Dihydroorotase	pyrC	-0.11	0.16	46.37	6	18.9
Q2FY66	Glucose-6-phosphate 1-dehydrogenase	zwf	-0.11	0.60	56.97	10	21.9
Q2FX19	Conserved hypothetical phage protein	SAOUHSC_02087	-0.11	0.10	35.63	5	15.6
Q2G1W2	Phosphoenolpyruvate carboxykinase [ATP]	pckA	-0.11	0.26	59.38	16	37.4
Q2G113	30S ribosomal protein S6	rpsF	-0.11	0.35	11.60	4	40.8
Q2FVT8	Putative uncharacterized protein	SAOUHSC_02604	-0.12	0.09	31.73	3	13
Q2G2S7	Putative uncharacterized protein	SAOUHSC_01975	-0.12	0.32	46.22	6	20.6
Q2FWM1	Sucrose-6-phosphate dehydrogenase, putative	SAOUHSC_02268	-0.12	0.30	57.93	6	15.2
Q93T05	DNA mismatch repair protein MutL	mutL	-0.12	0.97	76.85	6	10.5
Q2FV34	Putative uncharacterized protein	SAOUHSC_02905	-0.12	0.15	11.58	2	25.5
Q2FY41	Elongation factor P	efp	-0.12	0.16	20.55	7	36.8
Q2G0M6	Ribulokinase	araB	-0.13	0.08	61.01	5	11.9
Q2FYM3	Putative uncharacterized protein	SAOUHSC_01415	-0.13	0.35	30.08	5	21.6
Q2G0S3	Bifunctional protein GlmU	glmU	-0.13	0.14	48.50	5	14.2
Q2FWY8	Aspartyl/glutamyl-tRNA(Asn/Gln) amidotransferase subunit C	gatC	-0.13	0.47	11.27	2	27
Q2FW91	Arginase	SAOUHSC_02409	-0.13	0.39	33.26	10	29.1
Q2G268	Phosphopantothenoilcysteine decarboxylase/phosphopantothenate--cysteine ligase	SAOUHSC_01178	-0.13	0.10	44.14	5	19
Q2FXH2	Leucine--tRNA ligase	leuS	-0.13	1.36	91.79	12	22.9
Q2FZX0	Protein NagD homolog	nagD	-0.13	1.61	27.95	6	25.9
Q2G0J0	Phosphate acetyltransferase	SAOUHSC_00574	-0.13	0.42	34.95	13	56.4
Q7X2S2	Carbamate kinase 2	arcC2	-0.14	0.42	34.33	7	36.4
Q2FXY2	Putative uncharacterized protein	SAOUHSC_01698	-0.14	0.32	11.05	3	40.6
Q2FYZ9	DNA mismatch repair protein MutS	mutS	-0.14	0.14	99.90	11	12.6
Q2FX94	Fumarate hydratase class II	fumC	-0.14	0.51	51.11	11	27.8
Q2FVH3	2-dehydropantoate 2-reductase	SAOUHSC_02739	-0.14	0.41	34.44	3	13.2
Q2G2D0	Translation initiation factor IF-2	infB	-0.14	1.06	77.87	24	38.3

Q2G0Q8	Cysteine synthase	SAOUHSC_00488	-0.15	0.59	32.98	15	63.9
Q2FZ36	Succinyl-CoA ligase [ADP-forming] subunit alpha	SAOUHSC_01218	-0.15	0.44	31.54	9	43.7
Q2G218	L-lactate dehydrogenase 1	ldh1	-0.15	0.26	34.58	10	34.1
Q9ZAH5	Alanine racemase 1	alr1	-0.15	0.71	42.82	3	7.9
Q2G030	Triosephosphate isomerase	tpiA	-0.15	0.20	27.29	11	50.2
Q2FZ10	Putative competence-damage inducible protein	cinA	-0.15	0.14	43.27	5	14.6
Q2G0V0	Lipoprotein	SAOUHSC_00426	-0.15	0.13	30.46	3	13.9
Q2G163	Pseudouridine-5'-phosphate glycosidase	psuG	-0.15	0.28	32.87	6	20.5
Q2G0W8	Putative uncharacterized protein	SAOUHSC_00406	-0.16	0.76	49.26	8	31.7
Q2FXS8	50S ribosomal protein L21	rplU	-0.16	0.44	11.33	8	67.6
Q2G2T6	Putative uncharacterized protein	SAOUHSC_00015	-0.16	0.13	73.78	9	14.8
Q2FVV2	Putative uncharacterized protein	SAOUHSC_02589	-0.16	0.31	33.00	6	29.7
Q2G0J8	Phosphomethylpyrimidine kinase	SAOUHSC_00562	-0.16	0.62	29.86	8	35.1
Q2FVC2	Pyrophosphohydrolase, putative	SAOUHSC_02791	-0.16	0.15	14.89	2	16.9
Q2FVN3	HTH-type transcriptional regulator SarZ	sarZ	-0.16	0.97	17.44	4	29.7
Q2FZV4	Putative uncharacterized protein	SAOUHSC_00881	-0.16	0.09	13.55	2	14.5
Q2FWJ3	Serine-protein kinase RsbW	rsbW	-0.16	0.57	17.92	4	30.8
Q2FXZ2	Chaperone protein DnaK	dnaK	-0.17	1.27	66.36	27	50.8
Q2G015	Clumping factor A	clfA	-0.17	0.45	96.45	11	15.9
Q2FXP9	Translation initiation factor IF-3	infC	-0.17	1.79	20.21	4	26.9
Q2FWZ0	Aspartyl/glutamyl-tRNA(Asn/Gln) amidotransferase subunit B	gatB	-0.17	0.64	53.66	25	50.5
Q2FZ16	Putative uncharacterized protein	SAOUHSC_01255	-0.17	0.43	48.62	5	11.4
Q2G028	Enolase	eno	-0.17	0.72	47.12	19	55.8
Q2FUX7	Arginine deiminase	arcA	-0.17	0.45	46.91	19	44.8
Q2FY89	Helix-turn-helix domain protein	SAOUHSC_01575	-0.17	0.68	27.02	5	24.9
Q2G1S3	Adenylosuccinate synthetase	purA	-0.18	0.28	47.58	9	31.4
Q2FZG4	Pyruvate dehydrogenase complex, E1 component, alpha subunit, putative	SAOUHSC_01040	-0.18	1.89	41.38	9	34.6
Q2G280	Putative uncharacterized protein	SAOUHSC_01999	-0.18	0.38	17.26	4	26.5
Q2G1R9	Methionine--tRNA ligase	metG	-0.18	0.56	74.89	14	23.3
Q2FVX8	Molybdopterin biosynthesis moaB, putative	SAOUHSC_02544	-0.18	0.14	18.50	2	15.5
Q2FY54	2-oxoisovalerate dehydrogenase, E2 component, dihydrolipoamide acetyltransferase, putative	SAOUHSC_01611	-0.18	1.54	46.73	7	17.7
Q2FWM4	Accessory gene regulator protein A	SAOUHSC_02265	-0.18	0.44	24.25	3	9.6
Q2FWE5	Serine hydroxymethyltransferase	glyA	-0.19	0.95	45.17	10	28.6
Q2FVQ2	Uncharacterized lipoprotein	SAOUHSC_02650	-0.19	0.38	23.36	6	55
Q2G0T9	Alpha amylase family protein, putative	SAOUHSC_00438	-0.19	0.28	63.51	3	6.8
O05204	Alkyl hydroperoxide reductase subunit F	ahpF	-0.19	0.82	54.72	11	25.2
Q2FYV1	Putative uncharacterized protein	SAOUHSC_01323	-0.19	0.48	29.82	5	26.6
Q2FW03	DNA topoisomerase 3	topB	-0.19	0.97	81.55	11	17.4
Q2G1C8	Putative uncharacterized protein	SAOUHSC_00197	-0.19	1.07	44.73	14	34.7
Q2G2G4	Inositol monophosphatase family protein, putative	SAOUHSC_01055	-0.19	1.25	30.47	3	13.8
Q2FVA3	D-lactate dehydrogenase, putative	SAOUHSC_02830	-0.19	0.16	34.80	7	24.4
Q2G2D7	Putative uncharacterized protein	SAOUHSC_02447	-0.19	0.45	36.27	7	26.7
Q2FYU4	GMP reductase	guaC	-0.20	0.19	36.12	2	7.4
Q2FZ46	Signal recognition particle protein	ffh	-0.20	0.39	50.71	6	16.5
Q2FXI9	Putative uncharacterized protein	SAOUHSC_01857	-0.20	0.72	144.65	26	27.2
Q2FZ37	Succinyl-CoA ligase [ADP-forming] subunit beta	sucC	-0.20	1.36	42.06	19	52.6
Q2G2B2	Surface protein G	sasG	-0.20	0.52	178.52	27	39.6
Q2FZ04	Putative uncharacterized protein	SAOUHSC_01267	-0.20	0.51	31.36	3	13.9
Q2FZP9	UPF0477 protein	SAOUHSC_00951	-0.20	0.36	19.33	11	56.8
Q2G2P2	Globin domain protein	SAOUHSC_00204	-0.21	0.92	42.91	7	24.7
Q2FZT4	Uncharacterized protein	SAOUHSC_00906	-0.21	0.67	33.11	11	55.7
Q2FYJ3	L-threonine dehydratase catabolic TdcB	tdcB	-0.21	0.82	37.31	11	45.7
Q2FZW6	D-alanine--poly(phosphoribitol) ligase subunit 1	dlrA	-0.21	0.59	54.67	9	26
Q2G2A3	Dihydrolipoyl dehydrogenase	SAOUHSC_01043	-0.21	0.42	49.48	17	46.6
P02976	Immunoglobulin G-binding protein A	spa	-0.21	1.60	56.44	28	57.4
Q2FZZ9	Putative uncharacterized protein	SAOUHSC_00835	-0.21	0.79	13.60	4	37.3
Q2FXL7	Alanine dehydrogenase 2	ald2	-0.21	0.23	40.11	18	56.2
Q2G1Q4	Putative uncharacterized protein	SAOUHSC_00049	-0.21	0.98	121.73	17	19
Q2G0T4	Nucleoid-associated protein	SAOUHSC_00444	-0.21	0.41	11.60	2	26.7
Q2FZH8	Putative uncharacterized protein	SAOUHSC_01026	-0.22	0.93	44.77	6	19.2
Q2G0G1	Alcohol dehydrogenase	adh	-0.22	0.56	36.05	18	57.7
Q2FZ75	Aspartate carbamoyltransferase	pyrB	-0.22	0.59	33.26	5	19.8
Q2FYQ2	Putative uncharacterized protein	SAOUHSC_01383	-0.22	0.41	69.28	8	20
Q2FWH4	UDP-N-acetylmuramoyl-tripeptide--D-alanyl-D-alanine ligase	SAOUHSC_02317	-0.22	0.49	50.05	8	14.6

8 - Supporting Information

Q2FZH7	Putative uncharacterized protein	SAOUHSC_01027	-0.22	0.31	20.09	3	18.9
Q2FZU5	Glutamate dehydrogenase	SAOUHSC_00895	-0.22	0.97	45.76	12	38.9
Q2FVC3	Putative uncharacterized protein	SAOUHSC_02790	-0.22	1.04	109.90	14	19
Q2FVG5	Putative uncharacterized protein	SAOUHSC_02747	-0.22	0.48	23.80	3	15.6
Q2FWC6	Putative uncharacterized protein	SAOUHSC_02372	-0.22	0.33	25.86	4	17.5
Q2G2G9	Regulatory protein RecX	recX	-0.23	1.66	32.24	4	14.3
Q2FY08	Glycine--tRNA ligase	glyQS	-0.23	1.85	53.62	13	27.6
Q2FZ20	Polyribonucleotide nucleotidyltransferase	pnp	-0.23	0.90	77.36	19	28.2
Q2FYY3	Putative uncharacterized protein	SAOUHSC_01290	-0.23	0.49	7.86	2	36.8
Q2FYN4	Diaminopimelate decarboxylase	lysA	-0.23	0.59	47.03	4	13.8
Q2FZ50	3-oxoacyl-[acyl-carrier-protein] synthase 3	fabH	-0.23	0.57	33.88	4	19.5
Q2FWL2	tRNA N6-adenosine threonylcarbamoyltransferase	tsaD	-0.24	0.48	36.82	5	17.3
Q2G266	Primosomal protein N	SAOUHSC_01179	-0.24	1.00	92.52	10	12
Q2FWD4	UDP-N-acetylglucosamine 1-carboxyvinyltransferase	murA	-0.24	0.40	45.07	8	26.3
Q2FW06	50S ribosomal protein L3	rplC	-0.24	0.33	23.72	6	28.6
Q2G0Q3	Lysine--tRNA ligase	lysS	-0.24	1.41	56.72	16	35.6
Q2FZ82	Isoleucine--tRNA ligase	ileS	-0.24	1.19	104.88	12	15.3
Q2FVC1	Phosphoglucomutase	pgcA	-0.24	0.55	62.38	11	23.4
Q2FYY6	Glutamine synthetase	SAOUHSC_01287	-0.24	0.41	50.84	12	37.4
Q2FYM1	2-oxoglutarate dehydrogenase E1 component	odhA	-0.25	0.96	105.34	14	21.2
Q2FY35	Probable glycine dehydrogenase (decarboxylating) subunit 2	gcvPB	-0.25	1.32	54.78	12	24.9
Q2FYI6	Putative uncharacterized protein	SAOUHSC_01460	-0.25	0.99	43.33	4	16.8
Q2G236	NH(3)-dependent NAD(+) synthetase	nadE	-0.25	0.23	30.70	9	41.4
Q2FY79	Transcriptional regulatory protein SrrA	srrA	-0.25	1.44	28.16	3	13.3
Q2FVV6	Putative uncharacterized protein	SAOUHSC_02585	-0.25	1.68	26.62	6	26.1
Q2FYK4	UPF0403 protein	SAOUHSC_01436	-0.26	1.14	16.01	5	40
Q2FZ53	3-oxoacyl-(Acyl-carrier-protein) reductase, putative	SAOUHSC_01199	-0.26	1.85	25.89	15	80.7
Q2FY01	Putative uncharacterized protein	SAOUHSC_01673	-0.26	0.87	34.91	6	22.9
Q2FWE8	ATP synthase subunit alpha	atpA	-0.26	0.96	54.58	15	30.3
Q2FXM7	Acetyl-coenzyme A carboxylase carboxyl transferase subunit alpha	accA	-0.26	0.25	35.07	4	20.1
Q2FZY7	ABC transporter, ATP-binding protein, putative	SAOUHSC_00847	-0.26	1.19	28.28	6	30.4
Q2FYS9	Aconitate hydratase 1	SAOUHSC_01347	-0.26	0.80	98.97	20	28.6
Q2G2A5	Pyruvate dehydrogenase complex, E1 component, pyruvate dehydrogenase beta subunit, putative	SAOUHSC_01041	-0.26	2.74	35.25	12	48
Q2FXR8	Valine--tRNA ligase	valS	-0.27	1.57	101.72	19	24.5
Q2G1Z4	Proline--tRNA ligase	proS	-0.27	0.41	63.86	7	16.9
Q2FVI7	Glycerate kinase, putative	SAOUHSC_02723	-0.27	0.23	40.66	6	20.3
Q2FYG1	Glycerol-3-phosphate dehydrogenase [NAD(P)+]	gpsA	-0.27	0.91	36.07	8	36.7
Q2FZ48	Signal recognition particle receptor FtsY	ftsY	-0.27	1.58	46.59	9	28.6
Q2FY52	2-oxoisovalerate dehydrogenase, E1 component, alpha subunit, putative	SAOUHSC_01613	-0.27	0.52	36.23	4	19.7
Q2FW32	DNA-directed RNA polymerase subunit alpha	rpoA	-0.27	0.71	35.01	12	38.9
Q2G0F8	Arginine--tRNA ligase	argS	-0.28	1.48	62.38	22	46.8
Q2FZ67	Ribosomal RNA small subunit methyltransferase B	SAOUHSC_01184	-0.28	1.11	50.11	8	18.9
Q2FXT6	Queuine tRNA-ribosyltransferase	tgt	-0.28	0.75	43.31	2	4.7
O06446	Protein translocase subunit SecA 1	secA1	-0.28	1.39	95.96	25	32.7
Q2FZ21	Ribosome-recycling factor	frr	-0.28	1.28	20.35	8	57.6
Q2FWB8	Purine nucleoside phosphorylase DeoD-type	deoD	-0.28	0.27	25.91	3	9.3
Q2FY34	Probable glycine dehydrogenase (decarboxylating) subunit 1	gcvPA	-0.28	0.91	49.72	10	26.6
Q2FXU7	Putative uncharacterized protein	SAOUHSC_01735	-0.28	1.01	28.64	4	15.6
Q2G1G7	Putative uncharacterized protein	SAOUHSC_00156	-0.28	2.71	39.87	8	20.5
Q2FVZ4	Lipid II:glycine glycytransferase	femX	-0.29	1.69	48.52	10	29.5
Q2FWY9	Glutamyl-tRNA(Gln) amidotransferase subunit A	gatA	-0.29	1.69	52.82	15	36.1
Q2FZ89	Cell division protein FtsZ	ftsZ	-0.29	0.55	41.04	15	43.6
Q2G2R8	Staphopain A	sspP	-0.29	1.02	44.26	6	19.3
Q2FWD7	Transcription termination factor Rho	rho	-0.29	1.46	49.97	12	28.8
Q2FV76	HMG-CoA synthase, putative	SAOUHSC_02860	-0.29	1.10	43.21	12	40.5
Q2FXL5	Acetate kinase	ackA	-0.29	1.07	44.04	15	46.2
Q2G0L0	Putative uncharacterized protein	SAOUHSC_00550	-0.29	0.13	24.92	4	18.1
Q2FW39	30S ribosomal protein S9	rpsI	-0.29	0.46	14.83	6	31.1
Q2FY68	Pyrraline-5-carboxylate reductase	SAOUHSC_01597	-0.29	2.72	28.76	4	16.9
Q2FZA1	Uncharacterized N-acetyltransferase	SAOUHSC_01138	-0.29	0.23	17.00	2	12.3
Q2FUY2	Clumping factor B	clfB	-0.29	1.08	93.59	13	24.4
Q2FVB2	Fructose-1,6-bisphosphatase class 3	fbp	-0.29	1.00	76.17	14	26.8
Q2G2M6	Cysteine--tRNA ligase	cysS	-0.29	1.57	53.69	12	28.1

Q2FYLO	Phosphotransferase system enzyme IIA, putative	SAOUHSC_01430	-0.29	0.28	17.96	8	63.3
Q2FY16	Probable endonuclease 4	nfo	-0.29	0.57	33.16	8	31.8
Q2FZU7	FMN oxidoreductase, putative	SAOUHSC_00893	-0.30	0.63	42.11	7	27.7
Q2FV77	3-hydroxy-3-methylglutaryl coenzyme A reductase	SAOUHSC_02859	-0.30	0.49	46.24	7	23.5
Q2FY10	Putative pyruvate, phosphate dikinase regulatory protein	SAOUHSC_01664	-0.30	1.12	30.78	6	22.8
Q2FZW0	Putative uncharacterized protein	SAOUHSC_00875	-0.30	1.29	39.40	8	27.7
Q2FY59	Peptidase T, putative	SAOUHSC_01606	-0.30	1.26	40.26	6	22.8
Q2G2F0	Putative uncharacterized protein	SAOUHSC_01968	-0.30	0.64	15.95	6	39.3
Q2FVR9	Isopentenyl-diphosphate delta-isomerase	fni	-0.31	0.36	38.77	5	12
Q2FXL1	Probable tRNA sulfurtransferase	thil	-0.31	0.76	46.21	6	17.4
Q2FYM7	TelA-like protein	SAOUHSC_01408	-0.31	1.04	43.41	13	42.1
Q2FWC3	S-ribosylhomocysteine lyase	luxS	-0.31	0.31	17.51	4	27.6
Q2FZU0	Glucose-6-phosphate isomerase	pgi	-0.31	0.20	49.82	13	33.2
Q2G2A4	Dihydrolipoamide S-acetyltransferase component of pyruvate dehydrogenase complex E2, putative	SAOUHSC_01042	-0.31	2.19	46.35	16	37.7
Q2G036	ATP-dependent Clp protease proteolytic subunit	clpP	-0.31	0.66	21.51	6	22.6
Q2G2U9	Transcriptional regulator SarA	sarA	-0.31	0.57	14.72	7	40.3
Q2FWZ8	Bacterial non-heme ferritin	ftnA	-0.31	0.63	19.59	5	33.7
Q2FWL5	ABC transporter, ATP-binding protein, putative	SAOUHSC_02274	-0.32	1.38	74.46	5	10.6
Q2FVY0	Molybdopterin biosynthesis protein moeA, putative	SAOUHSC_02542	-0.32	0.57	45.02	9	31.3
Q2G0B1	HTH-type transcriptional regulator MgrA	mgrA	-0.32	1.60	17.09	9	42.9
Q2FYJ0	Putative uncharacterized protein	SAOUHSC_01455	-0.32	0.95	133.11	12	13
Q2FWB5	Putative uncharacterized protein	SAOUHSC_02383	-0.32	1.00	52.95	7	23.2
Q2FZD2	Thioredoxin	trxA	-0.32	0.19	11.44	5	52.9
Q2FXA4	Ferrochelatase	hemH	-0.32	0.57	35.07	7	32.9
Q2G032	Glyceraldehyde-3-phosphate dehydrogenase	SAOUHSC_00795	-0.33	0.22	36.28	14	48.5
Q2FXI8	Putative uncharacterized protein	SAOUHSC_01858	-0.33	0.46	21.69	5	25.3
Q53727	ATP-dependent DNA helicase PcrA	pcrA	-0.33	1.95	84.07	12	20.4
Q2FZQ7	Tryptophan--tRNA ligase	trpS	-0.33	0.42	36.91	10	35.3
Q2FWF4	UDP-N-acetylglucosamine 1-carboxyvinyltransferase	murA	-0.34	0.82	44.94	7	19
Q2G1U1	Fibronectin-binding protein A-related	SAOUHSC_01175	-0.34	1.08	65.78	14	29.4
P48860	50S ribosomal protein L7/L12	rplL	-0.34	0.43	12.71	8	74.6
Q2FVK8	2,3-bisphosphoglycerate-dependent phosphoglycerate mutase	gpmA	-0.34	0.57	26.68	8	39
Q2FY53	2-oxoisovalerate dehydrogenase, E1 component, beta subunit, putative	SAOUHSC_01612	-0.34	2.01	36.06	6	24.8
Q2FZT6	ATP-dependent helicase/deoxyribonuclease subunit B	addB	-0.34	0.54	134.50	7	6.6
Q2FWC1	Pyrimidine-nucleoside phosphorylase	pdp	-0.34	1.33	46.31	15	43.4
Q2FZ58	Uncharacterized protein	SAOUHSC_01193	-0.35	1.40	60.52	12	30.8
Q2FYPO	Aspartate-semialdehyde dehydrogenase	asd	-0.35	0.54	36.28	5	18.2
Q2G252	Ribosomal RNA large subunit methyltransferase H	rlmH	-0.35	0.40	18.31	5	34.6
Q2FZY6	Putative uncharacterized protein	SAOUHSC_00848	-0.35	0.81	48.55	6	21.8
Q2FZQ3	Enoyl-[acyl-carrier-protein] reductase [NADPH] FabI	fabI	-0.35	1.46	28.02	4	14.8
Q2G031	Phosphoglycerate kinase	pgk	-0.35	0.80	42.60	14	32.1
Q2FYM2	Dihydrolipoyllysine-residue succinyltransferase component of 2-oxoglutarate dehydrogenase complex	odhB	-0.35	1.42	46.67	15	39.8
Q2FXK6	30S ribosomal protein S4	rpsD	-0.36	1.15	23.01	10	37.5
Q2G1C7	Putative uncharacterized protein	SAOUHSC_00198	-0.36	1.41	56.21	13	35.1
Q2FY46	Exodeoxyribonuclease 7 large subunit	xseA	-0.36	1.63	50.89	5	12.6
Q2G1D0	Acetyl-CoA acetyltransferase, putative	SAOUHSC_00195	-0.36	1.02	41.84	8	35.8
Q2FWY1	Probable manganese-dependent inorganic pyrophosphatase	ppaC	-0.36	1.64	34.07	12	31.4
Q2FWF0	ATP synthase subunit beta	atpD	-0.36	1.27	51.40	16	43
Q2G0L8	Putative uncharacterized protein	SAOUHSC_00542	-0.36	1.19	31.84	9	42.9
Q2G0E8	Putative uncharacterized protein	SAOUHSC_00658	-0.37	0.75	12.79	2	25
Q2FZ55	Phosphate acyltransferase	plsX	-0.37	1.69	35.43	7	30.5
Q2G1D8	Formate acetyltransferase	pflB	-0.37	0.99	84.86	41	53.5
Q2FZR9	3-oxoacyl-[acyl-carrier-protein] synthase 2	SAOUHSC_00921	-0.37	1.28	43.74	11	37.7
Q2G2Q0	DNA gyrase subunit A	gyrA	-0.37	1.39	99.35	10	15.3
Q2FYJ2	Alanine dehydrogenase 1	ald1	-0.37	1.69	40.22	10	30.4
Q2G1Y6	GTP-binding protein TypA, putative	SAOUHSC_01058	-0.37	1.55	69.20	14	26.3
Q2FZJ0	Phosphoribosylformylglycinamide synthase subunit PurL	purL	-0.37	0.89	79.54	10	17.3
Q2G294	Acetyl-CoA synthetase, putative	SAOUHSC_01846	-0.37	1.39	64.36	11	23.4
Q2G235	Nicotinate phosphoribosyltransferase	SAOUHSC_02133	-0.37	1.55	54.80	14	34.6
Q2FXW7	Transcription elongation factor GreA	greA	-0.38	0.56	17.74	7	69.6
Q2FXT3	Holliday junction ATP-dependent DNA helicase RuvA	ruvA	-0.38	0.32	22.26	5	28.5

8 - Supporting Information

Q2FVK2	Gamma-hemolysin component C	hlgC	-0.38	0.30	35.61	5	18.7
Q2G296	Formate--tetrahydrofolate ligase	fhs	-0.38	1.23	59.86	18	44
Q2FYG6	Heptaprenyl diphosphate syntase component II, putative	SAOUHSC_01486	-0.38	1.62	35.59	2	7
Q2FV14	Acetyl-CoA synthetase, putative	SAOUHSC_02929	-0.38	2.04	59.75	10	21.6
Q2FW16	50S ribosomal protein L14	rplN	-0.38	0.69	13.14	7	50.8
O34090	Porphobilinogen deaminase	hemC	-0.38	1.45	34.35	8	31.8
Q2FZ09	Protein RecA	recA	-0.38	1.02	34.88	11	48.1
Q2FZG9	Ribonuclease J 1	rnj1	-0.38	1.54	62.67	15	32.4
Q2FXU8	Putative uncharacterized protein	SAOUHSC_01734	-0.39	1.34	46.28	7	20.5
Q05615	3-phosphoshikimate 1-carboxyvinyltransferase	aroA	-0.39	0.36	47.00	6	20.4
Q2FVQ0	Putative uncharacterized protein	SAOUHSC_02652	-0.39	0.57	32.87	6	26.3
Q2FZ39	Ribosome biogenesis GTPase A	SAOUHSC_01214	-0.39	1.27	33.38	6	17
Q2G2U6	Transcriptional regulatory protein WalR	walR	-0.39	1.19	27.19	6	27.9
Q2G1S4	Replicative DNA helicase	SAOUHSC_00018	-0.39	0.81	52.57	4	8.2
Q2G091	ABC transporter, ATP-binding protein	SAOUHSC_00729	-0.39	0.40	72.60	7	14.5
Q2FXR4	Glutamate-1-semialdehyde 2,1-aminomutase 1	hemL1	-0.39	1.15	46.39	12	40.7
Q2FWL6	Redox-sensing transcriptional repressor Rex	rex	-0.39	1.06	23.60	6	30.8
Q2FYT8	Transketolase	SAOUHSC_01337	-0.39	1.17	68.36	25	46.1
Q2G0S7	Pur operon repressor	SAOUHSC_00467	-0.39	1.19	30.40	9	37.6
Q2FW62	Putative uncharacterized protein	SAOUHSC_02445	-0.40	0.57	37.27	5	18
Q2G1A6	Ribokinase, putative	SAOUHSC_00239	-0.40	0.65	32.45	5	22
Q2FZJ6	Bifunctional protein f0D	fold	-0.40	1.23	30.84	12	46.2
Q2FW66	Alkaline shock protein 23	asp23	-0.40	1.45	19.19	6	42.6
Q2FZD3	Endonuclease MutS2	mutS2	-0.40	2.79	88.66	11	14.3
Q2FW38	50S ribosomal protein L13	rplM	-0.41	0.49	16.33	8	39.3
Q2FZ28	ATP-dependent protease ATPase subunit HslU	hslU	-0.41	0.81	52.31	11	31
Q2FW12	30S ribosomal protein S3	rpsC	-0.41	1.62	24.10	12	48.8
Q2FVW4	Putative 2-hydroxyacid dehydrogenase	SAOUHSC_02577	-0.41	1.62	34.67	14	59.6
Q2FXM8	ATP-dependent 6-phosphofructokinase	pfkA	-0.41	1.74	34.84	9	30.1
Q2G1M1	3-ketoacyl-acyl carrier protein reductase, putative	SAOUHSC_00086	-0.41	0.80	27.22	6	37.6
Q2FZ19	Ribonuclease J 2	rnj2	-0.41	2.15	62.60	13	20.1
Q2FWA0	Glutamine--fructose-6-phosphate aminotransferase [isomerizing]	glmS	-0.41	1.88	65.85	16	29.5
Q2FV17	Fructose-bisphosphate aldolase class 1	fda	-0.42	0.58	33.05	21	65.5
Q2FYG2	DNA-binding protein HU, putative	SAOUHSC_01490	-0.42	0.57	9.63	11	82.2
Q2FZ72	Carbamoyl-phosphate synthase large chain	carB	-0.42	2.25	117.18	27	30.3
Q2FYG0	GTPase Der	der	-0.42	1.08	48.98	5	17.4
Q2FZY3	UPF0051 protein	SAOUHSC_00851	-0.42	1.23	52.53	11	23.7
Q2FXM1	Putative uncharacterized protein	SAOUHSC_01814	-0.42	3.45	15.23	5	39.4
Q2G1C9	Putative uncharacterized protein	SAOUHSC_00196	-0.42	1.06	84.61	28	38.4
Q2FX12	Low molecular weight protein-tyrosine-phosphatase PtpA	ptpA	-0.42	0.42	17.49	2	16.9
Q2FW10	30S ribosomal protein S19	rpsS	-0.42	0.85	10.62	4	35.9
Q2FZU9	Putative peptidyl-prolyl cis-trans isomerase	SAOUHSC_00891	-0.42	1.10	21.62	6	44.2
Q2G1Z8	DNA polymerase III PolC-type	polC	-0.43	0.34	162.46	7	6.5
Q2FZH5	Phosphoenolpyruvate-protein phosphotransferase	SAOUHSC_01029	-0.43	0.69	63.22	7	15.7
Q2FW08	50S ribosomal protein L23	rplW	-0.43	2.09	10.61	6	51.6
Q2FWN4	60 kDa chaperonin	groL	-0.43	1.63	57.66	23	57.1
Q2FZD8	Phenylalanine--tRNA ligase beta subunit	pheT	-0.43	0.76	88.92	12	17.8
Q2G1W4	S-adenosylmethionine synthase	metK	-0.44	1.45	43.64	9	24.2
Q2FZ32	DNA topoisomerase 1	topA	-0.44	0.93	79.11	7	16
Q2FZR3	Oligopeptide ABC transporter, substrate-binding protein, putative	SAOUHSC_00927	-0.44	0.24	61.57	3	7.1
Q2FZ25	30S ribosomal protein S2	rpsB	-0.44	2.69	29.09	14	48.2
Q2G295	Catabolite control protein A	SAOUHSC_01850	-0.44	1.37	36.06	13	48
Q2G1T9	DNA-directed RNA polymerase subunit omega	rpoZ	-0.44	0.40	8.15	3	50
Q2G270	Putative uncharacterized protein	SAOUHSC_02568	-0.44	0.55	12.53	2	23.1
Q2G029	2,3-bisphosphoglycerate-independent phosphoglycerate mutase	gpml	-0.44	0.57	56.42	8	20.6
Q2FY27	Glucokinase, putative	SAOUHSC_01646	-0.44	1.41	35.08	7	32.3
Q2FXQ7	ATP-dependent Clp protease ATP-binding subunit ClpX	clpX	-0.44	1.56	46.30	9	25
Q2FXM6	Acetyl-coenzyme A carboxylase carboxyl transferase subunit beta	accD	-0.44	2.44	31.87	8	33.7
Q2FXX2	UPF0271 protein	SAOUHSC_01708	-0.44	0.53	27.45	3	12.4
Q2FWB9;Q2G224	Deoxyribose-phosphate aldolase	deoC	-0.44	0.60	23.33	7	38.6
Q2G2M3	Putative uncharacterized protein	SAOUHSC_00513	-0.45	1.50	27.21	7	29.4

Q2G1C0	2-C-methyl-D-erythritol 4-phosphate cytidyltransferase	ispD	-0.45	1.81	26.66	7	38.7
Q2FY33	Aminomethyltransferase	gcvT	-0.45	1.13	40.46	9	30.6
Q2FV74	ATP-dependent Clp protease ATP-binding subunit ClpL	clpL	-0.45	1.59	77.84	22	35.4
Q2G0N0	Elongation factor Tu	tuf	-0.45	1.16	43.10	23	74.1
Q2FZ22	Uridylate kinase	pyrH	-0.45	2.44	26.15	5	22.5
Q2FWI8	mRNA interferase MazF	mazF	-0.45	0.69	13.44	4	20.8
Q2G0Q7	Dihydropteroate synthase	SAOUHSC_00489	-0.45	0.12	29.52	3	15.4
Q2FWN3	10 kDa chaperonin	groS	-0.45	0.31	10.42	4	43.6
Q2FZA9	Carbamate kinase 1	arcC1	-0.45	1.53	33.60	10	37.1
Q2G2G7	UPF0637 protein	SAOUHSC_01054	-0.46	1.26	24.02	4	21.1
Q2FW07	50S ribosomal protein L4	rplD	-0.46	1.73	22.46	6	40.6
Q2FXU4	Histidine--tRNA ligase	hisS	-0.46	0.85	48.28	5	14.8
P95689	Serine--tRNA ligase	serS	-0.46	1.08	48.64	17	40.7
Q2G0L5	Serine-aspartate repeat-containing protein C	sdrC	-0.46	1.95	107.79	22	28.9
Q2G047	UvrABC system protein B	SAOUHSC_00779	-0.46	1.46	37.48	7	24.1
Q2FXA3	Uroporphyrinogen decarboxylase	hemE	-0.46	2.02	39.35	5	18.8
Q2FY06	GTPase Era	era	-0.46	0.94	34.27	6	17.4
Q2G2U0	N-acetylglucosamine-6-phosphate deacetylase	SAOUHSC_00710	-0.46	1.17	43.13	7	22.6
Q2FXJ0	UDP-N-acetylmuramate--L-alanine ligase	murC	-0.46	0.65	49.19	4	11.4
Q2G1W0	Putative uncharacterized protein	SAOUHSC_02574	-0.46	0.66	40.74	5	20
Q2FW30	30S ribosomal protein S13	rpsM	-0.46	1.04	13.72	9	37.2
Q2G0P0	50S ribosomal protein L1	rplA	-0.47	0.94	24.71	9	46.5
Q2FXR7	Putative uncharacterized protein	SAOUHSC_01768	-0.47	0.98	21.42	3	17.7
Q2FXQ8	Probable GTP-binding protein EngB	engB	-0.47	0.35	22.69	4	30.6
Q2G0G6	Putative uncharacterized protein	SAOUHSC_00603	-0.47	2.17	35.46	5	27.2
Q2FZD9	Phenylalanine--tRNA ligase alpha subunit	pheS	-0.47	1.59	40.11	9	23.3
Q2G2Q3	tRNA pseudouridine synthase B	truB	-0.47	0.56	34.59	5	16.7
Q2FY50	DNA repair protein RecN	SAOUHSC_01615	-0.48	0.74	64.32	5	10.6
Q2FXV6	tRNA-specific 2-thiouridylase MnmA	mnmA	-0.48	1.06	42.15	7	20.4
Q2G0L4	Serine-aspartate repeat-containing protein D	sdrD	-0.48	1.46	146.09	33	40
Q2FW23	30S ribosomal protein S5	rpsE	-0.48	2.15	17.74	9	56.6
Q2FXQ4	Putative uncharacterized protein	SAOUHSC_01781	-0.48	0.62	36.43	4	15.2
Q2G0N1	Elongation factor G	fusA	-0.49	3.04	76.61	25	49.4
Q2FZ23	Elongation factor Ts	tsf	-0.49	2.48	32.49	15	60.8
Q2G077	Ribonucleotide-disphosphate reductase beta chain, putative	SAOUHSC_00743	-0.49	1.01	37.51	4	16.1
Q2FX90	Putative uncharacterized protein	SAOUHSC_01987	-0.49	1.61	22.34	6	33.7
Q2G1K9	Aldehyde-alcohol dehydrogenase	SAOUHSC_00113	-0.49	1.97	94.94	28	40.3
Q2G1X1	Putative uncharacterized protein	SAOUHSC_01120	-0.49	0.32	8.90	2	40.3
Q2G1Y5	L-lactate dehydrogenase 2	ldh2	-0.49	0.77	34.42	12	48.9
Q2G2S0	Adenylosuccinate lyase	purB	-0.49	1.44	49.60	10	23.2
Q2FXN4	Isocitrate dehydrogenase [NADP]	SAOUHSC_01801	-0.49	2.41	46.42	7	22
Q2FXY7	Elongation factor 4	lepA	-0.49	2.57	68.17	8	18.9
Q2FXN9	DNA polymerase	SAOUHSC_01797	-0.49	1.29	99.19	17	27.3
Q2FZC6	Glutamate racemase	murI	-0.49	0.89	29.70	5	26.3
Q2FXE8	Putative uncharacterized protein	SAOUHSC_01901	-0.49	1.14	25.71	11	51.9
Q2FZ92	UDP-N-acetylmuramoylalanine--D-glutamate ligase	murD	-0.49	1.29	49.84	8	17.6
Q2FZ86	Cell division protein SepF	sepF	-0.50	1.31	21.02	2	17.1
Q2FW22	50S ribosomal protein L18	rplR	-0.50	1.25	13.10	6	51.3
Q2G1Y0	DNA ligase	ligA	-0.50	0.61	75.08	13	21.3
Q2FYS4	DNA topoisomerase 4 subunit A	parC	-0.50	1.59	91.00	16	22.6
Q2FXP7	Threonine--tRNA ligase	thrS	-0.50	2.23	74.49	16	24.5
Q2G1G6	N-acetylmuramic acid 6-phosphate etherase	murQ	-0.50	0.26	32.38	4	13.4
Q2FW20	30S ribosomal protein S8	rpsH	-0.50	1.01	14.83	8	57.6
Q2FXV0	Putative uncharacterized protein	SAOUHSC_01732	-0.50	0.82	12.77	2	28.4
Q2FXJ5	Tyrosine--tRNA ligase	tyrS	-0.50	1.84	47.60	9	26.2
Q2FW11	50S ribosomal protein L22	rplV	-0.50	0.82	12.84	7	58.1
Q2G1G2	Type I site-specific deoxyribonuclease, HsdR family, putative	SAOUHSC_00162	-0.50	1.95	109.23	16	16.6
Q2FWD6	Putative aldehyde dehydrogenase	SAOUHSC_02363	-0.51	1.85	51.97	14	32.4
Q2FZ54	Malonyl CoA-acyl carrier protein transacylase	SAOUHSC_01198	-0.51	1.03	33.64	9	31.8
Q2G274	DNA gyrase subunit B	gyrB	-0.51	1.78	72.54	13	17.5
Q2FW79	UPF0457 protein	SAOUHSC_02425	-0.51	1.67	10.01	3	41.9
Q2FV3	Threonine synthase	SAOUHSC_01321	-0.51	1.21	37.87	8	27.2
Q2FZX4	Lipoyl synthase	lipA	-0.51	1.52	34.89	7	22.3
Q2G2C9	Putative uncharacterized protein	SAOUHSC_01245	-0.51	1.10	11.54	2	24.8
Q2G0S2	Ribose-phosphate pyrophosphokinase	prs	-0.52	1.95	35.28	9	29

8 - Supporting Information

Q2FW18	50S ribosomal protein L5	rplE	-0.52	1.69	20.27	14	63.7
Q2G0P5	ATP-dependent Clp protease ATP-binding subunit ClpC	clpC	-0.52	2.15	91.04	27	36.9
Q2G293	Putative uncharacterized protein	SAOUHSC_01847	-0.52	0.36	24.78	5	28.6
Q2FXU1	GTP pyrophosphokinase	SAOUHSC_01742	-0.52	1.67	83.69	9	15.8
Q2FZT1	Putative uncharacterized protein	SAOUHSC_00909	-0.52	0.44	31.67	3	15
Q2FWJ5	S1 RNA binding domain protein	SAOUHSC_02297	-0.52	2.08	80.93	25	36.7
Q2G0M5	Uncharacterized epimerase/dehydratase	SAOUHSC_00535	-0.53	1.74	36.05	9	33.6
Q2G046	UvrABC system protein A	uvrA	-0.53	1.57	105.37	15	23.4
Q2FZB0	Ornithine carbamoyltransferase	argF	-0.53	1.05	37.52	9	31.2
Q2FYZ5	Glycerol kinase	glpK	-0.53	1.54	55.63	16	31.9
Q2FUS9	UPF0312 protein	SAOUHSC_03022	-0.53	0.92	18.66	2	14.6
Q2G0E9	Putative uncharacterized protein	SAOUHSC_00656	-0.54	1.26	21.26	5	27.8
Q2FV67	1-pyrroline-5-carboxylate dehydrogenase	rocA	-0.54	1.09	56.87	23	54.3
Q2FZP4	Peptide chain release factor 3	prfC	-0.54	1.40	59.60	4	7.9
Q2FZG8	UPF0356 protein	SAOUHSC_01036	-0.54	0.31	8.75	3	55.6
Q2FY43	Acetyl-CoA carboxylase, biotin carboxylase	SAOUHSC_01623	-0.54	1.26	50.05	9	27.3
Q2G1N7	HTH-type transcriptional regulator SarS	sarS	-0.54	0.80	29.89	4	18.8
Q2FYG7	Nucleoside diphosphate kinase	ndk	-0.55	1.31	16.58	5	40.9
Q2FY15	DEAD-box ATP-dependent RNA helicase CshB	cshB	-0.55	1.44	51.08	11	29.7
Q2G078	Ribonucleoside-diphosphate reductase	SAOUHSC_00742	-0.55	1.39	82.60	15	23.2
Q2FXP2	Glyceraldehyde-3-phosphate dehydrogenase	SAOUHSC_01794	-0.55	2.56	36.98	11	42.2
Q2G0N5	DNA-directed RNA polymerase subunit beta'	rpoC	-0.55	1.84	135.41	42	38.1
Q2FUQ5	Putative uncharacterized protein	SAOUHSC_03049	-0.55	1.32	32.20	4	22.2
Q2G0Q1	Pyridoxal biosynthesis lyase PdxS	pdxS	-0.55	1.26	31.99	9	35.9
Q2FXV9	Alanine--tRNA ligase	alaS	-0.56	1.67	98.52	16	26.5
Q2FW31	30S ribosomal protein S11	rpsK	-0.56	1.42	13.88	5	40.3
Q2FZS8	ATP-dependent Clp protease, ATP-binding subunit ClpB	SAOUHSC_00912	-0.56	3.13	98.33	33	42.8
Q2G0Q0	Glutamine amidotransferase subunit PdxT	pdxT	-0.56	0.54	20.63	3	16.1
Q2FZH6	Phosphocarrier protein hpr, putative	SAOUHSC_01028	-0.56	0.35	9.50	4	58
Q2FY88	Exonuclease family	SAOUHSC_01576	-0.57	0.60	35.90	9	28.1
Q2G069	UDP-N-acetylenolpyruvoylglucosamine reductase	murB	-0.57	0.82	33.80	3	11.7
Q2FXT1	GTPase Obg	obg	-0.57	1.27	47.24	13	37
Q2FZ16	Bifunctional purine biosynthesis protein PurH	purH	-0.57	0.42	54.35	8	16.5
Q2G024	Ribonuclease R	rnr	-0.57	1.73	90.43	10	12.9
P60393	Ribosomal RNA small subunit methyltransferase H	rsmH	-0.57	2.68	35.68	5	19.3
Q2FXA0	UPF0342 protein	SAOUHSC_01977	-0.57	0.39	13.31	6	58.8
Q2FXQ3	Putative uncharacterized protein	SAOUHSC_01782	-0.58	0.37	22.95	5	26.7
Q2FW81	Probable uridylyltransferase	SAOUHSC_02423	-0.58	1.14	44.89	12	33.2
Q2G0C6	Putative uncharacterized protein	SAOUHSC_00679	-0.59	0.67	33.24	2	8.3
P0A086	Peptide methionine sulfoxide reductase MsrA 2	msrA2	-0.59	0.83	20.59	4	19.2
P0A0G2	50S ribosomal protein L30	rpmD	-0.59	0.76	6.55	7	72.9
Q2FZ77	Bifunctional protein PyrR	pyrR	-0.60	1.68	19.86	8	49.1
P47768	DNA-directed RNA polymerase subunit beta	rpoB	-0.60	2.86	133.22	35	32.1
Q2FYP2	ABC transporter, ATP-binding protein, putative	SAOUHSC_01392	-0.60	1.66	60.26	13	25.9
Q2FVL8	Assimilatory nitrite reductase [NAD(P)H], large subunit, putative	SAOUHSC_02684	-0.60	2.36	88.66	15	23.5
Q2G115	Ribosome-binding ATPase YchF	ychF	-0.60	1.89	40.59	11	41.4
Q2G2Q4	Ribosome-binding factor A	rbfA	-0.61	1.26	13.52	4	41.4
Q2G2D2	Transcription termination-antitermination factor, putative	SAOUHSC_01243	-0.63	1.47	43.74	9	25.8
Q2G0N9	50S ribosomal protein L10	rplJ	-0.63	1.04	17.71	4	36.7
Q2FZ49	Chromosome partition protein Smc	smc	-0.63	0.72	136.75	14	15
Q2G2H5	Chromosomal replication initiator protein DnaA	dnaA	-0.63	1.25	51.97	9	17.4
Q2G1B9;Q2G1C4	Putative uncharacterized protein	SAOUHSC_00226	-0.64	1.69	38.45	6	16.4
Q2G050	Excinuclease ABC, B subunit	SAOUHSC_00776	-0.64	2.84	39.82	7	23
Q2FXI6	Putative uncharacterized protein	SAOUHSC_01860	-0.65	0.87	11.86	3	34
P0A0F4	50S ribosomal protein L11	rplK	-0.65	1.79	14.87	7	45
Q2FXM9	Pyruvate kinase	pyk	-0.65	3.23	63.10	29	66.3
Q2FWD8	50S ribosomal protein L31 type B	rpmE2	-0.65	0.62	9.72	2	31
Q2G2C1	Pyruvate carboxylase	SAOUHSC_01064	-0.66	1.35	128.55	41	46.2
Q2FWE9	ATP synthase gamma chain	atpG	-0.66	1.86	29.47	10	46
Q2G1T6	UTP--glucose-1-phosphate uridylyltransferase	gtaB	-0.67	1.86	32.45	6	17.7
Q2FZ50	Ribonuclease 3	rnc	-0.67	0.88	27.92	5	23.5
Q2FX95	Ribosomal large subunit pseudouridine synthase, RluD subfamily, putative	SAOUHSC_01982	-0.67	1.18	31.44	4	17.2
Q2FZ68	Methionyl-tRNA formyltransferase	fmt	-0.68	1.00	34.21	9	34.7
Q2FWE6	Uracil phosphoribosyltransferase	upp	-0.69	1.13	23.05	7	44.5

Q2G0X6;Q2FXD0	Type I restriction-modification system, M subunit	SAOUHSC_00397	-0.69	1.54	56.14	5	11.4
Q2FYH6	Asparagine--tRNA ligase	asnS	-0.70	1.77	49.16	11	28.4
Q2G111	30S ribosomal protein S18	rpsR	-0.70	0.59	9.31	3	25
Q9FOR1	HTH-type transcriptional regulator SarR	sarR	-0.70	0.98	13.67	6	34.8
Q2G0Y6	GMP synthase [glutamine-hydrolyzing]	guaA	-0.71	2.50	58.23	6	18.3
Q2FWC9	Putative uncharacterized protein	SAOUHSC_02370	-0.72	1.30	33.11	4	15.7
Q2FZ42	50S ribosomal protein L19	rplS	-0.73	1.24	13.36	6	37.9
Q2G2F8	ATP synthase subunit b	atpF	-0.73	0.94	19.54	7	43.9
Q2G093	Lipoteichoic acid synthase	ltaS	-0.73	0.27	74.40	11	24.3
Q2FWW3	Putative uncharacterized protein	SAOUHSC_02158	-0.74	1.09	48.12	8	24.8
Q2FWH5	DEAD-box ATP-dependent RNA helicase CshA	cshA	-0.74	1.61	56.94	16	40.1
Q2G0T5	DNA polymerase III, gamma and tau subunits, putative	SAOUHSC_00442	-0.74	1.20	62.46	7	15.4
P0A0J3	Superoxide dismutase [Mn] 1	sodA	-0.74	1.38	22.71	3	22.6
P0A0H0	30S ribosomal protein S12	rpsL	-0.75	0.84	15.29	3	13.1
Q2FWH3	D-alanine--D-alanine ligase	ddl	-0.75	0.97	40.23	8	32.3
Q2G2J2	Staphylococcal secretory antigen ssaA2	ssaA2	-0.75	0.57	29.33	6	47.9
Q2FY49	Arginine repressor	argR	-0.77	0.40	17.10	2	22
Q2FZ78	Pseudouridine synthase	SAOUHSC_01163	-0.77	1.51	34.60	5	16.1
Q2FXV8	Putative uncharacterized protein	SAOUHSC_01723	-0.80	0.54	93.05	6	10.7
Q2G0Y9	Xanthine phosphoribosyltransferase	xpt	-0.81	1.74	20.88	4	25
Q2G1X0	Alpha-hemolysin	hly	-0.81	0.68	35.97	14	50.8
Q2FZL8	Putative uncharacterized protein	SAOUHSC_00982	-0.83	0.57	46.62	4	10.2
Q2FZM7	Putative uncharacterized protein	SAOUHSC_00973	-0.85	0.99	27.73	4	19.6
Q2FW14	50S ribosomal protein L29	rpmC	-0.86	1.80	8.09	5	55.1
Q2FZK7	Bifunctional autolysin	atl	-0.91	1.34	137.38	42	40.6
Q2G065	Putative uncharacterized protein	SAOUHSC_00756	-0.92	0.72	41.80	4	9.6
P60430	50S ribosomal protein L2	rplB	-0.93	1.29	30.16	12	51.6
Q2G1Z9	NAD kinase	nadK	-0.95	0.50	30.77	2	7.1
Q2FVK5	Immunoglobulin-binding protein sbi	sbi	-0.95	0.77	50.07	13	29.1
Q2FV28	Putative uncharacterized protein	SAOUHSC_02911	-0.98	0.92	27.79	2	10
Q2G234	Nitric oxide synthase oxygenase	SAOUHSC_02134	-0.99	1.06	41.71	5	18.4
Q2FZP6	UDP-N-acetylmuramoyl-L-alanyl-D-glutamate--L-lysine ligase	murE	-1.05	0.70	54.10	12	25.4
P48940	30S ribosomal protein S7	rpsG	-1.05	2.87	17.79	7	40.4
Q2G0D1	HTH-type transcriptional regulator SarX	sarX	-1.10	1.14	14.18	6	44.5
Q2G170	5'-nucleotidase, lipoprotein e(P4) family	SAOUHSC_00284	-1.17	1.24	33.35	4	22.3
Q2FXQ1	50S ribosomal protein L20	rplT	-1.20	1.59	13.69	2	16.1
Q2FWN9	Uncharacterized leukocidin-like protein 2	SAOUHSC_02243	-1.22	1.98	40.43	9	28.5
Q2FWP0	Uncharacterized leukocidin-like protein 1	SAOUHSC_02241	-1.24	2.37	38.69	4	17.8
Q2G0F2	Putative uncharacterized protein	SAOUHSC_00617	-1.32	1.16	18.59	5	30.4
Q2G189	Putative uncharacterized protein	SAOUHSC_00257	-1.34	1.13	11.04	5	70.1
Q2G012	Extracellular matrix protein-binding protein emp	emp	-1.46	1.37	38.48	8	23.2
Q2FWE7	ATP synthase subunit delta	atpH	-1.48	1.53	20.50	5	30.2
Q2FWW1	MHC class II analog protein	SAOUHSC_02161	-1.50	1.11	65.57	19	35.8
Q2G1U6	Regulatory protein Spx	spxA	-1.60	0.88	15.44	3	22.1
Q2FWM8	Delta-hemolysin	hld	-1.75	0.37	2.98	3	84.6
Q2FV52	Probable transglycosylase IsaA	isaA	-1.75	1.57	24.20	5	39.9
Q2G0U9	N-acetylmuramoyl-L-alanine amidase sle1	sle1	-2.05	1.86	35.84	5	19.5
Q2G2T8	Putative uncharacterized protein	SAOUHSC_00712	-2.91	0.87	32.36	2	7.2

Table S10: MIC determination for **PK150** and **SFN** in transposon mutants (USA300, Nebraska Transposon mutant library).

Transposon mutant	Uniprot ID (USA300)	Gene name (USA300)	Uniprot ID (NCTC 8325, homologous protein)	Protein names (NCTC 8325)	Gene names (NCTC 8325, ordered locus)	MIC (μM)	
						PK150	SFN
NE1076	A0A0H2XKJ6	SAUSA300_2289	Q2FVS2	Putative uncharacterized protein	SAOUHSC_02620	0.3	3
NE112	Q2FK70	SAUSA300_0194	Q2G1G5	PTS system EIBC component	SAOUHSC_00158	0.3	3
NA1204	A0A0H2XIZ6	SAUSA300_2489	Q2FV70	Putative uncharacterized protein	SAOUHSC_02866	0.3	3
NE1270	A0A0H2XH18	SAUSA300_0913	Q2FZQ2	Putative uncharacterized protein	SAOUHSC_00948	0.3	3
NE1615	A0A0H2XI48	SAUSA300_0618	Q2G2D8	ABC transporter, substrate-binding protein, putative	SAOUHSC_00634	0.3	3
NE166	A0A0H2XIH0	SAUSA300_0230	Q2G1C5	Membrane protein, putative	SAOUHSC_00200	0.3	3
NE1884	Q2FID4	SAUSA300_0844	Q2FZV7	NADH dehydrogenase-like protein	SAOUHSC_00878	0.3	3
NE1886	A0A0H2XIX8	SAUSA300_0992	Q2FZG5	Putative uncharacterized protein	SAOUHSC_01039	0.3	3
NE291	A0A0H2XJ64	SAUSA300_2328	Q2FVN6	Putative uncharacterized protein	SAOUHSC_02666	0.3	3
NE323	A0A0H2XJS2	SAUSA300_0362	Q2G117	Putative uncharacterized protein	SAOUHSC_00344	0.3	3
NE419	A0A0H2XIR9	SAUSA300_2297	Q2G2W2	Putative uncharacterized protein	SAOUHSC_02628	0.3	3
NE646	Q2FF00	SAUSA300_2082	Q2FWD0	Probable DNA-directed RNA polymerase subunit delta	SAOUHSC_02369	0.3	3
NE721	A0A0H2XJU8	SAUSA300_2100	Q2FWA8	Lytic regulatory protein, putative	SAOUHSC_02390	0.3 - 1	10
NE733	A0A0H2XDX3	SAUSA300_0274	Q2G193	Putative uncharacterized protein	SAOUHSC_00253	0.3	3
NE779	A0A0H2XFZ5	SAUSA300_1254	Q2G2N2	Putative uncharacterized protein	SAOUHSC_01358	0.3	3
NE866	A0A0H2XER4	SAUSA300_2213	Q2FVZ5	Putative uncharacterized protein	SAOUHSC_02525	0.3	3
NE92	Q2FI17	SAUSA300_0963	Q2FZJ9	Probable quinol oxidase subunit 2	SAOUHSC_01002	0.3	3

Table S11: Mutations identified in SFN-resistant *S. aureus* NCTC 8325. Mutation positions are given for chromosome NC_007795.

ID	GN SAOUHSC	Descr.	RS#	Effect	Qual.	MPL	Pos.	WTB	MB	GN SAUSA300	TM
Q2FZQ6	_00944	RluD	2	MV	8544	S28T	915721	G	C	_0909	NE822
Q2FZQ6	_00944	RluD	3	MV	8390	A29T	915723	G	A	_0909	NE822
Q2G2M2	_01359	FmtC	2	FSV	6562	L595fs	1303264	ATT	A	_1255	NE1360
Q2FZS1	_00919	-60 to opp	3	UGV	6491		893950	T	C		
Q2FZ64	_01187	PknB	3	FSV	5402	A370fs	1139308	TG	T		
Q2FWM4	_02265	Protein A	1	MV	4425	S172R	2096521	C	A		
Q2G2M2	_01359	FmtC	1	FSV	4344	E32fs	1301574	CG	C	_1255	NE1360

ID, Uniprot ID; GN, Gene name; Descr., Description; RS#, Number of the resistant strain; MV, Missense variant; FSV, Frameshift variant; UGV, Upstream gene variant; MPL, Mutation at protein level; Pos., Position of mutation in the chromosome; WTB, Wild-type base; MB, Mutant base, USA300 homologous protein; TM, Transposon mutant (Nebraska Transposon Library).

Table S12: Proteins of the ABC transporter which confers resistance to arylomycin and renders SpsB non-essential.

Protein	Gene name (N315)	Gene name (NCTC 8325)	Description	Characteristics	MW [Da]
AyrR	SA0337	SAOUHSC_00331	Transcriptional regulator, Cro/Ci family-related protein	HTH_XRE superfamily	7,689
AyrA	SA0338	SAOUHSC_00332	Putative membrane protein	6 TMs DUF3169 superfamily	26,784
AyrB	SA0339	SAOUHSC_00333	ABC transporter, ATP-binding protein	Ccm AAA superfamily	31,594
AyrC	SA0340	SAOUHSC_00334	putative multi-drug ABC transporter permease	5 TMs ABC2_membrane superfamily	23,256

Table S13: Pfam database entries for peptidoglycan hydrolysing domains.

Pfam entry	Domain	Family	Domain full name
PF05257	CHAP	CHAP	CHAP domain
PF01510	Amidase	<i>Amidase_2</i>	N-acetylmuramoyl-L-alanine amidase
PF01520	Amidase	<i>Amidase_3</i>	N-acetylmuramoyl-L-alanine amidase
PF01464	Transglycosylase	<i>SLT</i>	Transglycosylase SLT domain
PF06737	Transglycosylase	<i>Transglycosylase</i>	Transglycosylase-like domain
PF01832	Glucosaminidase	<i>Glucosaminidase</i>	Mannosyl-glycoprotein endo-beta-N-acetylglucosaminidase
PF01551	Peptidase	<i>Peptidase_M23</i>	Peptidase family M23
PF01471	Putative peptidoglycan binding	<i>PG_binding_1</i>	Putative peptidoglycan binding domain

Table S14: Proteins, detected in the secretomes upon treatment with the inactive control compounds compared to DMSO (**PK150-C/DMSO** and **SFN-C/DMSO**) that were annotated as peptidoglycan hydrolases (PGH). Prediction of signal peptide by PrediSi is indicated in the column “SP” as “Y” or “N” for presence or absence of a predicted signal peptide. The abbreviations for of PGHs classes can be found beneath the table. Furthermore enrichment ratios (PR = \log_2 protein ratio) and *p*-values (PV = $-\log_{10}$ *p*-value (*t*-test)) are given. Ratios with values > 0.5 are shaded in gray.

Protein IDs	Protein names	PK150-C/ DMSO		SFN-C/ DMSO			
		SP	PGH	PR	PV	PR	PV
O33599	Glycyl-glycine endopeptidase LytM	Y	P	0.32	0.67	0.30	0.47
Q2FV55	Staphylococcal secretory antigen SsaA	Y	CH	0.19	0.14	0.12	0.10
Q2G0D4	Secretory antigen SsaA-like protein	Y	CH; LM	0.09	0.09	0.18	0.20
Q2G222	N-acetylmuramoyl-L-alanine amidase domain-containing protein	Y	CH; GA	-0.14	0.11	0.03	0.02
Q2G1W1	Secretory antigen SsaA, putative	Y	CH	0.05	0.04	-0.02	0.01
Q2FWF8	Probable TG SceD	Y	TG	0.11	0.12	0.33	0.38
Q2G0U9	N-acetylmuramoyl-L-alanine amidase sle1	Y	CH; LM	-0.09	0.12	-0.26	0.37
Q2G190	Putative uncharacterized protein	Y	CH	0.43	1.38	0.57	1.94
Q2G2J2	Staphylococcal secretory antigen ssaA2	Y	CH	-0.01	0.01	0.23	0.32
Q2FV52	Probable TG IsaA	Y	TG	-0.04	0.06	0.25	0.36
Q2FX77	Autolysin	N	CH	0.15	0.14	-0.24	0.28
Q9ZNI1	Probable cell wall hydrolase LytN	Y	CH; LM	0.35	0.43	0.31	0.29
Q2FZK7	Bifunctional autolysin	Y	GA	-0.05	0.07	0.10	0.19
Q2FV81	LM domain protein	N	CH	-0.24	0.20	-0.18	0.19
Q2FYL3	Putative uncharacterized protein	N	PB	-0.23	0.22	-0.14	0.13
Q2FVW2	N-acetylmuramoyl-L-alanine amidase, putative	N	GA	-0.56	0.30	-0.64	0.68
Q2FXF4	Putative uncharacterized protein	N	GA	-1.31	0.57	-0.35	0.23

SP, Signal Peptide predicted (by PrediSi), Y=yes, N=no; PGH, peptide hydrolase domain; CH, CHAP; GA, Glucosaminidase; LM, LysM; P, Peptidase; TG, Transglycosylase; PB, Putative peptidoglycan binding; PR, \log_2 protein ratio; PV, $-\log_{10}$ *p*-value (*t*-test)

Table S15: Enrichment analysis of peptidoglycan hydrolase domain-containing proteins (Pfam annotations: CHAP domain, LysM domain, amidase, transglycolase, glucosaminidase and peptidase M23 domain) using Fisher's exact test. Proteins with a \log_2 -fold enrichment of > 0.5 for compound- vs. DMSO-treatment were tested against the whole secretome as the background.

Category	Proteins with \log_2 protein ratio > 0.5		Secretome
	PK150/ PK150-C	SFN/ SFN-C	
Total proteins	72	112	806
„PGH domain AND predicted signal peptide“ proteins	8	7	12
Not „PGH domain AND predicted signal peptide“ proteins	64	105	794
Fisher Exact <i>p</i> -value (Secretome as background)	<0.0001	0.0048	

“The most beautiful thing we can experience is the mysterious.
It is the source of all true art and science”

— Albert Einstein

Danksagung

Abschließend möchte ich mich bei all den Menschen, die mich durch diese sehr intensive Zeit mit unzähligen Höhen und Tiefen begleitet und unterstützt haben, bedanken.

Ich möchte mich sehr herzlich bei Prof. Dr. Stephan A. Sieber für die herausragende Betreuung bedanken. Ich weiß sehr zu schätzen, dass Stephan es mir ermöglicht hat, meine Doktorarbeit an einem so ausgezeichnet ausgestatteten Lehrstuhl anfertigen zu dürfen und ich dabei eine so außerordentliche Bandbreite an Methoden nutzen konnte. Insbesondere möchte ich mich für sein stets offenes Ohr, die Begeisterung, Neugier und die vielen Ideen bedanken.

Mein Dank gilt meinem Zweitprüfer, Prof. Dr. Matthias Feige, für die Zeit und Mühe bei der Begutachtung meiner Arbeit. Ebenfalls für seine wertvolle Zeit danke ich meinem Prüfungsvorsitzenden, Prof. Dr. Michael Groll.

Weiterhin möchte ich mich bei allen meinen Kooperationspartnern für die angenehme und effiziente Zusammenarbeit bedanken. Dieser Dank gilt Dr. Katharina Rox, Dr. Megan C. Jennings, Maria Reinecke, Ilke M. Ugur, Prof. Dr. Bernhard Küster, Prof. Dr. Manfred Rohde, Prof. Dr. Eva Medina und Prof. Dr. Bill M. Wuest.

Für die Förderung während meiner Promotion danke ich dem Fonds der chemischen Industrie..

Ein großes Dankeschön geht an meinen Kollegen und Lab C-Sitznachbarn Philipp Kleiner. Seite an Seite haben wir mehrere Jahre an diesem Projekt geschwitzt und gemeinsam Freud und Leid geteilt, sowie uns gegenseitig unterstützt und motiviert.

Vielen lieben Dank an Markus Lakemeyer, Dr. Christian Fetzer und Jennifer Wiederspahn für das Korrekturlesen dieser Arbeit.

Ich möchte mich sehr herzlich bei Katja Bäuml für all die nervenaufreibenden Stunden an den Massenspektrometern bedanken. Ich kann mir niemand Besseren vorstellen, mit dem es trotzdem so viel Spaß gemacht hätte. Katja und Mona Wolff möchte ich zudem für die großartige tägliche Unterstützung im Labor bedanken. Vielen lieben Dank auch an Christina Brumer für Ihre tolle Arbeit.

Ich danke meinen tollen lieben Freunden aus dem Lab-Dschungel, insbesondere Dr. Franziska Mandl, Dr. Christian Fetzer, Markus Lakemeyer, Mathias Hackl und Thomas Gronauer für all die tollen Zeiten, die wir miteinander verbracht haben und für die unendliche Unterstützung. Ich werde die gemeinsame Zeit mit Euch sehr vermissen, insbesondere unsere entspannenden Kaffeepausen und die lustigen „Spieleabende“ und - nicht zu vergessen - die wissenschaftlichen Diskussionen, die oft entscheidende

Erkenntnisse gebracht haben. Außerdem wart ihr eine enorme seelische Unterstützung und habt es immer geschafft mich aufzumuntern, wenn ich es gebraucht habe. Ein sehr herzliches Dankeschön geht an alle meine Arbeitskollegen Anni Hoegl, Dr. Pavel Kielkowski, Matthias Stahl, Volker Kirsch, Dr. Nina Bach, Dr. Stephan Hacker, Dr. Weining Zhao, Barbara Hofbauer, Anja Fux, Caro Gleißner, Dóri Balogh, Ines Hübner, Robert Macsics, Martin Pfanzelt, Johnny Drechsel, Kyu Lee, Vadim Korotkov und Igor Pavlović für das wunderbare Arbeitsklima und die Hilfsbereitschaft. Auch bei meinen ehemaligen Kollegen und Freunden Dr. Maximilian Koch, Dr. Jürgen Eirich, Dr. Wolfgang Heydenreuter, Dr. Bianca Schwanhäußner, Dr. Jan Vomacka, Dr. Johannes Lehmann, Dr. Johannes Kreuzer, Dr. Maria Dahmen, Dr. Megan Wright, Dr. Roman Kolb möchte ich mich für die schöne Zeit bedanken. Bei den frischgebackenen Doktoranden Patrick Zanon, Josef Braun, Patrick Allihn, Theresa Rauh und Angela Muñoz bedanke ich mich ebenfalls für die zwar kurze, aber gute Zeit.

Vor allem aber auch möchte ich mich bei meinen tollen, schlaun, schönen, lustigen und einfach besten Freunden dafür bedanken, dass ihr immer für mich da wart und seid. Bei meiner allerliebsten Jenny dafür, dass mit dir einfach alles Spaß macht - ob Laborarbeit, Konzerte, Urlaube, Herumphilosophieren – einfach Alles. Vielen lieben Dank auch an meine liebe Frani und deine Familie für eure Warmherzigkeit und die unendliche Unterstützung. Ich danke Evi, Mäxli, Temssy, Sandy und Vivi für die unzähligen lustigen Abende, die oft die einzige Rettung nach schiefgelaufenen Labortagen waren. Janinalein und Timo danke ich dafür, dass ihr euch auch nach so langer Zeit räumlicher Trennung immer dafür interessiert und begeistert habt, was ich da so im Lab mache. Lenny, dir gilt ein ganz besonderer Dank, denn du bist innerhalb kürzester Zeit zu meinem besten Freund geworden, hast mich durch die anstrengendste Phase der Promotion begleitet und warst die großartigste Unterstützung, die man sich vorstellen kann.

Der größte Dank gilt meiner Mama - ohne deinen Mut, deine Intelligenz und Stärke hätte ich niemals die Möglichkeit bekommen, meine Doktorarbeit unter solch angenehmen Rahmenbedingungen in Angriff nehmen zu können und ohne deine unermüdliche emotionale Unterstützung und bedingungslose Liebe erfolgreich abzuschließen. Мама, огромное спасибо! Ich möchte mich vom ganzen Herzen auch bei dem Rest meiner Familie bedanken – insbesondere bei Ralf und meinen Großeltern – für die unzähligen weisen Ratschläge, die allerleckerste Nervennahrung und euren Glauben an mich.

Euer Lenchen

Für die beste Mama der Welt – meine ;)

